

LEARNING, MEMORY, AND SYNAPTIC PLASTICITY IN ALZHEIMER'S MODEL MICE

by

JASON KNIGHT CLARK

(Under the Direction of John J. Wagner)

ABSTRACT

Alzheimer's disease (AD) is a neurodegenerative disease of aging thought to be initiated by production of Amyloid- β peptide, which leads to synaptic dysfunction and progressive memory loss, and the eventual formation of β -Amyloid plaques and neurofibrillary Tau tangles. Working memory is one of the first cognitive impairments in AD. We therefore wanted to explore the cellular mechanisms underlying working memory impairments in AD utilizing a well-known triple transgenic mouse model of Alzheimer's disease (3xTg-AD) carrying mutations in APP, PS1, and Tau. We evaluated working memory using an 8-arm radial maze, and synaptic transmission and plasticity using an *ex vivo* hippocampal slice preparation to measure field Excitatory Post-Synaptic Potentials (fEPSP) in the CA1 region of ventral hippocampus. Unexpectedly, young 3xTg-AD mice at 3 months of age, typically considered to be presymptomatic, were significantly impaired in the spatial working memory task compared to Nontransgenic (NonTg) control mice. Measurements of fEPSPs to evaluate Long-Term Potentiation (LTP) as an indicator of long-term synaptic plasticity showed the NMDA receptor-dependent component of LTP (NMDAR LTP) was reduced in 3xTg-AD mice compared to NonTg mice. The remaining non-NMDA receptor-

dependent component of LTP (non-NMDAR LTP) however was increased, resulting in a total LTP that was not different between 3xTg-AD and NonTg mice. At 8 months of age, 3xTg-AD mice were again significantly impaired in the spatial working memory task, and NMDAR LTP was again reduced in 3xTg-AD mice. The non-NMDAR LTP however was also reduced in 3xTg-AD mice, resulting in a total LTP that was now reduced in 3xTg-AD mice. The majority (>90%) of non-NMDAR LTP is mediated by Voltage-Dependent Calcium Channels (VDCC), and attempts to block LTP using NMDAR and VDCC antagonists were unsuccessful, indicating 3xTg-AD mice have compensatory mechanisms for LTP expression that occur independently of NMDAR or non-NMDAR dependent mechanisms. In addition, 3xTg-AD mice also showed impairments in short-term synaptic plasticity and basal synaptic transmission at both 3 and 8 months of age. These impairments in synaptic transmission and plasticity coincide with impairments in spatial working memory, and understanding the nature of these altered mechanisms may lead to therapeutic targets for disorders such as AD.

INDEX WORDS: Alzheimer's disease, Synaptic Plasticity, Working Memory, LTP, Radial Maze, Amyloid- β , Hirano Body

LEARNING, MEMORY, AND SYNAPTIC PLASTICITY IN ALZHEIMER'S MODEL MICE

by

JASON KNIGHT CLARK

B.S., Georgia Southern University, 1998

M.S., The University of Georgia, 2007

A Dissertation Submitted to the Graduate Faculty of The University of Georgia in Partial
Fulfillment of the Requirements for the Degree

DOCTOR OF PHILOSOPHY

ATHENS, GEORGIA

2016

© 2016

Jason Knight Clark

All Rights Reserved

LEARNING, MEMORY, AND SYNAPTIC PLASTICITY IN ALZHEIMER'S MODEL MICE

by

JASON KNIGHT CLARK

Major Professor: John J. Wagner

Committee: Julie Coffield
James Lauderdale

Electronic Version Approved:

Suzanne Barbour
Dean of the Graduate School
The University of Georgia
May 2016

DEDICATION

To my family, for their support, encouragement, and patience.

ACKNOWLEDGEMENTS

I would like to begin by acknowledging and thanking Dr. John Wagner for the opportunity to learn, grow, and develop as a scientist under his guidance and direction throughout my graduate training. To the members of the Wagner Lab, whose discussions and contributions have been an invaluable source of creative thought. I would also like to thank Dr. Marcus Fechheimer and Dr. Ruth Furukawa. A portion of this work has been in collaboration with their research group, and they have been instrumental in the completion of this work. I would like to thank the members of my graduate committee, Dr. Jim Lauderdale and Dr. Julie Coffield, whose input is always valuable, and whose discussions always lead to new perspectives of my work. I would also like to thank the faculty and staff of the UGA department of Physiology and Pharmacology, who were always willing to help out in any way necessary, providing technical support and advice, and whose interactions made my time at UGA an enjoyable and engaging experience. Thank you all.

TABLE OF CONTENTS

	Page
ACKNOWLEDGEMENTS	v
CHAPTER	
1 INTRODUCTION AND LITERATURE REVIEW	1
1.1 Historical Perspective	1
1.2 General Overview of Alzheimer's Disease	3
1.3 General Overview of Learning and Memory	16
1.4 Memory and Synaptic Plasticity	22
1.5 Cellular Mechanisms of Synaptic Plasticity	27
1.6 NMDA Receptors in Complex Learning and Memory	41
1.7 Synaptic Impairment in Alzheimer's Disease	50
1.8 Final Thoughts	61
References	64
Figures	102
2 ALTERATIONS IN SYNAPTIC PLASTICITY COINCIDE WITH DEFICITS IN SPATIAL WORKING MEMORY IN 3xTg-AD MICE	118
Abstract	119
2.1 Introduction	120
2.2 Methods	122
2.3 Results	130

2.4 Discussion	136
References	146
Figures.....	152
3 ALTERATIONS IN SYNAPTIC TRANSMISSION AND SYNAPTIC PLASTICITY IN YOUNG 3xTg-AD MICE	160
Abstract.....	161
3.1 Introduction	162
3.2 Methods.....	164
3.3 Results.....	168
3.4 Discussion	173
References	183
Figures.....	187
4 OPEN FIELD BEHAVIOR IN YOUNG 3xTg-AD MICE.....	194
Abstract.....	195
4.1 Introduction	196
4.2 Methods.....	197
4.3 Results.....	199
4.4 Discussion	201
References	205
Figures.....	206
5 IMPAIRMENTS IN SPATIAL WORKING MEMORY IN A NOVEL MOUSE MODEL OF HIRANO BODY EXPRESSION	207
Abstract.....	208

5.1 Introduction	209
5.2 Methods	212
5.3 Results.....	223
5.4 Discussion	229
References	238
Figures.....	244
6 CONCLUSIONS AND FINAL THOUGHTS	260
6.1 Summary of Experimental Findings	260
6.2 The Big Picture	262
6.3 Where do we go from here?	264
6.4 A Final Thought on the Future of Alzheimer’s Disease Research...	269
References	271
Figures.....	273

CHAPTER 1

INTRODUCTION AND LITERATURE REVIEW

1.1 Historical Perspective

In 1901, Dr. Alois Alzheimer was a German psychiatrist working at *The Hospital for the Mentally Ill and for Epileptics* in Frankfurt, Germany. On November 25th 1901, Auguste Deter was admitted by her husband, and examined by Dr. Alzheimer. She was 51 years old. Her condition was described as being one of reduced comprehension and memory, disorientation, unpredictable behavior, paranoia, and pronounced psychosocial behavior (the general term for dementia at the time). Her husband described her to be delusional, carry items from one place to another hiding objects, and to cry out loudly believing someone was trying to kill her. Over the next four days, Dr. Alzheimer asked her a series of basic questions such as: "What is your name"? "Where you are"? "What is your husband's name"? She knew her first name and age, but could not remember her last name, husband's name, where she was, how long she had been there, where she lived, or what year it was. She was unable to determine what food she was eating, and when shown common recognizable objects, would forget them moments later. When asked to write her name, she could not, as she would forget what was asked of her, all the while repeating the phrase "Ich hab mich verloren" (I have lost myself). Dr. Alzheimer documented his observations, concluding his patient had: a complete disorientation of time and place, memory loss, confusion,

hallucinations, mistrust, and at times, complete helplessness. Over the next several years, Auguste D. became increasingly worse and eventually passed on April 8th 1906. By this time, Dr. Alzheimer had moved to the Royal Psychiatric Clinic in Munich under director Emil Kraepelin, but had continued to follow her case until her death. Upon learning of Auguste's passing a day later, Dr. Alzheimer requested her records and brain be sent to him for further study. Trained in pathology by a former colleague, Franz Nissl, and using a new silver staining technique of the time (Bielschowsky method), Dr. Alzheimer was able to examine sections of Auguste's brain with high contrast. Upon observation, there was profound neurodegeneration estimated at between 25%-30% of the cerebral cortex. There was also the description of two pathological features that would eventually go on to become the hallmarks of Alzheimer's disease:

“Distributed all over the cortex, but especially numerous in the upper layers, there are minute miliary foci which are caused by the deposition of a special substance in the cortex. This substance can be observed without dye, but it is very refractory to dyeing.”

“Inside of a cell which appears to be quite normal, one or several fibrils can be distinguished by their unique thickness and capacity for impregnation.”

These descriptions are referring to the characteristic β -Amyloid plaques and neurofibrillary tangles, respectively. These findings were published the following year in 1907 under the title “Über eine eigenartige Erkankung der Hirnrinde” (About a peculiar disease of the cerebral cortex) [1-3]. That same year, Fischer published a detailed account of the histopathological changes occurring in dementia [4], and the following year in 1908, Bonfiglio reported a similar case in a patient only 60 years old [5]. In 1909 Perusini published a paper consisting of five case studies on dementia [6], the first of which was a re-examination of Auguste D. from Dr. Alzheimer's original case, per Dr.

Alzheimer's request. While senile dementia was known to occur in some individuals of advanced age, this form of dementia was in relatively younger patients, and thus termed "presenile" dementia. It was however, in 1910 that Dr. Kraepelin published the medical textbook "Psychiatrie VIII Auflage" (Psychiatry, 8th edition) in which the eponym "Alzheimer's Disease" was first used as a tribute to his colleague [7]. In 1911, Dr. Alzheimer published his second case study of Alzheimer's disease from patient Johann F. [8]. These events marked the beginning of what would ultimately become the most widely studied memory disorder to date.

1.2 General Overview of Alzheimer's Disease

Alzheimer's disease (AD) is a neurodegenerative disease of aging. It is a global epidemic affecting nearly 35 million individuals worldwide [9]. It is the most common form of dementia in the elderly accounting for more than 50% of all cases [9, 10], and is the second most feared disease in the world after cancer [11]. Approximately 1 in 9 individuals in the United States over the age of 65 have AD [12]. This increases to 1 in 3 individuals over the age of 85 [12]. There is an estimated 4.7 million people currently living in the U.S. with AD, and this number is expected to increase to nearly 14 million by 2050 [12]. Health care costs in the United States alone total more than \$172 billion annually to provide care for these individuals [10]. It is a medical and economic problem that significantly and profoundly decreases the quality of life for both patients and their families.

Alzheimer's disease is present in two forms: a sporadic form (late-onset), and an autosomal dominant familial form (early-onset). While both forms have the same

characteristic pathological features, there are different mechanisms thought to drive each form. As much as 10% of cases occur before the age of 65 (early-onset) and may begin in the late 30's [10]. Signs of AD may vary but most commonly include memory loss, confusion, and disorientation [9]. Despite efforts to understand and treat AD, there is currently no known cure, and treatment options are limited. Progression cannot be stopped or reversed, and can only be minimally slowed, giving patients an additional 2-3 years at best once advanced symptoms begin.

Gross pathology of AD is characterized by cortical atrophy, reductions in hippocampal volume, and dilation of cerebral ventricles (Figure 1.1). Early stages of neurodegeneration begin with a loss of cholinergic input to brain regions important for cognitive function such as the hippocampus [13, 14], followed in late stages by widespread loss of both neurons and glia across multiple brain regions. Estimated brain atrophy in late-stage individuals is between 30%-40% of total cerebral volume [15, 16], and between 25%-40% of total hippocampal volume [17, 18]. Gross anatomical changes in AD can be directly imaged using structural MRI [19] (Figure 1.1C).

Histopathology of AD is characterized by the presence of extracellular accumulations of β -Amyloid plaques and intracellular neurofibrillary tangles of hyperphosphorylated Tau protein [20] (Figure 1.2). The emergence of β -Amyloid plaques begin in the cerebral cortex (stage 1) and progress to the hippocampus (stage 2), and eventually to other regions including the striatum, brainstem, and cerebellum (stage 3), while the emergence of neurofibrillary tangles begins considerably later than β -Amyloid plaques and follows the opposite pattern beginning in the hippocampal region and progressing to the cerebral cortex [20]. The presence of β -Amyloid deposits can be

imaged *in vivo* using the Amyloid binding radioactive tracer Pittsburgh compound B ($[^{11}\text{C}]\text{PiB}$) and Positron Emission Tomography [21] (Figure 1.1B). In addition to β -Amyloid plaques and neurofibrillary tangles, there is sometimes the presence of dense spherical intracellular inclusions called Lewy bodies, or rod shaped intracellular inclusions called Hirano bodies [9]. The onset of AD pathology leads to a series of inflammatory and metabolic events that ultimately result in synaptic loss and energy failure within the brain.

1.2.1 Amyloid Precursor Protein and the production of Amyloid- β

The most prominent pathological feature of AD is the accumulation of Amyloid- β ($\text{A}\beta$) peptides to form extracellular β -Amyloid plaques. $\text{A}\beta$ peptides are cleavage products of Amyloid Precursor Protein (APP) [22], an integral membrane protein concentrated in the synaptic membrane of neurons. APP has several functions including synapse formation, repair, and anterograde axonal transport. Neuronal activity increases the turnover rate of APP and there are two pathways responsible for APP processing: Amyloid producing and non-Amyloid producing (Figure 1.3). Both pathways occur in normal individuals with the non-amyloidogenic pathway being dominant. The non-amyloidogenic pathway involves the cleavage of APP by the membrane protein α -secretase at position 83 from the C-terminus. This produces a soluble $\text{APP}\alpha$ fragment that is released into the extracellular space. The remaining transmembrane C83 fragment is then subsequently cleaved by γ -secretase, a membrane bound complex of enzymes containing Presenilin (PS) 1 or 2, Nicastrin, anterior pharynx defective protein, and Presenilin enhancer 2. Cleavage by γ -secretase produces a small p3 fragment that is also released into the extracellular space, and an

APP intracellular domain (AICD) fragment that is released into the cytoplasm. AICD is known to be translocated to the nucleus upon phosphorylation, and has been implicated in intracellular signaling and gene expression [23, 24].

The amyloidogenic pathway involves the initial cleavage of APP by β -secretase, also known β -site APP cleaving enzyme 1 (BACE-1), at position 99 instead of 83 [25]. This produces a soluble APP β fragment that is released into the extracellular space. The remaining transmembrane C99 fragment is then subsequently cleaved by γ -secretase to produce a small A β peptide fragment that is released into the extracellular space, and an intracellular AICD fragment. A β peptides range in length from 33-49 amino acids with A β 40 and A β 42 being the most common, and both representing the dominant species overproduced in AD [26]. A small portion of A β is also produced intracellularly at both Endoplasmic Reticulum (ER) and Golgi sites, and may be secreted extracellularly [27, 28]. ER products are predominately A β 42, while Golgi products are predominately A β 40. In non-disease individuals, A β fragments are cleared from the extracellular space by astrocytes [29] and microglia [30] by endocytic scavenger receptors [31, 32], or degraded by neuronal and glial surface enzymes such as neprilysin [33, 34]. Astrocytes may also shuttle A β to the perivascular space where it enters systemic circulation and is degraded by liver enzymes [35].

AD individuals show increases in both APP and A β isoforms. Alternative splicing produces four isoforms of APP capable of producing A β peptides with APP695 being the most abundantly expressed followed by APP751, APP770, and APP714 [36-38]. APP751 and APP770 both carry the Kunitz protease inhibitor (KPI) domain which may offer protection against enzymatic degradation [39]. Both neurons and astrocytes

contain multiple isoforms of APP with neurons containing predominately APP695 (~80%), and glial cells containing predominately KPI-APP isoforms (~90%) [40]. The normal ratio of 695:751:770 in cerebral cortex of control individuals is 20:10:1, but decreases to 10:2:1 in the AD brain [36]. On average APP770 shows the largest increase (6.8 fold) followed by APP695 (3.3 fold) and APP751 (1.6 fold). APP variants differentially increase in different cerebral lobes in AD, and the largest increase occurs in the temporal lobe by APP770, increasing 12 fold over control brains, while both APP770 and APP695 increase more than 6 fold in frontal cortex over control brains [36]. KPI-APP variants have been positively correlated with plaque load in spontaneous AD patients, but also in plaques of non-demented controls [41]. In AD, there seems to be two events occurring concurrently, the increased expression of certain APP isoforms, particularly KPI-APP, and the increase in amyloidogenic processing to yield A β peptides. It could be that total APP expression in AD is not significantly different from non-AD individuals, but that mutations in APP influence alternative splicing mechanisms to preferentially produce specific isoforms, which are themselves more prone to amyloidogenic processing [42]. It is unclear if the change in APP expression occurs in both sporadic and familial AD patients to the same degree, or if the increase in KPI-APP in AD is primarily from neurons or glia, although one study does correlate increases in APP695 (non-KPI APP) in dementia patients with neurons, but not glia [43].

Mutations in *APP*, *PS1*, or *PS2* shifts APP processing towards the amyloidogenic pathway leading to an increase in A β production and favors the production of A β 42 [44-52]. Mutations in *APP* generally increase the affinity of β -secretase for APP. Some mutations increase total A β , increasing both A β 40 and A β 42, while others increase

A β 42 only, and significantly change the ratio between A β 42 and A β 40 [26]. There are no known mutations in β -secretase in AD. The mechanism of *PS* mutations is less clear but generally they increase the probability of cleaving the CT fragment in a way that favors A β 42 over A β 40. Most all *PS* mutations increase the A β 42/40 ratio by either increasing A β 42 or decreasing A β 40, or both [26]. Measurement of A β in the cerebral spinal fluid can be used as a biomarker for early detection of AD, and the A β 42/40 ratio has been shown to be a more accurate predictor of AD than total A β 42 [53].

Cell culture studies report A β 42 makes up around 10-18% of the total A β population when expressing wild-type alleles. Cells expressing various mutations of *APP* or *PS* show an increase in A β 42 production of approximately 1.5-2 fold with *APP* mutants [46], and up to 4-4.5 fold with *PS1* [48] or *PS2* [49] mutants. The overproduction and failure to adequately clear A β 42 initiates pathogenicity leading to AD. Soluble A β 42 monomers aggregate into oligomers of 2-14 peptides, of which, dimers, trimers, tetramers, and pentamers have been shown to be highly neurotoxic [54-58] with trimers being the most neurotoxic [56]. As monomer production continues, oligomeric pentamers form into decamers, which serve as nucleators for protofibrillar formation. Increasing molecular strain induces A β 42 protofibrils to undergo structural reconfiguration to a parallel, in-register β -sheet conformation, which allows rapid formation of insoluble A β 42 fibrils, and the addition of new monomers in a staggered unidirectional fashion [58]. In contrast, A β 40 can form oligomers of 200-400 peptides, and is slower to convert to the less toxic fibrillar form than A β 42, but also has a disorganized oligomeric form [59]. In addition, A β 40 oligomers and fibrils both show β -sheet morphology whereas A β 42 oligomers do not. This is attributed to the last two

additional residues that give A β 42 a different secondary structure, and allows A β 42 to form stable, ordered, intermediate oligomeric structures before continuing on to the less toxic fibrillar form [60, 61]. This represents a significant structural and functional difference between A β 40 and A β 42, and thus explains the more toxic nature of A β 42.

The hydrophobic insoluble nature of A β fibrils creates a problem for astrocytes and microglia attempting to clear fibrils from the extracellular space, allowing for the formation of the characteristic β -Amyloid plaques (also referred to as senile plaques or neuritic plaques). The interests by Glenner and Wong to determine the nature of circulating precursors for non-neuronal Amyloid deposits led to the discovery that the core composition of Amyloid deposits in meningeal vessels of AD and Down's syndrome patients (Amyloid angiopathy) was identical to that found in neuritic plaques of AD and Down's syndrome brains (Down's syndrome individuals typically develop AD-like pathology in their 30's due to overexpression of *APP* on chromosome 21) [62-64]. A few years later, it was determined that the core subunit of neuritic plaques was generated from the proteolytic processing of a larger cell-surface molecule (APP), allowing the full identification of the A β peptide as the central core of neuritic plaques in AD [65].

The β -Amyloid plaque is composed predominantly of A β peptides along with a small variety of other non-Amyloid constituents including soluble APP, proteoglycans, inflammatory compounds, ApoE, cholinesterase, and metal ions like Cu⁺², Zn⁺², and Fe^{+3/+2} [66-68]. Plaques are morphologically typed as diffuse, fibrillar, or densely compacted referring to the deposition pattern of A β fibrils, and are accompanied by an invading network of dystrophic neurites (disorganized neural projections occurring at

damaged or necrotic sites), most likely from axonal sprouting, that increase as the plaque matures [69] (Figure 1.2D). The fibrillar forms of both A β 40 and A β 42 have been identified in β -Amyloid plaques from AD patients, with A β 42 present in 100% of plaques and A β 40 present in about 33% of plaques from sporadic AD patients. In diffuse plaques present in early AD, and in AD patients carrying a mutation in *APP*, plaques were almost exclusively A β 42 positive and A β 40 negative [70-72]. Patients carrying *PS1* mutations also show a predominant A β 42 deposition with only a small fraction of plaques positive for A β 40 [72, 73]. In short, A β 42 deposition begins long before A β 40 deposition, and familial AD individuals have a much higher A β 42 deposition than sporadic AD individuals.

1.2.2 Tau protein and the formation of neurofibrillary tangles

The other major pathological feature of AD is the presence of intracellular neurofibrillary tangles of the protein Tau. Tau is abundantly expressed throughout the nervous system in both neurons and oligodendrocytes, and also in the kidneys, lung, and testis [74]. Tau is present in all compartments of the neuron but most concentrated in the axon [75]. There are 12 isoforms of Tau produced through alternative splicing which are characterized by the number of microtubule binding domains present and the number of N-terminal exons included. Tau is a multifunctional protein having multiple binding targets that include enzymes, cytoskeletal elements, signaling molecules, and lipids [74]. Tau itself does not have enzyme activity, but can activate or inhibit enzymes by binding to them [76-78], and also serves as a scaffold for assembly of enzyme complexes [76, 78].

The most well-studied role of Tau is that of a microtubule binding protein. The majority of Tau present in neurons is bound to microtubules in a gradient fashion along the axon with the highest concentrations near the axon terminal [74, 79]. While Tau is thought to promote assembly and stability, Tau-bound microtubules also have the highest turnover rate of any microtubule population [80]. Tau is subject to extensive post-translational modification by many different mechanisms including phosphorylation [81, 82], acetylation [83, 84], cross-linking [85], glycation [86], nitration [87, 88], and ubiquitination [89], just to name a few. Tau activity is highly regulated primarily through phosphorylation of serine/threonine residues. In AD, aberrant signaling causes Tau to become hyperphosphorylated, disrupting its normal physiological roles [90-94]. This leads to the disassociation of Tau from microtubules, and potentially other complexes, and the refolding into an abnormal conformation with high affinity for aggregation [95-97]. This leads to the formation of hyperphosphorylated soluble Tau oligomers that eventually aggregate to form insoluble filaments of neurofibrillary tangles [74] (Figure 1.4).

There are several known mutations in *Tau* that lead to hyperphosphorylation and formation of neurofibrillary tangles, and subsequently promote wide scale neurotoxicity in tauopathic conditions like frontotemporal lobar dementia [98]. But interestingly, there are no known mutations for *Tau* in AD [74]. All aberrant Tau activity in AD is through wild-type Tau that is mediated through aberrant A β signaling.

1.2.3 Apolipoprotein E4

As mentioned previously, astrocytes and microglia are responsible for clearing A β from the extracellular space by internalization and enzymatic degradation [29, 30].

The efficacy of A β clearance by astrocytes may be determined by Apolipoprotein E (ApoE). ApoE is a lipid binding protein primarily responsible for cholesterol transport, but also binds A β [29, 99]. It is produced systemically by many tissues but primarily by the liver, and in the CNS by astrocytes. ApoE has three variants (E2, E3, and E4), with each one imposing a different risk for developing AD. ApoE3 is the most common variant and individuals homozygous for E3 carry a neutral risk of 1. Individuals homozygous for ApoE4 carry the biggest risk with an odds ratio of 14.9, while individuals homozygous for ApoE2 carry the lowest risk with an odds ratio of 0.6, and seem to carry some protection against AD development [100]. ApoE4 mice clear A β less efficiently than either E2 or E3 variants [99], and actually promote A β plaque formation. ApoE4 binds A β with high affinity, promotes fibril formation, and is a component of β -Amyloid plaques [101, 102]. There is some controversy as to whether ApoE is even necessary for A β clearance since cultured astrocytes from ApoE^{-/-} knockouts clear A β with higher efficiency than any ApoE variant, suggesting ApoE4 provides interference to A β clearance [103]. This could occur by either promoting plaque formation, and/or competing for the same LRP-1 receptor on astrocytes, which has been shown to bind and internalize both A β and ApoE4 [104]. ApoE4 is the single largest genetic risk factor for the development of sporadic (late-onset) AD.

1.2.4 Calcium dysregulation and oxidative stress

Calcium dysregulation is another common feature of AD that has widespread and far reaching consequences. Since Ca²⁺ regulates many cellular processes from neurotransmitter release and synaptic plasticity to apoptosis, it is not surprising that an inability to regulate Ca²⁺ homeostasis leads to detrimental effects in neurons. Cytosolic

Ca²⁺ levels are partly regulated by Presenilin, which can act as passive leak channels on internal Ca²⁺ storage sites like ER [105]. Cultured embryonic mouse fibroblasts expressing transfected PS1 mutations specific to AD show increased cytosolic Ca²⁺ leak [105, 106], and cultured fibroblasts from mice carrying a PS1 knockin mutation show a potentiation of ligand-activated transient Ca²⁺ release from ER [107]. There is some evidence this is due to over filling of the ER [107], however this is controversial [108]. In neurons, Ca²⁺ release from the ER is predominately through either the IP₃ receptor (IP₃R), or the Ca²⁺ activated Ryanodine receptor (RyR). Hippocampal neurons from a triple transgenic mouse model of AD (3xTg-AD) carrying mutations in APP, PS1, and Tau, show significantly higher ligand-activated Ca²⁺ release from the ER compared to control mice [109, 110]. 3xTg-AD mice show an increase in IP₃R-mediated Ca²⁺ release that is not a result of increased IP₃R expression [111]. IP₃R activity is mediated by Presenilin through a functional association with the IP₃R, and PS1 and PS2 mutants specific to AD increase IP₃R current and alter gating kinetics [112]. This leads to an increase in resting intracellular Ca²⁺ levels that can be rescued by IP₃R antagonists [113]. Release of Ca²⁺ from IP₃Rs can then activate RyRs. Of the three known RyR isoforms, RyR2 shows nearly a 3 fold increase in mRNA expression in 3xTg-AD mice [109]. Comparatively, medial cortex tissue from human subjects show a significant increase in RyR2 mRNA expression from patients exhibiting mild cognitive impairment, and an increase in RyR3 mRNA expression in patients showing severe cognitive impairment from fully developed AD [114]. Increases in RyR2 mRNA expression from 3xTg-AD mice was shown at approximately 6 weeks of age, and may represent the mild cognitive impairment stage, although behavioral studies of cognition in 3xTg-AD mice at

that age have not been done, nor has evaluation of RyR3 mRNA expression in older animals when AD-like signs are more developed. Presenilins are also functionally associated with RyRs and have been shown to modulate their activity similar to the way they modulate IP₃Rs [115]. Presenilins and RyRs play important roles in regulating intracellular Ca²⁺ homeostasis and mediating synaptic processes such as neurotransmitter release [116, 117]. Transgenic mice carrying only a mutated PS1 knockin show increased IP₃R and RyR-mediated Ca²⁺ release similar to transgenic mice carrying multiple mutant alleles [118, 119]. ER-associated Presenilins carrying mutations specific to AD that function independently of those involved in A β production are most likely responsible for the early disruptions in Ca²⁺ homeostasis observed in AD model mice.

ER Ca²⁺ release is also linked to the control of mitochondrial associated anti- and proapoptotic pathways within specialized signaling microdomains through direct ER-mitochondrial membrane connections [120]. Mutated PS1 [121] and PS2 [122] proteins linked to RyR-dependent Ca²⁺ release sensitizes neurons to Ca²⁺ induced apoptosis through activation of Caspase 12 and 3 respectively. Sustained increases in cytosolic Ca²⁺ can also inhibit α -secretase activity, shifting activity of β -secretase and further increasing production of intracellular A β [123]. A β can form cationic leak channels in lipid membranes and allow influx of Ca²⁺ from extracellular or potentially intracellular Ca²⁺ stores [124]. A β aids in the production of both reactive oxygen and nitrogen species [125] producing oxidative stress in mitochondria. A β can also attack mitochondrial machinery directly, specifically cytochrome C [126] and Amyloid Binding

Alcohol Dehydrogenase (ABAD) [127], and A β accumulation has been found in mitochondria of both transgenic animals [128] and human AD patients [129].

In summary, increases in Ca²⁺ leakage, upregulation of RyRs, and potentiation of IP₃R and RyR current, all lead to a dysregulation of Ca²⁺ homeostasis that can lead to increases in intracellular A β and Ca²⁺ driven mechanisms detrimental to neuronal health such as mitochondrial collapse and Ca²⁺ induced apoptosis.

1.2.5 Hirano bodies and Lewy bodies

In addition to neurofibrillary tangles, there are two other types of inclusions that are sometimes present in AD pathology: Hirano bodies and Lewy bodies. First described by Asao Hirano in 1968 [130], Hirano bodies are rod shaped eosinophilic inclusions found in the brains of patients with several neurological conditions including Alzheimer's disease, Amyotrophic Lateral Sclerosis, Parkinson with dementia, Creutzfeldt-Jakob Disease, and to a much lesser extent, normal aging [130-133]. They are located primarily in the dendrites and cell bodies of hippocampal pyramidal neurons [132, 134] but are also present in glia [135]. Hirano bodies are paracrystalline structures composed predominately of filamentous actin (F-actin) [136, 137], a variety of actin binding proteins [138], microtubule associated proteins [139], and various enzymes, cytokines, and other proteins including Amyloid Precursor Protein Intracellular Domain [140] (AICD, the intracellular cleavage product of APP) and Tau [141]. Hirano bodies are distinguished from other types of actin based inclusions by their ultrastructure [132]. It is unclear what role, if any, Hirano bodies play, or what exactly their influence on cell physiology may be. There is evidence they may be both protective [142] and damaging [143]. The origin of their formation is also unclear.

The other type of inclusion commonly found in the brains of patients with some neurodegenerative conditions is Lewy bodies, discovered by Fritz Lewy in 1912 while working in the lab of Alois Alzheimer [144]. Lewy bodies are spherical shaped eosinophilic structures composed of aggregated α -synuclein, and make up a class of conditions termed α -synucleinopathies [145]. Lewy bodies are most commonly found in Parkinson disease, Parkinson with dementia, dementia with Lewy bodies, multiple system atrophy, and to a lesser extent, Alzheimer's disease [145]. Not all AD cases have Lewy bodies, and when present, they seem to be predominately located in the amygdala [146, 147], although some non-Lewy body α -synuclein inclusions do occur in the hippocampus of some AD patients [146], and α -synuclein is also a component of β -Amyloid plaques [148]. Aggregation of α -synuclein results from post-translational modifications such as phosphorylation [149, 150], nitration [151, 152], and ubiquitination [153], resulting in a misfolding of the α -synuclein protein into insoluble oligomers [154]. Mutations in α -synuclein may increase aberrant post-translational modification [155] and subsequent formation of Lewy bodies, which may contribute to neurotoxicity similar to neurofibrillary tangles.

1.3 General Overview of Learning and Memory

The hallmark sign of AD is cognitive impairment. This includes many aspects of cognition, but most commonly refers to memory loss, confusion, and disorientation that can severely affect problem solving and decision making abilities. Memory is the neural representation of information, and memory formation and function is composed of several steps: encoding (conversion of sensory information into a network

representation of information – the formation of a memory trace), consolidation (conversion of the memory trace from short-term to long-term storage), and retrieval (recall of the memory trace). Stored information of experiences can then be used to influence behavior or complete a specific task or challenge.

Memory is broadly organized into short-term and long-term storage systems. In brief, short-term memory is generally considered to have a time span of a few seconds to a few minutes, is unstable, and decays rapidly. Long-term memory however, is more stable and persistently maintained, and has a time span of a few minutes to decades, or a lifetime. Long-term memory can be divided into procedural (motor memory such as learning to throw a ball), or declarative, which is further divided into semantic (facts and figures) and episodic (autobiographical events relating to what, where, when, and why the events took place). The manipulation and use of short-term and long-term memory is through the cognitive process known as working memory. Working memory utilizes both informational storage and informational processing to perform cognitive tasks. The most currently accepted model of working memory is the Baddeley and Hitch model [156], which incorporates a multicomponent approach to managing complex tasks (Figure 1.5A).

The general idea behind this model proposes that working memory is governed by the central executive. This is the attentional and informational processing component of working memory that manages and oversees the other memory systems when performing multiple tasks simultaneously. When a cognitive task is performed, the central executive directs incoming sensory information, or retrieval of information from long-term memory storage, into several subtypes of short-term memory. Auditory

information is directed into the phonological loop and visual information is directed into the visuo-spatial sketch pad. Information is then loaded from these short-term memory areas into the episodic buffer, and then into the central executive for manipulation and processing of information. Information from long-term memory can also be loaded directly into the episodic buffer before proceeding to the central executive.

The central executive is believed to be located predominately in the prefrontal cortex of the frontal lobe with task specific localization in the dorsolateral [157], ventrolateral [158], and medial prefrontal cortex [159]. Imaging studies indicate both the prefrontal and parietal cortex, along with the medial temporal lobe, to be involved in working memory tasks [160-162], and indicate central executive functions may also be dependent on connections between these areas rather than localized to one specific region (Figure 1.5B). Short-term memory areas are spread over various cortices depending on whether visual or auditory information is being accessed [163]. Long-term memory is also widely distributed throughout the cortex with various components of a particular memory stored in different locations of the cortex pertaining to that specific modality of the memory [164, 165]. Working memory load can influence activation of different memory systems. Simple tasks with a small working memory load (remembering a set of three objects) involve short-term memory systems and are primarily prefrontal and parietal cortex dependent [166]. Increasing working memory load will also increase prefrontal cortex activity, but when working memory load exceeds the capacity of short-term memory systems (remembering more than seven objects for some amount of time while completing a separate unrelated cognitive task such as solving a math problem), long-term memory systems are activated [167, 168]. When

newly processed or incoming sensory information is directed for storage into long-term memory, even if only temporarily, the medial temporal lobe is specifically involved [167, 169]. Long-term memory is a tightly integrated component of working memory and there is considerable communication between the medial temporal lobe and prefrontal cortex [160, 170, 171]. Studies using functional MRI show an increase in prefrontal cortex and medial temporal lobe activity as working memory load increases [170], and studies show the medial prefrontal cortex and medial temporal lobe subserve different functional roles specific to working memory [172].

Medial temporal lobe structures important for memory consolidation include the hippocampal formation and associated parahippocampal cortices: the perirhinal, postrhinal and entorhinal cortices [173-175]. Information from all association cortices enter into the perirhinal and postrhinal cortices and then into the entorhinal cortex. The entorhinal cortex is the main entry point into the hippocampus. The hippocampus is a slightly curved cylindrical structure that runs anterior to posterior along the ventral portion of the medial temporal lobe in humans, but runs dorsal to ventral under the parietal lobe in quadrupeds (Figure 1.6). There are two hippocampi, one in each hemisphere, and each receives and returns information from virtually every sensory modality of the cortex, primarily through the entorhinal cortex (Figure 1.7A). The hippocampus (sometimes referred to as the hippocampal formation) contains three major regions: the dentate gyrus, the hippocampus proper, and the subiculum (Figure 1.7C & D). The dentate gyrus and the hippocampus proper each form a layer of densely packed excitatory neurons, and during development, each layer folds over on the other resulting in two curved interlocking layers. Neurons of the dentate gyrus are

granule cells and neurons of the hippocampus proper are pyramidal cells. The hippocampus proper contains three subregions designated CA1, CA2 and CA3, after *Cornu Ammonis* (ram's horn). The subiculum is the main exit point for information out of the hippocampus.

There are multiple entry and exit pathways of the hippocampus and a complete description is beyond the scope of this review, so only the relevant perforant, Mossy, and Schaffer pathways will be discussed here. The perforant pathway is the first of a trisynaptic circuit comprising the pyramidal cells of the entorhinal cortex, granule cells of the dentate gyrus, and pyramidal cells of CA3 and CA1 [176] (Figure 1.7D). Information coming in from the entorhinal cortex synapse on granule cell dendrites (EC→DG), granule cell axons (Mossy fibers) synapse on CA3 dendrites (DG→CA3), and CA3 axons (Schaffer collaterals) complete the circuit by synapsing on CA1 dendrites (CA3→CA1). CA1 axons synapse on subiculum pyramidal neurons which project to multiple regions including the perirhinal, entorhinal, parietal, and prefrontal cortices, and hypothalamus [177], or synapse directly with entorhinal cortex to complete a trisynaptic circuit loop [176]. All synapses in the trisynaptic circuit are excitatory glutamatergic synapses and activity within the circuit is regulated by a complex integration of GABAergic interneurons and modulatory input from cholinergic (medial septum) [178, 179], serotonergic (raphe nuclei) [180], dopaminergic (ventral tegmentum) [181], adrenergic (locus coeruleus) [182], and histaminergic [183] neurons. Other notable connections from the hippocampus occur through the fornix and include the mammillothalamic tract (mammillary bodies to anterior thalamic nuclei), cingulate gyrus,

and lateral septal nuclei. In short, the hippocampus receives input and projects output to multiple brain regions and is involved in many different cognitive processes.

In addition to the synaptic sequence described above, the entorhinal cortex also has direct input to CA3, CA1 and subiculum [173, 175]. CA3 serves as the pacemaker of the trisynaptic circuit and contains recurrent collateral feedback to itself, and is the key regulation point for consolidation of memory from short-term to long-term [184-187]. CA3 and CA1 work together to support different aspects of memory and lesions specific to CA3 or CA1 produce specific deficits in memory acquisition and consolidation [188-193]. For example, in associative learning tasks with spatial and temporal elements, CA3 contributes predominately to spatial coding while CA1 contributes to temporal elements [190, 193]. The greater the temporal load (holding information over some period of time), the greater importance of CA1 activity [191]. Importantly, both CA1 and subiculum have unidirectional, monosynaptic projections directly to the prefrontal cortex [194-196] (Figure 1.7B). Hippocampal and medial prefrontal cortex activity show coordinated phase-lock theta rhythms during working memory tasks involving exploratory spatial navigation [197]. The hippocampus also plays a role in retrieval of long-term (remote) memory and CA3 is specifically associated with retrieval precision [198], although evidence suggests that the hippocampus is not essential for retrieval of certain parts of remote memories [166]. One of the most famous patients in cognitive neuroscience history was Henry Molaison (H.M.), who underwent a double hippocampalectomy (and portions of the entorhinal cortex) in 1953 to relieve epileptic seizures [166]. The surgery was successful in controlling seizures, but afterwards H.M. developed severe anterograde amnesia and was unable to form new long-term explicit

memories. Despite this however, H.M. could still perform short-term memory tasks normally, and had intact procedural learning, despite not remembering performing or learning these tasks. H.M. was also able to recall fragments of remote memories prior to hippocampal removal, and the older the memory, the more complete the recall. Thus, the hippocampus may be the primary route for memory retrieval, but if damaged or absent, alternative pathways seem to exist. The hippocampus is however, essential in the formation of new explicit memories.

The hippocampus is not a storage site for memory *per se*, but rather a memory processing point for transition of a memory trace from short-term to long-term. The general idea is that short-term working memory traces route through the hippocampus, and if a particular trace is to be stored as a long-term memory, most likely influenced by extrahippocampal modulatory input, the hippocampus has the ability to modify the trace output in a way that allows for permanent storage within the cerebral cortex of the information the trace represents. A permanently stored trace is termed an engram. Once an engram is formed, the hippocampus may continue to modify and refine the engram for months to years [199].

1.4 Memory and Synaptic Plasticity

The cellular mechanism behind memory consolidation is thought to involve modification of the neural circuitry involved in the processing of an experience. Attention to an experience in the form of rehearsal, emotion, context, and state-dependent conditions can increase the probability that an experience will be committed to memory. These attentional modifiers can influence the activity of a memory trace,

thereby causing a change in the strength of the trace. It is believed that these changes occur at the synaptic level. The idea that a change in synaptic efficacy could lead to a learning process was first suggested by Ramon Y. Cajal in 1894 [200]. A more formal description of this idea came from Donald Hebb in “The Organization of Behavior” in 1949 [201], and has since been known as Hebbian learning. The ability of synapses to undergo changes in synaptic efficacy is known as synaptic plasticity.

Hebbian learning, also known as associative learning, predicts that spike-timing dependent plasticity induces changes in the strength of connection between synapses resulting in experience-dependent learning [202]. The early work of Eric Kandel demonstrated that changes in synaptic efficacy corresponds to changes in behavior (i.e., learning). Taking a reductionist approach, Kandel used the sea slug *Aplysia californica*, which has a simple nervous system, large neurons easily accessible to electrophysiological measurements, and responds well to behavioral modification. *Aplysia* has a water intake siphon that when tactilely stimulated, will produce a gill withdrawal reflex. Sensory neurons connected to the siphon are directly connected to motor neurons of the gill withdrawal muscles. When the siphon is repeatedly stimulated, the gill withdrawal reflex time will become longer, showing habituation. Simultaneous intracellular recordings from presynaptic sensory neurons and postsynaptic motor neurons demonstrated a reduction in the Excitatory Post-Synaptic Potential (EPSP) in the postsynaptic motor neuron during habituation of the gill withdrawal reflex [203]. Thus, habituation of the gill withdrawal reflex is due to a depression of synaptic efficacy.

Administration of a brief tail shock prior to siphon stimulation produces a sensitization and enhancement of the gill withdrawal reflex due to presynaptic facilitation of neurotransmitter release, resulting in an increase in the EPSP of the postsynaptic motor neuron [204]. Sensitization lasts approximately 15 min. Demonstration of Hebbian type associative learning by repeatedly pairing the gill withdrawal reflex with a tail shock will produce an enhanced gill withdrawal reflex that now last for several days [205, 206]. The motor neuron now shows a persistent increase in the EPSP in response to the activation of the presynaptic neuron during tactile stimulation of the siphon only [207]. This occurs through activation of serotonergic neurons in the tail that synapse on both the presynaptic sensory neuron of the siphon and the postsynaptic motor neuron of the gill withdrawal muscles. Serotonin enhances synaptic efficacy by persistent facilitation of neurotransmitter release through G-protein activated signaling mechanisms involving PKA, PKC, and CREB [208, 209].

Examples of changes in synaptic efficacy associated with learned behavior in mammals is best seen in studies of cued fear conditioning. This type of Hebbian learning associates a conditioned stimulus (such as an auditory tone) with some form of punishment (such as a footshock). This form of fear memory is strongly associated with the amygdala, the emotional learning and memory center, which also has strong connections with the hippocampus [210-212]. Auditory associated fibers from the medial geniculate nucleus of the thalamus synapse with neurons of the lateral amygdala. Field Excitatory Post-Synaptic Potentials (fEPSP) in the lateral amygdala occur in response to an auditory tone. When the tone is paired with a footshock, the animal learns to associate the sound of the tone with an unpleasant experience,

producing a conditioned fear response. The tone (fear cue) now evokes an increased fEPSP in the lateral amygdala [213]. When the paired association is extinguished, the fEPSP returns to baseline amplitude. Increased fEPSPs in the hippocampus have also been observed using inhibitory avoidance learning that pairs a foot shock with a location or condition, such as entering a particular room, and can be observed after only one trial of associative training [214].

As mentioned previously, increases in working memory load and activation of long-term memory mechanisms involve activation of hippocampal circuitry. Much attention has been devoted to studying synaptic plasticity in the hippocampus as it relates to memory, in particular spatial memory. Spatial navigation is a hippocampal dependent process making it ideal for the study of spatial memory. Rats trained in the Morris Water Maze (MWM) task, in which animals use visual cues to navigate to a hidden platform under the surface in a pool of water, show hippocampal dependent navigation [215-217] and lesioning of hippocampal areas produce deficits in spatial navigation and spatial reference memory [184-187, 190, 215, 216]. A functional MRI study shows activation of hippocampal activity during virtual reality navigation in humans [218]. Place cells in the hippocampus (location specific) [219, 220] and grid cells in the entorhinal cortex (positional orientation) [221] work together to create a cognitive map that allows successful navigation through an area. It is estimated that approximately 80% of CA3 and CA1 pyramidal neurons participate in place specific processing [222].

Direct measurement of changes in synaptic efficacy in the hippocampus in the awake behaving animal during a spatial navigation task has been difficult due to

technical challenges in collecting such data. The hippocampal network is also significantly more complex than what is observed in *Aplysia*, or even the medial geniculate-amygdala pathway. There are multiple synaptic check points that have the potential to be modified and the change in synaptic weights throughout a specific network are likely to play a role in the encoding, consolidation, and maintenance of a memory trace. There are however, several lines of evidence that support synaptic plasticity in the hippocampus as necessary for learning and memory.

If changes in synaptic efficacy are reflective of learning and memory, then there should be a measurable difference in synaptic efficacy after behavioral training. Indeed, rats exposed to spatially complex novel environments show an increase in fEPSP and population spike amplitude in the dentate gyrus compared to non-exposed controls [223]. The same observation occurs in rats after explorative learning in the MWM task and last for approximately 20 minutes [224]. Based on these observations, one can reasonably conclude that altering the ability of synapses to undergo changes in synaptic efficacy should impact learning and memory. It is hypothesized that variable patterns of synaptic weights throughout a network pertain to specific learning experiences [225]. Preventing synapses within a network from regulating variability in synaptic weights by artificially inducing a maximal increase in signal potentiation should produce a saturation effect, thereby interfering with learning. When perforant fibers (EC→DG) are tetanized with high frequency stimulation from bilaterally implanted electrodes to produce a persistent increase in fEPSPs in the dentate gyrus, a profound deficit in learning spatial information necessary to complete the Barnes maze is observed [226]. This finding was duplicated in the MWM as well [227]. Neither study had any effect on

already learned information, indicating this specifically disrupted the acquisition of new information. In the MWM, learning capability returned after the decay of potentiated fEPSPs back to baseline levels, which took approximately 1 hour [227]. In addition, a later study which took a similar approach using implanted electrodes for tetanic stimulation of the angular bundle perforant pathway to saturate the postsynaptic response in all hippocampal regions (DG, CA1, CA3, and subiculum) before MWM testing, was able to later determine the degree of saturation by measuring the amount of residual synaptic potentiation left over after MWM testing by administering an additional tetanic stimulation [228]. Performance in the MWM correlated to the amount of residual synaptic potentiation showing animals with the largest amounts of residual potentiation (least amount of initial saturation, i.e., greater potential for changes in synaptic efficacy) were the best performers, and animals with the lowest amounts of residual potentiation were the worst performers. Lastly, studies using the MWM show that age-related impairments in spatial long-term memory is significantly correlated with reductions in hippocampal synaptic potentiation in CA1 pyramidal neurons [229]. Thus, animals with the greatest potential to modulate changes in synaptic efficacy show the highest acquisition of spatial learning and memory.

1.5 Cellular Mechanisms of Synaptic Plasticity

The mechanisms by which changes in synaptic efficacy occur have been an area of intense research for over 50 years. Synaptic plasticity is the ability of neurons to change their strength of connection at the synapse. These changes can be short-term or long-term, and both presynaptic and postsynaptic neurons participate in synaptic

plasticity. The changes described for *Aplysia* are predominately presynaptic. In mammals, changes in long-term synaptic efficacy are predominately a postsynaptic mechanism involving changes in postsynaptic receptor density [230], although some presynaptic mechanisms that produce long-term facilitation of neurotransmitter release in specialized populations of CNS neurons, such as pyramidal neurons of the cerebral cortex and CA3 subregion of the hippocampus, have been described [231]. This review will focus on synaptic plasticity in mammals.

Short-term synaptic plasticity is typically a presynaptic event and usually involves the facilitation or depression of neurotransmitter release [232]. Synaptic efficacy changes over time in response to the recent history of the neuronal firing pattern. Early studies of axons at the neuromuscular junction demonstrated an increase in the EPSP of muscle cells upon repeated stimulations of presynaptic axons [233]. EPSPs will continue to increase with successive stimulations until a plateau is reached, which will be maintained until neurotransmitter is depleted. The mechanism behind short-term facilitation involves residual Ca^{2+} left over from the previous stimulation, that when combined with incoming Ca^{2+} from current stimulations, results in higher cytosolic Ca^{2+} and an increase in neurotransmitter release probability [232]. Whole cell recordings in presynaptic neurons with the addition of an intracellular photolabile Ca^{2+} chelater prevents both facilitation of neurotransmitter release and increases in EPSPs in the postsynaptic cell [234].

Short-term plasticity occurs very rapidly ($< 10\text{ms}$) and can modulate synaptic efficacy nearly instantaneously. Sustained external stimuli can modify network dynamics through short-term plasticity mechanisms. Transient external stimuli can also

modify network dynamics by prolongation of the neural signal through recurrent interactions between neurons within a circuit. Neurons that make up a circuit loop, or neurons within a specific region of a circuit (CA3 for example), that contain an autosynapse (axonal collaterals that synapse back on themselves) create a positive feedback loop sustaining neuronal activity by persistent recurrent firing within a group of neurons after the external stimuli has stopped, and are subject to short-term plasticity mechanisms that influence the recurrent signal and can modify network dynamics [235, 236]. This stimulus induced residual activity is thought to serve as the neural substrate for short-term information storage and represents our best and most current hypothesis for the short-term memory trace [237, 238].

Long-term synaptic plasticity is predominately a postsynaptic event leading to a Long-Term Potentiation (LTP) or Long-Term Depression (LTD) of synaptic strength [230]. In 1966, Terje Lømo began a PhD in the laboratory of Per Anderson at the University of Oslo in Norway. He was studying perforant pathway activation in the hippocampus of anaesthetized rabbits by stimulating the perforant pathway and measuring subsequent fEPSPs in the dendritic field of the dentate gyrus (EC→DG, synapse 1 of the trisynaptic circuit) [239]. It was during that time when he observed brief high stimulus trains (tetanus) delivered to the perforant fibers resulted in an increase in the synaptic efficacy of single pulse responses in the dentate gyrus that were stable for several hours [240]. Two years later in 1968, Tim Bliss joined the lab and together they published a more thorough account of Lømo's previous findings in what is now considered to be the primary reference for LTP [241]. Shortly after, LTP was demonstrated at every synapse in the trisynaptic circuit (EC→DG→CA3→CA1) for

both rat [242, 243] and mouse [244-246]. While other regions such as cortex, cerebellum, and amygdala all show the ability to modify synaptic efficacy, the hippocampus has become the standard model for studying synaptic plasticity and LTP, and much of what the field has learned about LTP has come from studies of *ex vivo* hippocampal slice preparations [230] (Figure 1.8).

1.5.1 Molecular mechanisms of NMDA receptor-dependent long-term potentiation

Long-term synaptic plasticity is an adaptation of synaptic efficacy based on the previous history of neuronal activity. The induction, expression, and maintenance of LTP at excitatory glutamatergic synapses depends on different underlying molecular mechanisms. Fast excitatory glutamatergic transmission results from activation of the postsynaptic α -amino-3-hydroxy-5-methyl-4-isoxazole-propionic acid (AMPA) receptor, and by itself is not sufficient to induce LTP. When a sufficient increase in presynaptic activation frequency occurs, a facilitation in neurotransmitter release (a short-term plasticity mechanism) results in a temporary increase in AMPA receptor activation and sustained depolarization of the postsynaptic membrane, allowing the activation of the postsynaptic N-methyl-D-aspartate (NMDA) receptor [247-249]. Both AMPA and NMDA receptors are ligand-gated ionotropic glutamate receptors permeable to cations with the NMDA receptor being highly permeable to Ca^{2+} ions [250, 251]. The NMDA receptor also contains a Mg^{2+} block in its ion pore and is not activated at subthreshold depolarizations. Only under conditions sufficient to depolarize the membrane enough to remove the Mg^{2+} block does the NMDA receptor activate and allow the influx of Ca^{2+} leading to a series of Ca^{2+} mediated processes responsible for the persistent expression of postsynaptic LTP [249, 252-256].

Activation of the NMDA receptor is sufficient for the induction of LTP, but in a synapse specific manner. Cortical pyramidal neurons, and hippocampal dentate granule and CA1 pyramidal neurons all show NMDA receptor-dependent LTP [230, 257, 258], however CA3 neurons at mossy fiber synapses do not, and are instead dependent on both presynaptic and postsynaptic kainate receptors for LTP induction [259-261]. Blockage of the NMDA receptor with the competitive antagonist 2-Amino-5-phosphonovalerate (APV) during the induction phase prevents LTP expression in cortical, granule and CA1 neurons [247, 257, 262], and has no effect on synaptic transmission before or after tetanizing stimulations [262, 263]. Induction of LTP in Mossy fiber CA3 neurons is unaffected by APV, and is instead blocked by the kainate specific antagonist LY382884 [259, 261]. The following is a brief description of the general mechanisms of NMDA receptor-dependent LTP.

Induction

Induction occurs from a transient facilitation of glutamate release and a transient increase in postsynaptic intracellular Ca^{2+} concentration [230]. The transient increase in postsynaptic Ca^{2+} during the induction phase is a necessary and sufficient mediator of LTP in hippocampal CA1 pyramidal cells [254] and blocking Ca^{2+} with Ca^{2+} chelators prevents LTP [254, 264, 265]. In hippocampal slice preparations it takes at least 1 sec, but not more than 2.5 sec, of increased Ca^{2+} concentration to induce LTP regardless of induction time, which can be significantly less [265]. When sufficient increases in intracellular Ca^{2+} concentration occur, Ca^{2+} binds calmodulin (Ca^{2+}/CaM), which in turn binds to and activates Calcium/Calmodulin-dependent Protein Kinase Type II (CaMKII), a serine/threonine protein kinase [266, 267]. Injection of CaMKII into hippocampal CA1

pyramidal cells [268], or viral transduction of constitutively active CaMKII to hippocampal slices [269], produces an increase in EPSPs that cannot be further potentiated with tetanus, nor does further potentiation result if tetanus induced LTP occurs first [268]. $\text{Ca}^{2+}/\text{CaM}$ induces potentiated EPSPs in hippocampal CA1 pyramidal cells through activation of CaMKII that are identical to potentiated EPSPs from tetanus induced LTP [268]. As with tetanus induced LTP, activation of CaMKII is synapse specific [270], but is also involved in synaptic tag and capture [271], a phenomenon by which induction of LTP at one synapse can sensitize surrounding synapses to induction. If $\text{Ca}^{2+}/\text{CaM}$ or CaMKII activity is blocked using Ca^{2+} chelators [254, 264, 265] or specific kinase inhibitors [266, 272-274], or in mutant mice lacking functional CaMKII [275, 276], LTP and spatial learning are severely impaired.

Expression

Activation of CaMKII initiates the expression of LTP. Studies of hippocampal slice preparations organize LTP expression into 3 stages. Stage 1 is composed of 3 parts and begins with post-tetanic potentiation (PTP) and last seconds to minutes, followed by short-term potentiation (STP) lasting approximately 30 min, and ends with early LTP (E-LTP) which typically last 1 hour post-induction. Intermediate and Late-LTP (L-LTP) is composed of stages 2 and 3 and are maintenance stages involving new protein synthesis from preexisting mRNA transcripts (stage 2) and transcription of new mRNA (stage 3).

Immediately following induction, a sharp rise in the EPSP can be observed due to the temporary facilitation of neurotransmitter release from the presynaptic neuron. High frequency tetanic stimulation increases presynaptic Ca^{2+} concentration in the

synaptic end bulb sufficient to bind calmodulin which initiates myosin light chain kinase (MLCK) to interact with myosin II, driving translocation of neurotransmitter vesicles from the slow releasing pool to the fast releasing pool, effectively increasing the size of the fast releasing Ready Releasable Pool, and thus facilitating the temporary increase in neurotransmitter release and PTP [277]

In the postsynaptic neuron, a sufficient rise in $\text{Ca}^{2+}/\text{CaM}$ drives CaMKII to become autophosphorylating at Thr286 on the α subunit [278], and Thr287 on the β subunit [279], and depending on the phosphorylation state of other sites (Thr305/306), can initiate either LTP or LTD [280]. Thr286 seems to be specifically associated with learning and memory and mutations at this location produce deficits in LTP and spatial learning without affecting other $\text{Ca}^{2+}/\text{CaM}$ dependent functions [278, 281]. When activated, CaMKII dissociates from F-actin and translocates from the cytosol to the postsynaptic density (PSD) by way of microtubule associated mechanisms [267, 282, 283]. Translocation efficiency is dependent on the expression ratio of α to β isoforms and dissociation from F-actin increases its own affinity to $\text{Ca}^{2+}/\text{CaM}$, thereby promoting and prolonging localization to the PSD [283].

Translocation of CaMKII into the PSD forms a CaMKII/NMDA receptor complex [267, 284, 285]. CaMKII binds both the NR2A and NR2B subunits of the NMDA receptor, but has a high affinity for the NR2B subunit [286, 287] that is regulated by the phosphorylation state of Ser1303 of the NR2B subunit [288]. The binding of CaMKII to NMDA receptors locks CaMKII into the active state by potentially configuring Thr286 into the catalytic site of neighboring subunits and effectively shielding it from phosphatase activity [286, 289]. The binding of CaMKII to NMDA receptors produce

CaMKII clusters that strategically localize CaMKII within NMDA receptor-mediated Ca^{2+} microdomains that further enhance CaMKII activity [290].

This configuration localizes CaMKII in close proximity to synaptic AMPA receptors and provides a mechanism for CaMKII phosphorylation of individual receptors. There are multiple phosphorylation sites located on the C-terminal tail of the GluR1 subunit. CaMKII phosphorylates AMPA receptors at Ser831 of the GluR1 subunit [291, 292] producing an increase in the unitary conductance by lowering the activation energy required for opening, and also increasing the frequency of opening [293, 294]. Phosphorylation of Ser831 correlates with autophosphorylation of CaMKII and is blocked by CaMKII inhibitors such as KN-62 [291].

Transient increases in postsynaptic Ca^{2+} from LTP induction induces lateral diffusion of extrasynaptic AMPA receptors into the synaptic field and upregulation of AMPA receptor density [295]. Real-time imaging of surface AMPA receptor dynamics using single molecule fluorescence microscopy (quantum dot coupling to AMPA receptor antibodies) show AMPA receptors in the extrasynaptic membrane undergo freely moving fast and slow lateral diffusion through what appears to be Brownian motion, while AMPA receptors within the synaptic field are more stationary [296, 297]. NMDA receptor-dependent synaptic activity induces a transient increase in AMPA receptor mobility followed by rapid incorporation and immobilization of extrasynaptic AMPA receptors into the synaptic field [298-300], presumably by rapid Ca^{2+} dependent phosphorylation events that promote trapping within the PSD. The AMPA receptor auxiliary subunit stargazin is a transmembrane AMPA receptor regulatory protein (TARP) associated with the GluR1 subunit, and is the major regulator of membrane

trafficking for AMPA receptors [301-308]. Phosphorylation of the C-terminal PDZ binding domain of stargazin by either CaMKII or PKC [305] promotes incorporation of AMPA receptors into the synaptic field by interaction of stargazin with PSD-95, thereby stabilizing and anchoring AMPA receptors within the PSD [301-303, 307].

Phosphorylation of the AMPA receptor GluR1 subunit at Ser818 and Thr840 by PKC also influences incorporation into the synaptic field [309, 310]. PKC also phosphorylates Ser831 on GluR1, the same as CaMKII [294, 311], changing receptor kinetics. It is unclear whether phosphorylation of Ser831 by either CaMKII or PKC occurs before or after movement of AMPA receptors into the synaptic field, and may represent a separate step from the initial fast phosphorylation of Ser831 by the CaMKII/NMDA complex. Stargazin has also been shown to regulate AMPA receptor kinetics by increasing channel opening rate [304, 306, 312].

Induction of LTP also promotes insertion of intracellular AMPA receptors into the extrasynaptic membrane through exocytosis of AMPA receptor containing endosomes [295]. This replenishes the extrasynaptic receptor pool and allows additional receptors to further incorporate into the synaptic field. There are numerous studies indicating this process is regulated by phosphorylation of Ser845 on the C-terminal tail of the GluR1 subunit by PKA [313-315]. The C-terminal of the GluR1 subunit is also associated with synaptic associated protein 97 (SAP97), which anchors AMPA receptors (AMPA receptor containing endosomes) to the actin cytoskeleton [316, 317]. Phosphorylation of GluR1 by PKA [313-315] and SAP97 by CaMKII [317, 318] initiates trafficking of AMPA receptor containing endosomes to the extrasynaptic membrane utilizing the actin motor protein myosin VI through a SAP97/myosin VI complex [319] where it docks with

the extrasynaptic membrane at perisynaptic exocytic zones through SNARE-mediated fusion [299].

Fast upregulation of AMPA receptors into the extrasynaptic membrane or synaptic field are primarily GluR1 containing receptors. AMPA receptors occur as heteromeric tetramers typically consisting of homomeric dimer dimers from four possible subunit isoforms (GluR1-4), and most commonly occur as GluR1/2 or GluR2/3 heteromers. GluR1 containing receptors are responsible for fast upregulation in response to LTP induction, while GluR2/3 receptors are typically for maintenance of existing AMPA receptors and are responsible for the normal cycling of AMPA receptors into and out of the synaptic membrane [320]. Thus, after upregulation of GluR1 containing subunits as a result of synaptic plasticity, GluR1 containing receptors are gradually switched out for GluR2/3 receptors [321]. Each subunit has its own set of regulatory proteins that contribute to the trafficking and diffusion of AMPA receptors into and out of the synaptic field. When regulatory proteins for GluR1 (4.1N/G, SAP97, AKAP150/79) and GluR2 (NSF/AP2, GRIP/ABP, PICK1) are both present, such as in GluR1/2 receptors, GluR1 regulatory mechanisms take dominance over GluR2 [320, 322]. The regulatory proteins associated with each subunit bind to the C-terminal tail, and the GluR2 subunit exists in an alternative splice variant with either a short or long C-terminal tail. It is possible that fast acting GluR1/2 receptors contain the long C-terminal tail, while the GluR2/3 receptors contain the short C-terminal tail, owing to the GluR1 dominance in GluR1/2 receptors.

Maintenance

Maintenance of LTP involves the persistent enhancement of synaptic efficacy through activation of proteins that serve as a molecular switch from E-LTP to L-LTP. Intermediate (stage 2, hours 2-3) and L-LTP (stage 3, > 3 hours) involves protein synthesis and production of new AMPA receptors along with a variety of other proteins important for dendritic spine enhancement. Sustained activation of kinases such as PKA and PKC during E-LTP leads to activation of MAPKs such as ERK1/2, which activate Mnk1, which activate eIF4E/G forming an eIF4E,G/4A/Mnk1 complex that initiates translation of preexisting mRNAs (CaMKII, PKC, PSD-95, F-actin, etc...) located within the dendrites [323-326]. This leads to remodeling and enhancement of the PSD and actin cytoskeleton resulting in spine enlargement, or in some cases splitting to form perforated spines, that results in multiple synaptic contacts [327-329]. Both GluR1 and GluR2 subunit mRNA is also found localized within dendrites indicating AMPA receptors can also be synthesized at dendritic locations [330]. All necessary organelles for protein production are present within the dendrites including ribosomes, dendritic extensions of ER, and Golgi outposts that allow AMPA receptors and other membrane bound proteins to be synthesized and packaged into endosomes and transported to spines along dendritic microtubules using dynein and kinesin motor proteins [329, 331, 332].

NMDA receptor density is also upregulated during the maintenance phase of LTP to maintain the correct AMPA/NMDA receptor ratio. The rapid change in receptor ratio observed after induction and during E-LTP is temporary and NMDA receptor potentiation is delayed by approximately 2 hours in cortical pyramidal neurons from both

slice and culture studies [333]. There is some work that challenges the timing of NMDA receptor trafficking, showing a more rapid increase in adult CA1 neurons [334], but the overwhelming majority of literature concludes NMDA receptor trafficking occurs with a substantial delay, if at all, compared to AMPA receptors [335]. NMDA receptors are heteromeric tetramers similar to AMPA receptors and exist as a homomeric NR1 dimer with a homo- or heteromeric NR2(A-D) dimer. NMDA receptor trafficking is driven by the NR2 subunit owing to its long cytoplasmic tail with binding sites for multiple regulatory proteins [336]. The general hypothesis is that NR2B containing receptors are mostly extrasynaptic and are responsible for incorporation of new NMDA receptors into the synaptic field which are then replaced with the more stable NR2A containing receptors [337, 338]. Transgenic mice with overexpression of the NR2B subunit show enhanced LTP in hippocampus and increased learning and memory in the MWM [339]. NMDA receptor trafficking has not received the same attention as AMPA receptor trafficking, and literature on the exact mechanisms are somewhat fragmented. The process seems to be regulated, at least in part, by mGluR1/5 activation [340, 341] and the interaction of CaMKII, PKC and MAPK signaling pathways [342-344].

The final stage of LTP involves transcription of new gene products (stage 3). There are multiple pathways that can lead to plasticity induced transcription with most of them converging on the activation of the transcription factor CREB (cAMP Response Element Binding protein) [345]. Activation of CREB in neurons occurs through a variety of Ca²⁺ mediated pathways, most notably Ca²⁺/CaM activation of CaMKIV [346] and Adenylate cyclase [347], which induces cAMP activation of PKA [348]. CaMKII also activates CREB and has been shown to function as both a positive and negative

regulator through phosphorylation at an additional site [346], as opposed to negative regulation through phosphatase activity utilizing the more well-known Calcineurin/PP1 or ATF4 pathway [345, 349]. Modulatory neurotransmitter systems also influence transcription through activation of MAPK signaling pathways and are themselves influenced by PKA interaction with ERKs for translocation of ERKs to the nucleus (TrkB/EGF/EphB2 receptor activation → SOS → RAS/RAF → MEK → ERK1/2 → RSK → CREB) [345, 350, 351]. Phosphorylation of CREB by either CaMKII [346], CaMKIV [346], PKA [352], or RSK [353] at Ser133 relieves CREB inhibition allowing recruitment of CREB binding protein (CBP) and transcriptional activation of immediate early genes such as *zif268*, *Arc*, *c-fos*, *BDNF*, and *C/EBPs* (CCAAT Enhancer Binding Protein) [345]. Some immediate early genes are themselves transcription factors that activate transcription of late response genes for various other associated synaptic physiology proteins [345]. Transcribed mRNA important for synaptic enhancement is either translated within the soma for axonal-somatic synapses, or packaged into mRNA containing granules and transported into dendrites along microtubules using the kinesin motor protein KIF5 [329, 354], or actin filaments via the Myosin Va motor protein [355], for local translation near dendritic spines. This process is activity dependent and glutamatergic signaling has been shown to promote bidirectional modulation and clustering of *Arc* and AMPA receptor mRNAs at synaptic sites in cultured hippocampal neurons [356-358].

Inhibition of translation or transcription show profound effects on LTP and learning and memory. Recordings of fEPSPs in hippocampal slices that have been microdissected to disconnect CA1 dendrites from the soma show normal STP and E-

LTP, then begin to decay 2-3 hours post-tetanus compared to intact hippocampal slices, which show robust L-LTP for at least 10 hours post-tetanus. When protein synthesis inhibitors are applied, LTP begins to decay approximately 1 hour post-tetanus [359, 360]. This demonstrates not only that persistence of LTP past the E-LTP stage is reliant upon translation of local preexisting dendritic mRNAs, but also that continued persistence beyond 3 hours post-tetanus is dependent on transcription and continued translation of new gene products. Blocking translation of Arc mRNA in the hippocampus of awake behaving animals with infused anti-sense oligomers impairs long-term memory in a spatial reference task using the MWM while leaving short-term memory and task acquisition unaffected. Maze performance coincides with the impairment of L-LTP *in vivo* of behaviorally naive awake animals [361]. CREB mutant mice with targeted disruptions in several CREB isoforms show profound impairments in long-term memory performance in the MWM and fear conditioning that coincides with the absence of L-LTP, while short-term memory performance and STP and E-LTP remain intact [362]. Mutant mice of the CREB downstream immediate early gene *zif268* have impaired long-term memory, impaired spatial representation, and impaired L-LTP, although studies indicate this deficiency may be partially overcome with rehearsal training [363, 364].

Until recently, a constitutively active isoform of PKC known as PKM ζ was thought to serve as a master molecular switch for consolidation and maintenance of long-term memory. Mice given an inhibitor of PKM ζ known as ZIP (Zeta Inhibitory Peptide), show profound deficits in learning and memory and L-LTP [365]. Not only that, ZIP has the ability to reverse established L-LTP in hippocampal slices up to 5 hours post-tetanus

[366], and erase recently formed memories up to a month later [367]. This prompted many articles exploring the nature of ZIP and PKM ζ . That all changed in 2013 when two different groups produced PKM ζ knockout mice that showed normal learning and memory and L-LTP [368, 369]. When ZIP is given to PKM ζ KOs, they display the same impairments in learning and LTP as wild-type mice, even erasure of recently formed memories [369]. This suggests ZIP is acting outside of PKM ζ inhibition and efforts to determine exactly which molecules and processes ZIP is acting on is an active area of intense research. Despite the elusiveness of the ZIP target, this does not diminish the fact that LTP is still representative of stored information, and the erasure of LTP results in the erasure of associated information.

1.6 NMDA Receptors in Complex Learning and Memory

As discussed previously, LTP is associated with increases in cognitive performance. Blocking NMDA receptors to prevent LTP in brain regions important for cognitive function impairs behavioral performance in LTP dependent tasks. Intracerebral ventricular (i.c.v.) or intrahippocampal infusion of the NMDA receptor antagonist APV directly into the brains of awake behaving animals results in significant impairments in both reference memory (use of previously learned rules or information to complete a task) and working memory (holding information in a temporary memory buffer for use in problem solving).

The standard test for reference memory is the Morris Water Maze developed by Richard Morris in 1986 [217]. In this task, animals swim in a pool of opaque water to find a hidden platform submerged just beneath the surface in order to escape. Animals

use visual cues in the surrounding environment to orient themselves and navigate to the escape platform. Performance is measured by escape latency (time to platform – less is better), a probe test (how much time the animal spends in the area where the platform was previously located – more is better) and reversal training (how quickly the animal learns a new location of the platform – less is better). In rats, i.c.v. infusion of APV at concentrations shown to also block hippocampal LTP *in vivo* (as low as 10 mM) show impaired escape latency, probe test, and reversal training [370, 371]. Pretraining animals to proficiency in a spatial navigation task prior to APV infusion however, has shown conflicting results. One study shows only minimal improvement in escape latency in pretrained animals with APV, compared to untrained animals with APV [370], while the other shows pretraining negates the effects of APV, allowing animals to perform similarly to control animals without APV [372]. Both studies however, agree that pretraining significantly improves probe test results. Infusion of APV directly into the dorsal hippocampus also produces impairments in learning acquisition and probe trials at a range of concentrations (10-30 mM) that also block LTP *in vivo*. Interestingly, pretraining to proficiency prior to APV infusion can negate the effects of APV at low doses (10 mM), but not at high doses (20, 30 mM) [373]. Pretraining however, does not seem to influence or rescue spatial learning in the MWM when there is a new (but similar) task that is sufficiently novel and performed under the influence of APV [374].

While the MWM is an accepted test of spatial reference memory, a more stringent test of reference memory, and working memory, can be achieved using the Radial Arm Maze (RAM) developed by Olton and Samuelson in 1976 [375]. The RAM consists of a circular central hub with 6, 8, or 16 arms extending out from the center hub

with equal distance between each arm. The most common configuration is the 8-arm radial maze. Animals use external visual cues to orient themselves and navigate through the maze to retrieve a food reward at the end of each arm. After collecting the reward, animals must return to the central hub before making the next choice. The basic reference memory task involves only 4 of the 8 arms being baited with food while the other 4 are not. The location of the food does not change from day to day, forcing the animal to remember the location of each food reward (reference memory) in order to successfully complete the task. Entering 1 of the 4 arms that does not contain food is an error in reference memory. Reentering an arm previously visited during a testing session, regardless if the arm originally contained food or not, is an error in short-term working memory.

Testing various aspects of working memory gives the RAM more flexibility than the MWM, and is the more common use of this type of maze. A standard test of short-term working memory is the uninterrupted 8-arm task, in which animals are to retrieve a food reward from all 8 arms without reentering any previously visited arms. A more stringent working memory test that involves long-term working memory is the 8-arm task with an interposed delay. In this task, the test is interrupted after the first 4 correct choices and the animal is returned to the home cage for a specified amount of time. Upon returning to the central hub, the animal must retrieve the remaining food rewards from the 4 unvisited arms of the earlier session. The RAM uses a Win-Shift learning strategy in which a successful outcome (a “win”) encourages the animal to then choose a different option (a “shift”), as opposed to a Win-Stay strategy that encourages the animal to continue with the same successful choice. This type of learning involves a

decision making process dependent on the use of trial specific information that must be held in memory for an extended period of time, then utilized in order to successfully complete the remainder of the task (the animal must remember the first 4 correct choices from trial 1 in order to complete the last 4 correct choices in trial 2 while avoiding previous wins from both trials). Rats begin to show impairments with a delay of approximately 2 hours [376]. A retention curve for the limits of working memory in mice has not been explored.

Studies exploring effects of NMDA receptor antagonists on learning and acquisition of RAM tasks are surprisingly rare, although some using the non-competitive channel blocker MK-801 do exist, and show profound impairments on task acquisition [377, 378]. Instead, many studies focus on different types of working memory performance after an animal has already learned the RAM task, the equivalent of pretraining seen in the MWM. Rats trained to proficiency in the reference memory task (4/8 arms baited) show impairments in both short-term working and reference memory when 20 or 40 mM APV is infused to dorsal hippocampus 15 minutes prior to testing [379], while rats receiving continuous i.c.v. infusion of 30 mM APV show no impairments in either short-term working or reference memory [377]. Results in the uninterrupted 8-arm task (8/8 arms baited) also show mixed results with some studies indicating an impairment in short-term working memory with dorsal hippocampal infusion of APV 15-20 minutes prior to testing [376, 380], while one study with continuous i.c.v. infusion showed no impairment in the uninterrupted 8-arm task [381], and another with i.c.v. infusion showed a substantial impairment [377]. Rats in these studies were all trained to proficiency prior to APV infusion and used similar concentrations of APV at

approximately 30 mM. These differences could arise due to the level of proficiency each study achieved prior to testing, or differences in APV administration (dorsal hippocampal versus intraventricular) which may result in differences in the way multiple brain regions interact with each other. Two of these studies ([379, 380]) had very low n-values, averaging approximately 3 animals per treatment group, compared to the other studies that averaged approximately 8 animals per group. Behavioral testing in animals can show considerable variance between subjects, and n-values of even 8 subjects is probably borderline for what is acceptable to draw reliable conclusions.

Regardless of whether APV is administered to the hippocampus directly, or to the ventricles, studies agree that either is sufficient to produce impairments in the 8-arm task with an interposed delay [376, 381]. Administration of APV before trial 1 or trial 2 show impairments in trial 2. Trial 2 tests both long-term working memory (information held from trial 1) and short-term working memory (information immediately used during trial 2). When a 2 hour delay is imposed between trials, impairments in both types of working memory can be seen depending on when APV is administered [376]. If APV is administered prior to trial 1, long-term working memory is impaired in trial 2, but not short-term working memory (animals enter arms visited in trial 1, but do not reenter arms once visited). Working memory errors from trial 1 are low due to the simplicity of trial 1 and probability of choosing any 4 unvisited arms successfully, even if by chance. If given APV prior to trial 2, animals make short-term working memory errors that also result in long-term working memory errors. This indicates that even though trial 1 may be successful, preventing short-term working memory during trial 2 also prevents utilization of long-term working memory information. This fits with the Baddeley-Hitch

model which suggests working memory circuits must be functional in order to utilize both short-term and long-term memory mechanisms, or in this case, temporary long-term memory in the form of long-term working memory. Given the effects of NMDA receptor antagonists on trial 2 performance when administered prior to trial 1, it is believed that long-term working memory utilizes hippocampal dependent LTP mechanisms to retain working memory information for later use in subsequent trials. This hypothesis has not been directly tested however, and can only be inferred as virtually no studies explore the correlation between long-term working memory and LTP (or STP), but only show associations.

Further complexity arises when non-NMDA receptor-dependent mechanisms of LTP occur. Grover and Teyler have demonstrated at least two forms of LTP coexist at CA3→CA1 synapses, NMDA and non-NMDA receptor-dependent, with the latter occurring via activation of the high threshold L-type Voltage-Dependent Calcium Channel (VDCC) [382-384]. Immuno-gold labeling and electron microscopy of rat CA1 pyramidal neurons indicate VDCCs are located throughout the dendritic tree and soma at both synaptic and extrasynaptic locations with proportionally higher concentrations occurring in apical dendrites [385]. VDCCs have a higher threshold of activation than dendritic Na_P , Na_V or Ca_T channels, so local depolarization sufficient for generating dendritic action potentials, or activation of NMDA receptors, does not necessarily activate L-type channels. In rat CA1 neurons of hippocampal slices, a weak tetanizing stimulation (25 Hz 1s, 1x) induces fast onset LTP that is completely blocked in the presence of 25 μ M APV. A strong tetanizing stimulation (200 Hz 0.5s, x4) produces a late-onset LTP even in the presence of up to 100 μ M APV, that is significantly blocked

by the L-type VDCC antagonist Nifedipine [382]. Thus, when sufficient stimulation occurs, activation of VDCCs results in a non-NMDA receptor-dependent component of LTP. In summary, high frequency stimulation can result in the induction of both NMDA receptor-dependent and non-NMDA receptor-dependent (VDCC) activation of LTP mechanisms (Figure 1.9).

Activation of VDCCs have been shown to induce signaling mechanisms similar to NMDA receptor activation, including activation of CaMKII specifically in the head and neck of dendritic spines [270]. There also seems to be distinct signaling between NMDA receptor and L-type VDCC LTP: serine/threonine kinase inhibitors block NMDA receptor LTP, but not L-type VDCC LTP, while tyrosine kinase inhibitors block L-type VDCC LTP but not NMDA receptor LTP [384]. There is even some evidence apical versus basal L-type VDCCs show differences in signaling activation [386]. Studies of learning and memory suggest VDCCs play a specific role in the processing of memory during the consolidation phase. I.p. injections of the L-type VDCC antagonist Verapamil show no effect on the acquisition of a spatial reference memory task (4/8 arms baited) using the 8-arm radial maze [387, 388]. After the final day of training, a delay period of 10 days is used to evaluate long-term retention of spatial information. During the retention test under the same drug conditions, animals show a profound impairment in long-term spatial reference memory. Short-term working memory performance during the reference memory task are mixed however, and different studies (from the same lab) show impairments in one study [388], but not the other [387]. This is in contrast to animals from the same studies that are given i.p. injections of MK-801, which do show impairments in reference memory during task acquisition, but are still able to improve.

Results of the retention test are again mixed between studies with one showing no impairment [388] and the other showing impairments in reference memory but not short-term working memory [387]. Animals given both MK-801 and Verapamil together show nearly a complete block of acquisition and memory during all testing. Mice with an L-type VDCC knockout ($Ca_v1.2$) in the hippocampus show impairments in L-LTP and spatial learning in a modified MWM task [389], while mice with a L-type VDCC conditional knockout of the same channel in both hippocampus and cortex show normal learning acquisition and normal probe trials in a standard MWM task, but 30 days later show significant impairment during a probe trial [390], indicating a failure to retain long-term spatial information. The role of VDCCs specifically in a long-term working memory task, such as an 8-arm radial maze task with an interposed delay, have not been evaluated.

The studies described above generally show no impairment in learning when L-type VDCCs are blocked during the acquisition of the task itself, but seem to show profound impairments some time later when task specific information is required to repeat the task. A one-time dose of Nifedipine directly into the dorsal hippocampus immediately following a probe trial after acquisition of standard MWM task, shows a significant impairment in subsequent probe trials both 24 hours and 5 days later [391]. If Nifedipine is given 30 minutes after the probe trial instead of immediately after, animals show normal performance in subsequent probe trials. This indicates that L-type VDCCs play a role in consolidation and reconsolidation of long-term memories, and this consolidation process occurs within a very narrow time window after the task is completed. When memories are initially formed, the memory trace is said to be in a

liable state to which it is subject to deterioration. If the trace goes through a consolidation phase, it becomes an engram. When that information is retrieved, the trace is reactivated and if task specific reinforcement occurs (platform present, e.g., a training trial), the trace is strengthened. If however, task specific information is not present during retrieval (platform not present, e.g., a probe test), the non-reinforced retrieval causes the trace to become liable again, and the trace must be reconsolidated. Reconsolidation of long-term memory is L-type VDCC-dependent. Reconsolidation is also protein synthesis and CaMKII dependent, and blocking either during the reconsolidation process produces the same effect as blocking L-type VDCCs [391, 392]. Blocking NMDA receptors during the reconsolidation process by direct infusion of APV into the dorsal hippocampus seems to have no effect on reconsolidation [391].

The role of NMDA receptors and VDCCs in learning and memory also seem to be subject to the effects of aging. While both forms of LTP exist throughout the lifespan, young animals display predominately NMDA receptor-mediated LTP. As animals age, there is a natural decline in NMDA receptor-mediated LTP, and an increase in L-type VDCC-mediated LTP [393]. This increase in L-type VDCC LTP in aged animals is believed to play a compensatory role in cognitive function. Animals tested in the MWM show young animals (6 months of age) perform better than aged animals (24 months of age), and have higher NMDA receptor LTP than aged animals [394]. There are however, two distinct groups within the aged animals: aged impaired and aged unimpaired. When separated by performance, aged unimpaired animals have higher L-type VDCC LTP than aged impaired animals. This indicates animals that are

able to effectively adjust the NMDA receptor to L-type VDCC ratio as they age, are better able to maintain cognitive function throughout the lifespan.

Our understanding of NMDA receptors and VDCCs (and others) in learning and memory is under continuous revision. NMDA receptors and VDCCs seem to have specific roles in different types of memory, and seem to modulate different aspects of learning and memory. Some of these differences may even be synapse specific (CA3 versus CA1 synapses). Their role in associational and spatial reference memory is the most well studied, while working memory data is still somewhat fragmented. A summary of the roles of NMDA receptors and VDCCs in spatial reference memory is shown in Figure 1.10.

1.7 Synaptic Impairment in Alzheimer's Disease

In a previous section, we described the mechanisms involved in the production of A β 42. In this section, we discuss the consequences of increased A β 42 production and the impact on synaptic physiology and cognition.

Alzheimer's disease is a disease of synaptic failure, driven by the excessive production of A β 42 and the hyperphosphorylation of Tau. The effects of A β 42 on synaptic physiology include impairments in basal synaptic transmission, and impairments in both short-term and long-term synaptic plasticity mechanisms. A β 42 shows a hormetic dose response, meaning small amounts may be beneficial, but moderate and excessive amounts are deleterious. APP processing increases during periods of normal synaptic activity, especially during synaptic plasticity events [395], and picomolar concentrations (~200 pM) of A β 42 have been shown to increase

performance in the MWM and increase LTP in the CA1 subregion when acutely applied to hippocampal slices *ex vivo* [396]. A β 40 has also been shown to increase LTP in the dentate gyrus when acutely applied *ex vivo* at nanomolar concentrations (~200nM) [397]. Thus, both A β 40 and A β 42 may be beneficial in small doses. Increasing concentrations of either A β 40 or A β 42 however, show deleterious effects once a neurotoxic threshold is crossed, with A β 42 (10 pM) having a significantly lower threshold for toxicity than A β 40 (400 pM) when measured *in vivo* at CA1 after i.c.v. injection of A β [398].

Direct comparisons of the effects of A β under different conditions is difficult due to the different variants of A β used in research. Studies have demonstrated that A β 40, A β 42, the C-terminal fragment of β -APP, and the A β fragment consisting of amino acids (25-35), are all capable of eliciting an effect on synaptic physiology [398, 399]. A β 42 and A β (25-35) are the two most common and potent A β variants available, with A β (25-35) representing the active neurotoxic fragment of the A β peptide [400]. In addition, most studies involving the application of synthetic or naturally isolated A β to brain tissue for neurophysiological or cognitive studies consists of a heterogeneous mixture of monomers, oligomers, and fibrillar forms. It has been demonstrated that the monomer form does not significantly contribute to pathology [54], and the fibrillar form is only mildly pathogenic [401, 402]. Most studies now agree the soluble oligomeric form of A β is the most detrimental to synaptic physiology [54], neuronal viability [401, 402], and cognitive function. I.c.v. injection of soluble A β oligomers produces impairments in learning and memory, but i.c.v. injection of monomer or fibrillar forms of A β do not [55, 403, 404].

Impairments in functional synaptic plasticity is likely the underlying cause of cognitive impairment in AD, and the application of A β 40, A β 42 or A β (25-35) all produce significant impairments in synaptic plasticity. Acute application of exogenous A β to hippocampal slices *ex vivo* produces a significant reduction in LTP in CA1 [56, 57, 396, 399, 405] and dentate gyrus [399, 406-408] without affecting basal synaptic transmission. *In vivo* measurements after i.c.v. injection of A β also show significant reductions in LTP in CA1 pyramidal neurons [54, 398, 405, 409, 410], and it is the soluble oligomeric form of A β , not the monomeric form, responsible for these reductions [54]. A β impairs LTP in a concentration- and time-dependent manner. Higher concentrations are increasingly more effective than lower concentrations at disrupting synaptic function for both A β 40 [410] and A β 42 [406, 409], however lower concentrations can have similar effects as higher concentrations if animals are exposed to A β for longer periods of time [409]. As a result, animals exposed to A β also have significant impairments in cognitive function. I.c.v. injection of either A β 40 or A β 42 produces impairments in spatial reference memory in the MWM [411-415], spatial working memory in the RAM [416] and Y-maze [412-414], passive avoidance behavior (a non-spatial reference memory test) [57, 412-415], novel object recognition (NOR) (a non-spatial working memory test) [403], and an alternating lever cyclic ratio test (a complex lever press assay for sequence learning) [55, 416]. Taken together, A β induced impairments in synaptic plasticity are most likely responsible for the impaired cognitive behavior observed in A β exposed animals.

Direct application of A β has been useful for studying acute effects within a short time frame, but long-term exposure outcomes and developmental progression of A β

pathophysiology is best accomplished through the use of transgenic animals. The engineering of mice carrying human transgenes with mutations in APP, PS1, or PS2 have aided greatly in the understanding of how A β affects cognition and neurophysiology over the course of months to years of continuous exposure. A variety of different mutations in *APP* have been described and are typically named based on the geographic region in which these mutations were discovered, although that's not always the case. For example *APP(Swe)* refers to a particular mutation first identified in a family from Sweden [417]. There are currently 44 different *APP* mutations listed in the Alzforum.org mutation database, 25 of which are classified as pathogenic. Of these, 9 have been incorporated into transgenic mouse models with the Swedish (K670N/M671L), London (V717I), and Indiana (V717F) mutations being the most commonly used. For the Presenilins, there are 230 known mutations in *PS1* (212 are pathogenic, 11 have been incorporated into transgenic models) and 39 in *PS2* (16 are pathogenic but only 1 has been incorporated into transgenic models). There is even one known *APP* mutation that offers protection against AD by inhibiting β -secretase from recognizing APP, preventing A β production [418].

Transgenic models have confirmed that overexpression of mutated forms of APP and PS characterized in AD patients do in fact lead to histological and behavioral disturbances consistent with the AD phenotype and physiological alterations consistent with exogenous A β exposure. APP transgenic mice have reduced LTP in CA1 [419-421], CA3 [422], and dentate gyrus [419, 423], and show impairments in reference memory [420, 424, 425] and short-term working memory [419, 424, 425] in the MWM, RAM, Y/T-maze, and NOR test. APP transgenic mice also recapitulate AD

histopathology [420, 424, 426, 427]. APP mice show increased A β 42 production and β -Amyloid plaque formation beginning on average around 10 months of age, and range from diffuse plaques in early stages to dense core plaques in late stages. A β 42 deposition occurs first, with A β 40 deposition following later. In addition, dystrophic neurites (indicative of hyperphosphorylated Tau) and GFAP+ reactive astrocytes (an indication of injury/inflammatory response) are associated with mature plaques. Synaptic decline and cytoskeletal alterations are also detected, and one study has even reported the presence of Hirano body-like structures [427]. Unlike AD patients, APP mice do not seem to show widespread neuronal loss or full neurofibrillary tangle formation, but this could be a factor of age as most studies do not continue past 18 months.

PS mice show a delay in disease progression compared to APP mice. PS1 transgenic mice show an increase in LTP [428-431] and a reduction in the threshold for inducing LTP [432] in CA1 of younger (3-4 month old) mice. This increase is transient however, and normalizes to wild-type levels around 10 months of age, and by 13-14 months of age develop reduced LTP [431]. By comparison, APP mice begin to show reduced LTP on average between 5-6 months [420, 421]. PS1 mice also show delayed cognitive impairment relative to APP models. At least five different PS1 mutations do not produce cognitive impairment in reference memory in the MWM up to at least 10 months of age [430, 432-434], although one study reported a slight impairment at 10 months [435], and there have been mixed results in NOR tests [430, 434]. Some reports even show enhanced cognition occurring around 6 months of age [430, 434], a time when LTP is known to be enhanced in PS1 mice. By comparison, most APP mice

begin to show deficits on average between 6-9 months. While some PS1 mice do show hyperphosphorylation of Tau and the beginnings of dystrophic neurites around 10 months (but not neurofibrillary tangles) [430, 435], they lack detectable β -Amyloid plaques up to at least 17 months of age despite having significantly increased levels of A β 42 as early as 6 months [434, 436-438] and staining positive for intracellular A β 42 [438]. PS mice also show a potentiated intracellular Ca²⁺ response to glutamate exposure, which could account for the facilitation of LTP and enhanced cognition at younger ages, but also sensitizes neurons to Ca²⁺ induced excitotoxicity [432, 439]. The enhanced Ca²⁺ response observed in young transgenic animals may temporarily offset the deleterious effects of increased A β production. PS mice show an increase in spine density at 6 months, the same time as increased LTP and enhanced cognition, that decreases to control levels around 10 months [431], but eventually begin to show neuronal loss around 13 months [438], presumably due to Ca²⁺ induced excitotoxic mechanisms.

The most popular transgenic models of AD are ones that coexpress mutated forms of both APP and PS1. APP/PS1 mice show the same pathology as individual APP or PS1 mice carrying the same mutations, but at a highly accelerated rate. A β 42 is increased and definitive plaque formation is observed around 6 months in APP/PS1 mice [440], compared to 12 months in APP mice [424]. Behavioral and physiological measurements are highly variable in APP/PS1 mice. APP mice show impairments in short-term working memory at 3 months in the Y-maze, and in reference memory around 9 months in the MWM [424]. APP/PS1 mice also show impairments in the Y-maze at 3 months, but show normal cognition in the MWM up to 14 months [441].

Another study however, using the same APP/PS1 model, report short-term working memory deficits at 3 months and reference memory deficits at 6 months in the radial arm water maze [442] (a hybrid of the RAM and MWM where animals must swim to a submerged escape platform at the end of one of the arms). Studies of synaptic plasticity show APP mice have reduced LTP in CA1 at 12 months [443, 444], but may begin as early as 6-7 months [445] with no change in PPF or basal synaptic transmission at any age tested up to at least 16 months [419]. APP/PS1 mice show significant reductions in LTP in CA1 as early as 3 months [442].

The APP/PS1 model discussed above refers to a model produced by crossing APP(Swe) x PS1(M146L), but it should be noted that a variety of different APP/PS1 models exist and each combination of APP/PS1 mutations will produce a different phenotypic expression of AD [26, 446]. Add this in combination to mice engineered with transgenes verses knockins, or transgenes under a variety of different promoters, or any number of other production variables, and the number of available models becomes quite numerous, and results between them can vary greatly. Some models overexpress wild-type APP by itself, or with mutant PS, that may show some aspects of AD [447-449], and some others combine multiple mutations within the same gene such as the 5xFAD mouse (APP carrying Swedish/London/Florida mutations, and PS1 carrying M146L/L286V mutations) that develops plaques after only 60 days [450]. One of the more popular AD models overexpress mutant forms of APP, PS1, and Tau (3xTg-AD), and forms both plaques and full neurofibrillary tangles [451]. Thus, when evaluating the literature it is important to note exactly which models are used in order to make the appropriate comparisons between studies.

1.7.1 Mechanisms of Amyloid- β induced neurotoxicity

There are numerous studies showing soluble oligomeric A β in the absence of β -Amyloid plaques is highly neurotoxic (see above sections). Transgenic AD mice support the hypothesis that soluble A β is the pathogenic initiator of AD and not β -Amyloid plaques. Transgenic mice show impairments in LTP and cognition when soluble A β 42 levels rise, and long before β -Amyloid plaques appear [420, 421, 423, 425, 426, 452], and cognitive impairment in both mice and humans correlate with soluble A β levels, but not with plaque load [453-457]. Plaques appear to be a late-stage end product of A β fibrillization and have minimal impact on AD progression. That is not to say however, that plaques are completely inert. Plaques may not contribute directly to behavioral deficits or pathophysiology, but they do attract reactive astrocytes and activated microglia that promote chronic inflammation which will impact neurophysiology (LTP) [458], and inflammation has been shown to be a highly prevalent part of AD pathology [459].

How then does soluble A β exert its effects on synaptic physiology and subsequently behavior? Impairments in LTP and cognition occur long before synaptic decline and neuronal loss. 3xTg-AD mice have similar dendritic spine density as wild-type mice in both the hippocampus and cortex up to around 13 months of age [460], yet these mice show reductions in LTP and cognition by 6 months of age [451, 461]. The rise in soluble oligomeric A β 42 that strongly correlates with synaptic dysfunction, and has been shown to be the pathogenic initiator of AD, must have effects prior to synaptic or neuronal loss that are responsible for these impairments, even if degeneration is the eventual outcome. The reduction in LTP observed in AD mice seems to be driven in

part by activity dependent LTD. Activation of LTD mechanisms leads to a reduction in synaptic AMPA receptors, and thus a reduced synaptic response [230]. The presence of A β has been shown to facilitate LTD mechanisms and the removal of AMPA receptors from the synaptic membrane [462-464]. In addition, AMPA receptor trafficking to the synaptic membrane during LTP has also been shown to be impaired in the presence of A β [463-465]. In support of reduced AMPA receptor expression in AD, there is evidence that 3xTg-AD mice may change expression levels of AMPA receptor subunits as they age, although the only study to date is inconclusive due to low observations [466]. This study suggests there is an overall reduction in GluR subunit expression in aged 3xTg-AD mice (12 months of age) that supports studies showing a reduction in AMPA receptor expression as a result of AD pathology [467]. Interestingly, control mice show an age dependent increase in GluR2 subunit expression, while 3xTg-AD mice show a significant reduction in all GluR subunits except GluR2. The GluR2 subunit regulates Ca²⁺ permeability and this difference in GluR2 subunit expression may allow for a potential compensatory mechanism that would resist changes to the Ca²⁺ impermeable/permeable AMPA receptor ratio in 3xTg-AD mice. In summary, one current hypothesis to explain reduced LTP in AD is that both LTD and LTP mechanisms may be occurring simultaneously, resulting in an average of the two.

Glutamatergic signaling: Metabotropic glutamate receptors and NMDA receptors

LTD at hippocampal CA3→CA1 synapses is mediated by NMDA receptors or metabotropic glutamate receptors (mGluR) [468, 469]. Exogenously applied A β to hippocampal slices produces a reduction in LTP that can be rescued in the presence of mGluR antagonists [470]. In addition to LTD facilitation, A β has also been shown to

sensitize neurons to subthreshold activation of LTD, both of which can be blocked in the presence of mGluR antagonists [471]. Activation of extrasynaptic NR2B containing NMDA receptors can also contribute to reduced LTP, which can be partially rescued by NR2B antagonists, although not to control levels [472]. Both mGluR and extrasynaptic NR2B containing receptors utilize overlapping signaling pathways such as p38 MAPK signaling that could lead to downstream activation of LTD mechanisms, and blocking p38 signaling improves A β induced impairments in LTP [470, 473]. A β induced reduction of LTP may be driven predominately by impairments in glutamate clearance rather than interactions between A β and mGluR or NR2B containing receptors directly. Application of a glutamate scavenger enzyme prevents A β induced LTD facilitation [471] and rescues LTP [472] similar to mGluR or NR2B antagonists. Likewise, application of a glutamate reuptake inhibitor produces LTD facilitation and reduced LTP similar to exogenously applied A β [471, 472].

Cholinergic signaling: Nicotinic acetylcholine receptors

A β interferes with cholinergic signaling, and manipulation of the cholinergic system is an active area of AD research. Cholinergic neurons of the basal forebrain have wide spread projections to the cortex and hippocampus [474, 475], and neurons from this region are one of the first to show substantial neurodegeneration in AD [476, 477], along with a significant reduction in nicotinic receptors throughout the AD brain [478]. Modulation of hippocampal pyramidal, granule, and interneuron activity by Acetylcholine (ACh) can affect both LTP and LTD depending on the timing of ACh receptor activation during glutamatergic or GABAergic transmission [479, 480]. A β 42 binds to both the α 7 and α 4 β 2 nicotinic acetylcholine receptors and significantly reduces

cationic current when activated by nicotine [481]. Both A β 40 and A β 42 have been shown to bind the α 7 nicotinic acetylcholine receptor (α 7nAChR) at the α -bungarotoxin site, with A β 42 binding at much higher affinity than A β 40 [482, 483]. Whole cell slice recordings show A β 42, but not A β 40, reduces α 7nAChR current by approximately 40% in hippocampal interneurons [484].

Application of nicotine facilitates LTP in CA1 and dentate gyrus of hippocampal slices [485, 486]. Blocking nicotinic receptors reduces LTP in CA1, indicating an important modulatory role in LTP induction. When co-applied with A β 42, nicotine rescues A β 42 induced impairments in LTP in both CA1 and dentate gyrus [485, 487]. Application of other agonists specific for α 7nAChRs have also demonstrated rescue of LTP in the presence of A β [487]. In addition, co-application of an α 7nAChR antagonist with A β [470], or application of A β to hippocampal slices from an α 7 knockout mouse [485], does not worsen A β induced impairments of LTP. Chronic nicotine injections prior to and during continuous i.c.v. infusion of A β 42 completely rescues short-term working and reference memory in rats [488, 489], and transgenic APP- α 7 KO mice have shown improvements in MWM performance and LTP at CA1 [490].

The α 7nAChR is Ca²⁺ permeable, providing another avenue for Ca²⁺ dysregulation, and influences LTP specifically through PKA activation associated with the α 7nAChR [485], and blocking PKA prevents nicotinic enhancement and the rescue of LTP in the presence of A β . Like the mGluR and NR2B containing receptors, MAPK signaling is also modulated by α 7nAChR signaling [491]. In summary, A β may interfere with nicotinic signaling by either antagonizing nicotinic receptors, or influencing receptor density by causing bound receptors to be internalized, either of which will affect

cholinergic modulation of synaptic activity through dysregulation of intracellular signaling cascades important for plasticity, and subsequently cognition.

Cellular Prion Protein and hyperphosphorylation of Tau

A β has been shown to bind to and activate the cellular Prion Protein (PrP) with nanomolar affinity [492], and antibody targeting and inhibition of PrP rescues A β induced impairments in LTP and LTD facilitation [492-494]. Binding of A β to PrP utilizes the associated membrane spanning protein caveolin-1 [495] to activate the tyrosine kinase Fyn [496]. Fyn is currently the most likely candidate driving the hyperphosphorylation of Tau. Fyn has been shown to be associated with Tau during microtubule extension [497] and the synaptic scaffolding protein PSD-95 [498]. Tau is necessary for Fyn to localize into dendritic spines where it phosphorylates the NR2B subunit of dendritic NMDA receptors [498]. A β drives the mislocalization of excessive Tau/Fyn into dendritic spines [499] where it phosphorylates NMDA receptors and it thought to contribute to excitotoxicity. This also explains the localization of hyperphosphorylated Tau present in dystrophic neurites.

1.8 Final Thoughts

In summary, synaptic plasticity is the ability of synapses to change their strength of connection in response to activity dependent stimuli. Activation of NMDA receptors and L-type VDCCs results in a long-term potentiation of synaptic strength through activation of postsynaptic Ca²⁺ mediated pathways. This ultimately leads to an upregulation of postsynaptic AMPA receptors and a potentiation of the synaptic signal. LTP is associated with learning and memory, and represents a cellular model for

information storage in the central nervous system. Preventing LTP by blocking either NMDA receptors or L-type VDCCs produces impairments in cognitive performance.

Alzheimer's disease is a disease aging and of synaptic failure brought on by the aberrant production of the Amyloid- β peptide. Animal models exist to study the biochemical, behavioral, and physiological progression of AD, with most studies focusing on cellular pathways for A β production. Although studies characterizing the basic parameters of learning and neurophysiology have been done in some models, less attention has been given to the specific subtypes of cognitive impairments in these models, such as impairments in different types of memory, and the physiological processes driving these behaviors. In addition, different AD models develop AD pathology and impairments in distinctly different ways, and characterization in one model does not necessarily apply to all models.

Long-term working memory deficit is one of the first types of memory impairments observed in AD patients, however the physiological mechanism behind this is unknown. This specific memory impairment is also unexplored in AD mouse models outside of delayed alternation using a T-maze, which is a relatively simple task, and does not model daily challenges of patients with mild cognitive impairment or early AD. Very few studies to date have explored synaptic plasticity mechanisms as they relate to memory impairments in AD. In this dissertation, the investigation of NMDA receptor and VDCC-dependent LTP as it relates to working memory in AD is explored using a well-known 3xTg-AD model mouse that produces both plaques and tangles. Given the effects of VDCCs on learning and memory in the aged animal, and the alterations in Ca²⁺ signaling in AD, exploring the relationship between NMDA receptors, VDCCs, and

AD could lead to a more precise understanding of how AD pathology influences deficits in specific types of working memory, and the underlying synaptic alterations that may contribute to these impairments. The characterization of a novel mouse model of Hirano bodies, a cellular inclusion observed in some neurodegenerative diseases including AD, will also be explored to determine the influence of these pathological structures on cognition and synaptic plasticity.

References

1. Alzheimer, A., *Über eine eigenartige Erkankung der Hirnrinde*. Allgemeine Zeitschrift für Psychiatrie und Psychisch-Gerichtliche Medizin, 1907. **64**: p. 146-148.
2. Alzheimer, A., et al., *An English translation of Alzheimer's 1907 paper, "Über eine eigenartige Erkankung der Hirnrinde"*. Clin Anat, 1995. **8**(6): p. 429-31.
3. Maurer, K., S. Volk, and H. Gerbaldo, *Auguste D and Alzheimer's disease*. Lancet, 1997. **349**(9064): p. 1546-9.
4. Fischer, O., *Miliare Nekrosen mit drüsigen Wucherungen der Neurofibrillen, eine regelmäßige Veränderung der Hirnrinde bei seniler Demenz*. Monatsschr Psychiatr Neurol, 1907. **22**: p. 361-372.
5. Bonfiglio, F., *Di speciali reperti in un caso di probabile sifilide cerebrale*. Riv Sper Freniatria, 1908. **34**: p. 196-206.
6. Perusini, G., *Über klinisch und histologisch eigenartige psychische Erkrankungen des späteren Lebensalters*. Histologische und Histopathologische Arbeiten., 1909: p. 297-351.
7. Kraepelin, E., *Psychiatrie: Ein Lehrbuch für Studierende und Ärzte*. VIII ed. 1910, Leipzig, Germany.
8. Alzheimer, A., *Über eigenartige Krankheitsfälle des späteren Alters*. Zeitschrift für die Gesamte Neurologie und Psychiatrie, 1911. **4**: p. 356-385.
9. Querfurth, H.W. and F.M. LaFerla, *Alzheimer's disease*. N Engl J Med, 2010. **362**(4): p. 329-44.
10. Association, A.s., *Alzheimer's Disease Facts and Figures*. Alzheimer's & Dementia, 2014. **10**(2).
11. Films, H., *The Alzheimer's Project*, in *HBO Documentary Series* 2012, HBO Films.
12. Hebert, L.E., et al., *Alzheimer disease in the United States (2010-2050) estimated using the 2010 census*. Neurology, 2013. **80**(19): p. 1778-83.
13. Ikonovic, M.D., et al., *Cortical alpha7 nicotinic acetylcholine receptor and beta-amyloid levels in early Alzheimer disease*. Arch Neurol, 2009. **66**(5): p. 646-51.
14. Lombardo, S. and U. Maskos, *Role of the nicotinic acetylcholine receptor in Alzheimer's disease pathology and treatment*. Neuropharmacology, 2014.

15. Forstl, H., et al., *Brain atrophy in normal ageing and Alzheimer's disease. Volumetric discrimination and clinical correlations*. Br J Psychiatry, 1995. **167**(6): p. 739-46.
16. Double, K.L., et al., *Topography of brain atrophy during normal aging and Alzheimer's disease*. Neurobiol Aging, 1996. **17**(4): p. 513-21.
17. Peng, G.P., et al., *Correlation of hippocampal volume and cognitive performances in patients with either mild cognitive impairment or Alzheimer's disease*. CNS Neurosci Ther, 2015. **21**(1): p. 15-22.
18. Dolek, N., et al., *Comparison of hippocampal volume measured using magnetic resonance imaging in Alzheimer's disease, vascular dementia, mild cognitive impairment and pseudodementia*. J Int Med Res, 2012. **40**(2): p. 717-25.
19. Vemuri, P. and C.R. Jack, Jr., *Role of structural MRI in Alzheimer's disease*. Alzheimers Res Ther, 2010. **2**(4): p. 23.
20. Serrano-Pozo, A., et al., *Neuropathological alterations in Alzheimer disease*. Cold Spring Harb Perspect Med, 2011. **1**(1): p. a006189.
21. Mathis, C.A., B.J. Lopresti, and W.E. Klunk, *Impact of amyloid imaging on drug development in Alzheimer's disease*. Nucl Med Biol, 2007. **34**(7): p. 809-22.
22. Shoji, M., et al., *Production of the Alzheimer amyloid beta protein by normal proteolytic processing*. Science, 1992. **258**(5079): p. 126-9.
23. Chang, K.A., et al., *Phosphorylation of amyloid precursor protein (APP) at Thr668 regulates the nuclear translocation of the APP intracellular domain and induces neurodegeneration*. Mol Cell Biol, 2006. **26**(11): p. 4327-38.
24. Cao, X. and T.C. Sudhof, *A transcriptionally [correction of transcriptively] active complex of APP with Fe65 and histone acetyltransferase Tip60*. Science, 2001. **293**(5527): p. 115-20.
25. Vassar, R., et al., *Beta-secretase cleavage of Alzheimer's amyloid precursor protein by the transmembrane aspartic protease BACE*. Science, 1999. **286**(5440): p. 735-41.
26. Weggen, S. and D. Beher, *Molecular consequences of amyloid precursor protein and presenilin mutations causing autosomal-dominant Alzheimer's disease*. Alzheimers Res Ther, 2012. **4**(2): p. 9.
27. Xia, W., et al., *Presenilin 1 regulates the processing of beta-amyloid precursor protein C-terminal fragments and the generation of amyloid beta-protein in endoplasmic reticulum and Golgi*. Biochemistry, 1998. **37**(47): p. 16465-71.

28. Hartmann, T., et al., *Distinct sites of intracellular production for Alzheimer's disease A beta40/42 amyloid peptides*. Nat Med, 1997. **3**(9): p. 1016-20.
29. Thal, D.R., *The role of astrocytes in amyloid beta-protein toxicity and clearance*. Exp Neurol, 2012. **236**(1): p. 1-5.
30. Lee, C.Y. and G.E. Landreth, *The role of microglia in amyloid clearance from the AD brain*. J Neural Transm, 2010. **117**(8): p. 949-60.
31. El Khoury, J., et al., *Scavenger receptor-mediated adhesion of microglia to beta-amyloid fibrils*. Nature, 1996. **382**(6593): p. 716-9.
32. Alarcon, R., et al., *Expression of scavenger receptors in glial cells. Comparing the adhesion of astrocytes and microglia from neonatal rats to surface-bound beta-amyloid*. J Biol Chem, 2005. **280**(34): p. 30406-15.
33. Iwata, N., et al., *Metabolic regulation of brain Abeta by neprilysin*. Science, 2001. **292**(5521): p. 1550-2.
34. Nalivaeva, N.N., et al., *The Alzheimer's amyloid-degrading peptidase, neprilysin: can we control it?* Int J Alzheimers Dis, 2012. **2012**: p. 383796.
35. Sagare, A.P., R.D. Bell, and B.V. Zlokovic, *Neurovascular dysfunction and faulty amyloid beta-peptide clearance in Alzheimer disease*. Cold Spring Harb Perspect Med, 2012. **2**(10).
36. Jacobsen, J.S., A.J. Blume, and M.P. Vitek, *Quantitative measurement of alternatively spliced amyloid precursor protein mRNA expression in Alzheimer's disease and normal brain by S1 nuclease protection analysis*. Neurobiol Aging, 1991. **12**(5): p. 585-92.
37. Tanaka, S., et al., *Tissue-specific expression of three types of beta-protein precursor mRNA: enhancement of protease inhibitor-harboring types in Alzheimer's disease brain*. Biochem Biophys Res Commun, 1989. **165**(3): p. 1406-14.
38. Golde, T.E., et al., *Expression of beta amyloid protein precursor mRNAs: recognition of a novel alternatively spliced form and quantitation in Alzheimer's disease using PCR*. Neuron, 1990. **4**(2): p. 253-67.
39. Donnelly, R.J., et al., *Isolation and expression of multiple forms of beta amyloid protein precursor cDNAs*. Prog Clin Biol Res, 1989. **317**: p. 925-37.
40. Rohan de Silva, H.A., et al., *Cell-specific expression of beta-amyloid precursor protein isoform mRNAs and proteins in neurons and astrocytes*. Brain Res Mol Brain Res, 1997. **47**(1-2): p. 147-56.

41. Zhan, S.S., et al., *APP with Kunitz type protease inhibitor domain (KPI) correlates with neuritic plaque density but not with cortical synaptophysin immunoreactivity in Alzheimer's disease and non-demented aged subjects: a multifactorial analysis*. Clin Neuropathol, 1995. **14**(3): p. 142-9.
42. Rockenstein, E.M., et al., *Levels and alternative splicing of amyloid beta protein precursor (APP) transcripts in brains of APP transgenic mice and humans with Alzheimer's disease*. J Biol Chem, 1995. **270**(47): p. 28257-67.
43. Procter, A.W., et al., *beta-Amyloid precursor protein isoforms show correlations with neurones but not with glia of demented subjects*. Acta Neuropathol, 1994. **88**(6): p. 545-52.
44. Citron, M., et al., *Mutation of the beta-amyloid precursor protein in familial Alzheimer's disease increases beta-protein production*. Nature, 1992. **360**(6405): p. 672-4.
45. Cai, X.D., T.E. Golde, and S.G. Younkin, *Release of excess amyloid beta protein from a mutant amyloid beta protein precursor*. Science, 1993. **259**(5094): p. 514-6.
46. Suzuki, N., et al., *An increased percentage of long amyloid beta protein secreted by familial amyloid beta protein precursor (beta APP717) mutants*. Science, 1994. **264**(5163): p. 1336-40.
47. Borchelt, D.R., et al., *Familial Alzheimer's disease-linked presenilin 1 variants elevate Abeta1-42/1-40 ratio in vitro and in vivo*. Neuron, 1996. **17**(5): p. 1005-13.
48. Citron, M., et al., *Additive effects of PS1 and APP mutations on secretion of the 42-residue amyloid beta-protein*. Neurobiol Dis, 1998. **5**(2): p. 107-16.
49. Walker, E.S., et al., *Presenilin 2 familial Alzheimer's disease mutations result in partial loss of function and dramatic changes in Abeta 42/40 ratios*. J Neurochem, 2005. **92**(2): p. 294-301.
50. Tamaoka, A., et al., *APP717 missense mutation affects the ratio of amyloid beta protein species (A beta 1-42/43 and a beta 1-40) in familial Alzheimer's disease brain*. J Biol Chem, 1994. **269**(52): p. 32721-4.
51. Findeis, M.A., *The role of amyloid beta peptide 42 in Alzheimer's disease*. Pharmacol Ther, 2007. **116**(2): p. 266-86.
52. Scheuner, D., et al., *Secreted amyloid beta-protein similar to that in the senile plaques of Alzheimer's disease is increased in vivo by the presenilin 1 and 2 and APP mutations linked to familial Alzheimer's disease*. Nat Med, 1996. **2**(8): p. 864-70.

53. Lewczuk, P., et al., *Neurochemical diagnosis of Alzheimer's dementia by CSF Abeta42, Abeta42/Abeta40 ratio and total tau*. *Neurobiol Aging*, 2004. **25**(3): p. 273-81.
54. Walsh, D.M., et al., *Naturally secreted oligomers of amyloid beta protein potently inhibit hippocampal long-term potentiation in vivo*. *Nature*, 2002. **416**(6880): p. 535-9.
55. Cleary, J.P., et al., *Natural oligomers of the amyloid-beta protein specifically disrupt cognitive function*. *Nat Neurosci*, 2005. **8**(1): p. 79-84.
56. Townsend, M., et al., *Effects of secreted oligomers of amyloid beta-protein on hippocampal synaptic plasticity: a potent role for trimers*. *J Physiol*, 2006. **572**(Pt 2): p. 477-92.
57. Shankar, G.M., et al., *Amyloid-beta protein dimers isolated directly from Alzheimer's brains impair synaptic plasticity and memory*. *Nat Med*, 2008. **14**(8): p. 837-42.
58. Ahmed, M., et al., *Structural conversion of neurotoxic amyloid-beta(1-42) oligomers to fibrils*. *Nat Struct Mol Biol*, 2010. **17**(5): p. 561-7.
59. Chimon, S., et al., *Evidence of fibril-like beta-sheet structures in a neurotoxic amyloid intermediate of Alzheimer's beta-amyloid*. *Nat Struct Mol Biol*, 2007. **14**(12): p. 1157-64.
60. Chen, Y.R. and C.G. Glabe, *Distinct early folding and aggregation properties of Alzheimer amyloid-beta peptides Abeta40 and Abeta42: stable trimer or tetramer formation by Abeta42*. *J Biol Chem*, 2006. **281**(34): p. 24414-22.
61. Mastrangelo, I.A., et al., *High-resolution atomic force microscopy of soluble Abeta42 oligomers*. *J Mol Biol*, 2006. **358**(1): p. 106-19.
62. Glenner, G.G. and C.W. Wong, *Alzheimer's disease: initial report of the purification and characterization of a novel cerebrovascular amyloid protein*. *Biochem Biophys Res Commun*, 1984. **120**(3): p. 885-90.
63. Glenner, G.G. and C.W. Wong, *Alzheimer's disease and Down's syndrome: sharing of a unique cerebrovascular amyloid fibril protein*. *Biochem Biophys Res Commun*, 1984. **122**(3): p. 1131-5.
64. Masters, C.L., et al., *Amyloid plaque core protein in Alzheimer disease and Down syndrome*. *Proc Natl Acad Sci U S A*, 1985. **82**(12): p. 4245-9.
65. Kang, J., et al., *The precursor of Alzheimer's disease amyloid A4 protein resembles a cell-surface receptor*. *Nature*, 1987. **325**(6106): p. 733-6.

66. Cole, G.M., et al., *Accumulation of amyloid precursor fragment in Alzheimer plaques*. *Neurobiol Aging*, 1991. **12**(2): p. 85-91.
67. Atwood, C.S., et al., *Senile plaque composition and posttranslational modification of amyloid-beta peptide and associated proteins*. *Peptides*, 2002. **23**(7): p. 1343-50.
68. Masters, C.L. and D.J. Selkoe, *Biochemistry of amyloid beta-protein and amyloid deposits in Alzheimer disease*. *Cold Spring Harb Perspect Med*, 2012. **2**(6): p. a006262.
69. Dickson, T.C. and J.C. Vickers, *The morphological phenotype of beta-amyloid plaques and associated neuritic changes in Alzheimer's disease*. *Neuroscience*, 2001. **105**(1): p. 99-107.
70. Iwatsubo, T., et al., *Visualization of A beta 42(43) and A beta 40 in senile plaques with end-specific A beta monoclonals: evidence that an initially deposited species is A beta 42(43)*. *Neuron*, 1994. **13**(1): p. 45-53.
71. Mann, D.M., et al., *Predominant deposition of amyloid-beta 42(43) in plaques in cases of Alzheimer's disease and hereditary cerebral hemorrhage associated with mutations in the amyloid precursor protein gene*. *Am J Pathol*, 1996. **148**(4): p. 1257-66.
72. Ishii, K., et al., *Distinguishable effects of presenilin-1 and APP717 mutations on amyloid plaque deposition*. *Neurobiol Aging*, 2001. **22**(3): p. 367-76.
73. Ishii, K., et al., *Increased A beta 42(43)-plaque deposition in early-onset familial Alzheimer's disease brains with the deletion of exon 9 and the missense point mutation (H163R) in the PS-1 gene*. *Neurosci Lett*, 1997. **228**(1): p. 17-20.
74. Morris, M., et al., *The many faces of tau*. *Neuron*, 2011. **70**(3): p. 410-26.
75. Trojanowski, J.Q., et al., *Distribution of tau proteins in the normal human central and peripheral nervous system*. *J Histochem Cytochem*, 1989. **37**(2): p. 209-15.
76. Lee, G., et al., *Tau interacts with src-family non-receptor tyrosine kinases*. *J Cell Sci*, 1998. **111 (Pt 21)**: p. 3167-77.
77. Perez, M., et al., *Tau--an inhibitor of deacetylase HDAC6 function*. *J Neurochem*, 2009. **109**(6): p. 1756-66.
78. Reynolds, C.H., et al., *Phosphorylation regulates tau interactions with Src homology 3 domains of phosphatidylinositol 3-kinase, phospholipase Cgamma 1, Grb2, and Src family kinases*. *J Biol Chem*, 2008. **283**(26): p. 18177-86.
79. Mandell, J.W. and G.A. Banker, *A spatial gradient of tau protein phosphorylation in nascent axons*. *J Neurosci*, 1996. **16**(18): p. 5727-40.

80. Fanara, P., et al., *Changes in microtubule turnover accompany synaptic plasticity and memory formation in response to contextual fear conditioning in mice.* Neuroscience, 2010. **168**(1): p. 167-78.
81. Scales, T.M., et al., *Tyrosine phosphorylation of tau by the SRC family kinases Ick and fyn.* Mol Neurodegener, 2011. **6**: p. 12.
82. Lee, G., et al., *Phosphorylation of tau by fyn: implications for Alzheimer's disease.* J Neurosci, 2004. **24**(9): p. 2304-12.
83. Min, S.W., et al., *Acetylation of tau inhibits its degradation and contributes to tauopathy.* Neuron, 2010. **67**(6): p. 953-66.
84. Cohen, T.J., et al., *The acetylation of tau inhibits its function and promotes pathological tau aggregation.* Nat Commun, 2011. **2**: p. 252.
85. Wilhelmus, M.M., et al., *Transglutaminases and transglutaminase-catalyzed cross-links colocalize with the pathological lesions in Alzheimer's disease brain.* Brain Pathol, 2009. **19**(4): p. 612-22.
86. Ledesma, M.D., et al., *Analysis of microtubule-associated protein tau glycation in paired helical filaments.* J Biol Chem, 1994. **269**(34): p. 21614-9.
87. Reyes, J.F., et al., *Selective tau tyrosine nitration in non-AD tauopathies.* Acta Neuropathol, 2012. **123**(1): p. 119-32.
88. Reyes, J.F., et al., *Tyrosine nitration within the proline-rich region of Tau in Alzheimer's disease.* Am J Pathol, 2011. **178**(5): p. 2275-85.
89. Cripps, D., et al., *Alzheimer disease-specific conformation of hyperphosphorylated paired helical filament-Tau is polyubiquitinated through Lys-48, Lys-11, and Lys-6 ubiquitin conjugation.* J Biol Chem, 2006. **281**(16): p. 10825-38.
90. Wood, J.G., et al., *Neurofibrillary tangles of Alzheimer disease share antigenic determinants with the axonal microtubule-associated protein tau (tau).* Proc Natl Acad Sci U S A, 1986. **83**(11): p. 4040-3.
91. Nukina, N. and Y. Ihara, *One of the antigenic determinants of paired helical filaments is related to tau protein.* J Biochem, 1986. **99**(5): p. 1541-4.
92. Lee, V.M., et al., *A68: a major subunit of paired helical filaments and derivatized forms of normal Tau.* Science, 1991. **251**(4994): p. 675-8.
93. Kondo, J., et al., *The carboxyl third of tau is tightly bound to paired helical filaments.* Neuron, 1988. **1**(9): p. 827-34.

94. Duong, T., et al., *Microtubule-associated proteins tau and amyloid P component in Alzheimer's disease*. Brain Res, 1993. **603**(1): p. 74-86.
95. Bibow, S., et al., *Structural impact of proline-directed pseudophosphorylation at AT8, AT100, and PHF1 epitopes on 441-residue tau*. J Am Chem Soc, 2011. **133**(40): p. 15842-5.
96. Jeganathan, S., et al., *Proline-directed pseudo-phosphorylation at AT8 and PHF1 epitopes induces a compaction of the paperclip folding of Tau and generates a pathological (MC-1) conformation*. J Biol Chem, 2008. **283**(46): p. 32066-76.
97. Steinhilb, M.L., et al., *Tau phosphorylation sites work in concert to promote neurotoxicity in vivo*. Mol Biol Cell, 2007. **18**(12): p. 5060-8.
98. Stanford, P.M., et al., *Frequency of tau mutations in familial and sporadic frontotemporal dementia and other tauopathies*. J Neurol, 2004. **251**(9): p. 1098-104.
99. Castellano, J.M., et al., *Human apoE isoforms differentially regulate brain amyloid-beta peptide clearance*. Sci Transl Med, 2011. **3**(89): p. 89ra57.
100. Farrer, L.A., et al., *Effects of age, sex, and ethnicity on the association between apolipoprotein E genotype and Alzheimer disease. A meta-analysis. APOE and Alzheimer Disease Meta Analysis Consortium*. JAMA, 1997. **278**(16): p. 1349-56.
101. Namba, Y., et al., *Apolipoprotein E immunoreactivity in cerebral amyloid deposits and neurofibrillary tangles in Alzheimer's disease and kuru plaque amyloid in Creutzfeldt-Jakob disease*. Brain Res, 1991. **541**(1): p. 163-6.
102. Ma, J., et al., *Amyloid-associated proteins alpha 1-antichymotrypsin and apolipoprotein E promote assembly of Alzheimer beta-protein into filaments*. Nature, 1994. **372**(6501): p. 92-4.
103. Verghese, P.B., et al., *ApoE influences amyloid-beta (Abeta) clearance despite minimal apoE/Abeta association in physiological conditions*. Proc Natl Acad Sci U S A, 2013. **110**(19): p. E1807-16.
104. Sagare, A.P., et al., *A lipoprotein receptor cluster IV mutant preferentially binds amyloid-beta and regulates its clearance from the mouse brain*. J Biol Chem, 2013. **288**(21): p. 15154-66.
105. Tu, H., et al., *Presenilins form ER Ca²⁺ leak channels, a function disrupted by familial Alzheimer's disease-linked mutations*. Cell, 2006. **126**(5): p. 981-93.
106. Nelson, O., et al., *Familial Alzheimer disease-linked mutations specifically disrupt Ca²⁺ leak function of presenilin 1*. J Clin Invest, 2007. **117**(5): p. 1230-9.

107. Leissring, M.A., et al., *Capacitative calcium entry deficits and elevated luminal calcium content in mutant presenilin-1 knockin mice*. J Cell Biol, 2000. **149**(4): p. 793-8.
108. Shilling, D., et al., *Lack of evidence for presenilins as endoplasmic reticulum Ca²⁺ leak channels*. J Biol Chem, 2012. **287**(14): p. 10933-44.
109. Chakroborty, S., et al., *Deviant ryanodine receptor-mediated calcium release resets synaptic homeostasis in presymptomatic 3xTg-AD mice*. J Neurosci, 2009. **29**(30): p. 9458-70.
110. Stutzmann, G.E., et al., *Enhanced ryanodine receptor recruitment contributes to Ca²⁺ disruptions in young, adult, and aged Alzheimer's disease mice*. J Neurosci, 2006. **26**(19): p. 5180-9.
111. Shilling, D., et al., *Suppression of InsP3 receptor-mediated Ca²⁺ signaling alleviates mutant presenilin-linked familial Alzheimer's disease pathogenesis*. J Neurosci, 2014. **34**(20): p. 6910-23.
112. Cheung, K.H., et al., *Gain-of-function enhancement of IP3 receptor modal gating by familial Alzheimer's disease-linked presenilin mutants in human cells and mouse neurons*. Sci Signal, 2010. **3**(114): p. ra22.
113. Lopez, J.R., et al., *Increased intraneuronal resting [Ca²⁺] in adult Alzheimer's disease mice*. J Neurochem, 2008. **105**(1): p. 262-71.
114. Bruno, A.M., et al., *Altered ryanodine receptor expression in mild cognitive impairment and Alzheimer's disease*. Neurobiol Aging, 2012. **33**(5): p. 1001 e1-6.
115. Rybalchenko, V., et al., *The cytosolic N-terminus of presenilin-1 potentiates mouse ryanodine receptor single channel activity*. Int J Biochem Cell Biol, 2008. **40**(1): p. 84-97.
116. Wu, B., et al., *Presenilins regulate calcium homeostasis and presynaptic function via ryanodine receptors in hippocampal neurons*. Proc Natl Acad Sci U S A, 2013. **110**(37): p. 15091-6.
117. Zhang, C., et al., *Presenilins are essential for regulating neurotransmitter release*. Nature, 2009. **460**(7255): p. 632-6.
118. Chan, S.L., et al., *Presenilin-1 mutations increase levels of ryanodine receptors and calcium release in PC12 cells and cortical neurons*. J Biol Chem, 2000. **275**(24): p. 18195-200.
119. Stutzmann, G.E., et al., *Dysregulated IP3 signaling in cortical neurons of knock-in mice expressing an Alzheimer's-linked mutation in presenilin1 results in exaggerated Ca²⁺ signals and altered membrane excitability*. J Neurosci, 2004. **24**(2): p. 508-13.

120. Pinton, P., et al., *Calcium and apoptosis: ER-mitochondria Ca²⁺ transfer in the control of apoptosis*. *Oncogene*, 2008. **27**(50): p. 6407-18.
121. Chan, S.L., et al., *Presenilin-1 mutations sensitize neurons to DNA damage-induced death by a mechanism involving perturbed calcium homeostasis and activation of calpains and caspase-12*. *Neurobiol Dis*, 2002. **11**(1): p. 2-19.
122. Lee, S.Y., et al., *PS2 mutation increases neuronal cell vulnerability to neurotoxicants through activation of caspase-3 by enhancing of ryanodine receptor-mediated calcium release*. *FASEB J*, 2006. **20**(1): p. 151-3.
123. Pierrot, N., et al., *Intraneuronal amyloid-beta 1-42 production triggered by sustained increase of cytosolic calcium concentration induces neuronal death*. *J Neurochem*, 2004. **88**(5): p. 1140-50.
124. Lin, H., R. Bhatia, and R. Lal, *Amyloid beta protein forms ion channels: implications for Alzheimer's disease pathophysiology*. *FASEB J*, 2001. **15**(13): p. 2433-44.
125. Varadarajan, S., et al., *Review: Alzheimer's amyloid beta-peptide-associated free radical oxidative stress and neurotoxicity*. *J Struct Biol*, 2000. **130**(2-3): p. 184-208.
126. Simonian, N.A. and B.T. Hyman, *Functional alterations in Alzheimer's disease: selective loss of mitochondrial-encoded cytochrome oxidase mRNA in the hippocampal formation*. *J Neuropathol Exp Neurol*, 1994. **53**(5): p. 508-12.
127. Borger, E., et al., *Mitochondrial beta-amyloid in Alzheimer's disease*. *Biochem Soc Trans*, 2011. **39**(4): p. 868-73.
128. Caspersen, C., et al., *Mitochondrial Abeta: a potential focal point for neuronal metabolic dysfunction in Alzheimer's disease*. *FASEB J*, 2005. **19**(14): p. 2040-1.
129. Hirai, K., et al., *Mitochondrial abnormalities in Alzheimer's disease*. *J Neurosci*, 2001. **21**(9): p. 3017-23.
130. Hirano, A., et al., *The fine structure of some intraganglionic alterations. Neurofibrillary tangles, granulovacuolar bodies and "rod-like" structures as seen in Guam amyotrophic lateral sclerosis and parkinsonism-dementia complex*. *J Neuropathol Exp Neurol*, 1968. **27**(2): p. 167-82.
131. Fechtner, M., et al., *Hirano bodies in health and disease*. *Trends Mol Med*, 2002. **8**(12): p. 590-1.
132. Hirano, A., *Hirano bodies and related neuronal inclusions*. *Neuropathol Appl Neurobiol*, 1994. **20**(1): p. 3-11.

133. Mitake, S., K. Ojika, and A. Hirano, *Hirano bodies and Alzheimer's disease*. Kaohsiung J Med Sci, 1997. **13**(1): p. 10-8.
134. Gibson, P.H. and B.E. Tomlinson, *Numbers of Hirano bodies in the hippocampus of normal and demented people with Alzheimer's disease*. J Neurol Sci, 1977. **33**(1-2): p. 199-206.
135. Gibson, P.H., *Light and electron microscopic observations on the relationship between Hirano bodies, neuron and glial perikarya in the human hippocampus*. Acta Neuropathol, 1978. **42**(3): p. 165-71.
136. Goldman, J.E., *The association of actin with Hirano bodies*. J Neuropathol Exp Neurol, 1983. **42**(2): p. 146-52.
137. Galloway, P.G., G. Perry, and P. Gambetti, *Hirano body filaments contain actin and actin-associated proteins*. J Neuropathol Exp Neurol, 1987. **46**(2): p. 185-99.
138. Maciver, S.K. and C.R. Harrington, *Two actin binding proteins, actin depolymerizing factor and cofilin, are associated with Hirano bodies*. Neuroreport, 1995. **6**(15): p. 1985-8.
139. Peterson, C., et al., *High molecular weight microtubule-associated proteins bind to actin lattices (Hirano bodies)*. Acta Neuropathol, 1988. **77**(2): p. 168-74.
140. Munoz, D.G., D. Wang, and B.D. Greenberg, *Hirano bodies accumulate C-terminal sequences of beta-amyloid precursor protein (beta-APP) epitopes*. J Neuropathol Exp Neurol, 1993. **52**(1): p. 14-21.
141. Galloway, P.G., et al., *Hirano bodies contain tau protein*. Brain Res, 1987. **403**(2): p. 337-40.
142. Furgerson, M., M. Fechheimer, and R. Furukawa, *Model Hirano bodies protect against tau-independent and tau-dependent cell death initiated by the amyloid precursor protein intracellular domain*. PLoS One, 2012. **7**(9): p. e44996.
143. Furgerson, M., et al., *Hirano body expression impairs spatial working memory in a novel mouse model*. Acta Neuropathol Commun, 2014. **2**: p. 131.
144. Rodrigues e Silva, A.M., et al., *Who was the man who discovered the "Lewy bodies"?* Mov Disord, 2010. **25**(12): p. 1765-73.
145. Kim, W.S., K. Kagedal, and G.M. Halliday, *Alpha-synuclein biology in Lewy body diseases*. Alzheimers Res Ther, 2014. **6**(5): p. 73.
146. Arai, Y., et al., *Alpha-synuclein-positive structures in cases with sporadic Alzheimer's disease: morphology and its relationship to tau aggregation*. Brain Res, 2001. **888**(2): p. 287-296.

147. Lippa, C.F., et al., *Lewy bodies contain altered alpha-synuclein in brains of many familial Alzheimer's disease patients with mutations in presenilin and amyloid precursor protein genes*. Am J Pathol, 1998. **153**(5): p. 1365-70.
148. Ueda, K., et al., *Molecular cloning of cDNA encoding an unrecognized component of amyloid in Alzheimer disease*. Proc Natl Acad Sci U S A, 1993. **90**(23): p. 11282-6.
149. Anderson, J.P., et al., *Phosphorylation of Ser-129 is the dominant pathological modification of alpha-synuclein in familial and sporadic Lewy body disease*. J Biol Chem, 2006. **281**(40): p. 29739-52.
150. Nakamura, T., et al., *Activated Fyn phosphorylates alpha-synuclein at tyrosine residue 125*. Biochem Biophys Res Commun, 2001. **280**(4): p. 1085-92.
151. Chavarria, C. and J.M. Souza, *Oxidation and nitration of alpha-synuclein and their implications in neurodegenerative diseases*. Arch Biochem Biophys, 2013. **533**(1-2): p. 25-32.
152. Giasson, B.I., et al., *Oxidative damage linked to neurodegeneration by selective alpha-synuclein nitration in synucleinopathy lesions*. Science, 2000. **290**(5493): p. 985-9.
153. Nonaka, T., T. Iwatsubo, and M. Hasegawa, *Ubiquitination of alpha-synuclein*. Biochemistry, 2005. **44**(1): p. 361-8.
154. Uversky, V.N., *Alpha-synuclein misfolding and neurodegenerative diseases*. Curr Protein Pept Sci, 2008. **9**(5): p. 507-40.
155. Higuchi, S., et al., *Mutation in the alpha-synuclein gene and sporadic Parkinson's disease, Alzheimer's disease, and dementia with lewy bodies*. Exp Neurol, 1998. **153**(1): p. 164-6.
156. Baddeley, A., *Working memory: theories, models, and controversies*. Annu Rev Psychol, 2012. **63**: p. 1-29.
157. Barbey, A.K., M. Koenigs, and J. Grafman, *Dorsolateral prefrontal contributions to human working memory*. Cortex, 2013. **49**(5): p. 1195-205.
158. Wolf, R.C., N. Vasic, and H. Walter, *Differential activation of ventrolateral prefrontal cortex during working memory retrieval*. Neuropsychologia, 2006. **44**(12): p. 2558-63.
159. Euston, D.R., A.J. Gruber, and B.L. McNaughton, *The role of medial prefrontal cortex in memory and decision making*. Neuron, 2012. **76**(6): p. 1057-70.

160. Stern, C.E., et al., *Medial temporal and prefrontal contributions to working memory tasks with novel and familiar stimuli*. Hippocampus, 2001. **11**(4): p. 337-46.
161. Collette, F. and M. Van der Linden, *Brain imaging of the central executive component of working memory*. Neurosci Biobehav Rev, 2002. **26**(2): p. 105-25.
162. Axmacher, N., et al., *Sustained neural activity patterns during working memory in the human medial temporal lobe*. J Neurosci, 2007. **27**(29): p. 7807-16.
163. D'Esposito, M. and B.R. Postle, *The cognitive neuroscience of working memory*. Annu Rev Psychol, 2015. **66**: p. 115-42.
164. Frankland, P.W. and B. Bontempi, *The organization of recent and remote memories*. Nat Rev Neurosci, 2005. **6**(2): p. 119-30.
165. Bruce, D., *Fifty years since Lashley's In search of the Engram: refutations and conjectures*. J Hist Neurosci, 2001. **10**(3): p. 308-18.
166. Squire, L.R. and J.T. Wixted, *The cognitive neuroscience of human memory since H.M.* Annu Rev Neurosci, 2011. **34**: p. 259-88.
167. Jeneson, A. and L.R. Squire, *Working memory, long-term memory, and medial temporal lobe function*. Learn Mem, 2012. **19**(1): p. 15-25.
168. Lewis-Peacock, J.A. and B.R. Postle, *Temporary activation of long-term memory supports working memory*. J Neurosci, 2008. **28**(35): p. 8765-71.
169. Axmacher, N., et al., *Interaction of working memory and long-term memory in the medial temporal lobe*. Cereb Cortex, 2008. **18**(12): p. 2868-78.
170. Schon, K., et al., *Greater working memory load results in greater medial temporal activity at retrieval*. Cereb Cortex, 2009. **19**(11): p. 2561-71.
171. Preston, A.R. and H. Eichenbaum, *Interplay of hippocampus and prefrontal cortex in memory*. Curr Biol, 2013. **23**(17): p. R764-73.
172. Yoon, T., et al., *Prefrontal cortex and hippocampus subserve different components of working memory in rats*. Learn Mem, 2008. **15**(3): p. 97-105.
173. van Strien, N.M., N.L. Cappaert, and M.P. Witter, *The anatomy of memory: an interactive overview of the parahippocampal-hippocampal network*. Nat Rev Neurosci, 2009. **10**(4): p. 272-82.
174. Furtak, S.C., et al., *Functional neuroanatomy of the parahippocampal region in the rat: the perirhinal and postrhinal cortices*. Hippocampus, 2007. **17**(9): p. 709-22.

175. Kerr, K.M., et al., *Functional neuroanatomy of the parahippocampal region: the lateral and medial entorhinal areas*. Hippocampus, 2007. **17**(9): p. 697-708.
176. Neves, G., S.F. Cooke, and T.V. Bliss, *Synaptic plasticity, memory and the hippocampus: a neural network approach to causality*. Nat Rev Neurosci, 2008. **9**(1): p. 65-75.
177. O'Mara, S., *The subiculum: what it does, what it might do, and what neuroanatomy has yet to tell us*. J Anat, 2005. **207**(3): p. 271-82.
178. Yun, S.H., et al., *Cholinergic modulation of synaptic transmission and plasticity in entorhinal cortex and hippocampus of the rat*. Neuroscience, 2000. **97**(4): p. 671-6.
179. Gulyas, A.I., L. Acsady, and T.F. Freund, *Structural basis of the cholinergic and serotonergic modulation of GABAergic neurons in the hippocampus*. Neurochem Int, 1999. **34**(5): p. 359-72.
180. Olvera-Cortes, M.E., et al., *Serotonergic modulation of hippocampal theta activity in relation to hippocampal information processing*. Exp Brain Res, 2013. **230**(4): p. 407-26.
181. Pezze, M. and T. Bast, *Dopaminergic modulation of hippocampus-dependent learning: blockade of hippocampal D1-class receptors during learning impairs 1-trial place memory at a 30-min retention delay*. Neuropharmacology, 2012. **63**(4): p. 710-8.
182. O'Dell, T.J., et al., *beta-Adrenergic receptor signaling and modulation of long-term potentiation in the mammalian hippocampus*. Learn Mem, 2015. **22**(9): p. 461-71.
183. Brown, R.E., et al., *Histaminergic modulation of synaptic plasticity in area CA1 of rat hippocampal slices*. Neuropharmacology, 1995. **34**(2): p. 181-90.
184. Gilbert, P.E. and A.M. Brushfield, *The role of the CA3 hippocampal subregion in spatial memory: a process oriented behavioral assessment*. Prog Neuropsychopharmacol Biol Psychiatry, 2009. **33**(5): p. 774-81.
185. Gilbert, P.E. and R.P. Kesner, *The role of the dorsal CA3 hippocampal subregion in spatial working memory and pattern separation*. Behav Brain Res, 2006. **169**(1): p. 142-9.
186. Florian, C. and P. Roulet, *Hippocampal CA3-region is crucial for acquisition and memory consolidation in Morris water maze task in mice*. Behav Brain Res, 2004. **154**(2): p. 365-74.

187. Stupien, G., C. Florian, and P. Roulet, *Involvement of the hippocampal CA3-region in acquisition and in memory consolidation of spatial but not in object information in mice*. *Neurobiol Learn Mem*, 2003. **80**(1): p. 32-41.
188. Daumas, S., et al., *Encoding, consolidation, and retrieval of contextual memory: differential involvement of dorsal CA3 and CA1 hippocampal subregions*. *Learn Mem*, 2005. **12**(4): p. 375-82.
189. Bahar, A.S., P.R. Shirvalkar, and M.L. Shapiro, *Memory-guided learning: CA1 and CA3 neuronal ensembles differentially encode the commonalities and differences between situations*. *J Neurosci*, 2011. **31**(34): p. 12270-81.
190. Lee, I., T.S. Jerman, and R.P. Kesner, *Disruption of delayed memory for a sequence of spatial locations following CA1- or CA3-lesions of the dorsal hippocampus*. *Neurobiol Learn Mem*, 2005. **84**(2): p. 138-47.
191. Farovik, A., L.M. Dupont, and H. Eichenbaum, *Distinct roles for dorsal CA3 and CA1 in memory for sequential nonspatial events*. *Learn Mem*, 2010. **17**(1): p. 12-17.
192. Hunsaker, M.R., B. Lee, and R.P. Kesner, *Evaluating the temporal context of episodic memory: the role of CA3 and CA1*. *Behav Brain Res*, 2008. **188**(2): p. 310-5.
193. Hunsaker, M.R., et al., *The role of CA3 and CA1 in the acquisition of an object-trace-place paired-associate task*. *Behav Neurosci*, 2006. **120**(6): p. 1252-6.
194. Parent, M.A., et al., *Identification of the hippocampal input to medial prefrontal cortex in vitro*. *Cereb Cortex*, 2010. **20**(2): p. 393-403.
195. Jay, T.M., et al., *Excitatory Amino Acid Pathway from the Hippocampus to the Prefrontal Cortex. Contribution of AMPA Receptors in Hippocampo-prefrontal Cortex Transmission*. *Eur J Neurosci*, 1992. **4**(12): p. 1285-1295.
196. Jay, T.M. and M.P. Witter, *Distribution of hippocampal CA1 and subicular efferents in the prefrontal cortex of the rat studied by means of anterograde transport of Phaseolus vulgaris-leucoagglutinin*. *J Comp Neurol*, 1991. **313**(4): p. 574-86.
197. Jones, M.W. and M.A. Wilson, *Theta rhythms coordinate hippocampal-prefrontal interactions in a spatial memory task*. *PLoS Biol*, 2005. **3**(12): p. e402.
198. Chadwick, M.J., H.M. Bonnici, and E.A. Maguire, *CA3 size predicts the precision of memory recall*. *Proc Natl Acad Sci U S A*, 2014. **111**(29): p. 10720-5.
199. Dudai, Y., *The restless engram: consolidations never end*. *Annu Rev Neurosci*, 2012. **35**: p. 227-47.

200. Cajal, R.Y., *The Croonian Lecture: La Fine Structure des Centres Nerveux*. Proceedings of the Royal Society of London, 1894. **55**: p. 444-468.
201. Hebb, D.O., *The Organization of Behavior*. 1949, New York, NY: Wiley.
202. Caporale, N. and Y. Dan, *Spike timing-dependent plasticity: a Hebbian learning rule*. *Annu Rev Neurosci*, 2008. **31**: p. 25-46.
203. Castellucci, V., et al., *Neuronal mechanisms of habituation and dishabituation of the gill-withdrawal reflex in Aplysia*. *Science*, 1970. **167**(3926): p. 1745-8.
204. Castellucci, V. and E.R. Kandel, *Presynaptic facilitation as a mechanism for behavioral sensitization in Aplysia*. *Science*, 1976. **194**(4270): p. 1176-8.
205. Carew, T.J., E.T. Walters, and E.R. Kandel, *Classical conditioning in a simple withdrawal reflex in Aplysia californica*. *J Neurosci*, 1981. **1**(12): p. 1426-37.
206. Walters, E.T., T.J. Carew, and E.R. Kandel, *Associative Learning in Aplysia: evidence for conditioned fear in an invertebrate*. *Science*, 1981. **211**(4481): p. 504-6.
207. Carew, T.J., E.T. Walters, and E.R. Kandel, *Associative learning in Aplysia: cellular correlates supporting a conditioned fear hypothesis*. *Science*, 1981. **211**(4481): p. 501-4.
208. Montarolo, P.G., et al., *A critical period for macromolecular synthesis in long-term heterosynaptic facilitation in Aplysia*. *Science*, 1986. **234**(4781): p. 1249-54.
209. Byrne, J.H. and E.R. Kandel, *Presynaptic facilitation revisited: state and time dependence*. *J Neurosci*, 1996. **16**(2): p. 425-35.
210. Maren, S., *Long-term potentiation in the amygdala: a mechanism for emotional learning and memory*. *Trends Neurosci*, 1999. **22**(12): p. 561-7.
211. Rodrigues, S.M., G.E. Schafe, and J.E. LeDoux, *Molecular mechanisms underlying emotional learning and memory in the lateral amygdala*. *Neuron*, 2004. **44**(1): p. 75-91.
212. Pitkanen, A., et al., *Reciprocal connections between the amygdala and the hippocampal formation, perirhinal cortex, and postrhinal cortex in rat. A review*. *Ann N Y Acad Sci*, 2000. **911**: p. 369-91.
213. Rogan, M.T., U.V. Staubli, and J.E. LeDoux, *Fear conditioning induces associative long-term potentiation in the amygdala*. *Nature*, 1997. **390**(6660): p. 604-7.
214. Whitlock, J.R., et al., *Learning induces long-term potentiation in the hippocampus*. *Science*, 2006. **313**(5790): p. 1093-7.

215. Sutherland, R.J., B. Kolb, and I.Q. Whishaw, *Spatial mapping: definitive disruption by hippocampal or medial frontal cortical damage in the rat*. *Neurosci Lett*, 1982. **31**(3): p. 271-6.
216. Morris, R.G., et al., *Place navigation impaired in rats with hippocampal lesions*. *Nature*, 1982. **297**(5868): p. 681-3.
217. Morris, R., *Developments of a water-maze procedure for studying spatial learning in the rat*. *J Neurosci Methods*, 1984. **11**(1): p. 47-60.
218. Maguire, E.A., et al., *Knowing where and getting there: a human navigation network*. *Science*, 1998. **280**(5365): p. 921-4.
219. O'Keefe, J., *Place units in the hippocampus of the freely moving rat*. *Exp Neurol*, 1976. **51**(1): p. 78-109.
220. Muller, R.U. and J.L. Kubie, *The effects of changes in the environment on the spatial firing of hippocampal complex-spike cells*. *J Neurosci*, 1987. **7**(7): p. 1951-68.
221. Hafting, T., et al., *Microstructure of a spatial map in the entorhinal cortex*. *Nature*, 2005. **436**(7052): p. 801-6.
222. Rotenberg, A., et al., *Mice expressing activated CaMKII lack low frequency LTP and do not form stable place cells in the CA1 region of the hippocampus*. *Cell*, 1996. **87**(7): p. 1351-61.
223. Sharp, P.E., B.L. McNaughton, and C.A. Barnes, *Enhancement of hippocampal field potentials in rats exposed to a novel, complex environment*. *Brain Res*, 1985. **339**(2): p. 361-5.
224. Moser, E.I., *Learning-related changes in hippocampal field potentials*. *Behav Brain Res*, 1995. **71**(1-2): p. 11-8.
225. Martin, S.J., P.D. Grimwood, and R.G. Morris, *Synaptic plasticity and memory: an evaluation of the hypothesis*. *Annu Rev Neurosci*, 2000. **23**: p. 649-711.
226. McNaughton, B.L., et al., *Long-term enhancement of hippocampal synaptic transmission and the acquisition of spatial information*. *J Neurosci*, 1986. **6**(2): p. 563-71.
227. Castro, C.A., et al., *Recovery of spatial learning deficits after decay of electrically induced synaptic enhancement in the hippocampus*. *Nature*, 1989. **342**(6249): p. 545-8.
228. Moser, E.I., et al., *Impaired spatial learning after saturation of long-term potentiation*. *Science*, 1998. **281**(5385): p. 2038-42.

229. Bach, M.E., et al., *Age-related defects in spatial memory are correlated with defects in the late phase of hippocampal long-term potentiation in vitro and are attenuated by drugs that enhance the cAMP signaling pathway*. Proc Natl Acad Sci U S A, 1999. **96**(9): p. 5280-5.
230. Malenka, R.C. and M.F. Bear, *LTP and LTD: an embarrassment of riches*. Neuron, 2004. **44**(1): p. 5-21.
231. Castillo, P.E., *Presynaptic LTP and LTD of excitatory and inhibitory synapses*. Cold Spring Harb Perspect Biol, 2012. **4**(2).
232. Zucker, R.S. and W.G. Regehr, *Short-term synaptic plasticity*. Annu Rev Physiol, 2002. **64**: p. 355-405.
233. Katz, B. and R. Miledi, *Estimates of quantal content during 'chemical potentiation' of transmitter release*. Proc R Soc Lond B Biol Sci, 1979. **205**(1160): p. 369-78.
234. Kamiya, H. and R.S. Zucker, *Residual Ca²⁺ and short-term synaptic plasticity*. Nature, 1994. **371**(6498): p. 603-6.
235. Bains, J.S., J.M. Longacher, and K.J. Staley, *Reciprocal interactions between CA3 network activity and strength of recurrent collateral synapses*. Nat Neurosci, 1999. **2**(8): p. 720-6.
236. Hasselmo, M.E., E. Schnell, and E. Barkai, *Dynamics of learning and recall at excitatory recurrent synapses and cholinergic modulation in rat hippocampal region CA3*. J Neurosci, 1995. **15**(7 Pt 2): p. 5249-62.
237. Jaaskelainen, I.P., et al., *Short-term plasticity as a neural mechanism supporting memory and attentional functions*. Brain Res, 2011. **1422**: p. 66-81.
238. Fuster, J.M. and G.E. Alexander, *Neuron activity related to short-term memory*. Science, 1971. **173**(3997): p. 652-4.
239. Lømo, T., *The discovery of long-term potentiation*. Philos Trans R Soc Lond B Biol Sci, 2003. **358**(1432): p. 617-20.
240. Lømo, T., *Frequency potentiation of excitatory synaptic activity in the dentate area of the hippocampal formation*. Acta Physiologica Scandinavica, 1966. **68**(Supplement 277): p. 128.
241. Bliss, T.V. and T. Lømo, *Long-lasting potentiation of synaptic transmission in the dentate area of the anaesthetized rabbit following stimulation of the perforant path*. J Physiol, 1973. **232**(2): p. 331-56.
242. Douglas, R.M. and G.V. Goddard, *Long-term potentiation of the perforant path-granule cell synapse in the rat hippocampus*. Brain Res, 1975. **86**(2): p. 205-15.

243. Alger, B.E. and T.J. Teyler, *Long-term and short-term plasticity in the CA1, CA3, and dentate regions of the rat hippocampal slice*. Brain Res, 1976. **110**(3): p. 463-80.
244. Kostopoulos, G., C. Psarropoulou, and H.L. Haas, *Membrane properties, response to amines and to tetanic stimulation of hippocampal neurons in the genetically epileptic mutant mouse tottering*. Exp Brain Res, 1988. **72**(1): p. 45-50.
245. Payne, K., et al., *Evoked potentials and long-term potentiation in the mouse dentate gyrus after stimulation of the entorhinal cortex*. Exp Neurol, 1982. **75**(1): p. 134-48.
246. Skrebitsky, V.G. and V.S. Vorobyev, *A study of synaptic plasticity in hippocampal slices*. Acta Neurobiol Exp (Wars), 1979. **39**(6): p. 633-42.
247. Collingridge, G.L., S.J. Kehl, and H. McLennan, *Excitatory amino acids in synaptic transmission in the Schaffer collateral-commissural pathway of the rat hippocampus*. J Physiol, 1983. **334**: p. 33-46.
248. Harris, E.W., A.H. Ganong, and C.W. Cotman, *Long-term potentiation in the hippocampus involves activation of N-methyl-D-aspartate receptors*. Brain Res, 1984. **323**(1): p. 132-7.
249. Malenka, R.C. and R.A. Nicoll, *NMDA-receptor-dependent synaptic plasticity: multiple forms and mechanisms*. Trends Neurosci, 1993. **16**(12): p. 521-7.
250. Mayer, M.L., G.L. Westbrook, and P.B. Guthrie, *Voltage-dependent block by Mg²⁺ of NMDA responses in spinal cord neurones*. Nature, 1984. **309**(5965): p. 261-3.
251. Nowak, L., et al., *Magnesium gates glutamate-activated channels in mouse central neurones*. Nature, 1984. **307**(5950): p. 462-5.
252. Collingridge, G.L., C.E. Herron, and R.A. Lester, *Frequency-dependent N-methyl-D-aspartate receptor-mediated synaptic transmission in rat hippocampus*. J Physiol, 1988. **399**: p. 301-12.
253. Herron, C.E., et al., *Frequency-dependent involvement of NMDA receptors in the hippocampus: a novel synaptic mechanism*. Nature, 1986. **322**(6076): p. 265-8.
254. Malenka, R.C., et al., *Postsynaptic calcium is sufficient for potentiation of hippocampal synaptic transmission*. Science, 1988. **242**(4875): p. 81-4.
255. Perkel, D.J. and R.A. Nicoll, *Evidence for all-or-none regulation of neurotransmitter release: implications for long-term potentiation*. J Physiol, 1993. **471**: p. 481-500.

256. Kauer, J.A., R.C. Malenka, and R.A. Nicoll, *A persistent postsynaptic modification mediates long-term potentiation in the hippocampus*. *Neuron*, 1988. **1**(10): p. 911-7.
257. Kirkwood, A., et al., *Common forms of synaptic plasticity in the hippocampus and neocortex in vitro*. *Science*, 1993. **260**(5113): p. 1518-21.
258. Feldman, D.E., *Synaptic mechanisms for plasticity in neocortex*. *Annu Rev Neurosci*, 2009. **32**: p. 33-55.
259. Bortolotto, Z.A., et al., *Kainate receptors are involved in synaptic plasticity*. *Nature*, 1999. **402**(6759): p. 297-301.
260. Schmitz, D., J. Mellor, and R.A. Nicoll, *Presynaptic kainate receptor mediation of frequency facilitation at hippocampal mossy fiber synapses*. *Science*, 2001. **291**(5510): p. 1972-6.
261. Zalutsky, R.A. and R.A. Nicoll, *Comparison of two forms of long-term potentiation in single hippocampal neurons*. *Science*, 1990. **248**(4963): p. 1619-24.
262. Errington, M.L., M.A. Lynch, and T.V. Bliss, *Long-term potentiation in the dentate gyrus: induction and increased glutamate release are blocked by D(-)aminophosphonovalerate*. *Neuroscience*, 1987. **20**(1): p. 279-84.
263. Goldman, R.S., L.E. Chavez-Noriega, and C.F. Stevens, *Failure to reverse long-term potentiation by coupling sustained presynaptic activity and N-methyl-D-aspartate receptor blockade*. *Proc Natl Acad Sci U S A*, 1990. **87**(18): p. 7165-9.
264. Lynch, G., et al., *Intracellular injections of EGTA block induction of hippocampal long-term potentiation*. *Nature*, 1983. **305**(5936): p. 719-21.
265. Malenka, R.C., B. Lancaster, and R.S. Zucker, *Temporal limits on the rise in postsynaptic calcium required for the induction of long-term potentiation*. *Neuron*, 1992. **9**(1): p. 121-8.
266. Wang, J.H. and P.T. Kelly, *Postsynaptic injection of CA2+/CaM induces synaptic potentiation requiring CaMKII and PKC activity*. *Neuron*, 1995. **15**(2): p. 443-52.
267. Lisman, J., R. Yasuda, and S. Raghavachari, *Mechanisms of CaMKII action in long-term potentiation*. *Nat Rev Neurosci*, 2012. **13**(3): p. 169-82.
268. Lledo, P.M., et al., *Calcium/calmodulin-dependent kinase II and long-term potentiation enhance synaptic transmission by the same mechanism*. *Proc Natl Acad Sci U S A*, 1995. **92**(24): p. 11175-9.
269. Pettit, D.L., S. Perlman, and R. Malinow, *Potentiated transmission and prevention of further LTP by increased CaMKII activity in postsynaptic hippocampal slice neurons*. *Science*, 1994. **266**(5192): p. 1881-5.

270. Lee, S.J., et al., *Activation of CaMKII in single dendritic spines during long-term potentiation*. Nature, 2009. **458**(7236): p. 299-304.
271. Redondo, R.L., et al., *Synaptic tagging and capture: differential role of distinct calcium/calmodulin kinases in protein synthesis-dependent long-term potentiation*. J Neurosci, 2010. **30**(14): p. 4981-9.
272. Otmakhov, N., L.C. Griffith, and J.E. Lisman, *Postsynaptic inhibitors of calcium/calmodulin-dependent protein kinase type II block induction but not maintenance of pairing-induced long-term potentiation*. J Neurosci, 1997. **17**(14): p. 5357-65.
273. Ito, I., H. Hidaka, and H. Sugiyama, *Effects of KN-62, a specific inhibitor of calcium/calmodulin-dependent protein kinase II, on long-term potentiation in the rat hippocampus*. Neurosci Lett, 1991. **121**(1-2): p. 119-21.
274. Malinow, R., H. Schulman, and R.W. Tsien, *Inhibition of postsynaptic PKC or CaMKII blocks induction but not expression of LTP*. Science, 1989. **245**(4920): p. 862-6.
275. Silva, A.J., et al., *Deficient hippocampal long-term potentiation in alpha-calcium-calmodulin kinase II mutant mice*. Science, 1992. **257**(5067): p. 201-6.
276. Silva, A.J., et al., *Alpha calcium/calmodulin kinase II mutant mice: deficient long-term potentiation and impaired spatial learning*. Cold Spring Harb Symp Quant Biol, 1992. **57**: p. 527-39.
277. Balakrishnan, V., G. Srinivasan, and H. von Gersdorff, *Post-tetanic potentiation involves the presynaptic binding of calcium to calmodulin*. J Gen Physiol, 2010. **136**(3): p. 243-5.
278. Giese, K.P., et al., *Autophosphorylation at Thr286 of the alpha calcium-calmodulin kinase II in LTP and learning*. Science, 1998. **279**(5352): p. 870-3.
279. Miller, S.G., B.L. Patton, and M.B. Kennedy, *Sequences of autophosphorylation sites in neuronal type II CaM kinase that control Ca²⁺(+)-independent activity*. Neuron, 1988. **1**(7): p. 593-604.
280. Pi, H.J., et al., *Autonomous CaMKII can promote either long-term potentiation or long-term depression, depending on the state of T305/T306 phosphorylation*. J Neurosci, 2010. **30**(26): p. 8704-9.
281. Bach, M.E., et al., *Impairment of spatial but not contextual memory in CaMKII mutant mice with a selective loss of hippocampal LTP in the range of the theta frequency*. Cell, 1995. **81**(6): p. 905-15.
282. Lemieux, M., et al., *Translocation of CaMKII to dendritic microtubules supports the plasticity of local synapses*. J Cell Biol, 2012. **198**(6): p. 1055-73.

283. Shen, K. and T. Meyer, *Dynamic control of CaMKII translocation and localization in hippocampal neurons by NMDA receptor stimulation*. Science, 1999. **284**(5411): p. 162-6.
284. Sanhueza, M., et al., *Role of the CaMKII/NMDA receptor complex in the maintenance of synaptic strength*. J Neurosci, 2011. **31**(25): p. 9170-8.
285. Gardoni, F., et al., *Calcium/calmodulin-dependent protein kinase II is associated with NR2A/B subunits of NMDA receptor in postsynaptic densities*. J Neurochem, 1998. **71**(4): p. 1733-41.
286. Bayer, K.U., et al., *Interaction with the NMDA receptor locks CaMKII in an active conformation*. Nature, 2001. **411**(6839): p. 801-5.
287. Barria, A. and R. Malinow, *NMDA receptor subunit composition controls synaptic plasticity by regulating binding to CaMKII*. Neuron, 2005. **48**(2): p. 289-301.
288. Raveendran, R., et al., *Phosphorylation status of the NR2B subunit of NMDA receptor regulates its interaction with calcium/calmodulin-dependent protein kinase II*. J Neurochem, 2009. **110**(1): p. 92-105.
289. Lisman, J. and S. Raghavachari, *Biochemical principles underlying the stable maintenance of LTP by the CaMKII/NMDAR complex*. Brain Res, 2014.
290. Merrill, M.A., et al., *Activity-driven postsynaptic translocation of CaMKII*. Trends Pharmacol Sci, 2005. **26**(12): p. 645-53.
291. Barria, A., et al., *Regulatory phosphorylation of AMPA-type glutamate receptors by CaM-KII during long-term potentiation*. Science, 1997. **276**(5321): p. 2042-5.
292. Mammen, A.L., et al., *Phosphorylation of the alpha-amino-3-hydroxy-5-methylisoxazole4-propionic acid receptor GluR1 subunit by calcium/calmodulin-dependent kinase II*. J Biol Chem, 1997. **272**(51): p. 32528-33.
293. Benke, T.A., et al., *Modulation of AMPA receptor unitary conductance by synaptic activity*. Nature, 1998. **393**(6687): p. 793-7.
294. Kristensen, A.S., et al., *Mechanism of Ca²⁺/calmodulin-dependent kinase II regulation of AMPA receptor gating*. Nat Neurosci, 2011. **14**(6): p. 727-35.
295. Makino, H. and R. Malinow, *AMPA receptor incorporation into synapses during LTP: the role of lateral movement and exocytosis*. Neuron, 2009. **64**(3): p. 381-90.
296. Tardin, C., et al., *Direct imaging of lateral movements of AMPA receptors inside synapses*. EMBO J, 2003. **22**(18): p. 4656-65.

297. Borgdorff, A.J. and D. Choquet, *Regulation of AMPA receptor lateral movements*. Nature, 2002. **417**(6889): p. 649-53.
298. Pickard, L., et al., *Transient synaptic activation of NMDA receptors leads to the insertion of native AMPA receptors at hippocampal neuronal plasma membranes*. Neuropharmacology, 2001. **41**(6): p. 700-13.
299. Lu, W., et al., *Activation of synaptic NMDA receptors induces membrane insertion of new AMPA receptors and LTP in cultured hippocampal neurons*. Neuron, 2001. **29**(1): p. 243-54.
300. Shi, S.H., et al., *Rapid spine delivery and redistribution of AMPA receptors after synaptic NMDA receptor activation*. Science, 1999. **284**(5421): p. 1811-6.
301. Chen, L., et al., *Stargazin regulates synaptic targeting of AMPA receptors by two distinct mechanisms*. Nature, 2000. **408**(6815): p. 936-43.
302. Chetkovich, D.M., et al., *Phosphorylation of the postsynaptic density-95 (PSD-95)/discs large/zona occludens-1 binding site of stargazin regulates binding to PSD-95 and synaptic targeting of AMPA receptors*. J Neurosci, 2002. **22**(14): p. 5791-6.
303. Schnell, E., et al., *Direct interactions between PSD-95 and stargazin control synaptic AMPA receptor number*. Proc Natl Acad Sci U S A, 2002. **99**(21): p. 13902-7.
304. Tomita, S., et al., *Stargazin modulates AMPA receptor gating and trafficking by distinct domains*. Nature, 2005. **435**(7045): p. 1052-8.
305. Tomita, S., et al., *Bidirectional synaptic plasticity regulated by phosphorylation of stargazin-like TARPs*. Neuron, 2005. **45**(2): p. 269-77.
306. Turetsky, D., E. Garringer, and D.K. Patneau, *Stargazin modulates native AMPA receptor functional properties by two distinct mechanisms*. J Neurosci, 2005. **25**(32): p. 7438-48.
307. Bats, C., L. Groc, and D. Choquet, *The interaction between Stargazin and PSD-95 regulates AMPA receptor surface trafficking*. Neuron, 2007. **53**(5): p. 719-34.
308. Sumioka, A., D. Yan, and S. Tomita, *TARP phosphorylation regulates synaptic AMPA receptors through lipid bilayers*. Neuron, 2010. **66**(5): p. 755-67.
309. Boehm, J., et al., *Synaptic incorporation of AMPA receptors during LTP is controlled by a PKC phosphorylation site on GluR1*. Neuron, 2006. **51**(2): p. 213-25.

310. Lee, H.K., et al., *Identification and characterization of a novel phosphorylation site on the GluR1 subunit of AMPA receptors*. Mol Cell Neurosci, 2007. **36**(1): p. 86-94.
311. Jenkins, M.A. and S.F. Traynelis, *PKC phosphorylates GluA1-Ser831 to enhance AMPA receptor conductance*. Channels (Austin), 2012. **6**(1): p. 60-4.
312. Yamazaki, M., et al., *A novel action of stargazin as an enhancer of AMPA receptor activity*. Neurosci Res, 2004. **50**(4): p. 369-74.
313. Esteban, J.A., et al., *PKA phosphorylation of AMPA receptor subunits controls synaptic trafficking underlying plasticity*. Nat Neurosci, 2003. **6**(2): p. 136-43.
314. Roche, K.W., et al., *Characterization of multiple phosphorylation sites on the AMPA receptor GluR1 subunit*. Neuron, 1996. **16**(6): p. 1179-88.
315. Diering, G.H., A.S. Gustina, and R.L. Huganir, *PKA-GluA1 coupling via AKAP5 controls AMPA receptor phosphorylation and cell-surface targeting during bidirectional homeostatic plasticity*. Neuron, 2014. **84**(4): p. 790-805.
316. Leonard, A.S., et al., *SAP97 is associated with the alpha-amino-3-hydroxy-5-methylisoxazole-4-propionic acid receptor GluR1 subunit*. J Biol Chem, 1998. **273**(31): p. 19518-24.
317. Nikandrova, Y.A., et al., *Ca²⁺/calmodulin-dependent protein kinase II binds to and phosphorylates a specific SAP97 splice variant to disrupt association with AKAP79/150 and modulate alpha-amino-3-hydroxy-5-methyl-4-isoxazolepropionic acid-type glutamate receptor (AMPA) activity*. J Biol Chem, 2010. **285**(2): p. 923-34.
318. Mauceri, D., et al., *Calcium/calmodulin-dependent protein kinase II phosphorylation drives synapse-associated protein 97 into spines*. J Biol Chem, 2004. **279**(22): p. 23813-21.
319. Wu, H., et al., *Interaction of SAP97 with minus-end-directed actin motor myosin VI. Implications for AMPA receptor trafficking*. J Biol Chem, 2002. **277**(34): p. 30928-34.
320. Passafaro, M., V. Piech, and M. Sheng, *Subunit-specific temporal and spatial patterns of AMPA receptor exocytosis in hippocampal neurons*. Nat Neurosci, 2001. **4**(9): p. 917-26.
321. Shi, S., et al., *Subunit-specific rules governing AMPA receptor trafficking to synapses in hippocampal pyramidal neurons*. Cell, 2001. **105**(3): p. 331-43.
322. Collingridge, G.L., J.T. Isaac, and Y.T. Wang, *Receptor trafficking and synaptic plasticity*. Nat Rev Neurosci, 2004. **5**(12): p. 952-62.

323. Klann, E. and T.E. Dever, *Biochemical mechanisms for translational regulation in synaptic plasticity*. Nat Rev Neurosci, 2004. **5**(12): p. 931-42.
324. Sutton, M.A. and E.M. Schuman, *Local translational control in dendrites and its role in long-term synaptic plasticity*. J Neurobiol, 2005. **64**(1): p. 116-31.
325. Kelleher, R.J., 3rd, et al., *Translational control by MAPK signaling in long-term synaptic plasticity and memory*. Cell, 2004. **116**(3): p. 467-79.
326. Banko, J.L., L. Hou, and E. Klann, *NMDA receptor activation results in PKA- and ERK-dependent Mnk1 activation and increased eIF4E phosphorylation in hippocampal area CA1*. J Neurochem, 2004. **91**(2): p. 462-70.
327. Yuste, R. and T. Bonhoeffer, *Morphological changes in dendritic spines associated with long-term synaptic plasticity*. Annu Rev Neurosci, 2001. **24**: p. 1071-89.
328. Toni, N., et al., *LTP promotes formation of multiple spine synapses between a single axon terminal and a dendrite*. Nature, 1999. **402**(6760): p. 421-5.
329. Shepherd, J.D. and R.L. Huganir, *The cell biology of synaptic plasticity: AMPA receptor trafficking*. Annu Rev Cell Dev Biol, 2007. **23**: p. 613-43.
330. Ju, W., et al., *Activity-dependent regulation of dendritic synthesis and trafficking of AMPA receptors*. Nat Neurosci, 2004. **7**(3): p. 244-53.
331. Hirokawa, N. and R. Takemura, *Molecular motors and mechanisms of directional transport in neurons*. Nat Rev Neurosci, 2005. **6**(3): p. 201-14.
332. Cui-Wang, T., et al., *Local zones of endoplasmic reticulum complexity confine cargo in neuronal dendrites*. Cell, 2012. **148**(1-2): p. 309-21.
333. Watt, A.J., et al., *A proportional but slower NMDA potentiation follows AMPA potentiation in LTP*. Nat Neurosci, 2004. **7**(5): p. 518-24.
334. Grosshans, D.R., et al., *LTP leads to rapid surface expression of NMDA but not AMPA receptors in adult rat CA1*. Nat Neurosci, 2002. **5**(1): p. 27-33.
335. Lau, C.G. and R.S. Zukin, *NMDA receptor trafficking in synaptic plasticity and neuropsychiatric disorders*. Nat Rev Neurosci, 2007. **8**(6): p. 413-26.
336. Chung, H.J., et al., *Regulation of the NMDA receptor complex and trafficking by activity-dependent phosphorylation of the NR2B subunit PDZ ligand*. J Neurosci, 2004. **24**(45): p. 10248-59.
337. Barria, A. and R. Malinow, *Subunit-specific NMDA receptor trafficking to synapses*. Neuron, 2002. **35**(2): p. 345-53.

338. Groc, L., et al., *NMDA receptor surface mobility depends on NR2A-2B subunits*. Proc Natl Acad Sci U S A, 2006. **103**(49): p. 18769-74.
339. Tang, Y.P., et al., *Genetic enhancement of learning and memory in mice*. Nature, 1999. **401**(6748): p. 63-9.
340. Lan, J.Y., et al., *Activation of metabotropic glutamate receptor 1 accelerates NMDA receptor trafficking*. J Neurosci, 2001. **21**(16): p. 6058-68.
341. Matta, J.A., et al., *mGluR5 and NMDA receptors drive the experience- and activity-dependent NMDA receptor NR2B to NR2A subunit switch*. Neuron, 2011. **70**(2): p. 339-51.
342. Yan, J.Z., et al., *Protein kinase C promotes N-methyl-D-aspartate (NMDA) receptor trafficking by indirectly triggering calcium/calmodulin-dependent protein kinase II (CaMKII) autophosphorylation*. J Biol Chem, 2011. **286**(28): p. 25187-200.
343. Kim, M.J., et al., *Differential roles of NR2A- and NR2B-containing NMDA receptors in Ras-ERK signaling and AMPA receptor trafficking*. Neuron, 2005. **46**(5): p. 745-60.
344. Lan, J.Y., et al., *Protein kinase C modulates NMDA receptor trafficking and gating*. Nat Neurosci, 2001. **4**(4): p. 382-90.
345. Lee, Y.S. and A.J. Silva, *The molecular and cellular biology of enhanced cognition*. Nat Rev Neurosci, 2009. **10**(2): p. 126-40.
346. Sun, P., et al., *Differential activation of CREB by Ca²⁺/calmodulin-dependent protein kinases type II and type IV involves phosphorylation of a site that negatively regulates activity*. Genes Dev, 1994. **8**(21): p. 2527-39.
347. Chetkovich, D.M. and J.D. Sweatt, *nMDA receptor activation increases cyclic AMP in area CA1 of the hippocampus via calcium/calmodulin stimulation of adenylyl cyclase*. J Neurochem, 1993. **61**(5): p. 1933-42.
348. Nguyen, P.V. and E.R. Kandel, *Brief theta-burst stimulation induces a transcription-dependent late phase of LTP requiring cAMP in area CA1 of the mouse hippocampus*. Learn Mem, 1997. **4**(2): p. 230-43.
349. Genoux, D., et al., *Protein phosphatase 1 is a molecular constraint on learning and memory*. Nature, 2002. **418**(6901): p. 970-5.
350. Impey, S., et al., *Cross talk between ERK and PKA is required for Ca²⁺ stimulation of CREB-dependent transcription and ERK nuclear translocation*. Neuron, 1998. **21**(4): p. 869-83.

351. Ying, S.W., et al., *Brain-derived neurotrophic factor induces long-term potentiation in intact adult hippocampus: requirement for ERK activation coupled to CREB and upregulation of Arc synthesis*. J Neurosci, 2002. **22**(5): p. 1532-40.
352. Ofir, R., et al., *CREB represses transcription of fos promoter: role of phosphorylation*. Gene Expr, 1991. **1**(1): p. 55-60.
353. Xing, J., D.D. Ginty, and M.E. Greenberg, *Coupling of the RAS-MAPK pathway to gene activation by RSK2, a growth factor-regulated CREB kinase*. Science, 1996. **273**(5277): p. 959-63.
354. Hirokawa, N., *mRNA transport in dendrites: RNA granules, motors, and tracks*. J Neurosci, 2006. **26**(27): p. 7139-42.
355. Balasanyan, V. and D.B. Arnold, *Actin and myosin-dependent localization of mRNA to dendrites*. PLoS One, 2014. **9**(3): p. e92349.
356. Dynes, J.L. and O. Steward, *Dynamics of bidirectional transport of Arc mRNA in neuronal dendrites*. J Comp Neurol, 2007. **500**(3): p. 433-47.
357. Grooms, S.Y., et al., *Activity bidirectionally regulates AMPA receptor mRNA abundance in dendrites of hippocampal neurons*. J Neurosci, 2006. **26**(32): p. 8339-51.
358. Steward, O. and P.F. Worley, *Selective targeting of newly synthesized Arc mRNA to active synapses requires NMDA receptor activation*. Neuron, 2001. **30**(1): p. 227-40.
359. Frey, U., et al., *Long-term potentiation induced in dendrites separated from rat's CA1 pyramidal somata does not establish a late phase*. Neurosci Lett, 1989. **97**(1-2): p. 135-9.
360. Vickers, C.A., K.S. Dickson, and D.J. Wyllie, *Induction and maintenance of late-phase long-term potentiation in isolated dendrites of rat hippocampal CA1 pyramidal neurones*. J Physiol, 2005. **568**(Pt 3): p. 803-13.
361. Guzowski, J.F., et al., *Inhibition of activity-dependent arc protein expression in the rat hippocampus impairs the maintenance of long-term potentiation and the consolidation of long-term memory*. J Neurosci, 2000. **20**(11): p. 3993-4001.
362. Bourtschuladze, R., et al., *Deficient long-term memory in mice with a targeted mutation of the cAMP-responsive element-binding protein*. Cell, 1994. **79**(1): p. 59-68.
363. Jones, M.W., et al., *A requirement for the immediate early gene Zif268 in the expression of late LTP and long-term memories*. Nat Neurosci, 2001. **4**(3): p. 289-96.

364. Renaudineau, S., et al., *Impaired long-term stability of CA1 place cell representation in mice lacking the transcription factor zif268/egr1*. Proc Natl Acad Sci U S A, 2009. **106**(28): p. 11771-5.
365. Pastalkova, E., et al., *Storage of spatial information by the maintenance mechanism of LTP*. Science, 2006. **313**(5790): p. 1141-4.
366. Serrano, P., Y. Yao, and T.C. Sacktor, *Persistent phosphorylation by protein kinase Mzeta maintains late-phase long-term potentiation*. J Neurosci, 2005. **25**(8): p. 1979-84.
367. Shema, R., T.C. Sacktor, and Y. Dudai, *Rapid erasure of long-term memory associations in the cortex by an inhibitor of PKM zeta*. Science, 2007. **317**(5840): p. 951-3.
368. Volk, L.J., et al., *PKM-zeta is not required for hippocampal synaptic plasticity, learning and memory*. Nature, 2013. **493**(7432): p. 420-3.
369. Lee, A.M., et al., *Prkcz null mice show normal learning and memory*. Nature, 2013. **493**(7432): p. 416-9.
370. Bannerman, D.M., et al., *Distinct components of spatial learning revealed by prior training and NMDA receptor blockade*. Nature, 1995. **378**(6553): p. 182-6.
371. Morris, R.G., et al., *Selective impairment of learning and blockade of long-term potentiation by an N-methyl-D-aspartate receptor antagonist, AP5*. Nature, 1986. **319**(6056): p. 774-6.
372. Morris, R.G., *Synaptic plasticity and learning: selective impairment of learning rats and blockade of long-term potentiation in vivo by the N-methyl-D-aspartate receptor antagonist AP5*. J Neurosci, 1989. **9**(9): p. 3040-57.
373. Inglis, J., S.J. Martin, and R.G. Morris, *Upstairs/downstairs revisited: spatial pretraining-induced rescue of normal spatial learning during selective blockade of hippocampal N-methyl-d-aspartate receptors*. Eur J Neurosci, 2013. **37**(5): p. 718-27.
374. Uekita, T. and H. Okaichi, *Pretraining does not ameliorate spatial learning deficits induced by intrahippocampal infusion of AP5*. Behav Neurosci, 2009. **123**(3): p. 520-6.
375. Olton, D.S. and R.J. Samuelson, *Remembrance of places passed: Spatial memory in rats*. Journal of Experimental Psychology: Animal Behavior Processes, 1976. **2** (2): p. 97-116.
376. Yoshihara, T. and Y. Ichitani, *Hippocampal N-methyl-D-aspartate receptor-mediated encoding and retrieval processes in spatial working memory: delay-interposed radial maze performance in rats*. Neuroscience, 2004. **129**(1): p. 1-10.

377. Caramanos, Z. and M.L. Shapiro, *Spatial memory and N-methyl-D-aspartate receptor antagonists APV and MK-801: memory impairments depend on familiarity with the environment, drug dose, and training duration*. Behav Neurosci, 1994. **108**(1): p. 30-43.
378. Shapiro, M.L. and C. O'Connor, *N-methyl-D-aspartate receptor antagonist MK-801 and spatial memory representation: working memory is impaired in an unfamiliar environment but not in a familiar environment*. Behav Neurosci, 1992. **106**(4): p. 604-12.
379. Yamada, K., et al., *Hippocampal AP5 treatment impairs both spatial working and reference memory in radial maze performance in rats*. Eur J Pharmacol, 2015. **758**: p. 137-41.
380. Kawabe, K., Y. Ichitani, and T. Iwasaki, *Effects of intrahippocampal AP5 treatment on radial-arm maze performance in rats*. Brain Res, 1998. **781**(1-2): p. 300-6.
381. Bolhuis, J.J. and I.C. Reid, *Effects of intraventricular infusion of the N-methyl-D-aspartate (NMDA) receptor antagonist AP5 on spatial memory of rats in a radial arm maze*. Behav Brain Res, 1992. **47**(2): p. 151-7.
382. Grover, L.M. and T.J. Teyler, *Two components of long-term potentiation induced by different patterns of afferent activation*. Nature, 1990. **347**(6292): p. 477-9.
383. Morgan, S.L. and T.J. Teyler, *VDCCs and NMDARs underlie two forms of LTP in CA1 hippocampus in vivo*. J Neurophysiol, 1999. **82**(2): p. 736-40.
384. Cavus, I. and T. Teyler, *Two forms of long-term potentiation in area CA1 activate different signal transduction cascades*. J Neurophysiol, 1996. **76**(5): p. 3038-47.
385. Leitch, B., et al., *Subcellular distribution of L-type calcium channel subtypes in rat hippocampal neurons*. Neuroscience, 2009. **164**(2): p. 641-57.
386. Cavus, I. and T.J. Teyler, *NMDA receptor-independent LTP in basal versus apical dendrites of CA1 pyramidal cells in rat hippocampal slice*. Hippocampus, 1998. **8**(4): p. 373-9.
387. Woodside, B.L., et al., *NMDA receptors and voltage-dependent calcium channels mediate different aspects of acquisition and retention of a spatial memory task*. Neurobiol Learn Mem, 2004. **81**(2): p. 105-14.
388. Borroni, A.M., et al., *Role of voltage-dependent calcium channel long-term potentiation (LTP) and NMDA LTP in spatial memory*. J Neurosci, 2000. **20**(24): p. 9272-6.

389. Moosmang, S., et al., *Role of hippocampal Cav1.2 Ca²⁺ channels in NMDA receptor-independent synaptic plasticity and spatial memory*. J Neurosci, 2005. **25**(43): p. 9883-92.
390. White, J.A., et al., *Conditional forebrain deletion of the L-type calcium channel Ca_v 1.2 disrupts remote spatial memories in mice*. Learn Mem, 2008. **15**(1): p. 1-5.
391. Da Silva, W.C., et al., *Memory reconsolidation and its maintenance depend on L-voltage-dependent calcium channels and CaMKII functions regulating protein turnover in the hippocampus*. Proc Natl Acad Sci U S A, 2013. **110**(16): p. 6566-70.
392. Rossato, J.I., et al., *Retrieval induces hippocampal-dependent reconsolidation of spatial memory*. Learn Mem, 2006. **13**(4): p. 431-40.
393. Shankar, S., T.J. Teyler, and N. Robbins, *Aging differentially alters forms of long-term potentiation in rat hippocampal area CA1*. J Neurophysiol, 1998. **79**(1): p. 334-41.
394. Boric, K., et al., *Potential adaptive function for altered long-term potentiation mechanisms in aging hippocampus*. J Neurosci, 2008. **28**(32): p. 8034-9.
395. Fazeli, M.S., et al., *Increase in extracellular NCAM and amyloid precursor protein following induction of long-term potentiation in the dentate gyrus of anaesthetized rats*. Neurosci Lett, 1994. **169**(1-2): p. 77-80.
396. Puzzo, D., L. Privitera, and A. Palmeri, *Hormetic effect of amyloid-beta peptide in synaptic plasticity and memory*. Neurobiol Aging, 2012. **33**(7): p. 1484 e15-24.
397. Wu, J., R. Anwyl, and M.J. Rowan, *beta-Amyloid-(1-40) increases long-term potentiation in rat hippocampus in vitro*. Eur J Pharmacol, 1995. **284**(3): p. R1-3.
398. Cullen, W.K., et al., *Block of LTP in rat hippocampus in vivo by beta-amyloid precursor protein fragments*. Neuroreport, 1997. **8**(15): p. 3213-7.
399. Chen, Q.S., et al., *Impairment of hippocampal long-term potentiation by Alzheimer amyloid beta-peptides*. J Neurosci Res, 2000. **60**(1): p. 65-72.
400. Pike, C.J., et al., *Structure-activity analyses of beta-amyloid peptides: contributions of the beta 25-35 region to aggregation and neurotoxicity*. J Neurochem, 1995. **64**(1): p. 253-65.
401. Resende, R., et al., *Neurotoxic effect of oligomeric and fibrillar species of amyloid-beta peptide 1-42: involvement of endoplasmic reticulum calcium release in oligomer-induced cell death*. Neuroscience, 2008. **155**(3): p. 725-37.
402. Dahlgren, K.N., et al., *Oligomeric and fibrillar species of amyloid-beta peptides differentially affect neuronal viability*. J Biol Chem, 2002. **277**(35): p. 32046-53.

403. Balducci, C., et al., *Synthetic amyloid-beta oligomers impair long-term memory independently of cellular prion protein*. Proc Natl Acad Sci U S A, 2010. **107**(5): p. 2295-300.
404. He, Y., et al., *Soluble oligomers and fibrillar species of amyloid beta-peptide differentially affect cognitive functions and hippocampal inflammatory response*. Biochem Biophys Res Commun, 2012. **429**(3-4): p. 125-30.
405. Freir, D.B., D.A. Costello, and C.E. Herron, *A beta 25-35-induced depression of long-term potentiation in area CA1 in vivo and in vitro is attenuated by verapamil*. J Neurophysiol, 2003. **89**(6): p. 3061-9.
406. Chen, Q.S., et al., *Alzheimer amyloid beta-peptide inhibits the late phase of long-term potentiation through calcineurin-dependent mechanisms in the hippocampal dentate gyrus*. Neurobiol Learn Mem, 2002. **77**(3): p. 354-71.
407. Wang, H.W., et al., *Soluble oligomers of beta amyloid (1-42) inhibit long-term potentiation but not long-term depression in rat dentate gyrus*. Brain Res, 2002. **924**(2): p. 133-40.
408. Lambert, M.P., et al., *Diffusible, nonfibrillar ligands derived from Abeta1-42 are potent central nervous system neurotoxins*. Proc Natl Acad Sci U S A, 1998. **95**(11): p. 6448-53.
409. Freir, D.B., C. Holscher, and C.E. Herron, *Blockade of long-term potentiation by beta-amyloid peptides in the CA1 region of the rat hippocampus in vivo*. J Neurophysiol, 2001. **85**(2): p. 708-13.
410. Freir, D.B. and C.E. Herron, *Nicotine enhances the depressive actions of A beta 1-40 on long-term potentiation in the rat hippocampal CA1 region in vivo*. J Neurophysiol, 2003. **89**(6): p. 2917-22.
411. Nitta, A., et al., *beta-Amyloid protein-induced Alzheimer's disease animal model*. Neurosci Lett, 1994. **170**(1): p. 63-6.
412. Yamada, K., et al., *Propentofylline improves learning and memory deficits in rats induced by beta-amyloid protein-(1-40)*. Eur J Pharmacol, 1998. **349**(1): p. 15-22.
413. Yamada, K., et al., *Improvement by nefiracetam of beta-amyloid-(1-42)-induced learning and memory impairments in rats*. Br J Pharmacol, 1999. **126**(1): p. 235-44.
414. Yamada, K., et al., *Protective effects of idebenone and alpha-tocopherol on beta-amyloid-(1-42)-induced learning and memory deficits in rats: implication of oxidative stress in beta-amyloid-induced neurotoxicity in vivo*. Eur J Neurosci, 1999. **11**(1): p. 83-90.

415. Noshita, T., N. Murayama, and S. Nakamura, *Effect of nicotine on neuronal dysfunction induced by intracerebroventricular infusion of amyloid-beta peptide in rats*. Eur Rev Med Pharmacol Sci, 2015. **19**(2): p. 334-43.
416. Poling, A., et al., *Oligomers of the amyloid-beta protein disrupt working memory: confirmation with two behavioral procedures*. Behav Brain Res, 2008. **193**(2): p. 230-4.
417. Mullan, M., et al., *A pathogenic mutation for probable Alzheimer's disease in the APP gene at the N-terminus of beta-amyloid*. Nat Genet, 1992. **1**(5): p. 345-7.
418. Jonsson, T., et al., *A mutation in APP protects against Alzheimer's disease and age-related cognitive decline*. Nature, 2012. **488**(7409): p. 96-9.
419. Chapman, P.F., et al., *Impaired synaptic plasticity and learning in aged amyloid precursor protein transgenic mice*. Nat Neurosci, 1999. **2**(3): p. 271-6.
420. Moechars, D., et al., *Early phenotypic changes in transgenic mice that overexpress different mutants of amyloid precursor protein in brain*. J Biol Chem, 1999. **274**(10): p. 6483-92.
421. Larson, J., et al., *Alterations in synaptic transmission and long-term potentiation in hippocampal slices from young and aged PDAPP mice*. Brain Res, 1999. **840**(1-2): p. 23-35.
422. Witton, J., et al., *Altered synaptic plasticity in the mossy fibre pathway of transgenic mice expressing mutant amyloid precursor protein*. Mol Brain, 2010. **3**: p. 32.
423. Jacobsen, J.S., et al., *Early-onset behavioral and synaptic deficits in a mouse model of Alzheimer's disease*. Proc Natl Acad Sci U S A, 2006. **103**(13): p. 5161-6.
424. Hsiao, K., et al., *Correlative memory deficits, Abeta elevation, and amyloid plaques in transgenic mice*. Science, 1996. **274**(5284): p. 99-102.
425. Dodart, J.C., et al., *Behavioral disturbances in transgenic mice overexpressing the V717F beta-amyloid precursor protein*. Behav Neurosci, 1999. **113**(5): p. 982-90.
426. Games, D., et al., *Alzheimer-type neuropathology in transgenic mice overexpressing V717F beta-amyloid precursor protein*. Nature, 1995. **373**(6514): p. 523-7.
427. Masliah, E., et al., *Comparison of neurodegenerative pathology in transgenic mice overexpressing V717F beta-amyloid precursor protein and Alzheimer's disease*. J Neurosci, 1996. **16**(18): p. 5795-811.

428. Parent, A., et al., *Synaptic transmission and hippocampal long-term potentiation in transgenic mice expressing FAD-linked presenilin 1*. Neurobiol Dis, 1999. **6**(1): p. 56-62.
429. Zaman, S.H., et al., *Enhanced synaptic potentiation in transgenic mice expressing presenilin 1 familial Alzheimer's disease mutation is normalized with a benzodiazepine*. Neurobiol Dis, 2000. **7**(1): p. 54-63.
430. Dewachter, I., et al., *Modulation of synaptic plasticity and Tau phosphorylation by wild-type and mutant presenilin1*. Neurobiol Aging, 2008. **29**(5): p. 639-52.
431. Auffret, A., et al., *Age-dependent impairment of spine morphology and synaptic plasticity in hippocampal CA1 neurons of a presenilin 1 transgenic mouse model of Alzheimer's disease*. J Neurosci, 2009. **29**(32): p. 10144-52.
432. Schneider, I., et al., *Mutant presenilins disturb neuronal calcium homeostasis in the brain of transgenic mice, decreasing the threshold for excitotoxicity and facilitating long-term potentiation*. J Biol Chem, 2001. **276**(15): p. 11539-44.
433. Janus, C., et al., *Spatial learning in transgenic mice expressing human presenilin 1 (PS1) transgenes*. Neurobiol Aging, 2000. **21**(4): p. 541-9.
434. Huang, X.G., et al., *Behavioral and neurochemical characterization of transgenic mice carrying the human presenilin-1 gene with or without the leucine-to-proline mutation at codon 235*. Exp Neurol, 2003. **183**(2): p. 673-81.
435. Wang, Y., et al., *Val97Leu mutant presenilin-1 induces tau hyperphosphorylation and spatial memory deficit in mice and the underlying mechanisms*. J Neurochem, 2012. **121**(1): p. 135-45.
436. Duff, K., et al., *Increased amyloid-beta42(43) in brains of mice expressing mutant presenilin 1*. Nature, 1996. **383**(6602): p. 710-3.
437. Oyama, F., et al., *Mutant presenilin 2 transgenic mouse: effect on an age-dependent increase of amyloid beta-protein 42 in the brain*. J Neurochem, 1998. **71**(1): p. 313-22.
438. Chui, D.H., et al., *Transgenic mice with Alzheimer presenilin 1 mutations show accelerated neurodegeneration without amyloid plaque formation*. Nat Med, 1999. **5**(5): p. 560-4.
439. Guo, Q., et al., *Increased vulnerability of hippocampal neurons to excitotoxic necrosis in presenilin-1 mutant knock-in mice*. Nat Med, 1999. **5**(1): p. 101-6.
440. Holcomb, L., et al., *Accelerated Alzheimer-type phenotype in transgenic mice carrying both mutant amyloid precursor protein and presenilin 1 transgenes*. Nat Med, 1998. **4**(1): p. 97-100.

441. Holcomb, L.A., et al., *Behavioral changes in transgenic mice expressing both amyloid precursor protein and presenilin-1 mutations: lack of association with amyloid deposits*. Behav Genet, 1999. **29**(3): p. 177-85.
442. Trinchese, F., et al., *Progressive age-related development of Alzheimer-like pathology in APP/PS1 mice*. Ann Neurol, 2004. **55**(6): p. 801-14.
443. Mitchell, J.C., et al., *X11beta rescues memory and long-term potentiation deficits in Alzheimer's disease APP^{swe} Tg2576 mice*. Hum Mol Genet, 2009. **18**(23): p. 4492-500.
444. Jung, J.H., et al., *Pathway-specific alteration of synaptic plasticity in Tg2576 mice*. Mol Cells, 2011. **32**(2): p. 197-201.
445. Balducci, C., et al., *The gamma-secretase modulator CHF5074 restores memory and hippocampal synaptic plasticity in plaque-free Tg2576 mice*. J Alzheimers Dis, 2011. **24**(4): p. 799-816.
446. Elder, G.A., M.A. Gama Sosa, and R. De Gasperi, *Transgenic mouse models of Alzheimer's disease*. Mt Sinai J Med, 2010. **77**(1): p. 69-81.
447. Citron, M., et al., *Mutant presenilins of Alzheimer's disease increase production of 42-residue amyloid beta-protein in both transfected cells and transgenic mice*. Nat Med, 1997. **3**(1): p. 67-72.
448. Yamaguchi, F., et al., *Transgenic mice for the amyloid precursor protein 695 isoform have impaired spatial memory*. Neuroreport, 1991. **2**(12): p. 781-4.
449. Quon, D., et al., *Formation of beta-amyloid protein deposits in brains of transgenic mice*. Nature, 1991. **352**(6332): p. 239-41.
450. Oakley, H., et al., *Intraneuronal beta-amyloid aggregates, neurodegeneration, and neuron loss in transgenic mice with five familial Alzheimer's disease mutations: potential factors in amyloid plaque formation*. J Neurosci, 2006. **26**(40): p. 10129-40.
451. Oddo, S., et al., *Triple-transgenic model of Alzheimer's disease with plaques and tangles: intracellular Abeta and synaptic dysfunction*. Neuron, 2003. **39**(3): p. 409-21.
452. Van Dam, D., et al., *Age-dependent cognitive decline in the APP23 model precedes amyloid deposition*. Eur J Neurosci, 2003. **17**(2): p. 388-96.
453. Zhang, W., et al., *Soluble Abeta levels correlate with cognitive deficits in the 12-month-old APP^{swe}/PS1^{dE9} mouse model of Alzheimer's disease*. Behav Brain Res, 2011. **222**(2): p. 342-50.

454. Steinerman, J.R., et al., *Distinct pools of beta-amyloid in Alzheimer disease-affected brain: a clinicopathologic study*. Arch Neurol, 2008. **65**(7): p. 906-12.
455. Kuo, Y.M., et al., *Water-soluble Abeta (N-40, N-42) oligomers in normal and Alzheimer disease brains*. J Biol Chem, 1996. **271**(8): p. 4077-81.
456. Nagy, Z., et al., *Relative roles of plaques and tangles in the dementia of Alzheimer's disease: correlations using three sets of neuropathological criteria*. Dementia, 1995. **6**(1): p. 21-31.
457. Nagy, Z., et al., *Hippocampal pathology reflects memory deficit and brain imaging measurements in Alzheimer's disease: clinicopathologic correlations using three sets of pathologic diagnostic criteria*. Dementia, 1996. **7**(2): p. 76-81.
458. Min, S.S., et al., *Chronic brain inflammation impairs two forms of long-term potentiation in the rat hippocampal CA1 area*. Neurosci Lett, 2009. **456**(1): p. 20-4.
459. Heppner, F.L., R.M. Ransohoff, and B. Becher, *Immune attack: the role of inflammation in Alzheimer disease*. Nat Rev Neurosci, 2015. **16**(6): p. 358-72.
460. Bittner, T., et al., *Multiple events lead to dendritic spine loss in triple transgenic Alzheimer's disease mice*. PLoS One, 2010. **5**(11): p. e15477.
461. Billings, L.M., et al., *Intraneuronal Ab causes the onset of early Alzheimer's disease-related cognitive deficits in transgenic mice*. Neuron, 2005. **45**: p. 675-688.
462. Hsieh, H., et al., *AMPA removal underlies Abeta-induced synaptic depression and dendritic spine loss*. Neuron, 2006. **52**(5): p. 831-43.
463. Rui, Y., et al., *Inhibition of AMPA receptor trafficking at hippocampal synapses by beta-amyloid oligomers: the mitochondrial contribution*. Mol Brain, 2010. **3**: p. 10.
464. Minano-Molina, A.J., et al., *Soluble oligomers of amyloid-beta peptide disrupt membrane trafficking of alpha-amino-3-hydroxy-5-methylisoxazole-4-propionic acid receptor contributing to early synapse dysfunction*. J Biol Chem, 2011. **286**(31): p. 27311-21.
465. Gu, Z., W. Liu, and Z. Yan, *{beta}-Amyloid impairs AMPA receptor trafficking and function by reducing Ca²⁺/calmodulin-dependent protein kinase II synaptic distribution*. J Biol Chem, 2009. **284**(16): p. 10639-49.
466. Cantanelli, P., et al., *Age-Dependent Modifications of AMPA Receptor Subunit Expression Levels and Related Cognitive Effects in 3xTg-AD Mice*. Front Aging Neurosci, 2014. **6**: p. 200.

467. D'Amelio, M., et al., *Caspase-3 triggers early synaptic dysfunction in a mouse model of Alzheimer's disease*. Nat Neurosci, 2011. **14**(1): p. 69-76.
468. Neyman, S. and D. Manahan-Vaughan, *Metabotropic glutamate receptor 1 (mGluR1) and 5 (mGluR5) regulate late phases of LTP and LTD in the hippocampal CA1 region in vitro*. Eur J Neurosci, 2008. **27**(6): p. 1345-52.
469. Gladding, C.M., S.M. Fitzjohn, and E. Molnar, *Metabotropic glutamate receptor-mediated long-term depression: molecular mechanisms*. Pharmacol Rev, 2009. **61**(4): p. 395-412.
470. Wang, Q., et al., *Block of long-term potentiation by naturally secreted and synthetic amyloid beta-peptide in hippocampal slices is mediated via activation of the kinases c-Jun N-terminal kinase, cyclin-dependent kinase 5, and p38 mitogen-activated protein kinase as well as metabotropic glutamate receptor type 5*. J Neurosci, 2004. **24**(13): p. 3370-8.
471. Li, S., et al., *Soluble oligomers of amyloid Beta protein facilitate hippocampal long-term depression by disrupting neuronal glutamate uptake*. Neuron, 2009. **62**(6): p. 788-801.
472. Li, S., et al., *Soluble A β oligomers inhibit long-term potentiation through a mechanism involving excessive activation of extrasynaptic NR2B-containing NMDA receptors*. J Neurosci, 2011. **31**(18): p. 6627-38.
473. Chen, X., et al., *Enhancement of long-term depression by soluble amyloid beta protein in rat hippocampus is mediated by metabotropic glutamate receptor and involves activation of p38MAPK, STEP and caspase-3*. Neuroscience, 2013. **253**: p. 435-43.
474. Woolf, N.J., M.C. Hernit, and L.L. Butcher, *Cholinergic and non-cholinergic projections from the rat basal forebrain revealed by combined choline acetyltransferase and Phaseolus vulgaris leucoagglutinin immunohistochemistry*. Neurosci Lett, 1986. **66**(3): p. 281-6.
475. Bigl, V., N.J. Woolf, and L.L. Butcher, *Cholinergic projections from the basal forebrain to frontal, parietal, temporal, occipital, and cingulate cortices: a combined fluorescent tracer and acetylcholinesterase analysis*. Brain Res Bull, 1982. **8**(6): p. 727-49.
476. Whitehouse, P.J., et al., *Alzheimer's disease and senile dementia: loss of neurons in the basal forebrain*. Science, 1982. **215**(4537): p. 1237-9.
477. Whitehouse, P.J., et al., *Alzheimer disease: evidence for selective loss of cholinergic neurons in the nucleus basalis*. Ann Neurol, 1981. **10**(2): p. 122-6.
478. Whitehouse, P.J., et al., *Nicotinic acetylcholine binding sites in Alzheimer's disease*. Brain Res, 1986. **371**(1): p. 146-51.

479. Ge, S. and J.A. Dani, *Nicotinic acetylcholine receptors at glutamate synapses facilitate long-term depression or potentiation*. J Neurosci, 2005. **25**(26): p. 6084-91.
480. Ji, D., R. Lape, and J.A. Dani, *Timing and location of nicotinic activity enhances or depresses hippocampal synaptic plasticity*. Neuron, 2001. **31**(1): p. 131-41.
481. Wu, J., et al., *beta-Amyloid directly inhibits human alpha4beta2-nicotinic acetylcholine receptors heterologously expressed in human SH-EP1 cells*. J Biol Chem, 2004. **279**(36): p. 37842-51.
482. Wang, H.Y., et al., *Amyloid peptide Abeta(1-42) binds selectively and with picomolar affinity to alpha7 nicotinic acetylcholine receptors*. J Neurochem, 2000. **75**(3): p. 1155-61.
483. Wang, H.Y., et al., *beta-Amyloid(1-42) binds to alpha7 nicotinic acetylcholine receptor with high affinity. Implications for Alzheimer's disease pathology*. J Biol Chem, 2000. **275**(8): p. 5626-32.
484. Pettit, D.L., Z. Shao, and J.L. Yakel, *beta-Amyloid(1-42) peptide directly modulates nicotinic receptors in the rat hippocampal slice*. J Neurosci, 2001. **21**(1): p. RC120.
485. Welsby, P.J., M.J. Rowan, and R. Anwyl, *Beta-amyloid blocks high frequency stimulation induced LTP but not nicotine enhanced LTP*. Neuropharmacology, 2007. **53**(1): p. 188-95.
486. Fujii, S., et al., *Acute and chronic nicotine exposure differentially facilitate the induction of LTP*. Brain Res, 1999. **846**(1): p. 137-43.
487. Kroker, K.S., et al., *Restoring long-term potentiation impaired by amyloid-beta oligomers: comparison of an acetylcholinesterase inhibitor and selective neuronal nicotinic receptor agonists*. Brain Res Bull, 2013. **96**: p. 28-38.
488. Srivareerat, M., et al., *Chronic nicotine restores normal Abeta levels and prevents short-term memory and E-LTP impairment in Abeta rat model of Alzheimer's disease*. Neurobiol Aging, 2011. **32**(5): p. 834-44.
489. Alkadhi, K.A., M. Srivareerat, and T.T. Tran, *Intensification of long-term memory deficit by chronic stress and prevention by nicotine in a rat model of Alzheimer's disease*. Mol Cell Neurosci, 2010. **45**(3): p. 289-96.
490. Dzievczapolski, G., et al., *Deletion of the alpha 7 nicotinic acetylcholine receptor gene improves cognitive deficits and synaptic pathology in a mouse model of Alzheimer's disease*. J Neurosci, 2009. **29**(27): p. 8805-15.
491. Dineley, K.T., et al., *Beta-amyloid activates the mitogen-activated protein kinase cascade via hippocampal alpha7 nicotinic acetylcholine receptors: In vitro and in*

- vivo mechanisms related to Alzheimer's disease.* J Neurosci, 2001. **21**(12): p. 4125-33.
492. Lauren, J., et al., *Cellular prion protein mediates impairment of synaptic plasticity by amyloid-beta oligomers.* Nature, 2009. **457**(7233): p. 1128-32.
493. Barry, A.E., et al., *Alzheimer's disease brain-derived amyloid-beta-mediated inhibition of LTP in vivo is prevented by immunotargeting cellular prion protein.* J Neurosci, 2011. **31**(20): p. 7259-63.
494. Hu, N.W., et al., *mGlu5 receptors and cellular prion protein mediate amyloid-beta-facilitated synaptic long-term depression in vivo.* Nat Commun, 2014. **5**: p. 3374.
495. Mouillet-Richard, S., et al., *Signal transduction through prion protein.* Science, 2000. **289**(5486): p. 1925-8.
496. Um, J.W., et al., *Alzheimer amyloid-beta oligomer bound to postsynaptic prion protein activates Fyn to impair neurons.* Nat Neurosci, 2012. **15**(9): p. 1227-35.
497. Klein, C., et al., *Process outgrowth of oligodendrocytes is promoted by interaction of fyn kinase with the cytoskeletal protein tau.* J Neurosci, 2002. **22**(3): p. 698-707.
498. Ittner, L.M., et al., *Dendritic function of tau mediates amyloid-beta toxicity in Alzheimer's disease mouse models.* Cell, 2010. **142**(3): p. 387-97.
499. Zempel, H., et al., *Abeta oligomers cause localized Ca(2+) elevation, missorting of endogenous Tau into dendrites, Tau phosphorylation, and destruction of microtubules and spines.* J Neurosci, 2010. **30**(36): p. 11938-50.
500. Snapphaan, L., et al., *Reduced medial temporal lobe functionality in stroke patients: a functional magnetic resonance imaging study.* Brain, 2009. **132**(Pt 7): p. 1882-8.

Figures

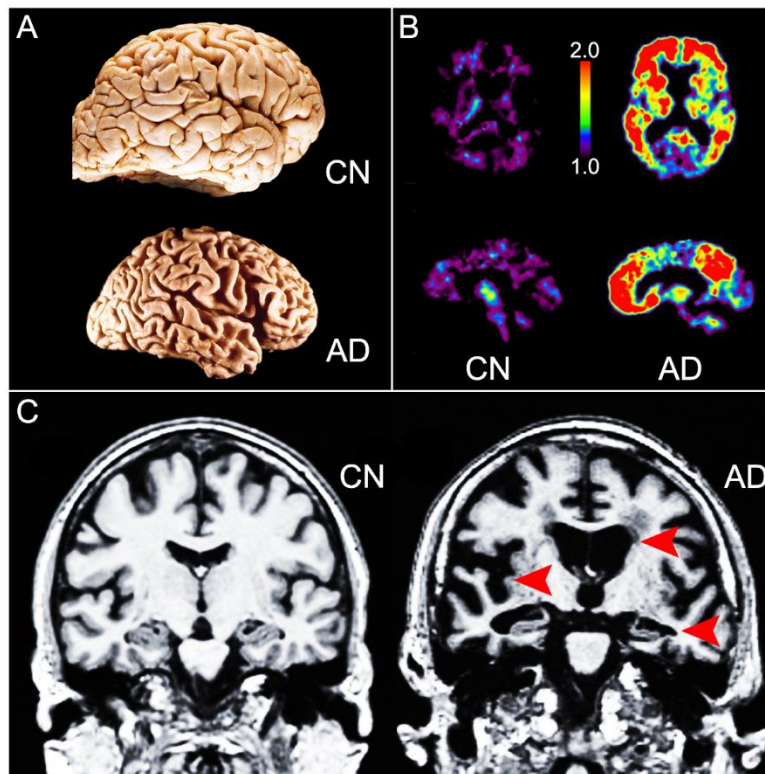


Figure 1.1. Gross pathology and clinical diagnostics of Alzheimer's disease. A) Comparison of brains from a cognitively normal (CN) individual and an Alzheimer's disease patient (AD). The AD brain has noticeable cortical atrophy showing a narrowing of gyri and widening of sulci, particularly in the frontal and temporal lobes. B) Positron Emission Tomography of CN and AD individuals with the Amyloid binding radioactive tracer Pittsburgh compound B ($[^{11}\text{C}]\text{PiB}$). Horizontal (top) and sagittal (bottom) planes show the highest signal intensity in the frontal, temporal, and parietal associational cortices in the AD patient. The low signal seen in the brainstem of the CN individual represents slow clearance of nonspecific binding $[^{11}\text{C}]\text{PiB}$. Intensity is measured in Logan distribution volume ratios, and relative to cerebellum. Scans were

measured 90 minutes post-administration of [^{11}C]PiB. C) Structural MRI of CN and AD individuals in the coronal plane. The AD patient shows several key anatomical changes indicated by the red arrows: dilation of cerebral ventricles (top arrow), atrophy of the medial temporal lobe (middle arrow), and a reduction in hippocampal volume (bottom arrow). Part (A) adapted from the University of Alabama at Birmingham Department of Pathology Public Digital Library. Part (B) adapted from Mathis et al., 2007 [21]. Part (C) adapted from Vemuri et al., 2010 [19].

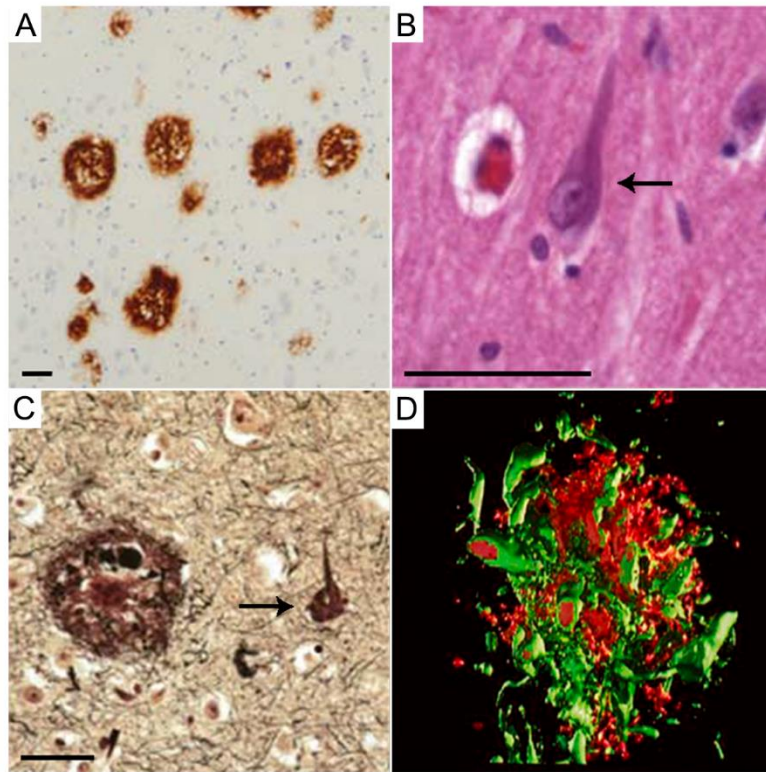


Figure 1.2. Histopathology of Alzheimer's disease. Photomicrographs of characteristic histopathological lesions found in Alzheimer's disease (AD). A) Immunohistochemistry of Amyloid- β deposition (brown deposits) showing plaque formation. B) Hematoxylin and Eosin stain highlighting a neurofibrillary tangle in a hippocampal pyramidal neuron (arrow). C) Silver stain showing both Amyloid- β deposition (large brown deposit) and neurofibrillary tangle (arrow). Scale bars = 100 μ m. D) 3D reconstruction of a β -Amyloid plaque generated from confocal microscopy imaging. The image shows an integrated relationship between extracellular Amyloid- β deposits (red) and dystrophic neurites containing hyperphosphorylated Tau (green). Parts (A, B, & C) adapted from Serrano-Pozo et al., 2011 [20]. Part (D) adapted from Masters et al., 2011 [68].

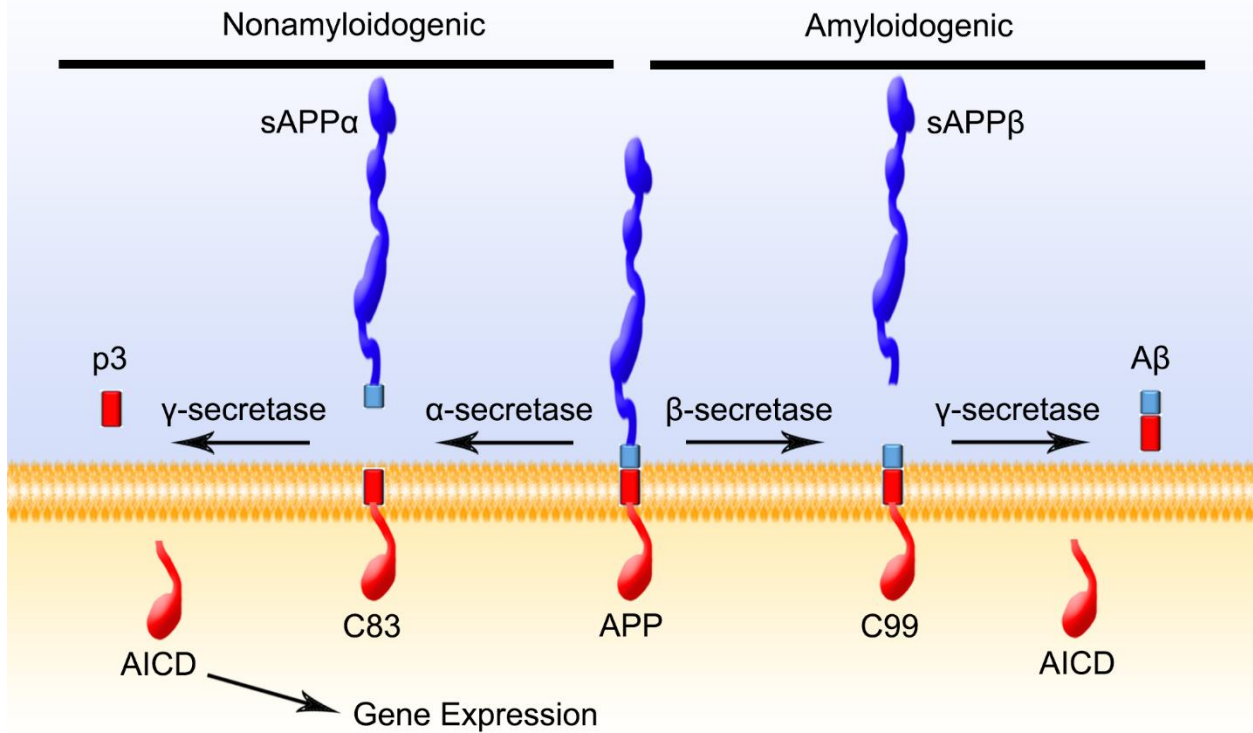


Figure 1.3. Amyloid Precursor Protein (APP) processing and Amyloid- β production. Two pathways exist for APP processing: nonamyloidogenic initiated by α -secretase, and amyloidogenic initiated by β -secretase. Cleavage products from both pathways are further processed by γ -secretase resulting in a p3 fragment from the nonamyloidogenic pathway, and Amyloid- β ($A\beta$) from the amyloidogenic pathway. In Alzheimer's disease (AD), the production of $A\beta$ results in β -Amyloid deposits from either the overproduction of $A\beta$ in familial AD, or failure to clear $A\beta$ in sporadic AD.

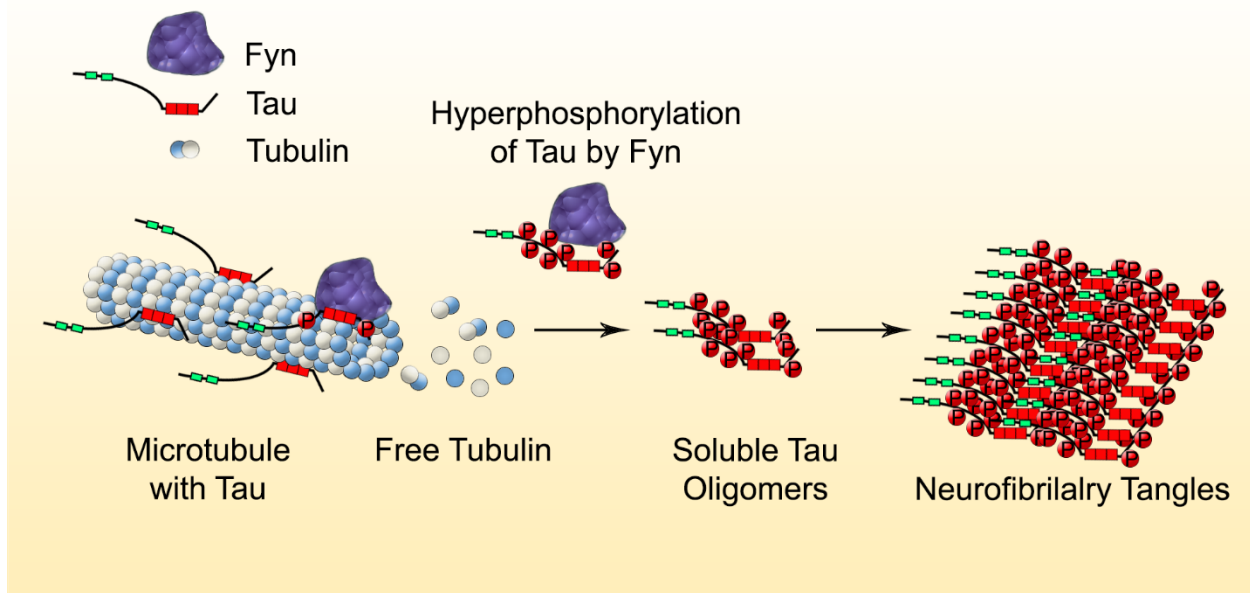


Figure 1.4. Hyperphosphorylation of Tau protein. Over activation of the tyrosine kinase Fyn results in hyperphosphorylation of the microtubule stabilizing protein Tau, resulting in microtubule destabilization and the formation of soluble Tau oligomers. Tau oligomers then aggregate to form insoluble neurofibrillary tangles characteristic of Alzheimer's disease.

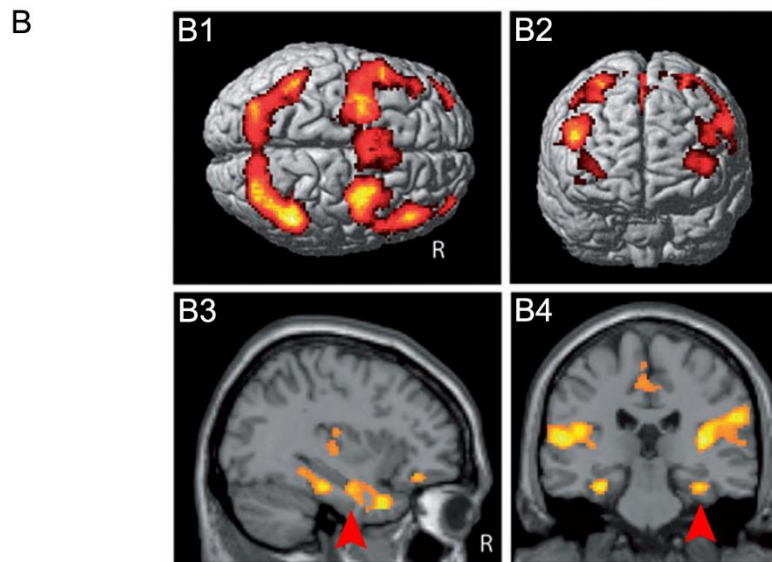
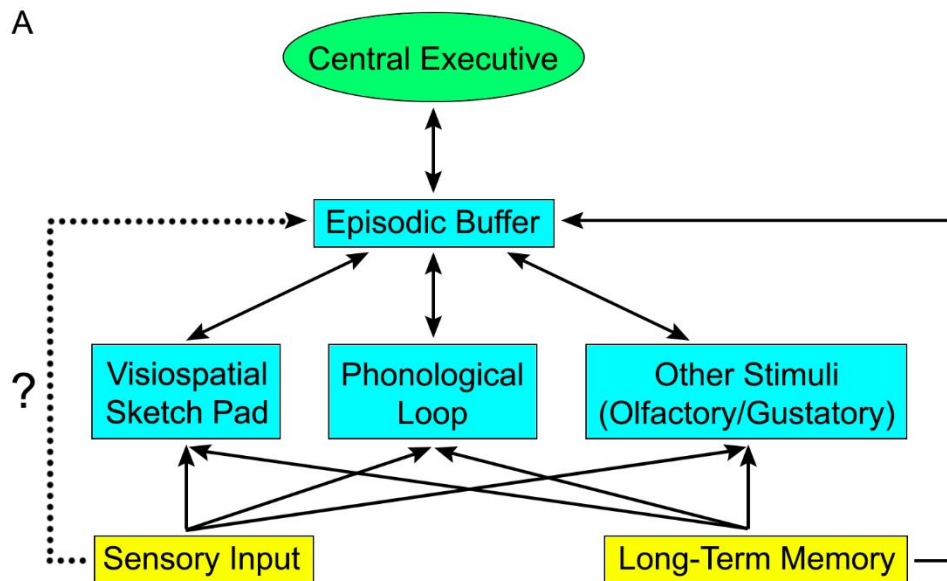


Figure 1.5. Neurobiology of working memory. A) Organizational model of working memory revised and adapted from Baddeley and Hitch's original 1974 model using a multicomponent approach for managing multiple tasks at one time. Sensory input and/or long-term memory information (yellow) is loaded into the short-term memory

component (blue), which is then managed by the central executive (green) to perform executive functions (e.g., problem solving, decision making). B) Functional MRI showing the anatomical representation of the central executive during a working memory task. B1 & B2 show a surface rendering of neural activity localized to parts of the frontal and parietal cortex. B3 & B4 show activation of the hippocampus (red arrows) through a parasagittal (B3) and coronal (B4) plane during the same task as performed in B1 & B2. Part (B) adapted from Shaphaan et al., 2009 [500].

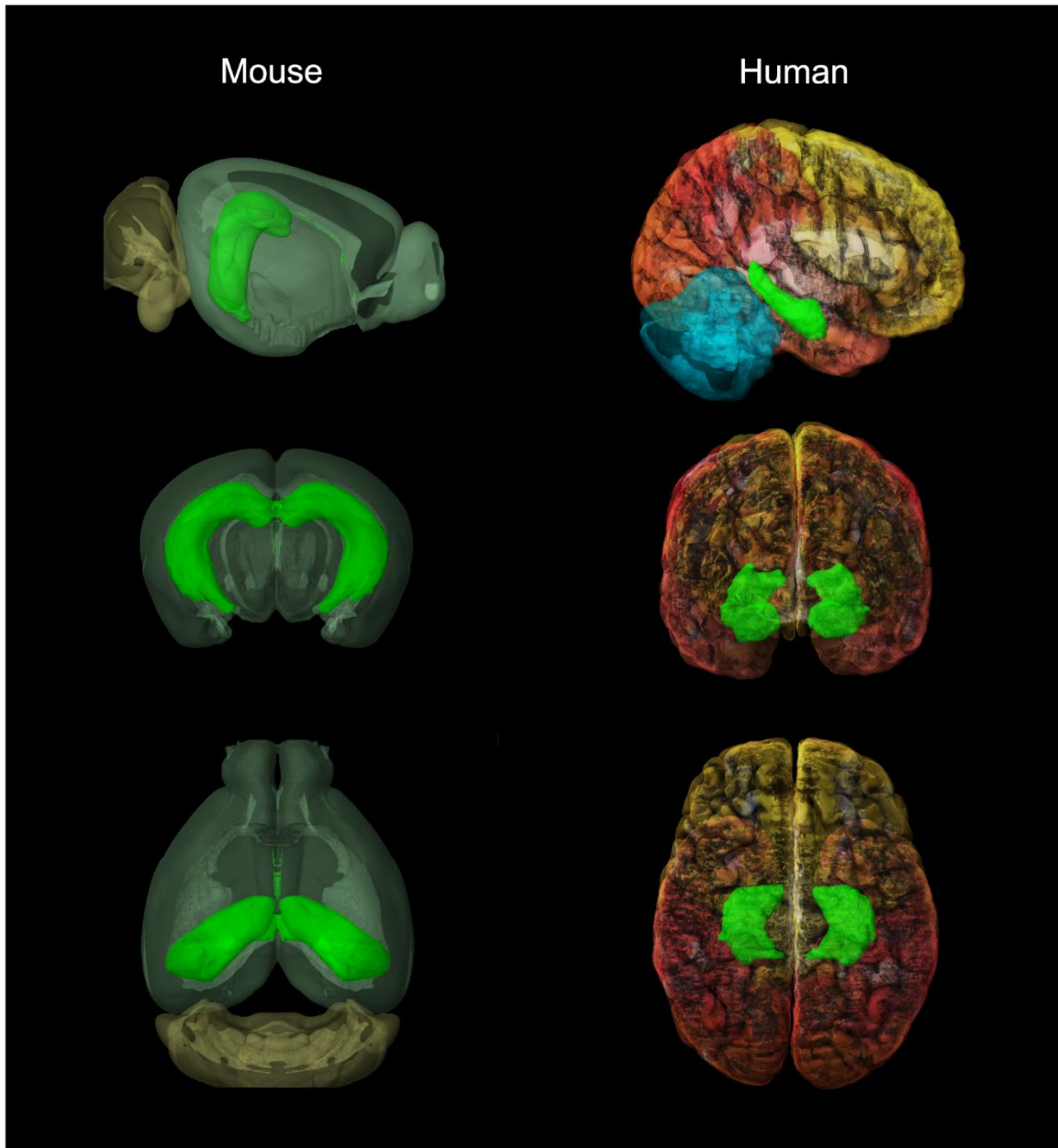


Figure 1.6. Comparative anatomy of mouse and human hippocampus. Anatomical location of the hippocampus in mouse (left column) and human (right column) from a sagittal view (top row), anterior view (middle row), and dorsal view (bottom row). The

hippocampus is highlighted in bright green. Images were generated from data obtained from the Allen Brain Atlas.

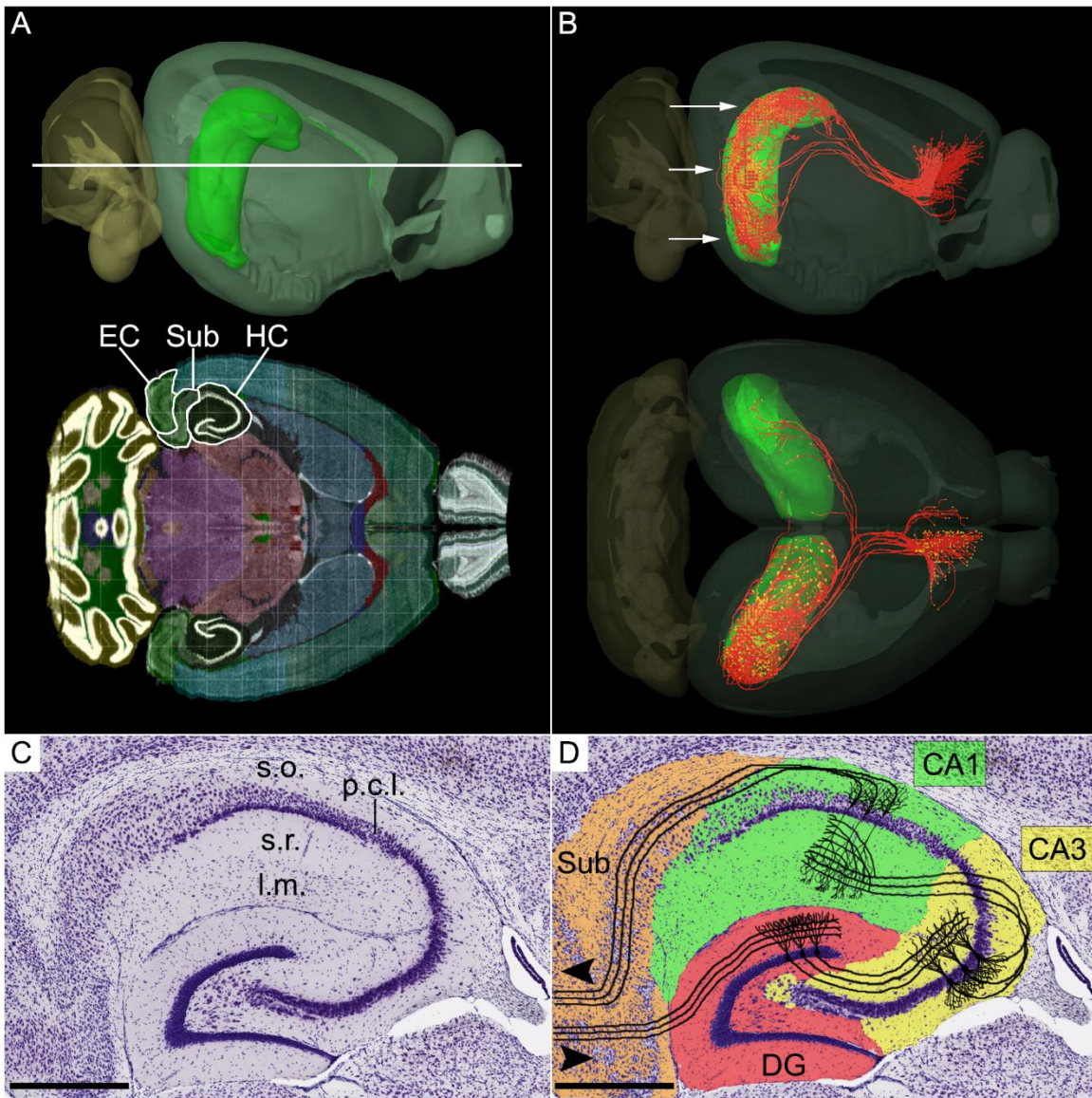


Figure 1.7. Hippocampal anatomy and circuitry. A) Horizontal section through mouse brain showing the location of the hippocampus (HC), subiculum (Sub), and entorhinal cortex (EC), all outlined in white. The white line (top image) indicates the plane of section shown below (bottom image). The hippocampus is highlighted in bright green. B) Injection of a recombinant adeno-associated viral vector-GFP tracer into CA1 and

subiculum of the right hippocampus highlighting the projection of axons (orange) out of the hippocampus and terminating in the prefrontal cortex (PFC). There are a total of six injection sites: dorsal CA1/Sub, middle CA1/Sub, ventral CA1/Sub. The approximate location of the dorsal, middle, and ventral injection sites are indicated by the white arrows. CA1 and subicular axons exit the hippocampus through the fornix (not shown) and exit the fornix to terminate in the PFC. Projections from the middle and ventral injection sites show the highest density of PFC synapses. Injections to other hippocampal regions (DG and CA3) showed no, or very weak, projections to PFC, respectively (data not shown). The CA1 and subiculum regions are highlighted in bright green (DG and CA3 regions have been omitted for clarity). Projections from CA1 and subiculum to other brain regions (e.g., EC) have been omitted for clarity. Tracer data was generated using serial 2-photon tomography. C) Nissl stain of mouse hippocampus with labeling of the major layers of the CA1 subregion: stratum oriens (s.o.), pyramidal cell layer (p.c.l.), stratum radiatum (s.r.), stratum lacunosum-moleculare (l.m.). D) Major regions of the hippocampus: dentate gyrus (DG, red), CA3 (yellow), CA1 (green), and subiculum (Sub, orange). Arrows indicate the direction of information flow through the hippocampus. Only neurons in the trisynaptic circuit are shown, other pathways have been omitted for clarity. Scale bar = 500 μ m. A & B were generated from projection data obtained from the Allen Brain Atlas. C & D unlabeled Nissl stain section acquired from brainmaps.org.

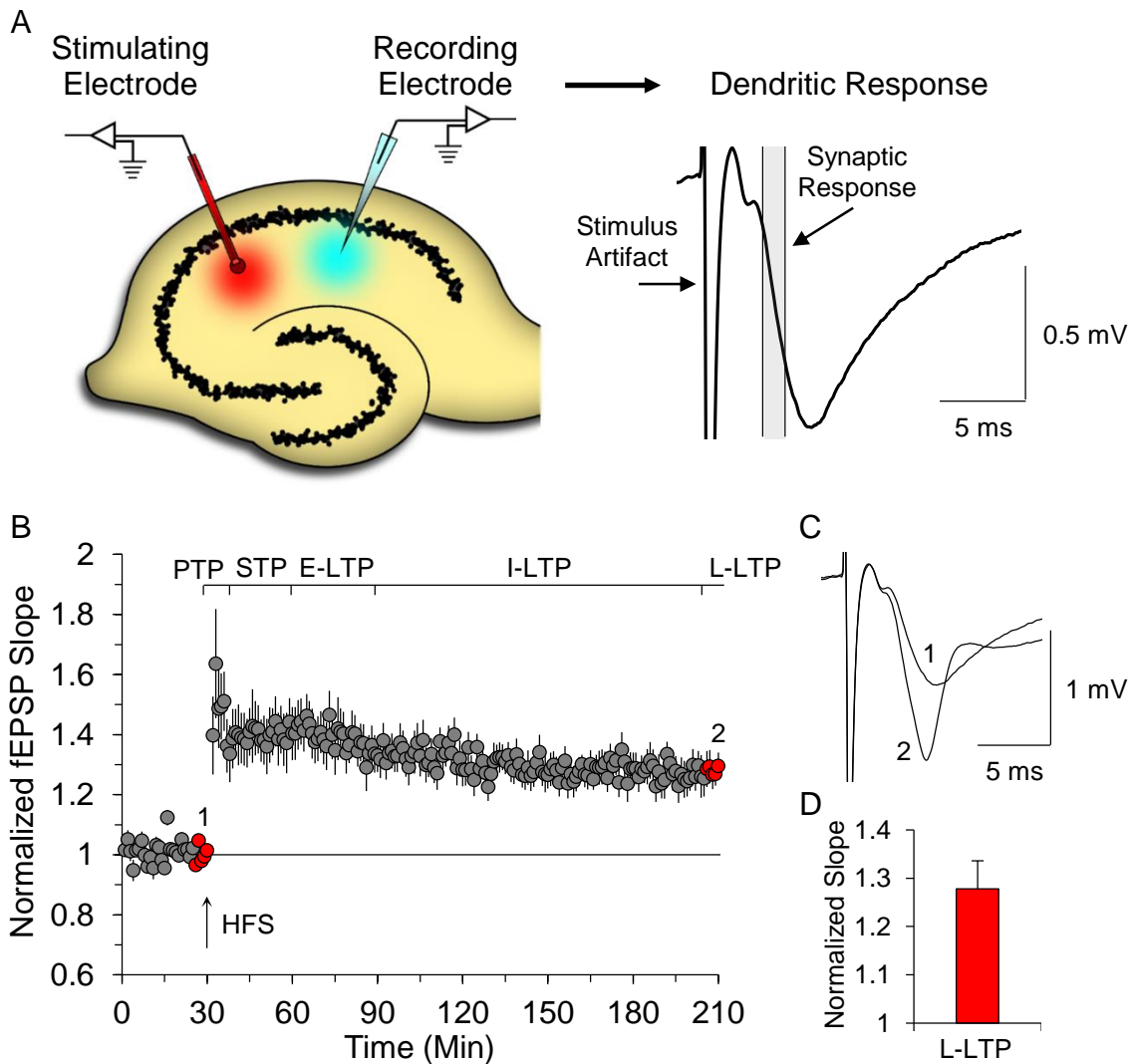


Figure 1.8. Recording of field Excitatory Post-Synaptic Potentials (fEPSP) in the *ex vivo* hippocampal slice. A) Diagram illustrating the location of stimulating and recording electrodes in the hippocampal slice preparation. The stimulating electrode is placed in the stratum radiatum of CA1 to stimulate Schaffer collateral axons from CA3 pyramidal neurons that synapse on CA1 dendrites. The recording electrode is placed in the same

layer of CA1 to record changes in the local field potential that result from local dendritic synaptic activity. An example of a fEPSP recording is shown to the right. The initial downward slope of the synaptic response (shaded blue area) is measured to generate the data points shown below in (B). B) Data plot summary of normalized fEPSP slope values demonstrating a typical Long-Term Potentiation (LTP) experiment. After 30 minutes of baseline recording, a high frequency stimulation (arrow, HFS) is delivered to the slice, resulting in an increase in the initial slope of the synaptic response. Values are normalized by dividing all slope values by the average of the 5 responses recorded immediately prior to HFS (red data points, 1). The last 5 normalized slope values recorded 3 hours post-HFS (red data points, 2) are averaged to determine the change in synaptic strength. The different components of the LTP time course are indicated above the data points: Post-Tetanic Potentiation (PTP), Short-Term Potentiation (STP), Early-LTP (E-LTP), Intermediate-LTP (I-LTP), Late-LTP (L-LTP). C) Averaged fEPSP recordings representing the 5 data points before HFS (1) and 5 data points 3 hours post-HFS (2) (generated from the red data points in part B). D) Quantification of LTP from the last 5 data points 3 hour-post HFS.

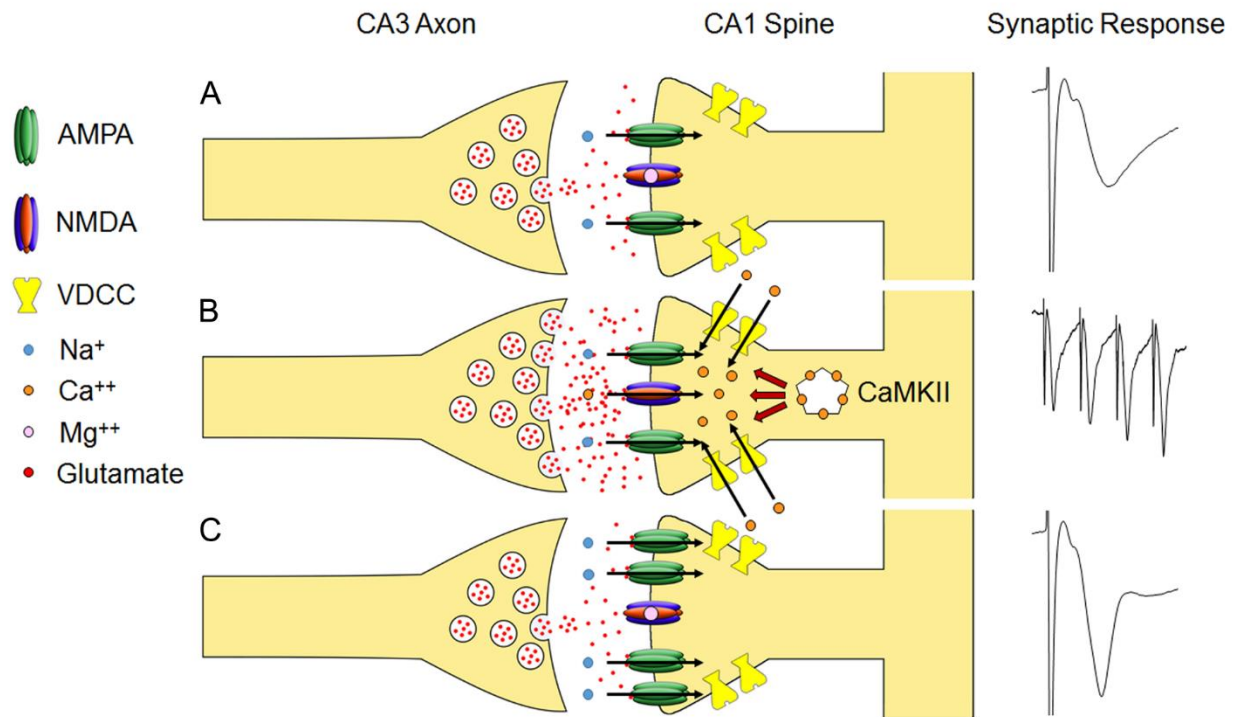


Figure 1.9. Cellular mechanisms of synaptic plasticity at CA3→CA1 synapses. A) Under basal activation, action potentials in CA3 axons trigger the release of glutamate from the presynaptic membrane. This results in the activation of postsynaptic AMPA receptors by glutamate, and the subsequent influx of Na^+ into CA1 dendritic spines causing a local depolarization at the postsynaptic membrane. B) High frequency activation of CA3 axons results in a temporary facilitation of neurotransmitter release (a form of short-term synaptic plasticity). Sustained activation of postsynaptic AMPA receptors allows sufficient depolarization to relieve the Mg^{2+} block in postsynaptic NMDA receptors, allowing for their activation by glutamate and subsequent influx of Ca^{2+} . Continued postsynaptic depolarization eventually triggers the activation of Voltage-Dependent Calcium Channels (VDCC), allowing for additional influx of Ca^{2+} .

Increased intracellular Ca^{2+} activates CaMKII, which initiates a series of signaling cascades resulting in the upregulation of surface AMPA receptors as depicted in (C).

C) A return to basal activation now shows a long-term potentiation of the synaptic response (a form of long-term synaptic plasticity) due to the upregulation of postsynaptic AMPA receptors, which upon activation results in an increased postsynaptic depolarization.

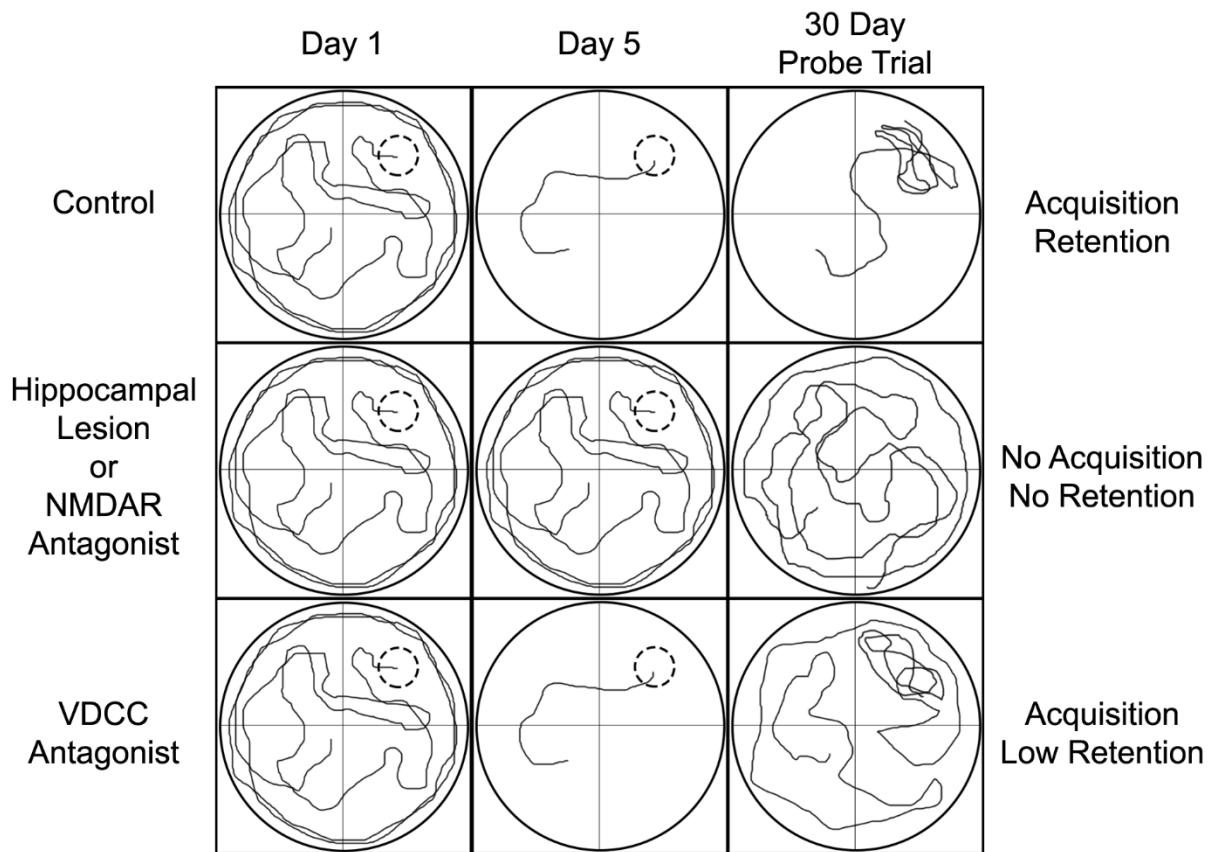


Figure 1.10. The role of NMDA receptors and VDCCs in spatial learning and memory of the Morris Water Maze task. Illustrations show the swim path for animals to reach a submerged escape platform (dashed circle) under different experimental conditions. Performance is improved over 5 days of training in the control and VDCC groups. In the 30 day probe trial, the escape platform has been removed and the number of crossings where the platform was previously located is measured. Only the control group shows retention of the platform location. Data represent a consensus of existing literature, see text for details.

CHAPTER 2

ALTERATIONS IN SYNAPTIC PLASTICITY COINCIDE WITH DEFICITS IN SPATIAL WORKING MEMORY IN 3xTg-AD MICE¹

¹ Clark JK, Furgerson M, Crystal JD, Fecheimer M, Furukawa R, Wagner JJ. *Alterations in synaptic plasticity coincide with deficits in spatial working memory in presymptomatic 3xTg-AD mice.* Neurobiology of Learning and Memory. 2015 Nov;125:152-62.
Reprinted here with permission.

Abstract

Alzheimer's disease is a neurodegenerative condition believed to be initiated by production of Amyloid- β peptide, which leads to synaptic dysfunction and progressive memory loss. Using a mouse model of Alzheimer's disease (3xTg-AD), an 8-arm radial maze was employed to assess spatial working memory. Unexpectedly, the younger (3 month old) 3xTg-AD mice were as impaired in the spatial working memory task as were the older (8 month old) 3xTg-AD mice when compared with age-matched NonTg control animals. Field potential recordings from the CA1 region of slices prepared from the ventral hippocampus were obtained to assess synaptic transmission and capability for synaptic plasticity. At 3 months of age, the NMDA receptor-dependent component of LTP was reduced in 3xTg-AD mice. However, the magnitude of the non-NMDA receptor-dependent component of LTP was concomitantly increased, resulting in a similar amount of total LTP in 3xTg-AD and NonTg mice. At 8 months of age, the NMDA receptor-dependent LTP was again reduced in 3xTg-AD mice, but now the non-NMDA receptor-dependent component was decreased as well, resulting in a significantly reduced total amount of LTP in 3xTg-AD compared with NonTg mice. Both 3 and 8 month old 3xTg-AD mice exhibited reductions in paired-pulse facilitation and NMDA receptor-dependent LTP that coincided with the deficit in spatial working memory. The early presence of this cognitive impairment and the associated alterations in synaptic plasticity demonstrate that the onset of some behavioral and neurophysiological consequences can occur before the detectable presence of plaques and tangles in the 3xTg-AD mouse model of Alzheimer's disease.

2.1 Introduction

Alzheimer's disease (AD) is a disease of aging characterized by progressive memory loss and dementia. It is differentiated from other forms of dementia based on two pathological hallmarks, Amyloid plaques and neurofibrillary tangles [1]. Amyloid plaques are derived from the aggregation of the Amyloid- β ($A\beta$) peptide, which is generated through sequential cleavage of the Amyloid Precursor Protein by β - and γ -secretase [2]. During disease progression, the microtubule associated protein Tau is subject to extensive post-translational modification including hyperphosphorylation and acetylation, modifications that are prerequisites to Tau aggregation and formation of neurofibrillary tangles [3]. The exact mechanisms linking these pathologies to memory impairment are unclear, however a growing body of evidence suggests the inability of neurons to maintain Ca^{2+} homeostasis may be an underlying factor during the early events of AD [4, 5].

One aspect of Ca^{2+} signaling related to learning and memory involves the cellular mechanisms underlying Long-Term Potentiation (LTP) of synaptic strength. LTP is a model for information storage within the brain, and synaptic plasticity is thought to play an important role in cognitive processes such as learning and memory [6, 7]. Large, transient increases in intracellular Ca^{2+} and subsequent activation of Ca^{2+} mediated responses lead to the induction and expression of LTP [8]. At least two different mechanisms of LTP are known to coexist at hippocampal CA3→CA1 synapses, N-methyl-D-aspartate receptor-dependent LTP (NMDAR LTP) and a non-NMDA receptor-dependent LTP (non-NMDAR LTP), with the latter predominantly mediated via activation of high threshold L-type Voltage-Dependent Calcium Channels (VDCC) [9-

11]. Pharmacological evidence indicates that both forms of LTP can contribute to spatial memory as either NMDAR antagonists [12] or Ca²⁺ channel antagonists [13] can impair spatial learning and memory.

NMDA receptors play an important role in assessments of spatial working memory using the radial arm maze [14-16]. More recent experiments, in which the NMDAR subunits NR2B and NR2A are specifically blocked by bilateral infusion of antagonists directly into the CA1 region of hippocampus, show a significant reduction in spatial working memory using a T-maze delayed alternation task [17]. NR2A^{-/-} mice show impairments in spatial working memory but not spatial reference memory in the 6-arm radial maze [18], demonstrating the contribution of specific NMDARs to specific memory functions. Finally, studies in humans have also shown that blockage of NMDARs with ketamine have decreased accuracy on spatial working memory tests [19].

A triple transgenic mouse model of Alzheimer's disease (3xTg-AD) has been developed that produces both β -Amyloid plaques and neurofibrillary Tau tangles [20-22]. We have further characterized this AD mouse model using both behavioral (spatial working memory using an 8-arm radial maze) and neurophysiological (extracellular recording from *ex vivo* slices in the CA1 region of ventral hippocampus) assessments. Our results demonstrate that 3xTg-AD mice have significant impairments in spatial working memory and significant alterations in neurotransmission and synaptic plasticity at both 3 and 8 months of age.

2.2 Methods

2.2.1 Animals and euthanasia

All animals used in this study were male mice and consisted of Alzheimer's disease model mice (3xTg-AD) homozygous for three mutant transgenes: APP(Swe), Psen1, and TauP301L, (B6/129-*Psen1*^{tm1Mpm} Tg(APP^{Swe}, tauP301L)1Lfa/Mmjax) obtained from the MMRRC (ID 034830-JAX) through Jackson Laboratories, and nontransgenic (NonTg) control mice (B6129SF2/J) from Jackson Laboratories (101045 JAX, Bar Harbor, ME). The generation of 3xTg-AD mice has been described elsewhere [22]. Briefly, two separate transgene constructs each encoding human *APP* cDNA (695 isoform) harboring the Swedish mutation (*KM670/671NL*), or human *Tau* cDNA (4R/0N) harboring the *P301L* mutation, each under control of mouse Thy1.2 regulatory elements, were comicroinjected into single-cell embryos from homozygous *PS1*_{M146V} knockin mice. Embryos were screened for cointegration of both cassettes to the same locus. Embryos were then reimplanted into foster mothers and the resulting offspring were genotyped to identify 3xTg-AD mice. Hemizygous F1 3xTg-AD mice were then crossed to produce 3xTg-AD mice homozygous for all three transgenes. Both 3xTg-AD and NonTg mice are on the same genetic and strain background (129/C57BL6 hybrid), except NonTg mice harbor the endogenous wild-type *PS1* gene. Breeding pairs for each group were obtained and animals were bred in house at the University of Georgia animal facilities. Mice were housed individually in an AAALAC accredited facility on a 12 hour light/dark timed schedule and had ad libitum access to food (except during behavioral studies) and water during this study. Mice began testing in the radial arm maze at approximately 2.5 and 7.5 months of age. After completion of radial arm maze

testing, 10 days elapsed before electrophysiological studies commenced to reduce any potential temporary enrichment from the maze environment. Euthanasia of mice occurred under deep anesthesia with halothane followed by decapitation. The University of Georgia Institutional Animal Care and Use Committee approved all animal protocols and experiments.

2.2.2 Radial arm maze apparatus and animal preparation

Learning and memory assessments were conducted using an 8-arm radial maze (Med Associates, St. Albans, VT) as described previously for rats [23]. This maze consists of a central chamber with 8 equally spaced arms extending outward. The central chamber is equipped with motorized guillotine doors positioned at the interface of the central chamber and arms. Each arm has two sets of photosensors to track movement of the animals into and out of the arms. At the distal end of each arm is a food trough with a 20 mm food dispenser activated by a photosensor to detect mouse head entries. The sides and top of each arm are composed of clear plastic to allow mice to use external visual cues to spatially navigate the maze. A computer in an adjacent room controls the maze events and data collection. Photosensor, food, and door data were collected using MED-PC software 4.0 (Med Associates, St. Albans, VT) with a resolution of 10 ms. A video camera was mounted above the maze to visualize the mice during the procedure.

Behavioral assessments in the radial arm maze were measured at either 3 or 8 months of age. Thirteen days prior to the start of behavioral testing, mice were individually housed and a 3 day average of individual animal body weight was determined. Mice were diet restricted to reduce and maintain a body weight of

approximately 87.0% of their free fed body weight for the duration of the behavioral testing. Mice were behaviorally shaped to associate a single head entry with obtaining a single sucrose-flavored food reward (Bio-Serve F0071, Frenchtown, NJ) by allowing each animal free access to 4 of the 8 arms until a single food reward from each arm was retrieved. Behavioral shaping was carried out once a day for 4 consecutive days prior to testing.

The maze was cleaned between subjects with 1/1250 diluted Coverage Plus NPD disinfectant (Steris Life Sciences, Mentor, OH) to prevent a previous mouse's scent from interfering with a subsequent mouse's performance. To further prevent a mouse from using scent cues, the entire maze was scent saturated using cotton bedding from the mouse's home cage after cleaning the maze.

2.2.3 Radial arm maze testing to assess spatial short-term working memory

Spatial short-term working memory was assessed using a standard 8-arm uninterrupted task. Each mouse was placed in the central chamber for a 2 minute acclimation period, after which all 8 doors simultaneously opened allowing free access to all arms for the duration of the testing session (8 arms open, 8 arms baited). Only a single food reward is delivered per baited arm, and a revisit to a previously visited food trough is considered an error in spatial short-term working memory. After collecting the last food reward, or after 15 minutes of elapsed time, the session ends and the doors close. For this task, the dependent variable is the number of errors in the first 8 choices. Comparisons are results obtained from the first 2 days and last 2 days of testing. The experiments are performed once a day, at the same time of day for 10 consecutive days. All mice achieved the criterion of no more than 2 errors within the

first 10 choices for 3 consecutive days by the 10th day of testing and were continued in the study. Following 10 consecutive days of spatial short-term memory testing, animals proceeded directly to the spatial long-term working memory task containing a retention interval delay.

2.2.4 Radial arm maze testing to assess spatial long-term working memory

On the following day after completion of spatial short-term working memory testing, spatial long-term working memory was tested using a modified delayed spatial win-shift assay. This is a 2-phase procedure similar to a standard 8-arm task with an interposed delay. This test consisted of a study phase and test phase, conducted in the same day for 10 consecutive days. For the initial study phase, the mouse was placed in the central chamber of the maze for a 2 minute acclimation period. After acclimation, only 4 of the 8 doors simultaneously opened, allowing free access to all open arms for the duration of the testing session (4 arms open, 4 arms baited). The 4 arm sequence during this phase was randomly chosen for each mouse on each day. Only a single food reward is delivered per baited arm, and a revisit to a previously visited food trough is considered an error in spatial short-term working memory. After collecting the last food reward, or after 15 minutes of elapsed time, the session ends and the doors close. The mouse was then subjected to a retention interval by returning to the home cage for 3 minutes while the maze is cleaned of any urine or feces that could potentially serve as visitation cues. The mouse was then returned to the central chamber to begin the subsequent test phase. After a 1 minute acclimation period (4 minute total interval), all 8 doors simultaneously opened allowing free access to all open arms for the duration of the testing session. Only arms that were previously closed during the study phase were

baited during the test phase (8 arms open, 4 arms baited). Each animal must collect the food reward available at the end of each of the 4 newly baited arms. Only a single food reward is delivered per baited arm, and a revisit to a previously baited food trough from the study phase was considered an error in spatial long-term working memory (maximum of 4 errors), and a revisit to any food trough during the test phase (whether baited in the training or test phase), was considered an error in spatial short-term working memory. All animals tested made only negligible short-term working memory errors during the test phase (NonTg, 0.09 errors in 4; 3xTg, 0.13 errors in 4, for both 3 and 8 months, data not shown) so both short-term and long-term working memory errors were combined into a total working memory error variable that we report herein as working memory errors. After collecting the last food reward, or after 15 minutes of elapsed time, the session ends and the doors close. In the test phase, the dependent variable is the number of errors in the first 4 choices. Comparisons are results obtained from the first 2 days and last 2 days of testing.

2.2.5 Chemicals and reagents

Except where noted, specialty chemicals and antibodies were obtained from Sigma Aldrich (St. Louis, MO).

2.2.6 Immunohistochemistry

Tissue from naive animals not used in behavioral or electrophysiological testing was fixed overnight with 4% paraformaldehyde at 4°C, embedded with paraffin, and cut into 6-10 µm sections using a Leica RM2155 microtome. Mounted sections were dewaxed in xylene and rehydrated in an ethanol gradient prior to antigen retrieval in boiling 50 mM sodium citrate plus 0.01% Tween 20 for 25 minutes. Endogenous

peroxidase activity was inhibited by incubating sections in 3% hydrogen peroxide for 10 minutes prior to washing with phosphate buffered saline (PBS) and blocking with 10 mg/ml bovine serum albumin in PBS overnight. The primary antibodies Beta-Amyloid Monoclonal antibody-10 (BAM-10), pTau-199/202, pTau231 (Acris Antibodies, San Diego, CA), and pTau396 were used at a concentration of 1/250, 1/200, 1/450, and 1/300, respectively. Secondary biotinylated goat anti-mouse and goat anti-rabbit antibodies were used at 1/450 dilution. Slices were incubated with 1/1000 streptavidin-HRP polymer complex (Vector Laboratory, Burlingame, CA). Slices were washed x3 for 5 minutes each between antibody and enzyme incubations with 0.02% Tween-20 in PBS. Diaminobenzidine enhanced substrate system was used according to the manufacturer's instructions. After washing off excess diaminobenzidine substrate, slides were counterstained with Gill's No. 2 hematoxylin prior to mounting coverslips. Sections were viewed with a Leica DM6000 B microscope (Wetzlar, Germany) with Hamamatsu ORCA-ER digital camera (Hamamatsu, Bridgewater, NJ).

2.2.7 Amyloid- β extraction

A β extraction was performed as previously described [24]. Briefly, ventral hippocampal tissue from behaviorally tested animals taken at the time of sacrifice for electrophysiological testing was obtained and stored at -80°C. The tissue was transferred to a Potter-Elvehjem homogenizer containing 4x brain volumes of 6.25 M guanidine HCl in 50 mM Tris buffered saline (50 mM Tris-HCl pH 8.0, 140 mM NaCl, 3 mM KCl, 5 mM EDTA, and 2 mM 1,10-phenanthroline) with 5 μ L protease inhibitor cocktail (5 mM EGTA, 1 mM DTT, 10 μ g/mL leupeptin, 1 μ L/mL pepstatin, 0.1 M PMSF, 0.1 M benzamidine, and 0.5 M ϵ -aminocaproic acid). After homogenization, samples

were transferred to a 1.5 mL microcentrifuge tube and rocked on a platform for 2 hours at room temperature before centrifugation at 12,000 rpm for 30 minutes. The supernatant was collected and stored at -80°C until the ELISA.

2.2.8 Enzyme-linked immunosorbent assay (ELISA)

ELISAs were performed as previously described [24-26]. Briefly, 96-well Costar plates were coated with 4.0 µg/mL BAM-10 for capture of all Aβ isoforms. Aβ 1-42 (Aβ42) levels were detected using a 1/250 dilution (2.5 µg/mL) of rabbit Aβ42 antibody. Wells were subsequently incubated with 100 µL of 1/500 biotinylated anti-rabbit antibody followed by incubation with (1/1000) Avidin D-horseradish peroxidase (Vector Laboratory, Burlingame, CA). Wells were washed x3 for 1 minute each with Tris buffered saline plus 0.05% Tween 20 after each incubation step. QuantaBlu substrate kit was used according to the manufacturers protocol (Pierce Biotechnology, Rockford, IL) and fluorescence of the HRP-substrate reaction was measured on a Biotek Synergy 2 plate reader (EX 320, EM 460) (Winooski, VT).

2.2.9 Extracellular field recording

Hippocampal slices were prepared from behaviorally tested 3 and 8 month old 3xTg-AD and NonTg mice 10-17 days after completion of radial arm maze testing. Mice were deeply anesthetized with halothane prior to decapitation. The brain was removed and submerged in ice-cold, oxygenated (95% O₂ / 5% CO₂) dissection artificial cerebrospinal fluid (ACSF) containing: 120 mM NaCl, 3 mM KCl, 4 mM MgCl₂, 1 mM NaH₂PO₄, 26 mM NaHCO₃, and 10 mM glucose. The brain was sectioned using a vibratome through the horizontal plane into 400 µm thick slices. The hippocampus was then dissected free from slices obtained between the levels of Bregma -4.0 mm to

Bregma -2.4 mm. We estimate such slices were from the ventral 35-40% of the hippocampus with respect to the longitudinal axis. We also excluded slices from the extreme 10% of the ventral pole, where it is difficult to clearly distinguish the CA1 pyramidal region from the CA2/3 and subicular regions. Slices were placed in a submersion recording chamber and perfused at approximately 1 ml/min with oxygenated (95% O₂ / 5% CO₂) standard ACSF containing: 120 mM NaCl, 3 mM KCl, 1.5 mM MgCl₂, 1 mM NaH₂PO₄, 2.5 mM CaCl₂, 26 mM NaHCO₃, and 10 mM glucose at room temperature. Slices recovered for 45 minutes at room temperature and an additional 45 minutes at 30°C. A bipolar stimulating electrode (Kopf Instruments, Tujunga, CA) was placed within the stratum radiatum of CA1 and an extracellular recording microelectrode (1.0 MΩ tungsten recording microelectrode, World Precision Instruments, Sarasota, FL) was positioned in the same layer of CA1. Field Excitatory Post-Synaptic Potentials (fEPSPs) were recorded at Schaffer collateral→CA1 synapses using a stimulus pulse consisting of a single square wave of 270 μs duration. Data were digitized at 10 kHz, low-pass filtered at 1 kHz, and analyzed with pCLAMP 10.2 software (Axon Instruments, Sunnyvale, CA). The initial slope of the population fEPSP was measured by fitting a straight line to a 1 ms window immediately following the fiber volley.

Stimulus response curves were obtained at the beginning of each experiment with stimulus pulses delivered at 40, 50, 60, 75, 90, 110, 130, and 150 μA once every 60 s (0.0167 Hz). For baseline recording, the stimulation intensity was adjusted to obtain a fEPSP of approximately 35-40% of the maximum response. Paired-pulse stimulations were performed at intervals of 50, 100, 200, and 500 ms. Five pairs of

pulses were performed and averaged together for each interval. The initial slope of the averaged second pulse was divided by the initial slope of the averaged first pulse to obtain the paired-pulse ratio for each slice. Synaptic responses for Long-Term Potentiation (LTP) experiments were normalized by dividing all fEPSP slope values by the average of the five responses recorded during the 5 minutes immediately prior to high frequency stimulation (HFS). LTP values for the 1 hour time point were determined by averaging 5 minutes of normalized slope values at 55-60 minutes post-HFS. The HFS protocol used to induce LTP in all experiments consisted of 4 episodes of 200 Hz/0.5 s stimulus trains (100 pulses x4) administered at 5 s inter-train intervals. In order to pharmacologically separate the NMDAR-dependent from the non-NMDAR-dependent component of LTP, the NMDAR antagonist D,L-AP5 (50 μ M) (Tocris Bioscience, Minneapolis, MN) was bath applied for 30 minutes prior to HFS, continued for 5 minutes post-HFS, and washed out for the remainder of recording. Reported n-values (x(y)) indicate the number of slices (x) and the number of animals (y) assessed.

2.2.10 Statistics

Tests of significance were performed using either ANOVA, or paired and independent t-tests as appropriate.

2.3 Results

Spatial working memory was evaluated in NonTg and 3xTg-AD mice at 3 and 8 months of age. Electrophysiological recordings of synaptic transmission and synaptic plasticity in the ventral hippocampal CA1 region of these same mice were obtained as well as quantification of total A β 42 levels.

2.3.1 Spatial memory testing

Spatial memory was tested in an 8-arm radial maze utilizing two different protocols. The first tested spatial short-term working memory utilizing an 8-arm uninterrupted task as shown in the top schematic diagram of Figure 2.1, and the second tested spatial long-term working memory utilizing a delayed spatial win-shift task as shown in the middle schematic diagram of Figure 2.1. The 8-arm uninterrupted task (8 arms open, 8 arms baited) showed no difference between genotypes at either 3 or 8 months of age (Figure 2.1A & B). Data from the 8-arm uninterrupted task (Figure 2.1A & B) were subjected to a 2 genotype (NonTg versus 3xTg-AD) x 2 training levels (first 2 versus last 2 days) x 2 ages (3 versus 8 months) mixed ANOVA. Within-subjects analysis showed there was a significant effect of training ($F(1,41)=26.472$, $p < 0.001$). None of the other factors were significant (all p values > 0.2). No significant effects were observed between-subjects. This indicates that both NonTg mice (3 month old, $n=11$; 8 month old, $n=11$) and 3xTg-AD mice (3 month old, $n=12$; 8 month old, $n=11$) performed similarly during the 10 days of testing, showing significant improvement from initial to terminal days, and demonstrating intact learning acquisition and spatial short-term working memory function.

Beginning on day 11, the same mice from the 8-arm uninterrupted task were evaluated using a delayed spatial win-shift assay as shown in the middle schematic diagram of Figure 2.1. In the study phase (4 arms open, 4 arms baited), mice at both 3 and 8 months of age showed no difference between genotypes (data not shown), as this task is a simplified version (4-arm uninterrupted task) of the 8-arm uninterrupted task depicted in the top schematic diagram of Figure 2.1. Upon completion of the study

phase, a 4 minute retention interval occurred before the subsequent test phase (8 arms open, 4 arms baited). Data from the test phase (Figure 2.1C & D) were subjected to a 2 genotype (NonTg versus 3xTg-AD) x 2 training levels (first 2 versus last 2 days) x 2 ages (3 versus 8 months) mixed ANOVA. Within-subjects analysis showed there was a significant effect of training ($F(1,41)=7.906$, $p < 0.01$) and a significant interaction of training x genotype ($F(1,41)=15.195$, $p < 0.001$). The significant interaction within-subjects demonstrates that the NonTg mice benefited from training more than did the 3xTg-AD mice. Follow up within-subjects comparisons with paired t-tests showed NonTg mice produced fewer errors as a consequence of training ($p < 0.01$ at both 3 and 8 months of age), whereas errors for 3xTg-AD mice remained unchanged despite training ($p > 0.05$ at both 3 and 8 months of age). Notably, the inability of 3xTg-AD mice to improve is not age-dependent. The mixed ANOVA showed no significant between-subjects effects, however a follow up between-subjects comparison using an independent t-test evaluating terminal performance (days 19-20) shows NonTg mice make fewer spatial working memory errors than 3xTg-AD mice at 8 months ($p < 0.05$; Figure 2.1D). This trend is also present at 3 months, but is not statistically significant ($p = 0.104$, Figure 2.1C). These results demonstrate that the onset of impairment of spatial working memory performance can be observed as early as 3 months of age in 3xTg-AD mice, but only after increasing memory load requirements using a rigorous delayed spatial win-shift assay that involves long-term working memory mechanisms.

2.3.2 Characterization of 3xTg-AD pathology and progression

To determine the histopathological state of 3xTg-AD mice, immunohistochemical analysis at 3 and 8 months was performed (Figure 2.2). Using a non-isoform specific

A β antibody (BAM-10), intraneuronal A β localization was detected in CA1 pyramidal neurons at both 3 and 8 months in 3xTg-AD mice, but not in NonTg mice. BAM-10 localization also revealed small disperse plaque deposits in the hippocampus of 8 month old 3xTg-AD mice, but not in NonTg or 3 month old 3xTg-AD mice. To determine relative levels of Tau hyperphosphorylation, three antibodies that recognize site-specific phosphorylation of Tau at Ser199/202, Thr231, and Ser396 were utilized. No detectable phospho-Tau within CA1 pyramidal neurons of NonTg or 3 month 3xTg-AD mice was found. However, in 8 month 3xTg-AD mice, phospho-Tau was readily detectable in CA1 pyramidal neurons of the hippocampus with all antibodies.

Since A β is suspected to be the initiating factor in the development of AD pathology, we wanted to determine if there were changes in hippocampal A β levels that coincide with the observed impairments in spatial working memory, and if individual A β levels correlated with behavioral measurements of cognitive performance. To quantify the amount of A β peptide, A β from ventral hippocampal brain tissue was extracted from the same mice that were tested in the radial arm maze. Since soluble A β (40 or 42), as well as total A β 40, has been shown to remain relatively stable with age in 3xTg-AD mice [20, 21], ELISAs were used to measure total A β 42 since it is the most abundant species in 3xTg-AD mice, and because of its more aggressive nature during disease progression (Figure 2.3A) [21, 22, 27]. The total A β 42 data were subjected to a 2 genotype (NonTg versus 3xTg-AD) x 2 ages (3 versus 8 months) ANOVA. There was a significant effect of age ($F(1,37)=68.4$, $p < 0.001$), genotype ($F(1,37)=616.6$, $p < 0.001$), and interaction of age x genotype ($F(1,37)=63.9$, $p < 0.001$). As can be seen in Figure 2.3A, the interaction confirms the visual impression that A β 42 accumulation significantly

increased as a function of age for the 3xTg-AD mice but not for the NonTg mice, which is consistent with the immunohistochemistry. At both 3 and 8 months of age, 3xTg-AD mice show a significant correlation between total A β 42 and spatial working memory as measured by the number of errors that occurred in the test phase before visiting the last baited arm (Figure 2.3B) (3 months: $r^2 = 0.354$; Pearson correlation coefficient 0.6, $p < 0.05$; 8 months: $r^2 = 0.404$, Pearson correlation coefficient 0.8, $p < 0.01$). The results suggest that within a given age cohort, increased levels of total A β 42 correlated with decreased cognitive performance. Additional comparisons between total LTP, NMDAR LTP, or non-NMDAR LTP and maze performance or A β 42 levels were also conducted but did not result in any significant correlations (Data not shown).

2.3.3 Electrophysiology

To determine if neurophysiological differences exist between 3xTg-AD and NonTg mice at 3 and 8 months of age, fEPSPs from the CA1 region of ventral hippocampal slices were recorded. Stimulus response curves were generated to evaluate the functional range of synaptic activity (Figure 2.4). At 3 months of age, baseline fEPSPs for both groups were largely similar. The 3xTg-AD mice ($n=54(12)$) exhibited significantly lower fEPSP slope values than NonTg mice ($n=56(11)$) at the highest stimulus intensities (Figure 2.4A, 130 and 150 μ A, $p < 0.05$). At 8 months of age, fEPSP slopes at intensities greater than 60 μ A were significantly reduced ($p < 0.01$) in 3xTg-AD mice ($n=39(11)$) compared to NonTg mice ($n=47(11)$) (Figure 2.4B).

Short-term synaptic plasticity was evaluated using a paired-pulse stimulus protocol to determine the degree of synaptic facilitation (Figure 2.5). At 3 months of age, both 3xTg-AD and NonTg mice showed paired-pulse facilitation at all intervals

tested except 500 ms (Figure 2.5A). The 3xTg-AD mice (n=54(12)) showed significantly less facilitation ($p < 0.01$) than NonTg mice (n=58(11)). Paired-pulse facilitation in 8 month old mice showed similar results, as the 3xTg-AD mice (n=36(11)) showed significantly less facilitation ($p < 0.01$) than NonTg mice (n=42(11)) at stimulus intervals of 50,100, and 200 ms (Figure 2.5B). In addition, a modest but significant difference ($p < 0.05$) in the 500 ms paired-pulse response was also present between 3xTg-AD and NonTg mice at 8 months of age.

Long-term synaptic plasticity was evaluated by inducing LTP using a multiple train stimulus induction protocol previously shown to elicit a compound potentiation consisting of both NMDAR and non-NMDAR components of LTP [28] (Figure 2.6). The non-NMDAR component of LTP was measured utilizing the selective NMDAR antagonist D,L-AP5 to block the NMDAR component of LTP. LTP data were subjected to a 2 genotype (NonTg versus 3xTg-AD) x 2 treatment group (No drug (total LTP) versus D,L-AP5 (non-NMDAR LTP)) ANOVA for multiple group comparisons at each age. The ANOVA revealed a significant effect of genotype ($F(1,94)=5.879$, $p < 0.05$) and treatment ($F(1,94)=10.926$, $p < 0.01$) at 3 months. While there was no statistical interaction of genotype x treatment, it was close to significance ($F(1,94)=3.730$, $p = 0.056$). At 8 months of age, there was a significant effect of treatment ($F(1,71)=13.366$, $p < 0.01$) and a significant interaction of genotype x treatment ($F(1,71)=5.533$, $p < 0.05$), indicating that genotype influenced the response to treatment. ANOVAs were followed by Tukey's post-hoc analysis to determine significance between specific treatment groups and between genotypes for each treatment.

At 3 months of age, there was no significant difference in total LTP between 3xTg-AD mice ($47 \pm 4\%$, $n=23(12)$) and NonTg mice ($45 \pm 2\%$, $n=25(10)$) (Figure 2.6A, B, & C). However, in the presence of D,L-AP5 ($50 \mu\text{M}$), the potentiated fEPSP slope value was significantly reduced in NonTg mice ($28 \pm 3\%$, $n=25(10)$) but not significantly altered in 3xTg-AD mice ($42 \pm 4\%$, $n=25(12)$) as compared with their respective total LTP values (Figure 2.6C). In addition, the non-NMDAR component of LTP was significantly greater ($p < 0.01$) in 3xTg-AD mice than in the NonTg mice (Figure 2.6C). At 8 months, total LTP was significantly reduced ($p < 0.05$) in 3xTg-AD mice ($31 \pm 4\%$, $n=15(11)$) compared to NonTg mice ($46 \pm 4\%$, $n=19(9)$) (Figure 2.6D, E, & F). These results agree with a previous report describing the timing of impairment in total LTP magnitude in the 3xTg-AD mice [22]. In the presence of D,L-AP5 ($50 \mu\text{M}$), the potentiated fEPSP slope value was again significantly reduced ($p < 0.01$) in NonTg mice ($24 \pm 2\%$, $n=23(11)$), and was not significantly altered in 3xTg-AD mice ($27 \pm 5\%$, $n=18(11)$) as compared to their respective total LTP values (Figure 2.6F). Note that the significant difference in the magnitude of the non-NMDAR component of LTP observed between the two genotypes at 3 months is not evident at 8 months of age (Figure 2.6C & F). Thus, the significant decrease in total LTP at 8 months of age in the 3xTg-AD mice is most likely due to the decrease in the non-NMDAR component of LTP.

2.4 Discussion

In this study, behavioral deficiencies in spatial working memory were found in the 3xTg-AD mouse model using the 8-arm radial maze. At both 3 and 8 months of age, these mice failed to demonstrate improvements in spatial working memory performance

in the test phase of a delayed spatial win-shift assay, compared to their NonTg counterparts (Figure 2.1C & D). This is in contrast to results from the 8-arm uninterrupted task, which assesses spatial short-term working memory and yielded similar improvement across session days in both 3xTg-AD and NonTg mice (Figure 2.1A & B). A significant decrease in paired-pulse facilitation was consistently observed in the 3xTg-AD mice at both 3 and 8 months of age (Figure 2.5), and although the total magnitude of LTP in the CA1 region of the hippocampus was equivalent for the NonTg and 3xTg-AD mice at 3 months, the contribution of non-NMDAR LTP was significantly greater in 3xTg-AD than NonTg mice (Figure 2.6). The impairment in spatial working memory in the test phase of our delayed spatial win-shift assay was concurrent with alterations in both short-term presynaptic plasticity and the NMDAR-dependent component of LTP in 3xTg-AD mice at both 3 and 8 months. In addition, impairments in spatial working memory of individual 3xTg-AD mice were positively correlated with total A β 42 levels in both of these age groups (Figure 2.3).

The results from the 8-arm uninterrupted task demonstrate that both NonTg and 3xTg-AD mice have intact spatial learning and navigation (i.e., they show equivalent levels of learning the rules required to complete the radial maze task, equivalent perception of spatial cues, equivalent levels of motivation and locomotor control). Due to the continuous nature of this task the working memory load is low, making the procedure dependent upon immediately accessible information from short-term memory [29, 30]. In order to specifically examine spatial working memory involving a long-term component, the mice were tested in a 2-phase delayed spatial win-shift assay, which included a retention interval delay of 4 minutes. The incorporation of a time delay

forces retention of trial-unique spatial information (i.e., the mice must remember which arms were visited in phase 1 in order to successfully complete phase 2), which increases working memory load beyond the capability of short-term memory. This allowed discrimination in performance between NonTg and 3xTg-AD mice, as the NonTg mice showed improvement across sessions but the 3xTg-AD mice did not. The test phase results suggest that 3xTg-AD mice have impaired spatial working memory (i.e., memory for daily location-specific information) when long-term working memory mechanisms are required. This is likely a profound impairment specifically for this type of spatial working memory, since the 8-arm uninterrupted task results indicated intact acquisition of the maze rules (making a general impairment in learning capability unlikely).

Assessments of spatial learning and memory depend upon intact hippocampal function [29, 31-33]. From analysis of anatomical, genetic, and functional data from primarily animal models, it was proposed that the dorsal and ventral sectors of the hippocampus are distinct entities, both anatomically and functionally [34]. However, there is some controversy to ascribing particular functions solely to the dorsal or ventral hippocampus (reviewed in [35]). More recently, a primary role for the ventral sector of the hippocampus in spatial working memory has been reported [36], as well as a report of ventral hippocampus involvement in goal-directed spatial learning [37]. Both of these observations are consistent with the presence of a direct anatomical connection between the ventral hippocampus and the medial prefrontal cortex [38, 39]. Finally, with respect to the possible relevance of the ventral hippocampus for being involved in early AD deficits, evidence indicates that early loss of hippocampal tissue in AD patients is

more prominent in the anterior (ventral) sector [40, 41]. Therefore, in the current studies we obtained electrophysiological recordings from hippocampal slices taken from the ventral third of the hippocampus to determine if synaptic function is altered in 3xTg-AD mice when behavioral impairments are evident in a spatial working memory task dependent upon intact ventral hippocampal function.

Basal synaptic transmission is largely similar between genotypes at 3 months of age, but at 8 months a reduction in the fEPSP responses were observed in both NonTg and 3xTg-AD mice, with the 3xTg-AD mice being significantly less responsive than the NonTg mice (Figure 2.4). This reduction in NonTg mice at 8 months is most likely due to a normal age-related decline of synaptic AMPAR activity, possibly related to reduced postsynaptic AMPAR activity [42, 43]. In the 8 month old 3xTg-AD mice, this age-related decline in synaptic transmission may be exaggerated due to A β -induced AMPAR trafficking [44] or changes in Ca²⁺ homeostasis [45]. Previous investigations of short-term synaptic plasticity have reported that measurements of paired-pulse facilitation in the CA1 region of both 1 and 6 month old 3xTg-AD mice are not significantly different from NonTg mice [22, 46]. In contrast, our results demonstrate the paired-pulse facilitation ratio is significantly decreased in 3xTg-AD mice at both 3 and 8 months of age (Figure 2.5). Other work has shown dysregulation of Ca²⁺ homeostasis in 3xTg-AD mice as early as 6 weeks of age [47]. Alterations in presynaptic Ca²⁺ levels would be expected to affect paired-pulse facilitation [48], however the specific underlying mechanism at work here is uncertain. Our observation of a reduction in paired-pulse ratio in ventral hippocampal slices from 3xTg-AD mice may be an early

neurophysiological indicator of a functional synaptic abnormality that is consistent with the dysregulation of Ca^{2+} homeostasis and excitatory neurotransmission [49].

In addition to evaluating short-term synaptic plasticity, we also investigated a form of long-term synaptic plasticity by evaluating the ability of mice to sustain a long-term potentiation of synaptic strength, LTP. At least two forms of LTP are known to coexist at CA3→CA1 synapses, NMDAR LTP and non-NMDAR LTP [9-11], both of which have been shown to be involved in spatial learning and memory [50, 51]. Our results demonstrate that NMDAR LTP was significantly reduced in 3xTg-AD mice at both 3 and 8 months of age, coinciding with the spatial working memory failure in the test phase of our delayed spatial win-shift assay. Interestingly, while the NMDAR component of LTP was reduced in 3xTg-AD mice, the non-NMDAR component of LTP increased. As a result, the combination of NMDAR LTP with non-NMDAR LTP yielded a total LTP that was not significantly different between 3xTg-AD and NonTg mice at 3 months of age. At 8 months however, 3xTg-AD mice showed a significant reduction in total LTP compared to NonTg mice. These results (no difference at 3 months, reduction at 8 months) are consistent with previous work [22].

The importance of NMDAR function in spatial working memory has been demonstrated in numerous studies. NMDARs that are pharmacologically blocked prior to behavioral tests of working memory [14-16, 51, 52], or knock-out mice with non-functional NMDARs due to missing NR2A or NR2B^{ΔFb} subunits [53, 54], show profound deficits in spatial working memory. Pharmacological blockade of NMDARs in wild-type animals assessed for short-term and working memory performance in spatial tasks similar to our own have impairments in working memory, but not short-term memory

[52]. Together these results suggest a specific role for NMDAR LTP in spatial working memory [14-16, 51-57]. In light of these findings, the reduction in NMDAR LTP we observed in 3xTg-AD mice at both 3 and 8 months of age appears likely to play a causative role in the spatial working memory impairment we have observed in the current study. Others have reported reduced NMDAR currents in CA1 pyramidal cells of either PS1 [58] or APP [59] mutant mice and reported reductions in LTP. Interestingly, in an APP/PS1 mutant mouse the loss of NMDAR-mediated cGMP production occurred without an associated loss of NMDAR density, demonstrating that a change in receptor expression is not required for altered signal transduction [60].

In unimpaired aged rats performing a reference memory task, the loss of NMDAR LTP was accompanied by a compensatory increase in non-NMDAR LTP [57]. In the current study, 3xTg-AD mice had increased non-NMDAR LTP at 3 months, an age they were thought to be cognitively unimpaired. This could account for previous findings which demonstrated that 3xTg-AD mice were unimpaired at 2 months in the Morris Water Maze (MWM) [20], as the MWM is primarily a test of spatial reference memory as opposed to spatial working memory [61, 62]. Furthermore, our studies indicated the majority of LTP in 3xTg-AD mice is non-NMDAR LTP at both 3 and 8 months of age. Thus the reduction in total LTP at 8 months is possibly due to reduced activation of VDCCs, as the majority of non-NMDAR LTP in wild-type animals is VDCC-dependent [28]. Interestingly, it has been reported that APP/PS1 mutant mice have reduced somatic Na⁺ currents resulting in reduced VDCC activation [63], this potentially could result in the decreased non-NMDAR LTP we observed in our 8 month old 3xTg-AD animals. Other possibilities for mechanisms involved in non-NMDAR LTP include

synaptic plasticity mediated by A β and metabotropic glutamate receptor signaling [64, 65], or NR2B containing NMDARs [66].

The 3xTg-AD mice used in our study are homozygous for three mutant transgenes: APP(Swe), Psen1, and TauP301L, with expression driven by the Thy1.2 promoter. In contrast to exogenously applied A β 42, neurons in 3xTg-AD mice are continuously exposed to A β 42 from a very young age and potential compensatory mechanisms to synaptic dysfunction could therefore develop as the mouse ages. The increased non-NMDAR LTP observed in the 3 month old mice of the current study may be an example of such compensation. It is important to note that such effects are likely not observed in acute slice studies. For example, the effects of acutely applied exogenous A β 42 to *ex vivo* slices are probably manifested via alterations of NMDAR LTP, but without the associated increase in non-NMDAR LTP.

The effect of A β 42 on synaptic loss and its consequences for memory functions are complex. The increase in A β 42 levels at 3 and 8 months in our mice coincides with the presence of intraneuronal A β at 3 months, and intraneuronal A β and β -Amyloid plaques at 8 months, and with the behavioral and electrophysiological alterations we have observed at these ages. A comparison of A β 42 levels with the total number of errors accrued in the test phase of our 8-arm radial maze task, show there is a significant relationship between total A β 42 levels and spatial working memory performance. At 8 months, total A β 42 was significantly higher than at 3 months, but without concomitantly increased detriment to maze performance. Given that soluble A β 42 levels remain constant over a period of 2-6 months in this 3xTg-AD model [20], the continued increase in total A β 42 measured at 8 months is likely due to its

accumulation within insoluble depositions. This may explain why an increase in total A β 42 levels at 8 months does not result in further decrement of maze performance if the age-associated accumulation of insoluble A β 42 is extraneous. These findings suggest that intraneuronal A β 42 may act as an initiator of synaptic impairment that drive impairments in cognitive performance. The first demonstration fully developed impairments in long-term spatial reference memory in 3xTg-AD mice occurs by 6 months, a time when β -Amyloid plaque is present [20]. The first signs of spatial reference memory impairment however, show up as impairments in day to day trial training at 4 months (3xTg-AD mice perform worse than NonTg mice on the first trial of each day during MWM acquisition training, but perform similarly by the last trial of each day, and perform similarly overall throughout the course of 5 consecutive days of training), a time when only intraneuronal A β is present. In another study using a 2xTg-AD (APP/PS1) model, a correlation between A β 42 levels and spatial reference memory impairment in the MWM was also only identified at a time when β -Amyloid plaque was present [67]. In human AD patients, the total amount of cortical A β 42 was positively correlated with mild clinical dementia prior to Tau pathology [68]. Transgenic mice that produce high levels of A β 42 but do not form β -Amyloid plaques or Tau pathology show significant synaptic loss and behavioral impairments similar to mice that do [69]. These observations add further support to the suggestion that soluble A β 42 may be important for early synaptic deficits associated with the disease state [70]. However, the total A β load may also be important, depending upon the behavioral endpoint being assessed. A multimetric statistical analysis of four transgenic mouse lines differing in A β deposition was assessed by a large battery of behavioral tests [71]. The results of this analysis

showed impaired acquisition and memory retention in the MWM were correlated with the “diffuse” and “compact” A β deposition in the brain, respectively. While relationships between A β 42 levels and spatial working memory performance were evident in the current study, correlations between A β 42 and other measures of electrophysiology were not found. For example, LTP values were not correlated with spatial working memory performance in the current study, although other forms of memory, such as spatial reference memory, have been shown to correlate to LTP [57].

In the current series of studies, we have characterized early behavioral and electrophysiological alterations, and total A β 42 in 3xTg-AD model mice. Our findings of behavioral impairment in spatial working memory at 3 months of age is at least 3 months before the observation of plaque formation in the hippocampus of these mice [20, 22]. Our findings of altered synaptic plasticity, such as decreased paired-pulse facilitation and decreased NMDAR LTP in the ventral hippocampus, coincide with significant impairments in radial arm maze performance, intraneuronal A β , and increased A β 42 levels. The linear relationship between A β 42 levels and spatial working memory errors demonstrates that individuals producing more A β 42 suffered greater memory impairment. These observations in 3xTg-AD mice show that physiological and behavioral deficiencies are present at an age previously referred to by many investigators as presymptomatic for these animals. Our additional finding that 3xTg-AD mice also exhibited an increase in non-NMDAR LTP at 3 months of age is intriguing, and warrants further investigation into this potentially adaptive mechanism during the early stages of AD. Such observations regarding the early functional and behavioral consequences of increased A β 42 in a mouse model of AD provides new insight at the

mechanistic level for potentially understanding the early cognitive impairments observed in AD patients.

Acknowledgments

Funding for this work was provided by NIH R01 N5046451 (www.ninds.nih.gov) to R. Furukawa and M. Fechtner. Disclosure statement: There are no conflicts of interest. All animal protocols and experiments were approved by the University of Georgia Institutional Animal Care and Use Committee.

References

1. Querfurth, H.W. and F.M. LaFerla, *Alzheimer's disease*. N Engl J Med, 2010. **362**(4): p. 329-44.
2. LaFerla, F.M., K.N. Green, and S. Oddo, *Intracellular amyloid-beta in Alzheimer's disease*. Nat Rev Neurosci, 2007. **8**(7): p. 499-509.
3. Morris, M., et al., *The many faces of tau*. Neuron, 2011. **70**(3): p. 410-26.
4. Yu, J.T., R.C. Cahng, and L. Tan, *Calcium dysregulation in Alzheimer's disease: from mechanisms to therapeutic opportunitites*. Prog. Neurobiol., 2009. **89**: p. 240-255.
5. Berridge, M.J., *Calcium signalling and Alzheimer's disease*. Neurochem. Res., 2011. **36**: p. 1149-1156.
6. Peng, S., et al., *Glutamate receptors and signal transduction in learning and memory*. Mol. Biol. Rep., 2011. **38**: p. 453-460.
7. Bliss, T. V. and G.L. Collingridge, *A synaptic model of memory: long-term potentiation in the hippocampus*. Nature, 1993. **361**: p. 31-39.
8. Citri, A. and R.C. Malenka, *Synaptic plasticity: multiple forms, functions, and mechanisms*. Neuropsychopharmacology, 2008. **33**: p. 18-41.
9. Morgan, S.L. and T.J. Teyler, *VDCCs and NMDARs underlie two forms of LTP in CA1 hippocampus in vivo*. J Neurophysiol, 1999. **82**(2): p. 736-40.
10. Cavus, I. and T. Teyler, *Two forms of long-term potentiation in area CA1 activate different signal transduction cascades*. J Neurophysiol, 1996. **76**(5): p. 3038-47.
11. Grover, L.M. and T.J. Teyler, *Two components of long-term potentiation induced by different patterns of afferent activation*. Nature, 1990. **347**(6292): p. 477-9.
12. Morris, R.G., et al., *Selective impairment of learning and blockade of long-term potentiation by an N-methyl-D-aspartate receptor antagonist, AP5*. Nature, 1986. **319**: p. 774-776.
13. Maurice, T., J. Bayle, and A. Privat, *Learning impairment following acute administration of the calcium channel antagonist nimodipine in mice*. Behav Pharmacol, 1995. **6**(2): p. 167-175.
14. Butelman, E.R., *A novel NMDA antagonist, MK-801, impairs performance in a hippocampal-dependent spatial learning task*. Pharm. Biochem. Behav., 1989. **34**: p. 13-16.

15. Bolhuis, J.J. and I.C. Reid, *Effects of intraventricular infusion of the N-methyl-D-aspartate (NMDA) receptor antagonist AP5 on spatial memory of rats in a radial arm maze*. Behav. Brain Res., 1992. **47**: p. 151-157.
16. Ward, L., S.E. Mason, and W.C. Abraham, *Effects of the NMDA antagonists CPP and MK-801 on radial arm maze performance in rats*. Pharm. Biochem. Behav., 1990. **35**: p. 785-790.
17. Zhang, X.H., et al., *Delay-dependent impairment of spatial working memory with inhibition of NR2B-containing NMDA receptors in hippocampal CA1 region of rats*. Mol. Brain, 2013. **6**: p. 13.
18. Niewoehner, B., et al., *Impaired spatial working memory but spared spatial reference memory following functional loss of NMDA receptors in the dentate gyrus*. Eur. J. Neurosci., 2007. **25**: p. 837-846.
19. Driesen, N.R., et al., *The impact of NMDA receptor blockade on human working memory-related prefrontal function and connectivity*. Neuropsychopharmacology, 2013. **38**: p. 2613-2622.
20. Billings, L.M., et al., *Intraneuronal Ab causes the onset of early Alzheimer's disease-related cognitive deficits in transgenic mice*. Neuron, 2005. **45**: p. 675-688.
21. Oddo, S., et al., *Amyloid deposition precedes tangle formation in a triple transgenic model of Alzheimer's disease*. Neurobiol Aging, 2003. **24**(8): p. 1063-70.
22. Oddo, S., et al., *Triple-transgenic model of Alzheimer's disease with plaques and tangles: intracellular Abeta and synaptic dysfunction*. Neuron, 2003. **39**(3): p. 409-21.
23. Babb, S.J. and J.D. Crystal, *Episodic-like memory in the rat*. Curr. Biol., 2006. **16**: p. 1317-1321.
24. Hemming, M.L., D. Selkoe, and W. Farris, *Effects of prolonged angiotensin-converting enzyme inhibitor treatment on amyloid beta-protein metabolism in mouse models of Alzheimer disease*. Neurobiol. Dis., 2007. **26**: p. 273-281.
25. Hemming, M.L. and D. Selkoe, *Amyloid beta-protein is degraded by cellular angiotensin-converting enzyme (ACE) and elevated by an ACE inhibitor*. J. Biol. Chem., 2005. **280**: p. 37644-37650.
26. Johnson-Wood, K., et al., *Amyloid precursor protein processing and A β 42 deposition in a transgenic mouse model of Alzheimer disease*. Proc. Natl. Acad. Sci. USA, 1997. **94**: p. 1550-1555.

27. Hardy, J., *A hundred years of Alzheimer's disease research*. Neuron, 2006. **52**: p. 3-13.
28. Grover, L.M. and T.J. Teyler, *Two components of long-term potentiation induced by different patterns of afferent activation*. Nature, 1990. **347**: p. 477-479.
29. Floresco, S.B., J.K. Seamans, and A.G. Phillips, *Selective roles for hippocampal, prefrontal cortical, and ventral striatal circuits in radial-arm maze tasks with or without a delay*. J. Neurosci., 1997. **17**: p. 1880-1890.
30. Baddeley, A., *Working memory*. Curr. Biol., 2010. **20**: p. R136-R140.
31. Jarrard, L.E., *On the role of the hippocampus in learning and memory in the rat*. Behav. Neural Biol., 1993. **60**: p. 9-26.
32. Olton, D.S. and B.C. Papas, *Spatial memory and hippocampal function*. Neuropsychologia, 1979. **17**: p. 668-682.
33. Becker, J.T., J.A. Walker, and D.S. Olton, *Neuroanatomical bases of spatial memory*. Brain Res., 1980. **200**: p. 307-320.
34. Fanselow, M.S. and H.W. Dong, *Are the dorsal and ventral hippocampus functionally distinct structures?* Neuron, 2010. **65**: p. 7-19.
35. Poppenk, J., et al., *Long-axis specialization of the human hippocampus*. Trends Cogn. Sci., 2013. **17**: p. 230-240.
36. O'Neill, P.K., J.A. Gordon, and T. Sigurdsson, *Theta oscillations in the medial prefrontal cortex are modulated by spatial working memory and synchronize with the hippocampus through its ventral subregion*. J. Neurosci., 2013. **33**: p. 1411-1424.
37. Ruediger, S., et al., *Goal-oriented searching mediated by ventral hippocampus early in trial-and-error learning*. Nat Neurosci, 2012. **15**(11): p. 1563-71.
38. Degenetais, E., et al., *Synaptic influence of hippocampus on pyramidal cells of the rat prefrontal cortex: an in vivo intracellular recording study*. Cereb Cortex, 2003. **13**(7): p. 782-92.
39. Tripathi, A., et al., *The hippocampal to prefrontal cortex circuit in mice: a promising electrophysiological signature in models for psychiatric disorders*. Brain Struct Funct, 2015.
40. Qiu, A., et al., *Regional shape abnormalities in mild cognitive impairment and Alzheimer's disease*. NeuroImage, 2009. **45**: p. 656-661.
41. Frisoni, G.B., et al., *Mapping local hippocampal changes in Alzheimer's disease and normal ageing with MRI at 3 Tesla*. Brain Pathol., 2008. **131**: p. 3266-3276.

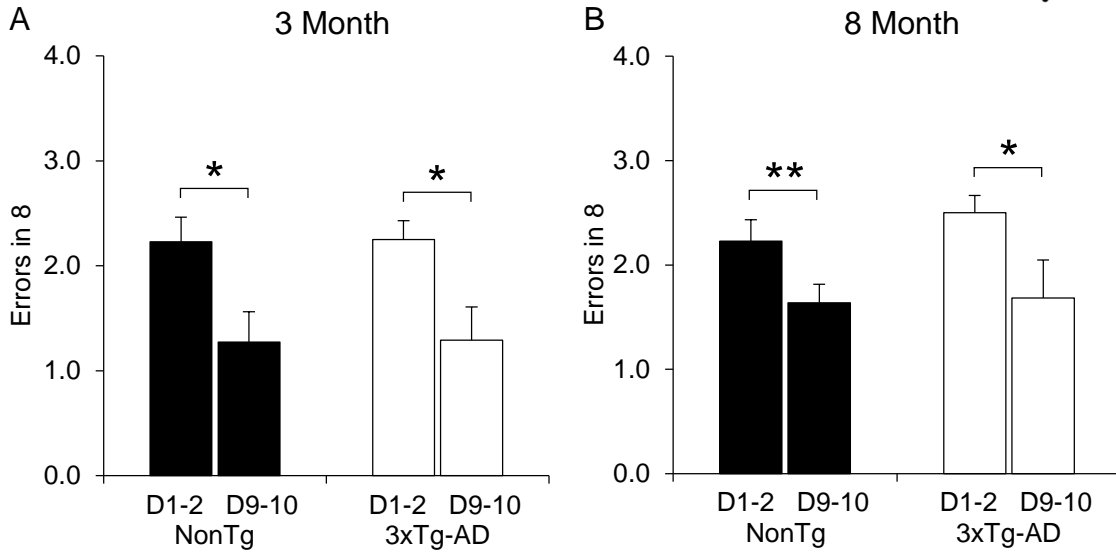
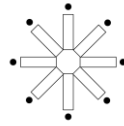
42. Kumar, A. and T.C. Foster, *Neurophysiology of Old Neurons and Synapses*, in *Brain Aging: Models, Methods, and Mechanisms*, D.R. Riddle, Editor. 2007: Boca Raton (FL).
43. Barnes, C.A., G. Rao, and G. Orr, *Age-related decrease in the Schaffer collateral-evoked EPSP in awake, freely behaving rats*. *Neural Plast*, 2000. **7**(3): p. 167-78.
44. Hsieh, H., et al., *AMPA removal underlies Abeta-induced synaptic depression and dendritic spine loss*. *Neuron*, 2006. **52**(5): p. 831-43.
45. Chakroborty, S., et al., *Early presynaptic and postsynaptic calcium signaling abnormalities mask underlying synaptic depression in presymptomatic Alzheimer's disease mice*. *J Neurosci*, 2012. **32**(24): p. 8341-53.
46. Chakroborty, S., et al., *Deviant ryanodine receptor-mediated calcium release resets synaptic homeostasis in presymptomatic 3xTg-AD mice*. *J Neurosci*, 2009. **29**(30): p. 9458-70.
47. Stutzmann, G.E., et al., *Enhanced ryanodine receptor recruitment contributes to Ca²⁺ disruptions in young, adult, and aged Alzheimer's disease mice*. *J. Neurosci.*, 2006. **26**: p. 5180-5189.
48. Zucker, R.S. and W.G. Regehr, *Short-term synaptic plasticity*. *Annu. Rev. Physiol.*, 2002. **64**: p. 355-405.
49. Paula-Lima, A.C., J. Brito-Moreira, and S.T. Ferreira, *Deregulation of excitatory neurotransmission underlying synapse failure in Alzheimer's disease*. *J. Neurochem.*, 2013. **126**: p. 191-2002.
50. Davis, S., S.P. Butcher, and R.G. Morris, *The NMDA receptor antagonist D-2-amino-5-phosphonopentanoate (D-AP5) impairs spatial learning and LTP in vivo at intracerebral concentrations comparable to those that block LTP in vitro*. *J. Neurosci.*, 1992. **12**: p. 21-34.
51. Borroni, A.M., et al., *Role of voltage-dependent calcium channel long-term potentiation (LTP) and NMDA LTP in spatial memory*. *J. Neurosci.*, 2000. **20**: p. 9272-9276.
52. Enomoto, T. and S.B. Floresco, *Disruptions in spatial working memory, but not short-term memory, induced by repeated ketamine exposure*. *Prog. Neuropsychopharmacol Biol. Psychiatry*, 2009. **33**: p. 668-675.
53. Bannerman, D.M., et al., *NMDA receptor subunit NR2A is required for rapidly acquired spatial working memory but not incremental spatial reference memory*. *J. Neurosci.*, 2008. **28**: p. 3623-3630.

54. von Engelhardt, J., et al., *Contribution of hippocampal and extra-hippocampal NR2B containing NMDA receptors to performance on spatial learning tasks.* Neuron, 2008. **60**: p. 846-860.
55. Shankar, S., T.J. Teyler, and N. Robbins, *Aging differentially alters forms of long-term potentiation in rat hippocampal area CA1.* J. Neurophysiol., 1998. **79**: p. 334-341.
56. Rosenzweig, E.S. and C.A. Barnes, *Impact of aging on hippocampal function: plasticity, network dynamics, and cognition.* Prog. Neurobiol., 2003. **69**: p. 143-179.
57. Boric, K., et al., *Potential adaptive function of altered long-term potentiation mechanisms in aging hippocampus.* J. Neurosci., 2008. **28**: p. 8034-8039.
58. Wang, Y., et al., *Presenilin-1 mutation impairs cholinergic modulation of synaptic plasticity and suppresses NMDA currents in hippocampus slices.* Neurobiol. Aging, 2009. **30**: p. 1061-1068.
59. Tozzi, A., et al., *Region- and age-dependent reductions of hippocampal long-term potentiation and NMDA to AMPA ratio in a genetic model of Alzheimer's disease.* Neurobiol. Aging, 2015. **36**: p. 123-133.
60. Duszczuk, M., et al., *in vivo hippocampal microdialysis reveals impairment of NMDA receptor-cGMP signaling in APP(SW) and APP(SW)/PS1(L166P) Alzheimer's transgenic mice.* Neurochem. Int., 2012. **61**: p. 976-980.
61. Morris, R.G., *Developments of a water-maze procedure for studying spatial learning in the rat.* J. Neurosci. Meth., 1984. **11**: p. 47-60.
62. Wenk, G.L., *Assessment of spatial memory using the radial arm maze and Morris water maze.* Curr. Protoc. Neurosci., 2004. **8**: p. unit 8.5A.
63. Brown, J.T., et al., *Altered intrinsic neuronal excitability and reduced Na⁺ currents in a mouse model of Alzheimer's disease.* Neurobiol. Aging, 2011. **32**: p. 2109 e2101-2114.
64. Wang, Q., et al., *Block of long-term potentiation by naturally secreted and synthetic amyloid beta-peptide in hippocampal slices is mediated via activation of the kinases c-Jun N-terminal kinase, cyclin-dependent kinase 5, and p38 mitogen-activated protein kinase as well as metabotropic glutamate receptor type 5.* J Neurosci, 2004. **24**(13): p. 3370-8.
65. Li, S., et al., *Soluble oligomers of amyloid Beta protein facilitate hippocampal long-term depression by disrupting neuronal glutamate uptake.* Neuron, 2009. **62**(6): p. 788-801.

66. Li, S., et al., *Soluble Abeta oligomers inhibit long-term potentiation through a mechanism involving excessive activation of extrasynaptic NR2B-containing NMDA receptors*. J Neurosci, 2011. **31**(18): p. 6627-38.
67. Puolivali, J., et al., *Hippocampal abeta 42 levels correlate with spatial memory deficit in APP and PS1 double transgenic mice*. Neurobiol. Dis., 2002. **9**: p. 339-347.
68. Naslund, J., et al., *Correlation between elevated levels of amyloid b-peptide in the brain and cognitive decline*. J. Am. Med. Assoc., 2000. **283**: p. 1571-1577.
69. Koistinaho, M., et al., *Specific spatial learning deficits become severe with age in beta-amyloid precursor protein transgenic mice that harbor diffuse beta-amyloid deposits but do not form plaques*. Proc. Natl. Acad. Sci. U. S. A., 2001. **98**: p. 14675-14680.
70. Mucke, L., et al., *High-level neuronal expression of Abeta₁₋₄₂ in wild type human amyloid protein precursor transgenic mice: synaptotoxicity without plaque formation*. J. Neurosci., 2000. **20**: p. 4050-4058.
71. Leighty, R.E., et al., *Use of multivariate statistical analysis to characterize and discriminate between the performance of four Alzheimer's transgenic mouse lines differing in Ab deposition*. Behav. Brain Res., 2004. **153**: p. 107-121.

Figures

8-Arm uninterrupted task: 8 Arms Open; 8 Arms Baited



Study Phase: 4 Arms Open; 4 Arms Baited



Retention Interval (4 min)

Test Phase: 8 Arms Open; 4 Arms Baited

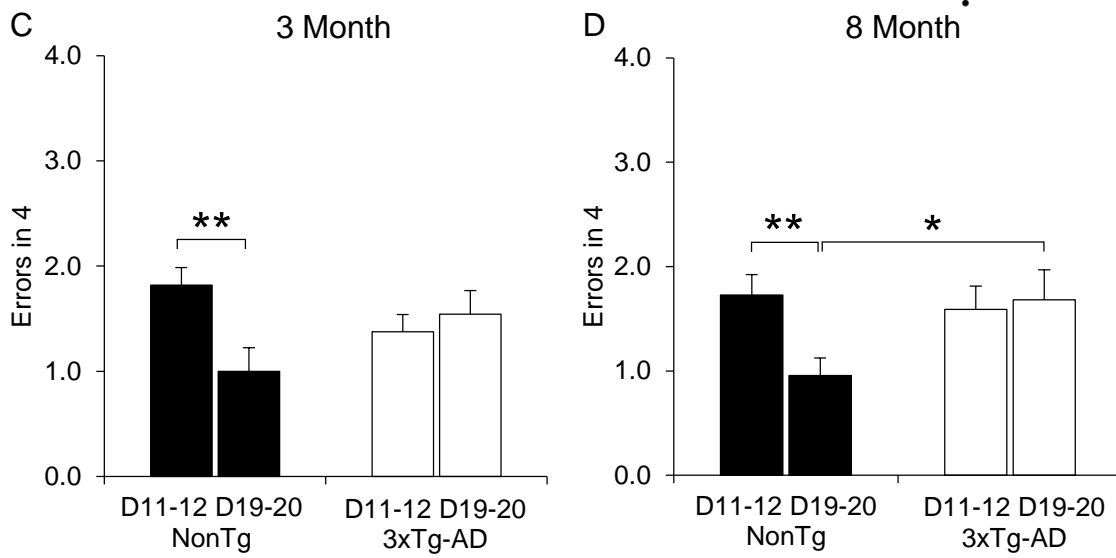
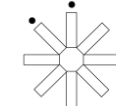


Figure 2.1. Short-term and working memory in the 8-arm radial maze. The Schematic above each data set illustrates the protocol used for testing. (•) represents baited arms. Blacked out arms represent inaccessible arms. A & B) 8-arm uninterrupted task for 3xTg-AD and NonTg control mice at 3 and 8 months. A) NonTg (black bars, n=11) and 3xTg-AD (open bars, n=12) mice at 3 months of age. B) NonTg (black bars, n=11) and 3xTg-AD (open bars, n=11) at 8 months of age. C & D) Test phase of the delayed spatial win-shift assay for 3xTg-AD and NonTg control mice at 3 and 8 months. C) NonTg (black bars, n=11) and 3xTg-AD (open bars, n=12) mice at 3 months of age. D) NonTg (black bars, n=11) and 3xTg-AD (open bars, n=11) mice at 8 months of age. Values represent the mean \pm SEM of the first 2 days or the last 2 days of testing for each phase from n animals. Significance was determined using mixed ANOVA, and paired and independent t-tests (* p < 0.05, ** p < 0.01).

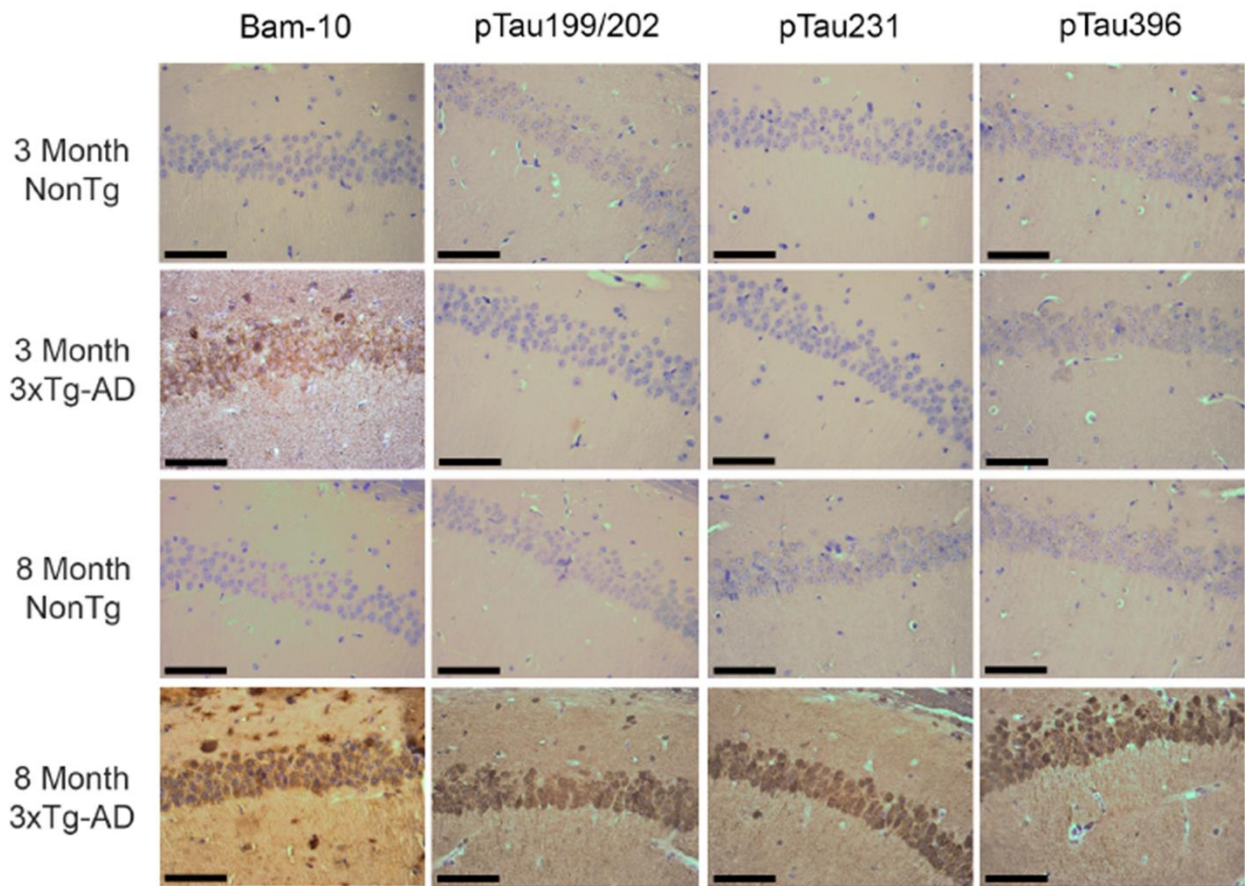


Figure 2.2. Characterization of Alzheimer's-type pathology in the CA1 region of ventral hippocampus in 3xTg-AD and NonTg control mice. Sections of 3xTg-AD and NonTg mice at 3 and 8 months were stained with BAM-10 (specific for total A β), pTau199/202 (site-specific phosphorylation of Tau at Ser 199 and 202), pTau231 (site-specific phosphorylation of Tau at Thr 231), and Tau396 (site-specific phosphorylation of Tau at Ser 396). 3xTg-AD mice exhibit intraneuronal A β at both 3 and 8 months. Small plaque deposits can be seen at 8 months, but not 3 months in 3xTg-AD mice. Phosphorylated Tau is present at 8 months but not 3 months in 3xTg-AD mice. Scale bar = 50 μ m.

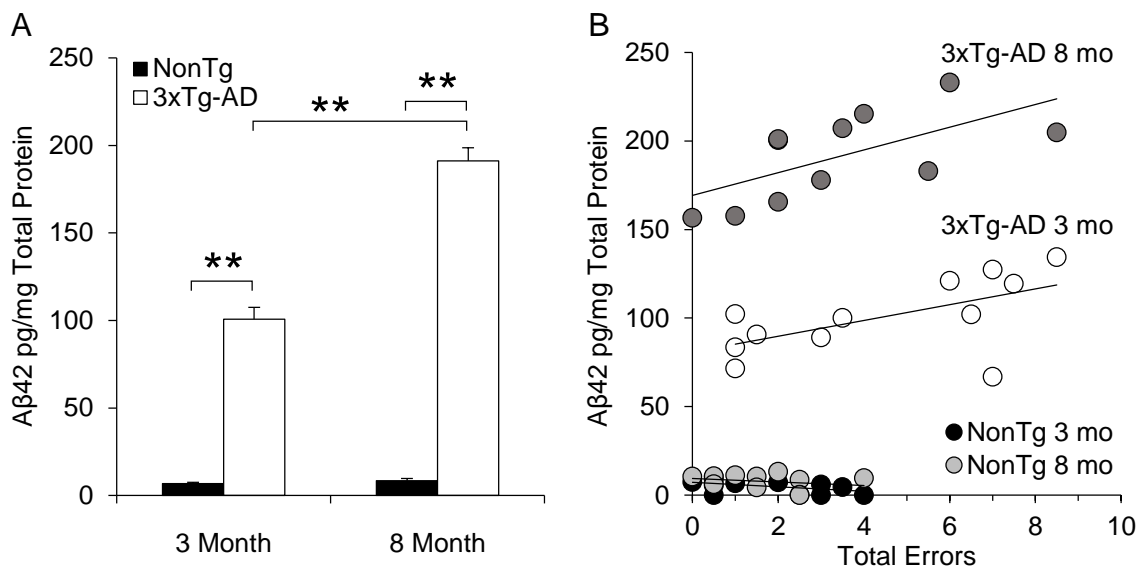


Figure 2.3. Aβ42 quantification and relation to maze performance in 3xTg-AD and NonTg control mice. A) Comparison of total Aβ42 levels in ventral hippocampal tissue at 3 and 8 months of age for 3xTg-AD (open bars, 3 months n=12, 8 months n=11) and NonTg (black bars, 3 months n=8, 8 months n=10) mice. Values represent the mean ± SEM from n animals. Significance was determined using ANOVA (* p < 0.05, ** p < 0.01). B) Scatter plot showing the relationship between total Aβ42 and total errors in the test phase at 3 and 8 months in 3xTg-AD (open/dark grey circles) and NonTg (black/light grey circles) mice. Values represent individual subject performance and Aβ42 quantification. Significance was determined using Pearson correlation. Both 3 (p < 0.05) and 8 (p < 0.01) month 3xTg-AD mice show a significant correlation between total errors and total Aβ42.

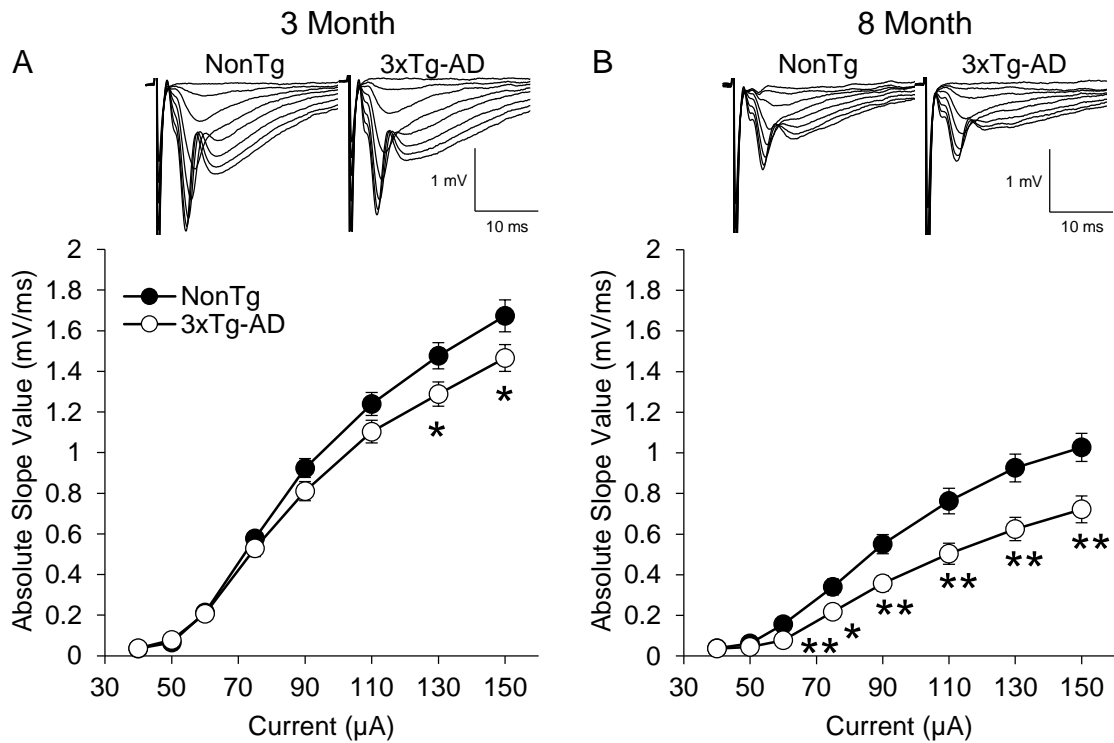


Figure 2.4. Field Excitatory Post-Synaptic Potentials (fEPSP) recorded from the CA1 region of ventral hippocampus in 3xTg-AD and NonTg control mice. A) Stimulus response curves for 3xTg-AD (open circles, n=54(12)) and NonTg (black circles, n=56(11)) mice at 3 months of age. Input intensities are 40, 50, 60, 75, 90, 110, 130, and 150 μ A. The averaged fEPSP sweeps are shown above the stimulus response curves. B) Same as panel A except at 8 months of age for 3xTg-AD (n=39(11)) and NonTg (n=47(11)) mice. Values represent the mean \pm SEM from n slices(animals). Significance was determined using independent t-tests (* $p < 0.05$, ** $p < 0.01$).

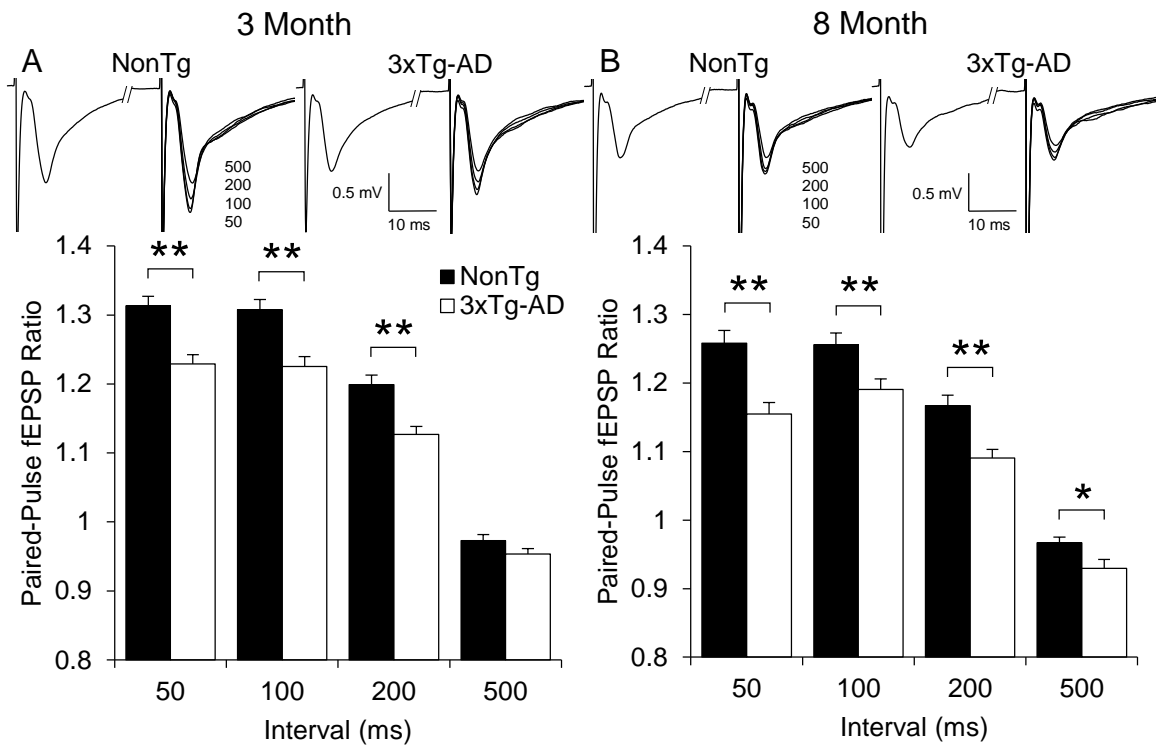


Figure 2.5. Paired-pulse field Excitatory Post-Synaptic Potentials (fEPSP) recorded from the CA1 region of ventral hippocampus in 3xTg-AD and NonTg control mice. A) Paired-pulse ratios at 50, 100, 200, and 500 ms intervals in 3xTg-AD (open bars, n=54(12)) and NonTg (black bars, n=58(11)) mice at 3 months of age. The averaged fEPSP sweeps are shown above the paired-pulse ratios. B) Same as panel A except at 8 months of age for 3xTg-AD (n=36(11)) and NonTg (n=42(11)) mice. Values represent the mean \pm SEM from n slices(animals). Significance was determined using independent t-tests (* p < 0.05, ** p < 0.01).

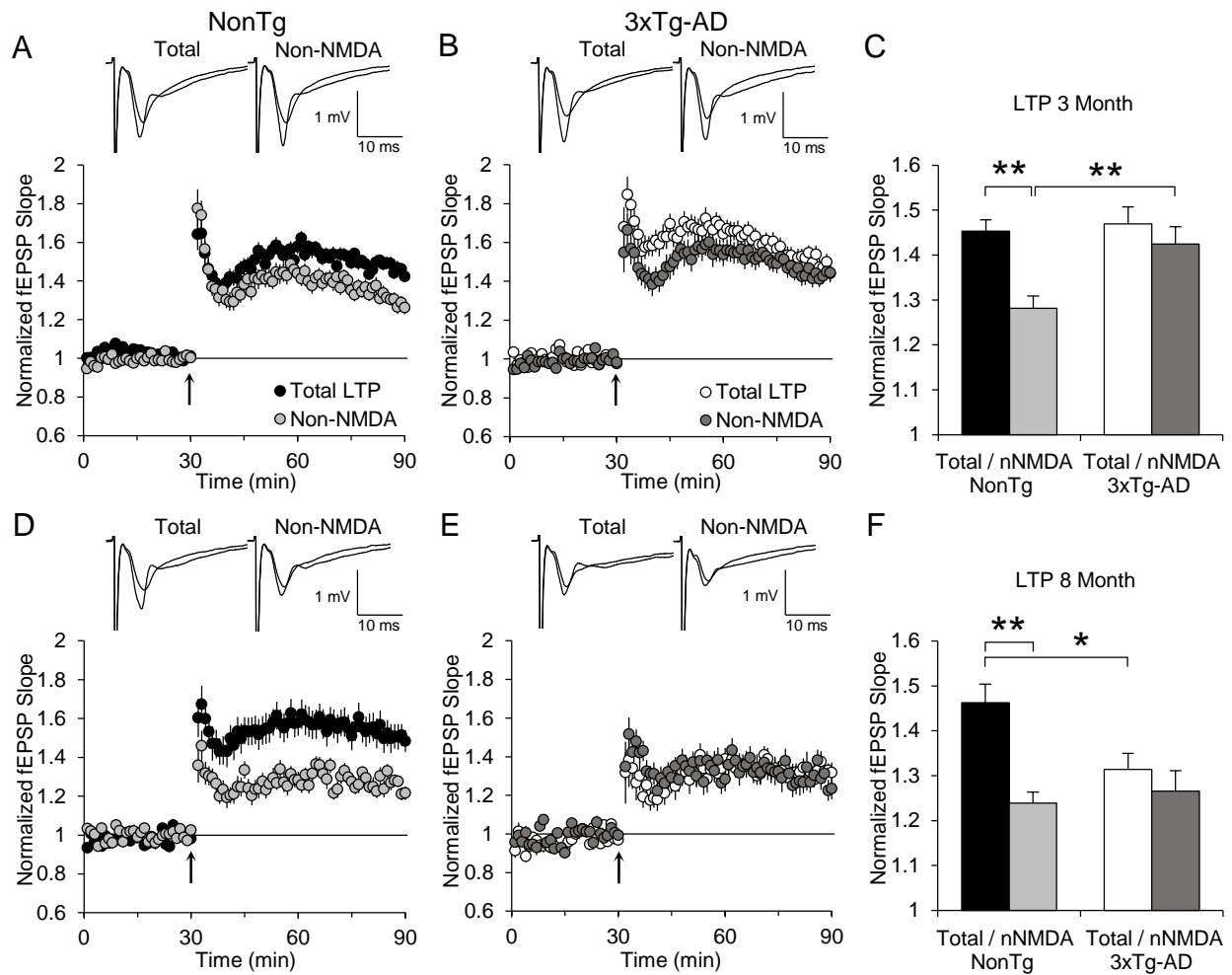


Figure 2.6. Long-Term Potentiation (LTP) of field Excitatory Post-Synaptic Potentials (fEPSP) recorded from the CA1 region of ventral hippocampus in 3xTg-AD and NonTg control mice. A) Summary plot of normalized fEPSP slope values in 3 month old NonTg mice for total LTP (black circles, (n=25(10)) and bath applied D,L-AP5 (50 μ M) representing non-NMDAR LTP (light grey circles, n=25(10)), before and after high frequency stimulation (HFS) (4 x 200Hz/0.5 s at 5 s intervals) indicated by the arrow at 30 minutes. The averaged fEPSP sweeps before and after HFS for total LTP and non-NMDAR LTP are shown above the plot. B) Same as panel A except in 3 month old

3xTg-AD mice for total LTP (open circles, (n=23(12)) and non-NMDAR LTP (dark grey circles, n=25(12)). C) Summary quantification of total LTP and non-NMDAR LTP for NonTg and 3xTg-AD mice at 1 hour post-HFS. D, E, & F) Same as A, B, & C above except at 8 months of age for NonTg (total LTP, n=17(9); non-NMDAR LTP, n=23(11)) mice and 3xTg-AD (total LTP, n=15(11); non-NMDAR LTP, n=18(11)) mice. Values represent the mean \pm SEM from n slices(animals). Significance was determined using ANOVA and independent t-tests (* p < 0.05, ** p < 0.01).

CHAPTER 3
ALTERATIONS IN SYNAPTIC TRANSMISSION AND SYNAPTIC PLASTICITY IN
YOUNG 3xTg-AD MICE¹

¹ Clark JK, Furukawa R, Fechheimer M, Wagner JJ. *Alterations in Locomotor Behavior and Synaptic Transmission and Plasticity in Young 3xTg-AD Mice*. Submitted to Neuroscience.

Abstract

Alzheimer's disease is a neurodegenerative condition thought to be initiated by production of the Amyloid- β peptide, which leads to synaptic dysfunction, and progressive memory and behavioral disturbances. Using a triple transgenic mouse model of Alzheimer's disease (3xTg-AD), we evaluated the onset of synaptic disturbances by measuring hippocampal synaptic plasticity in 3xTg-AD and NonTg control mice at 21 days, 2 months, and 3 months of age. Field potential recordings from the CA1 region of hippocampal slices were obtained to assess synaptic transmission and potential for synaptic plasticity. High frequency stimulations designed to invoke both NMDAR-dependent and VDCC-dependent components of Long-Term Potentiation (LTP) showed total LTP was similar between 3xTg-AD and NonTg mice at all ages tested, however application of the NMDAR antagonist AP5, and the VDCC antagonist Nifedipine, showed 3xTg-AD mice were resistant to AP5 at 2 months of age, and resistant to both AP5 and Nifedipine at 3 months of age, indicating additional compensatory mechanisms are present for inducing LTP in the 3xTg-AD model. NMDAR-mediated synaptic responses were not different between 3xTg-AD and NonTg mice, indicating these alterations were not due to changes in NMDAR activity. In addition, 3xTg-AD mice also showed a reduced paired-pulse facilitation ratio at 2 and 3 months of age, and a reduction in basal synaptic responses at 3 months of age. These findings should provide a new perspective on the early cellular mechanisms that occur in the early stages of Alzheimer's disease.

3.1 Introduction

Alzheimer's disease (AD) is a disease of aging, and the most common form of dementia accounting for more than 50% of all cases [1]. AD patients show deficits in cognitive processes that include progressive memory loss, confusion, and disorientation. AD pathology is characterized by the presence of extracellular β -Amyloid plaques and intracellular accumulations of hyperphosphorylated Tau protein leading to the formation of neurofibrillary tangles [2, 3]. The primary initiator of AD pathology is thought to be the overproduction of soluble Amyloid- β ($A\beta$) peptide, produced through sequential cleavage of Amyloid Precursor Protein by the membrane bound enzymes β - and γ -secretase [3]. The increased production of the $A\beta$ peptide leads to synaptic impairment and eventual neurodegeneration from excitotoxicity, oxidative stress, and apoptosis [1]. In addition, the dysregulation of Ca^{2+} homeostasis seems to be an early feature of AD pathology [4, 5]. Studies show AD neurons release excessive Ca^{2+} upon stimulation [6], and older neurons may have higher resting Ca^{2+} levels, making them more sensitive to Ca^{2+} regulated processes [7].

Ca^{2+} plays many roles in the cell. In neurons, it is responsible for a variety of functions including neurotransmitter release and synaptic plasticity, the modification of synaptic strength as a result of experience. Activation of postsynaptic glutamatergic N-methyl-D-aspartic acid (NMDA) receptors produces a transient increase in intracellular Ca^{2+} concentration, leading to a series of Ca^{2+} mediated responses that can lead to the Long-Term Potentiation (LTP) of the synaptic signal through upregulation of postsynaptic glutamatergic α -amino-3-hydroxy-5-methyl-4-isoxazole-propionic acid (AMPA) receptors [8-11]. LTP represents the most current model for information

storage in the CNS, and is therefore suspected to play important roles in cognitive processes such as learning and memory [12]. The hippocampus is one of the major brain regions important for mediating learning and memory, and at least two different mechanisms of LTP are known to coexist at hippocampal CA3→CA1 synapses, NMDA receptor-dependent LTP (NMDAR LTP) and non-NMDA receptor-dependent LTP (non-NMDAR LTP), with the latter predominately mediated via activation of high threshold L-type Voltage-Dependent Calcium Channels (VDCC) [13-15]. Both forms of LTP have been shown to be important for cognition, with the relative contribution of each form changing as the animal ages [16, 17]. Young animals rely primarily on NMDAR-dependent LTP, but this mechanism may naturally decrease with age, affecting cognitive performance in certain tasks. Some aged animals however, show a compensatory increase in non-NMDAR-dependent LTP, and it has been suggested that the ability to effectively alter the ratio between these two mechanisms may allow for compensation of reduced NMDAR-dependent mechanisms, and maintenance of cognitive abilities for some tasks [18]. Hippocampal function is one of the first significantly impacted processes observed in AD, and it is therefore important to understand how LTP mechanisms are affected during the early stages of AD.

A triple transgenic mouse model of Alzheimer's disease (3xTg-AD) has been developed that produces both β -Amyloid plaques and neurofibrillary Tau tangles [19]. In a previous study we showed 3xTg-AD mice have severe impairments in long-term working memory using the 8-arm radial maze at 3 months old, an age generally considered to be presymptomatic [20]. We also showed 3xTg-AD mice have altered NMDAR LTP that coincides with these impairments in working memory, despite having

total LTP that is not different from nontransgenic (NonTg) control mice. In the current study, we explore the early changes that occur in 3xTg-AD mice using a variety of neurophysiological (extracellular recording from *ex vivo* slices in the CA1 region of ventral hippocampus) assessments to investigate the age of onset and progression of these changes, and to further examine of the nature of the neurophysiological differences observed in our previous study. Our results indicate that 3xTg-AD mice develop significant differences in neurotransmission and synaptic plasticity at hippocampal CA3→CA1 synapses beginning between 1 and 2 months of age. By 3 months of age, 3xTg-AD mice show differences in both NMDAR- and VDCC-dependent mechanisms responsible for the induction and expression of LTP.

3.2 Methods

3.2.1 Animals and euthanasia

All animals used in this study were male mice and consisted of Alzheimer's disease model mice (3xTg-AD) homozygous for three mutant transgenes: APP(Swe), Psen1, and TauP301L, (B6/129-*Psen1*^{tm1Mpm} Tg(APP^{Swe}, tauP301L)1Lfa/Mmjax) obtained from the MMRRC (ID 034830-JAX) through Jackson Laboratories, and nontransgenic (NonTg) control mice (B6129SF2/J) from Jackson Laboratories (101045 JAX, Bar Harbor, ME). The generation of 3xTg-AD mice has been described elsewhere [19]. Briefly, two separate transgene constructs each encoding human *APP* cDNA (695 isoform) harboring the Swedish mutation (*KM670/671NL*), or human *Tau* cDNA (4R/0N) harboring the *P301L* mutation, each under control of mouse Thy1.2 regulatory elements, were comicroinjected into single-cell embryos from homozygous PS1^{M146V}

knockin mice. Embryos were screened for cointegration of both cassettes to the same locus. Embryos were then reimplanted into foster mothers and the resulting offspring were genotyped to identify 3xTg-AD mice. Hemizygous F1 3xTg-AD mice were then crossed to produce 3xTg-AD mice homozygous for all three transgenes. Both 3xTg-AD and NonTg mice are on the same genetic and strain background (129/C57BL6 hybrid), except NonTg mice harbor the endogenous wild-type *PS1* gene. Breeding pairs for each group were obtained and animals were bred in house at the University of Georgia animal facilities. Mice were housed in an AAALAC accredited facility on a 12 hour light/dark timed schedule and had ad libitum access to food and water during this study. Physiological testing occurred at three different time points: 21 days (20-22 days old), 2 months (60-67 days old), and 3 months (90-100 days old). Pre-weaned mice at 21 days were tested instead of 1 month old mice to avoid any stress induced effects from the weaning process that could potentially influence neurophysiological measurements. Euthanasia of mice occurred under deep anesthesia with halothane followed by decapitation. The University of Georgia Institutional Animal Care and Use Committee approved all animal protocols and experiments.

3.2.2 Chemicals and reagents

Except where noted, specialty chemicals were obtained from Sigma Aldrich (St. Louis, MO).

3.2.3 Extracellular field recording

Hippocampal slices were prepared from naive 21 day, 2 month, and 3 month old 3xTg-AD and NonTg mice. Mice were deeply anesthetized with halothane prior to decapitation. The brain was removed and submerged in ice-cold, oxygenated (95% O₂ /

5% CO₂) dissection artificial cerebrospinal fluid (ACSF) containing: 120 mM NaCl, 3 mM KCl, 4 mM MgCl₂, 1 mM NaH₂PO₄, 26 mM NaHCO₃, and 10 mM glucose. The brain was sectioned using a vibratome through the horizontal plane into 400 μm thick slices. The hippocampus was then dissected free from slices obtained between the levels of Bregma -4.0 mm to Bregma -2.4 mm. We estimate such slices were from the ventral 35-40% of the hippocampus with respect to the longitudinal axis. We also excluded slices from the extreme 10% of the ventral pole, where it is difficult to clearly distinguish the CA1 pyramidal region from the CA2/3 and subicular regions. Slices were placed in a submersion recording chamber and perfused at approximately 1 ml/min with oxygenated (95% O₂ / 5% CO₂) standard ACSF containing: 120 mM NaCl, 3 mM KCl, 1.5 mM MgCl₂, 1 mM NaH₂PO₄, 2.5 mM CaCl₂, 26 mM NaHCO₃, and 10 mM glucose at room temperature. Slices recovered for 45 minutes at room temperature and an additional 45 minutes at 30°C. A bipolar stimulating electrode (Kopf Instruments, Tujunga, CA) was placed within the stratum radiatum of CA1 and an extracellular recording microelectrode (1.0 MΩ tungsten recording microelectrode, World Precision Instruments, Sarasota, FL) was positioned in the same layer of CA1. Field Excitatory Post-Synaptic Potentials (fEPSPs) were recorded at Schaffer collateral→CA1 synapses using a stimulus pulse consisting of a single square wave of 270 μs duration. Data were digitized at 10 kHz, low-pass filtered at 1 kHz, and analyzed with pCLAMP 10.2 software (Axon Instruments, Sunnyvale, CA). The initial slope of the population fEPSP was measured by fitting a straight line to a 1 ms window immediately following the fiber volley.

Stimulus response curves were obtained at the beginning of each experiment with stimulus pulses delivered at 40, 50, 60, 75, 90, 110, 130, 150, 170, and 190 μA once every 60 s (0.0167 Hz). For baseline recording, the stimulation intensity was adjusted to obtain a fEPSP of approximately 35-40% of the maximum response. Paired-pulse stimulations were performed at an interval of 50 ms. Five pairs of pulses were performed and averaged together. The initial slope of the averaged second pulse was divided by the initial slope of the averaged first pulse to obtain the paired-pulse ratio for each slice. Synaptic responses for Long-Term Potentiation (LTP) experiments were normalized by dividing all fEPSP slope values by the average of the five responses recorded during the 5 minutes immediately prior to high frequency stimulation (HFS). LTP values for the 1 hour time point were determined by averaging 5 minutes of normalized slope values at 55-60 minutes post-HFS. Two different HFS protocols were used to induce LTP. The strong HFS protocol consisted of 4 episodes of 200 Hz/0.5 s stimulus trains (100 pulses x4) administered at 5 s inter-train intervals. The weak HSF protocol consisted of 1 episode of 50 Hz/0.5 s (25 pulses x1). In order to pharmacologically separate or block the NMDAR-dependent and non-NMDAR-dependent components of LTP, the NMDAR antagonist D,L-AP5 (50 μM) (Tocris Bioscience, Minneapolis, MN) and the L-type VDCC antagonist Nifedipine (20 μM) (Sigma Aldrich, St. Louis, MO) were bath applied for 30 minutes prior to HFS, continued for 10 minutes post-HFS, and washed out for the remainder of recording. Isolation of NMDAR-mediated fEPSPs was achieved using nominally Mg^{2+} free ACSF with high Ca^{2+} (4 μM) to maintain proper osmolarity. The AMPAR antagonist CNQX (10 μM) (Tocris Bioscience, Minneapolis, MN) and VDCC antagonist Nifedipine (20 μM) were

bath applied for the entirety of NMDAR-mediated fEPSP experiments. Reported n-values (x(y)) indicate the number of slices (x) and the number of animals (y) assessed.

3.2.4 Statistics

Tests of significance were performed using either ANOVA, or independent t-tests as appropriate.

3.3 Results

To determine if neurophysiological differences exist between 3xTg-AD and NonTg mice at 21 days, 2 months, and 3 months of age, electrophysiological recordings of fEPSPs from the CA1 region of ventral hippocampal slices were recorded to evaluate synaptic transmission and synaptic plasticity in this region.

Stimulus response curves were generated to evaluate the functional range of synaptic activity (Figure 3.1). Data were subjected to a 2 genotype (NonTg versus 3xTg-AD) x 10 stimulus intensity (40-190 μ A) mixed ANOVA. There was a significant effect of stimulus intensity at 21 days ($F(9,378)=206.648$, $p < 0.001$), 2 months ($F(9,126)=124.424$, $p < 0.001$), and 3 months ($F(9,441)=212.921$, $p < 0.001$), indicating a significant increase in synaptic response as stimulus intensity increased, as would be expected. There was no difference between genotypes at either 21 days (3xTg-AD, $n=21(8)$; NonTg, $n=23(9)$) (Figure 3.1A) or 2 months (3xTg-AD, $n=8(3)$; NonTg, $n=8(3)$) (Figure 3.1B). By 3 months however, there existed a significant difference between genotypes for synaptic response ($F(1,49)=9.303$, $p < 0.01$) (Figure 3.1C). Within-subjects analysis showed a significant interaction of stimulus intensity x genotype ($F(9,441)=2.482$, $p < 0.001$), indicating genotype influenced synaptic response as

stimulus intensities increased. Follow up between-subjects comparisons of stimulus intensity using independent t-tests showed 3xTg-AD mice (n=37(11)) have lower synaptic responses than NonTg mice (n=58(19)) at stimulus intensities $\geq 90 \mu\text{A}$ ($p < 0.05$).

Short-term synaptic plasticity was evaluated using a paired-pulse stimulus protocol to determine the degree of synaptic facilitation (Figure 3.2). Both 3xTg-AD and NonTg mice showed paired-pulse facilitation at all ages. The 3xTg-AD and NonTg mice showed similar levels of facilitation at 21 days (3xTg-AD, n=23(8); NonTg, n=25(9)), but by 2 months (3xTg-AD, n=23(8); NonTg, n=25(9)) and 3 months (3xTg-AD, n=23(8); NonTg, n=25(9)), 3xTg-AD mice showed significantly less facilitation than NonTg mice (2 months $p < 0.05$, 3 months $p < 0.01$), indicating impairments in short-term synaptic plasticity begin as early as 2 months of age.

Long-term synaptic plasticity was evaluated by inducing LTP using a multiple train stimulus induction protocol previously shown to elicit a compound potentiation consisting of both NMDAR and non-NMDAR-dependent components of LTP [15] (Figure 3.3). The non-NMDAR component of LTP was isolated by blocking the NMDAR component of LTP utilizing the selective NMDAR antagonist D,L-AP5. The remaining non-NMDAR component of LTP was blocked using the VDCC antagonist Nifedipine. Hippocampal slices from 21 day, 2 month, and 3 month old NonTg and 3xTg-AD mice were subjected to 3 treatment conditions: No drug (total LTP), D,L-AP5 (AP5), and AP5 and Nifedipine together (AP5/Nif). LTP data were subjected to a 2 genotype (NonTg versus 3xTg-AD) x 3 treatment group (No drug versus AP5 versus AP5/Nif) ANOVA for multiple group comparisons at each age. There was a significant effect of treatment at

21 days ($F(2,57)=2.425$, $p < 0.001$) and 2 months ($F(2,41)=12.684$, $p < 0.001$), but only at 3 months was there a significant effect of treatment ($F(2,44)=9.588$, $p < 0.001$) and genotype ($F(1,44)=10.195$, $p < 0.001$). Additional ANOVA by genotype for each age confirmed a significant effect of treatment for 3xTg-AD and NonTg mice at 21 days and 2 months, but only for NonTg mice at 3 months. A Tukey's post-hoc analysis was performed as a follow up to determine significance between treatments, and planned comparisons using independent t-tests were performed to evaluate similar treatments across genotype.

At 21 days, NonTg mice (total LTP, $n=14(5)$; AP5, $n=9(3)$; AP5/Nif, $n=11(4)$; $F(2,31)=51.522$, $p < 0.001$) and 3xTg-AD mice (total LTP, $n=10(4)$; AP5, $n=9(3)$; APV/Nif, $n=11(4)$; $F(2,26)=41.835$, $p < 0.001$) both showed similar results for LTP under each treatment condition (Figure 3.4A, B, & C). AP5 and AP5/Nif significantly reduced LTP from total LTP ($p < 0.01$), and AP5/Nif did not further decrease LTP from AP5 alone. There was no difference in LTP between NonTg and 3xTg-AD mice (across genotype) for total LTP, AP5, or AP5/Nif treatment groups. At 2 months, NonTg mice (total LTP, $n=8(3)$; AP5, $n=8(3)$; AP5/Nif, $n=9(3)$; $F(2,22)=12.271$, $p < 0.001$) showed similar results to those obtained at 21 days (Figure 3.4D & F), with AP5 and AP5/Nif treatments significantly reducing LTP from total LTP (AP5, $p < 0.05$; AP5/Nif, $p < 0.01$). While treatment with AP5/Nif was visibly lower than AP5 alone, it was not statistically different ($p = 0.12$). In contrast, 3xTg-AD mice (total LTP, $n=8(3)$; AP5, $n=7(3)$; AP5/Nif, $n=7(3)$; $F(2,19)=3.552$, $p < 0.05$) begin to show differences in response to treatment at 2 months (Figure 3.4E & F). AP5 did not significantly reduce LTP from total LTP ($p = 0.62$), however AP5/Nif did ($p < 0.05$). AP5 and AP5/Nif treatments were not

statistically different despite AP5/Nif being visibly lower ($p = 0.249$). As at 21 days, there was no difference across genotypes for any treatment group at 2 months. At 3 months, NonTg mice (total LTP, $n=10(4)$; AP5, $n=10(4)$; AP5/Nif, $n=11(4)$; $F(2,28)=17.585$, $p < 0.001$) again showed similar results to those at 21 days and 2 months (Figure 3.4G & I). AP5 and AP5/Nif significantly reduced LTP from total LTP ($p < 0.01$), with the addition that AP5/Nif further reduced LTP significantly over AP5 alone ($p < 0.05$). In stark contrast, 3xTg-AD mice (total LTP, $n=7(3)$; AP5, $n=6(3)$; AP5/Nif, $n=6(3)$; $F(2,16)=0.698$, $p = 0.51$), showed no difference in LTP between any treatment at 3 months (Figure 3.4H & I). Neither AP5 nor AP5/Nif significantly reduced LTP from total LTP (AP5, $p = 0.74$; AP5/Nif, $p = 0.49$), nor was LTP different between AP5/Nif and AP5 alone ($p = 0.91$). In addition, differences between NonTg and 3xTg-AD mice were now seen for AP5 ($p < 0.05$) and AP5/Nif groups ($p < 0.01$).

These results show there is a change in NMDAR LTP in 3xTg-AD mice beginning as early as 2 months, and established by 3 months. To determine if this change is a result of differences in NMDAR activity, fEPSPs were generated under conditions that isolate NMDAR-mediated synaptic responses. Basal synaptic activity as measured by fEPSPs is mediated by AMPARs. The NMDAR is not activated under basal stimulating conditions due to the presence of a Mg^{2+} block within the channel pore that is not relieved by subthreshold depolarizations of local dendritic fields. In order to pharmacologically isolate NMDAR-mediated fEPSPs under basal stimulating conditions, the AMPAR antagonist CNQX ($10 \mu M$), along with the VDCC antagonist Nifedipine ($20 \mu M$), and nominally Mg^{2+} free ACSF, were bath applied to hippocampal slices for recording. In order to evaluate the functional range of NMDAR-mediated synaptic

responses, stimulus response curves of NMDAR-mediated fEPSPs were generated (Figure 3.4A). Data from 3xTg-AD mice (n=15(5)) and NonTg mice (n=14(5)) were subjected to a 2 genotype (NonTg versus 3xTg-AD) x 10 stimulus intensity (40-190 μ A) mixed ANOVA. Results show there was a significant effect of stimulus intensity ($F(9,189)=195.574$, $p < 0.001$), as expected, and surprisingly, a statistical interaction of genotype x stimulus intensity ($F(9,189)=2.465$, $p < 0.05$), indicating that genotype influences synaptic response as stimulus intensity increases. This is likely due to the 3xTg-AD mice showing slightly higher NMDAR-mediated responses at lower intensity stimulations, but lower responses at higher intensity stimulations. There was not however, an overall effect of genotype ($F(1,21)=0.135$, $p = 0.717$), and a follow up between-subjects analysis confirmed there was no difference across genotype at any stimulus intensity tested, which agrees with the visual impression of the two curves. We next sought to determine if the presence of A β (or some other factor) in 3xTg-AD mice may be interfering with the efficacy of AP5. To evaluate this, basal synaptic activity of NMDAR-mediated fEPSPs was measured, and bath application of AP5 (50 μ M) was used to determine the effectiveness of AP5 antagonism (Figure 3.4B). Results showed no difference in the efficacy of AP5 antagonism on NMDAR-mediated fEPSPs between 3xTg-AD (n=11(5)) and NonTg mice (n=13(5)).

To further examine the contribution of NMDARs in long-term synaptic plasticity in 3xTg-AD mice, NMDAR LTP was induced in 3 month old 3xTg-AD (n=12(5)) and NonTg mice (n=13(5)), and evaluated in 5 minute increments for 30 minutes, and also at 1 hour, post-tetanus (Figure 3.5). The NMDAR component of LTP was isolated using a weak HFS protocol shown to elicit NMDAR-dependent-only LTP. In addition, the VDCC

antagonist Nifedipine (20 μ M) was bath applied as a precaution against possible inadvertent induction of non-NMDAR LTP. LTP data were subjected to a 2 genotype (NonTg versus 3xTg-AD) x 7 point elapsed time (0-30 minutes in 5 minute blocks, and at 1 hour) mixed ANOVA. There was a significant effect of time ($F(6,138)=28.758$, $p < 0.001$) and a significant interaction of genotype x time ($F(6,138)=5.327$, $p < 0.001$), indicating genotype influenced LTP as time progressed. This most likely is due to differences in LTP within the first 30 minutes post-tetanus. There was no overall effect of genotype ($F(1,23)=2.390$, $p = 0.136$), but follow up between-subjects analysis confirmed the first 10 minutes of LTP post-tetanus is different ($p < 0.05$) between 3xTg-AD and NonTg mice.

3.4 Discussion

In this study, we observed neurophysiological changes in both synaptic transmission and synaptic plasticity in 3xTg-AD mice. A significant change in baseline synaptic response at 3 months of age (Figure 3.1), and a significant reduction in paired-pulse facilitation at 2 and 3 months of age (Figure 3.2), were observed in 3xTg-AD mice. Total LTP in the CA1 region of ventral hippocampus was similar between 3xTg-AD and NonTg mice at all ages tested, but the apparent contribution of each component of LTP (NMDAR- or VDCC-dependent) was different in 3xTg-AD mice by 2 and 3 months of age respectively, compared to NonTg mice (Figure 3.3). Analysis of NMDAR-mediated fEPSPs indicate there are subtle differences in NMDAR-mediated synaptic responses that are present at 3 months of age (Figure 3.4), and while direct measurement of NMDAR LTP is similar between 3xTg-AD and NonTg mice after 1 hour, differences in

the LTP timecourse and NMDAR-dependent short-term potentiation were observed between genotypes (Figure 3.5).

The hallmark sign of AD is cognitive impairment, and the hippocampus is one of the major brain regions important for cognitive performance, and one of the first regions impacted by AD [21]. Our previous work has shown 3xTg-AD mice have a profound cognitive impairment that coincides with changes in NMDAR LTP at 3 months of age [20]. To investigate changes that occur in the hippocampus prior to these events, we obtained electrophysiological recordings from ventral hippocampal slices to determine the onset of altered synaptic function in 3xTg-AD mice.

Basal synaptic transmission is similar between genotypes at 21 days and 2 months of age, but at 3 months of age there is a reduction in synaptic response in 3xTg-AD mice at the higher stimulus intensities. This result is similar to what we have observed previously in these mice at 3 months [20]. The reduction in synaptic response does not seem to be due to synaptic loss, as 3xTg-AD and NonTg mice show similar dendritic spine density in the hippocampus and cortex up to around 13 months of age [22]. The observed reduction in synaptic response may be due to a reduction in postsynaptic AMPARs. There is evidence that A β promotes removal of AMPARs from the synaptic membrane through mGluR-dependent signaling mechanisms [23-25]. In our own experiments, application of the AMPAR antagonist CNQX (10 μ M) resulted in a complete block of basal synaptic transmission for both genotypes (data not shown), indicating our measurement of fEPSPs to assess basal synaptic transmission is AMPAR-mediated, supporting the hypothesis that 3xTg-AD mice may have reduced AMPAR activity at 3 months of age.

The paired-pulse facilitation ratio is significantly less in 3xTg-AD mice at 2 and 3 months, indicating an impairment in short-term synaptic plasticity by 2 months of age. Paired-pulse facilitation is mediated by presynaptic Ca^{2+} [26]. In addition to N-type Ca^{2+} channels associated with vesicle release, intracellular Ca^{2+} is also regulated by ER-associated Ca^{2+} activated Ryanodine receptors (RyR) and IP_3 -mediated receptors (IP_3R). Presenilins (PS) that function independently of those associated with $\text{A}\beta$ production play a role in regulating intracellular Ca^{2+} homeostasis by forming Ca^{2+} leak channels within the ER [27], and have functional associations with RyRs that modulate their activity [28]. Presenilin and RyR activity in presynaptic neurons have been shown to functionally mediate synaptic physiology such as neurotransmitter release [29, 30]. Mutated Presenilins of the type found in AD have been shown to increase both RyR expression and RyR-associated Ca^{2+} release in neurons of PS1 transgenic mice [31]. The 3xTg-AD mice used in our own studies carry the same mutated form of Presenilin (M146V), and these mice have been shown to have a potentiated release of intracellular Ca^{2+} via altered RyR and IP_3R activity [6, 32]. This leads to a dysregulation of intracellular Ca^{2+} homeostasis, and has been shown to alter vesicle release probability and increase spontaneous vesicle fusion events in 3xTg-AD mice as early as 6 weeks of age [32, 33]. Alterations such as these would surely be expected to affect paired-pulse facilitation, and our results at 2 and 3 months support this rationale. Previous investigations of short-term synaptic plasticity in 3xTg-AD mice have reported paired-pulse facilitation in the CA1 region is not different from NonTg mice at 4 [19] and 6-8 weeks of age [32], indicating the emergence of altered short-term synaptic plasticity begins by at least 2 months of age. One of these studies however, has reported no

difference in paired-pulse ratio between 3xTg-AD and NonTg mice at 6 months [19], which is in contrast to our current and previous findings that paired-pulse ratio is reduced at 3 months of age [20]. In our own studies, we report data from a substantially higher number of observations, which may explain, in addition to differences in experimental protocol, the differences reported for paired-pulse ratios. Our observation of a reduced paired-pulse ratio at 2 and 3 months is at an age when Ca^{2+} dysregulation is known to occur in 3xTg-AD mice, and would support the hypothesis that disruptions in Ca^{2+} homeostasis can lead to early changes in synaptic physiology in AD. Thus, the reduction of the paired-pulse ratio we observed in the CA1 region of 2 month old 3xTg-AD mice could potentially serve as an early indicator of a functional synaptic impairment that is supportive of a Ca^{2+} dysregulation hypothesis of AD [34].

To investigate the potential for long-term synaptic plasticity, we evaluated the ability of mice to sustain a long-term potentiation of synaptic strength. LTP represents the best and most current hypothesis for information storage in the CNS, and the hippocampus is an important brain region mediating information storage in learning and memory. Both NMDAR- and VDCC-dependent LTP coexist at hippocampal CA3→CA1 synapses [13-15], and the importance of NMDARs and VDCCs in cognition, especially in learning and memory, has been well established [17, 35-39]. Hippocampal function is one of the first resources compromised in AD, and it is therefore necessary to understand how these LTP mechanisms are affected in order to better understand the nature of cognitive diseases such as AD.

In a previous study, we found 3xTg-AD mice showed reduced NMDAR LTP compared to NonTg mice, and a subsequent increase in non-NMDAR LTP which

resulted in a total LTP that was not different between genotypes [20]. For our current study, we wanted to determine when these changes in NMDAR and non-NMDAR LTP begin to occur, and explore the nature of non-NMDAR LTP in 3xTg-AD mice. We did not find any difference between genotypes at 21 days for total LTP, or either component of LTP, indicating 3xTg-AD mice are neurophysiologically not different from NonTg mice at 21 days old. We also found total LTP is not different between genotypes at 2 and 3 months of age. Other groups have also reported total LTP in 3xTg-AD mice is not different from NonTg mice at 4 [19] and 6-8 weeks of age [6], with 6 months being the earliest report to date of total LTP being significantly reduced from NonTg mice [19]. The contribution of the NMDAR- and VDCC-dependent components of LTP were not reported in those studies. In the current study using 21 day, 2 month, and 3 month old NonTg mice, blocking NMDARs (AP5) significantly blocked LTP, and blocking NMDARs and VDCCs together (AP5/Nif) produced a $\geq 90\%$ block of LTP, similar to what other studies have shown using wild-type animals [13-15]. In 3xTg-AD mice however, we did not observe a significant block of LTP with AP5 at 3 months of age, duplicating the AP5 results from our previous study [20]. Additionally, we observed similar results at 2 months, indicating the change in the NMDAR contribution to LTP begins by 2 months of age. We hypothesized that the increase in non-NMDAR LTP was VDCC-dependent based on observations in wild-type animals, but our attempt to block the non-NMDAR component of LTP with the VDCC antagonist Nifedipine was unsuccessful. There was in fact, some reduction of LTP at 2 months of age with the application of both AP5 and Nifedipine together, although not as much as that seen in NonTg mice. By 3 months of

age however, the application of both AP5 and Nifedipine failed to significantly block LTP in 3xTg-AD mice.

Our initial hypothesis for the change in NMDAR LTP we observed in 3xTg-AD mice was that there may be a reduction in NMDAR activity or receptor density, but our measurement of NMDAR-mediated fEPSPs indicated no difference in NMDAR-mediated synaptic responses compared to NonTg mice. Previous studies specifically examining the density and expression of hippocampal NMDARs in both human AD patients [40, 41] and APP/PS1 transgenic mice [42] showed no difference in hippocampal NMDAR density from age-matched controls. We then considered the possibility that AP5 may have reduced efficacy in 3xTg-AD mice, potentially through a mechanism whereby A β directly interferes with AP5 binding to NMDARs, but application of AP5 to NMDAR-mediated fEPSPs showed no change in efficacy of AP5 in 3xTg-AD mice compared to NonTg mice, resulting in a complete block of NMDAR-mediated fEPSPs in both genotypes. These results prompted us to look at NMDAR LTP directly by inducing LTP using a stimulus protocol that activates NMDARs but not VDCCs. We found the initial stages post-HFS (PTP and STP) were significantly reduced in 3xTg-AD mice compared to NonTg mice, despite LTP being similar after 1 hour.

These findings suggest that while the net output of total LTP is similar between 3xTg-AD and NonTg mice, there are distinctly different mechanisms driving LTP. We have demonstrated that 3xTg-AD mice are resistant to drugs that typically block the majority (>90%) of LTP. Ca²⁺ is a mediator of LTP (and synaptic plasticity in general, both short-term and long-term), and increases in postsynaptic intracellular Ca²⁺ for the generation of LTP normally occur through activation of postsynaptic NMDARs or

VDCCs [8, 43]. Despite their exposure to antagonism however, LTP still occurs in 3xTg-AD mice at 3 months of age. Our studies, as well as others, indicate NMDARs and VDCCs function normally in 3xTg-AD mice at 3 months. Neither NMDAR nor VDCC current is different in 3xTg-AD mice compared to NonTg mice in either CA1, CA3, or dentate granule neurons until at least 12 months of age [44], so the rise in intracellular Ca^{2+} necessary to elicit LTP must be occurring through an alternative mechanism. The primary source of intracellular Ca^{2+} is the ER, which liberates Ca^{2+} through both IP_3 Rs and Ca^{2+} activated RyRs. Different induction protocols elicit different forms of LTP utilizing specific Ca^{2+} sources dependent on stimulus intensity [45]. NMDARs and RyRs are activated first, followed by IP_3 Rs, and finally VDCCs. Different induction protocols have also shown different results in the presence of $\text{A}\beta$ that are independent of NMDAR activity, and reductions in LTP observed in the presence of $\text{A}\beta$ cannot be explained by effects on NMDARs [46, 47]. As mentioned above, 3xTg-AD mice have been shown to have a dysregulation of intracellular Ca^{2+} homeostasis as a result of potentiated RyR activity that is most likely mediated by the functional association with mutated PS1. This results in an increase in RyR expression of nearly 3 fold in 3xTg-AD mice, and a functional potentiation of intracellular Ca^{2+} release upon activation [32].

How then, might the activation of Ca^{2+} activated RyRs occur under conditions that block external Ca^{2+} entry? One potential mechanism involves metabotropic glutamate receptor (mGluR) signaling. Postsynaptic mGluR signaling activates Phospholipase C (PLC), which results in the generation of IP_3 from PIP_2 . IP_3 activates the IP_3 R, releasing Ca^{2+} that then could activate RyRs. It has been demonstrated that

exposure to A β leads to excessive mGluR activation through interference with glutamate reuptake transporters, prolonging glutamate clearance and mGluR activation [23]. Activation of mGluRs in 3xTg-AD mice show an increase in IP₃R-mediated Ca²⁺ release that is not a result of increased IP₃R expression [48]. IP₃R activity is mediated by PS similar to RyRs, and PS1/2 FAD mutants increase IP₃R current and alter gating kinetics [49]. This leads to an increase in resting intracellular Ca²⁺ levels that can be rescued by IP₃R antagonists [7], and dysregulations in LTP that can be rescued by reducing IP₃R expression [48]. This potentially also explains the reduction in AMPAR-mediated synaptic response, and reductions in LTP observed in older 3xTg-AD mice, which may be a consequence of LTD dependent mechanisms also initiated by excessive mGluR signaling.

The strong 200 Hz stimulus protocol we have used to induce long-term plasticity is specifically designed to activate both NMDAR- and VDCC-dependent LTP, but the differences between genotype that mediate the induction of each component of LTP are only resolved with pharmacological intervention. The use of the weak 50 Hz stimulus protocol further resolves differences in LTP induction between 3xTg-AD and NonTg mice without the use of pharmacological intervention. These specific differences observed in 3xTg-AD mice could potentially contribute to previous observations of cognitive impairment at similar ages, including the working memory results of our previous study [20], as well as impairments observed in MWM training at 4 months, in which 3xTg-AD mice had small impairments in day to day memory during consecutive daily training, but overall performed similarly to control mice in repeated training within each day, and overall by the end of 5 days of training [51]. Cognitive performance in

these types of working memory tasks could be more dependent on short-term plasticity (neurotransmitter facilitation), or short-term potentiation mechanisms (neurotransmitter facilitation, AMPAR phosphorylation, AMPAR trafficking), rather than long-term potentiation mechanisms such as LTP (protein synthesis and gene expression). The timing of these behavioral tests occur in the time frame of minutes instead of hours, and measurements of short-term plasticity such as paired-pulse ratio, or short-term potentiation which occurs within the first 30 minutes after HFS, may actually be a better predictor of cognitive performance than 1 hour LTP in these specific tasks.

In the current study, we show 3xTg-AD mice have impairments in short-term and long-term synaptic plasticity by 2 months of age, and additional impairments in basal synaptic transmission by 3 months of age. Our results demonstrate that while the net output of total LTP is similar between 3xTg-AD and NonTg mice, NMDAR LTP and non-NMDAR LTP develop differently in 3xTg-AD mice compared to NonTg mice. We show that 3xTg-AD mice are resistant to drugs that typically block LTP, yet despite their resistance to NMDAR and VDCC antagonism, results from previous working memory studies show they still have a profound impairment in cognitive function at 3 months of age [20]. There is substantial evidence to support LTP as a mediator of learning and memory, and the degree of LTP can be correlated to cognitive performance [18, 52], but we have shown that just being able to generate LTP does not equate to cognitive performance in all tasks. LTP must be generated through the proper signaling mechanisms in the proper context for it to make the desired contribution to learning and memory performance. If not, the integrity of cognition may be compromised. Compensatory alterations in LTP induction and expression in 3xTg-AD mice can occur

independently of NMDAR or VDCC activation, and understanding the nature of these altered mechanisms may prove useful not only in understanding the precise role for each mechanism in learning and memory, but also may lead to therapeutic targets for memory disorders such as AD.

Acknowledgments

Funding for this work was provided by NIH R01 N5046451 (www.ninds.nih.gov) to R. Furukawa and M. Fechheimer. Disclosure statement: There are no conflicts of interest. All animal protocols and experiments were approved by the University of Georgia Institutional Animal Care and Use Committee.

References

1. Querfurth, H.W. and F.M. LaFerla, *Alzheimer's disease*. N Engl J Med, 2010. **362**(4): p. 329-44.
2. Morris, M., et al., *The many faces of tau*. Neuron, 2011. **70**(3): p. 410-26.
3. LaFerla, F.M., K.N. Green, and S. Oddo, *Intracellular amyloid-beta in Alzheimer's disease*. Nat Rev Neurosci, 2007. **8**(7): p. 499-509.
4. Yu, J.T., R.C. Chang, and L. Tan, *Calcium dysregulation in Alzheimer's disease: from mechanisms to therapeutic opportunities*. Prog Neurobiol, 2009. **89**(3): p. 240-55.
5. Berridge, M.J., *Calcium signalling and Alzheimer's disease*. Neurochem Res, 2011. **36**(7): p. 1149-56.
6. Stutzmann, G.E., et al., *Enhanced ryanodine receptor recruitment contributes to Ca²⁺ disruptions in young, adult, and aged Alzheimer's disease mice*. J Neurosci, 2006. **26**(19): p. 5180-9.
7. Lopez, J.R., et al., *Increased intraneuronal resting [Ca²⁺] in adult Alzheimer's disease mice*. J Neurochem, 2008. **105**(1): p. 262-71.
8. Malenka, R.C., et al., *Postsynaptic calcium is sufficient for potentiation of hippocampal synaptic transmission*. Science, 1988. **242**(4875): p. 81-4.
9. Kauer, J.A., R.C. Malenka, and R.A. Nicoll, *A persistent postsynaptic modification mediates long-term potentiation in the hippocampus*. Neuron, 1988. **1**(10): p. 911-7.
10. Herron, C.E., et al., *Frequency-dependent involvement of NMDA receptors in the hippocampus: a novel synaptic mechanism*. Nature, 1986. **322**(6076): p. 265-8.
11. Shi, S.H., et al., *Rapid spine delivery and redistribution of AMPA receptors after synaptic NMDA receptor activation*. Science, 1999. **284**(5421): p. 1811-6.
12. Bliss, T.V. and G.L. Collingridge, *A synaptic model of memory: long-term potentiation in the hippocampus*. Nature, 1993. **361**(6407): p. 31-9.
13. Morgan, S.L. and T.J. Teyler, *VDCCs and NMDARs underlie two forms of LTP in CA1 hippocampus in vivo*. J Neurophysiol, 1999. **82**(2): p. 736-40.
14. Cavus, I. and T. Teyler, *Two forms of long-term potentiation in area CA1 activate different signal transduction cascades*. J Neurophysiol, 1996. **76**(5): p. 3038-47.
15. Grover, L.M. and T.J. Teyler, *Two components of long-term potentiation induced by different patterns of afferent activation*. Nature, 1990. **347**(6292): p. 477-9.

16. Shankar, S., T.J. Teyler, and N. Robbins, *Aging differentially alters forms of long-term potentiation in rat hippocampal area CA1*. J Neurophysiol, 1998. **79**(1): p. 334-41.
17. Borroni, A.M., et al., *Role of voltage-dependent calcium channel long-term potentiation (LTP) and NMDA LTP in spatial memory*. J Neurosci, 2000. **20**(24): p. 9272-6.
18. Boric, K., et al., *Potential adaptive function for altered long-term potentiation mechanisms in aging hippocampus*. J Neurosci, 2008. **28**(32): p. 8034-9.
19. Oddo, S., et al., *Triple-transgenic model of Alzheimer's disease with plaques and tangles: intracellular Abeta and synaptic dysfunction*. Neuron, 2003. **39**(3): p. 409-21.
20. Clark, J.K., et al., *Alterations in synaptic plasticity coincide with deficits in spatial working memory in presymptomatic 3xTg-AD mice*. Neurobiol Learn Mem, 2015. **125**: p. 152-162.
21. de Flores, R., R. La Joie, and G. Chetelat, *Structural imaging of hippocampal subfields in healthy aging and Alzheimer's disease*. Neuroscience, 2015. **309**: p. 29-50.
22. Bittner, T., et al., *Multiple events lead to dendritic spine loss in triple transgenic Alzheimer's disease mice*. PLoS One, 2010. **5**(11): p. e15477.
23. Li, S., et al., *Soluble oligomers of amyloid Beta protein facilitate hippocampal long-term depression by disrupting neuronal glutamate uptake*. Neuron, 2009. **62**(6): p. 788-801.
24. Hsieh, H., et al., *AMPA removal underlies Abeta-induced synaptic depression and dendritic spine loss*. Neuron, 2006. **52**(5): p. 831-43.
25. Minano-Molina, A.J., et al., *Soluble oligomers of amyloid-beta peptide disrupt membrane trafficking of alpha-amino-3-hydroxy-5-methylisoxazole-4-propionic acid receptor contributing to early synapse dysfunction*. J Biol Chem, 2011. **286**(31): p. 27311-21.
26. Zucker, R.S. and W.G. Regehr, *Short-term synaptic plasticity*. Annu Rev Physiol, 2002. **64**: p. 355-405.
27. Nelson, O., et al., *Familial Alzheimer disease-linked mutations specifically disrupt Ca²⁺ leak function of presenilin 1*. J Clin Invest, 2007. **117**(5): p. 1230-9.
28. Rybalchenko, V., et al., *The cytosolic N-terminus of presenilin-1 potentiates mouse ryanodine receptor single channel activity*. Int J Biochem Cell Biol, 2008. **40**(1): p. 84-97.

29. Zhang, C., et al., *Presenilins are essential for regulating neurotransmitter release*. Nature, 2009. **460**(7255): p. 632-6.
30. Wu, B., et al., *Presenilins regulate calcium homeostasis and presynaptic function via ryanodine receptors in hippocampal neurons*. Proc Natl Acad Sci U S A, 2013. **110**(37): p. 15091-6.
31. Chan, S.L., et al., *Presenilin-1 mutations increase levels of ryanodine receptors and calcium release in PC12 cells and cortical neurons*. J Biol Chem, 2000. **275**(24): p. 18195-200.
32. Chakroborty, S., et al., *Deviant ryanodine receptor-mediated calcium release resets synaptic homeostasis in presymptomatic 3xTg-AD mice*. J Neurosci, 2009. **29**(30): p. 9458-70.
33. Chakroborty, S., et al., *Early presynaptic and postsynaptic calcium signaling abnormalities mask underlying synaptic depression in presymptomatic Alzheimer's disease mice*. J Neurosci, 2012. **32**(24): p. 8341-53.
34. Green, K.N. and F.M. LaFerla, *Linking calcium to Abeta and Alzheimer's disease*. Neuron, 2008. **59**(2): p. 190-4.
35. Bauer, E.P., G.E. Schafe, and J.E. LeDoux, *NMDA receptors and L-type voltage-gated calcium channels contribute to long-term potentiation and different components of fear memory formation in the lateral amygdala*. J Neurosci, 2002. **22**(12): p. 5239-49.
36. Davis, S., S.P. Butcher, and R.G. Morris, *The NMDA receptor antagonist D-2-amino-5-phosphonopentanoate (D-AP5) impairs spatial learning and LTP in vivo at intracerebral concentrations comparable to those that block LTP in vitro*. J Neurosci, 1992. **12**(1): p. 21-34.
37. Bolhuis, J.J. and I.C. Reid, *Effects of intraventricular infusion of the N-methyl-D-aspartate (NMDA) receptor antagonist AP5 on spatial memory of rats in a radial arm maze*. Behav Brain Res, 1992. **47**(2): p. 151-7.
38. Maurice, T., J. Bayle, and A. Privat, *Learning impairment following acute administration of the calcium channel antagonist nimodipine in mice*. Behav Pharmacol, 1995. **6**(2): p. 167-175.
39. Da Silva, W.C., et al., *Memory reconsolidation and its maintenance depend on L-voltage-dependent calcium channels and CaMKII functions regulating protein turnover in the hippocampus*. Proc Natl Acad Sci U S A, 2013. **110**(16): p. 6566-70.
40. Geddes, J.W., et al., *Density and distribution of NMDA receptors in the human hippocampus in Alzheimer's disease*. Brain Res, 1986. **399**(1): p. 156-61.

41. Panegyres, P.K., K. Zafiris-Toufexis, and B.A. Kakulas, *The mRNA of the NR1 subtype of glutamate receptor in Alzheimer's disease*. J Neural Transm (Vienna), 2002. **109**(1): p. 77-89.
42. Duszczyk, M., et al., *In vivo hippocampal microdialysis reveals impairment of NMDA receptor-cGMP signaling in APP(SW) and APP(SW)/PS1(L166P) Alzheimer's transgenic mice*. Neurochem Int, 2012. **61**(7): p. 976-80.
43. Schiller, J., Y. Schiller, and D.E. Clapham, *NMDA receptors amplify calcium influx into dendritic spines during associative pre- and postsynaptic activation*. Nat Neurosci, 1998. **1**(2): p. 114-8.
44. Wang, Y. and M.P. Mattson, *L-type Ca²⁺ currents at CA1 synapses, but not CA3 or dentate granule neuron synapses, are increased in 3xTgAD mice in an age-dependent manner*. Neurobiol Aging, 2014. **35**(1): p. 88-95.
45. Raymond, C.R. and S.J. Redman, *Different calcium sources are narrowly tuned to the induction of different forms of LTP*. J Neurophysiol, 2002. **88**(1): p. 249-55.
46. Smith, J.P., et al., *Stimulus pattern dependence of the Alzheimer's disease amyloid-beta 42 peptide's inhibition of long term potentiation in mouse hippocampal slices*. Brain Res, 2009. **1269**: p. 176-84.
47. Raymond, C.R., D.R. Ireland, and W.C. Abraham, *NMDA receptor regulation by amyloid-beta does not account for its inhibition of LTP in rat hippocampus*. Brain Res, 2003. **968**(2): p. 263-72.
48. Shilling, D., et al., *Suppression of InsP3 receptor-mediated Ca²⁺ signaling alleviates mutant presenilin-linked familial Alzheimer's disease pathogenesis*. J Neurosci, 2014. **34**(20): p. 6910-23.
49. Cheung, K.H., et al., *Gain-of-function enhancement of IP3 receptor modal gating by familial Alzheimer's disease-linked presenilin mutants in human cells and mouse neurons*. Sci Signal, 2010. **3**(114): p. ra22.
50. Cantanelli, P., et al., *Age-Dependent Modifications of AMPA Receptor Subunit Expression Levels and Related Cognitive Effects in 3xTg-AD Mice*. Front Aging Neurosci, 2014. **6**: p. 200.
51. Billings, L.M., et al., *Intraneuronal Ab causes the onset of early Alzheimer's disease-related cognitive deficits in transgenic mice*. Neuron, 2005. **45**: p. 675-688.
52. Bach, M.E., et al., *Age-related defects in spatial memory are correlated with defects in the late phase of hippocampal long-term potentiation in vitro and are attenuated by drugs that enhance the cAMP signaling pathway*. Proc Natl Acad Sci U S A, 1999. **96**(9): p. 5280-5.

Figures

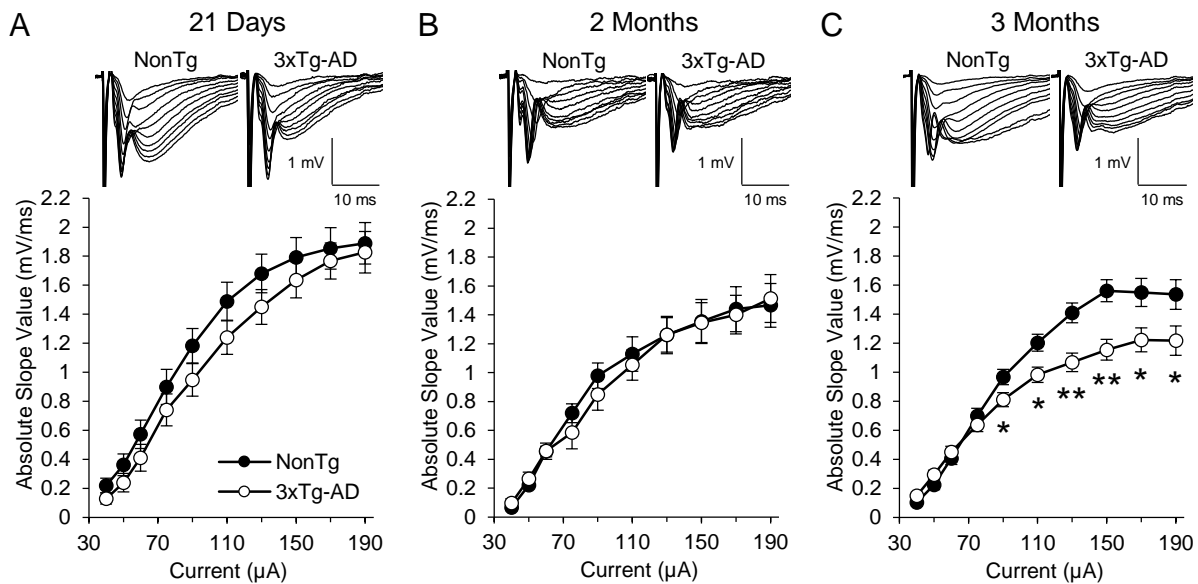


Figure 3.1. Field Excitatory Post-Synaptic Potentials (fEPSP) recorded from the CA1 region of ventral hippocampus in 3xTg-AD and NonTg control mice. A) Stimulus response curves for 3xTg-AD (open circles, n=21(8)) and NonTg (black circles, n=23(9)) mice at 21 days old. Input intensities are 40, 50, 60, 75, 90, 110, 130, 110, 150, and 190 μA. The averaged fEPSP sweeps are shown above the stimulus response curves. B) Same as panel A except at 2 months of age for 3xTg-AD (n=8(3)) and NonTg (n=8(3)) mice. C) Same as panel A except at 3 months of age for 3xTg-AD (n=37(11)) and NonTg (n=58(19)) mice. Values represent the mean ± SEM from n slices(animals). Significance was determined using repeated measures ANOVA and independent t-tests (* p < 0.05, ** p < 0.01).

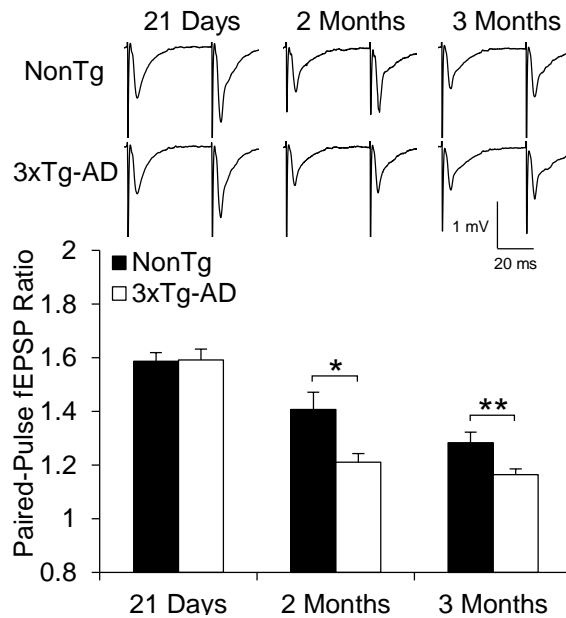


Figure 3.2. Paired-pulse field Excitatory Post-Synaptic Potentials (fEPSP) recorded from the CA1 region of ventral hippocampus in 3xTg-AD and NonTg control mice. A) Paired-pulse ratio in 3xTg-AD (open bars) and NonTg (black bars) mice at 21 days old (3xTg-AD, n=23(8); NonTg, n=25(9)), 2 months of age (3xTg-AD, n=8(3); NonTg, n=8(3)), and 3 months of age (3xTg-AD, n=39(11); NonTg, n=27(11)). The paired-pulse interval is 50 ms. The averaged fEPSP sweeps are shown above the paired-pulse ratios. Values represent the mean \pm SEM from n slices(animals). Significance was determined using independent t-tests (* $p < 0.05$, ** $p < 0.01$).

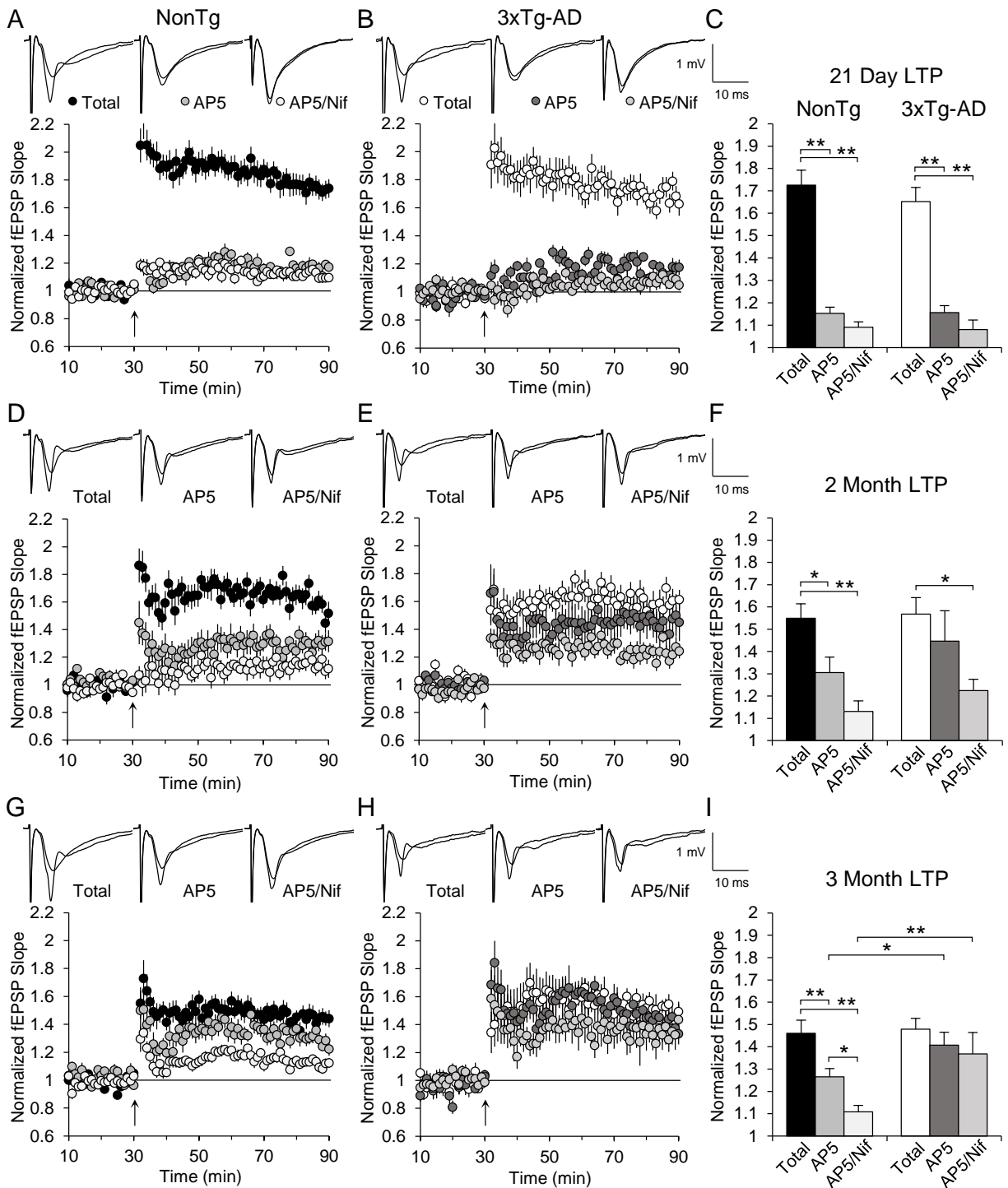


Figure 3.3. Long-Term Potentiation (LTP) of field Excitatory Post-Synaptic Potentials (fEPSP) recorded from the CA1 region of ventral hippocampus in 3xTg-AD and NonTg control mice. A) Summary plot of normalized fEPSP slope values in 21 day old NonTg mice for total LTP (black circles, (n=14(5)), bath applied D,L-AP5 (AP5) (50 μ M) (light grey circles, n=9(3)), and bath applied AP5 (50 μ M) and Nifedipine (20 μ M) together (AP5/Nif) (lightest circles, n=11(4)), before and after strong high frequency stimulation (HFS) (4 x 200 Hz/0.5 s at 5 s intervals) indicated by the arrow at 30 minutes. The averaged fEPSP sweeps before and after HFS for each condition are shown above the plot. B) Same as panel A except in 21 day old 3xTg-AD mice for total LTP (open circles, (n=10(4)), bath applied AP5 (dark grey circles, n=9(3)), and bath applied AP5/Nif (lightest circles, n=11(4)). C) Summary quantification of LTP for each condition for NonTg and 3xTg-AD mice at 1 hour post-HFS. D, E, & F) Same as A, B, & C above except at 2 months of age for NonTg (total LTP, n=8(3); AP5, n=8(3); AP5/Nif, n=9(3)) mice and 3xTg-AD (total LTP, n=8(3); AP5, n=7(3); AP5/Nif, n=7(3)) mice. G, H, & I) Same as A, B, & C above except at 3 months of age for NonTg (total LTP, n=10(4); AP5, n=10(4); AP5/Nif, n=11(4)) mice and 3xTg-AD (total LTP, n=7(3); AP5, n=6(3); AP5/Nif, n=6(3)) mice. Values represent the mean \pm SEM from n slices(animals). Significance was determined using ANOVA and independent t-tests (* p < 0.05, ** p < 0.01).

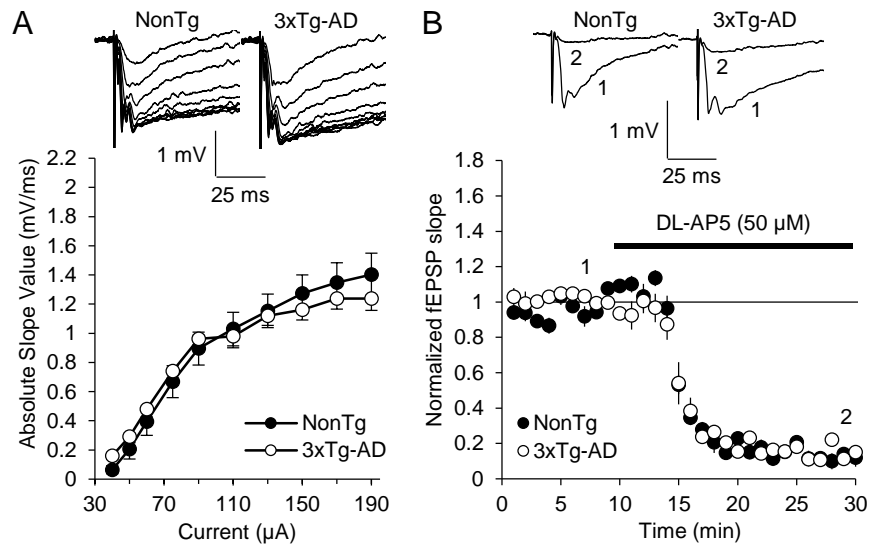


Figure 3.4. NMDAR-mediated field Excitatory Post-Synaptic Potentials (fEPSP) recorded from the CA1 region of ventral hippocampus in 3xTg-AD and NonTg control mice. A) Stimulus response curves for NMDAR-mediated fEPSPs in 3xTg-AD (open circles, n=15(5)) and NonTg (black circles, n=14(5)) mice at 3 months of age. Recordings are in nominally Mg^{2+} free ACSF in the presence of CNQX ($10 \mu M$) and Nifedipine ($20 \mu M$). Input intensities are 40, 50, 60, 75, 90, 110, 130, 110, 150, and 190 μA . The averaged fEPSP sweeps are shown above the stimulus response curves. B) Summary plot of normalized NMDAR-mediated fEPSP slope values in 3 month old 3xTg-AD (n=11(5)) and NonTg (n=13(5)) control mice before and after bath application of D,L-AP5 (AP5) ($50 \mu M$) as indicated by the line above the plot points at 10 minutes. After recordings in panel A, stimulatory intensity was returned to baseline and AP5 was bath applied. The averaged NMDAR-mediated fEPSP sweeps before and after AP5 application are shown above the plot (1=before AP5 application, 2=30 minutes after AP5 application). There was no difference between genotypes for NMDAR-mediated

fEPSPs to the sensitivity of AP5 antagonism. Values represent the mean \pm SEM from n slices(animals). Significance was determined using repeated measures ANOVA and independent t-tests (* $p < 0.05$, ** $p < 0.01$).

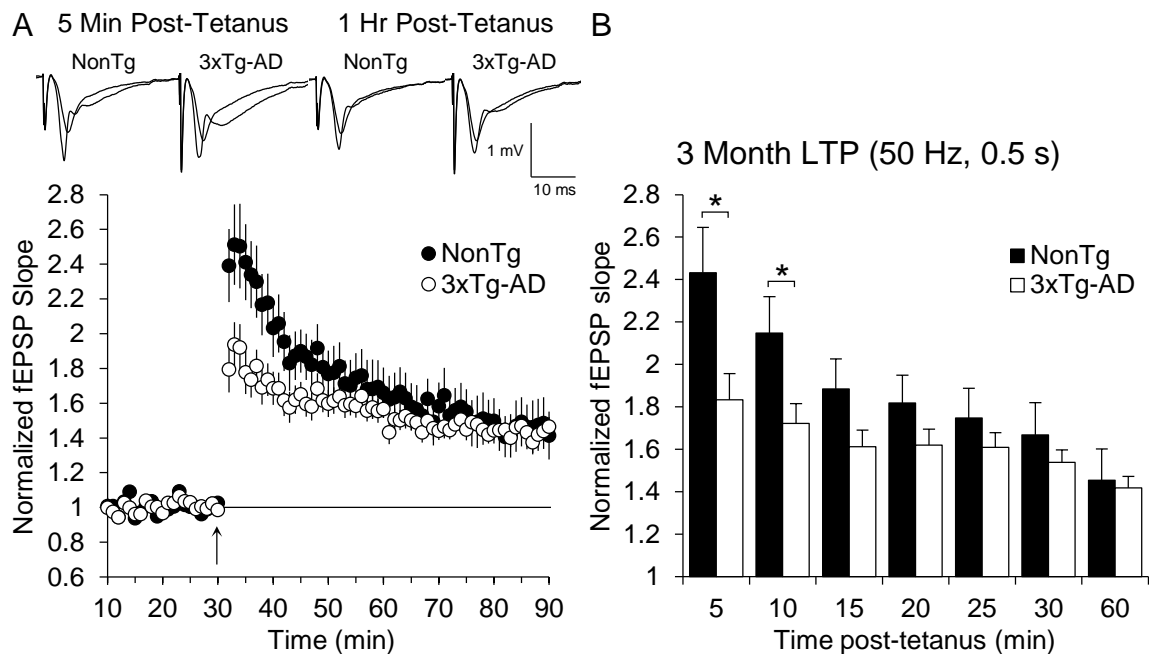


Figure 3.5. NMDA receptor-dependent Long-Term Potentiation (LTP) of field Excitatory Post-Synaptic Potentials (fEPSP) recorded from the CA1 region of ventral hippocampus in 3xTg-AD and NonTg control mice. A) Summary plot of normalized fEPSP slope values in 3 month old 3xTg-AD (open circles, (n=12(5)) and NonTg (black circles, (n=13(5)) mice, before and after weak high frequency stimulation (HFS) (1 x 50 Hz/0.5 s) indicated by the arrow at 30 minutes. Recordings are in standard ACSF in the presence of Nifedipine (20 μ M). The averaged fEPSP sweeps before and after HFS are shown above the plot. B) Summary quantification of LTP for 3xTg-AD and NonTg mice up to 1 hour post-HFS. Values represent the mean \pm SEM from n slices(animals). Significance was determined using independent t-tests (* $p < 0.05$, ** $p < 0.01$).

CHAPTER 4

OPEN FIELD BEHAVIOR IN YOUNG 3xTg-AD MICE¹

¹ Clark JK, Furukawa R, Fechheimer M, Wagner JJ. *Alterations in Locomotor Behavior and Synaptic Transmission and Plasticity in Young 3xTg-AD Mice*. Submitted to Neuroscience.

Abstract

Alzheimer's disease is a neurodegenerative condition thought to be initiated by production of the Amyloid- β peptide, which leads to synaptic dysfunction, and progressive memory and behavioral disturbances. Using a triple transgenic mouse model of Alzheimer's disease (3xTg-AD), we evaluated the onset of behavioral disturbances by measuring locomotor activity in 3xTg-AD and NonTg control mice at 21 days, 2 months, and 3 months of age. Using an open field arena, we measured the total locomotor activity, and crossings into a center zone, as a measure of the general psychological state of the animal and potential for anxiogenic behavior. 3xTg-AD mice show reduced locomotor activity at 21 days and 2 months of age, but not at 3 months of age compared to NonTg mice. At 21 days, NonTg mice display significantly higher center zone crossings compared to 3xTg-AD mice, which may be indicative of either anxiogenic behavior in 3xTg-AD mice, or hyperactivity in NonTg mice. All groups displayed habituation to the novel environment with the exception of NonTg mice at 21 days. These findings should provide a new perspective on the early behavioral disturbances that may occur in the early stages of Alzheimer's disease.

4.1 Introduction

Alzheimer's disease (AD) is a neurodegenerative disease of aging, and the most common form of dementia [1]. AD patients show deficits in cognitive processes that include progressive memory loss, confusion, and disorientation, but may also show behavioral changes that include increased agitation, anxiety, and sleep disturbances [2, 3]. AD pathology is characterized by the presence of extracellular β -Amyloid plaques and intracellular neurofibrillary tangles of hyperphosphorylated Tau protein [4, 5]. The primary initiator of AD pathology is thought to be the overproduction of soluble Amyloid- β (A β) peptide, produced through sequential cleavage of Amyloid Precursor Protein by the membrane bound enzymes β - and γ -secretase [5]. The increased production of the A β peptide leads to synaptic impairment and eventual neurodegeneration resulting in both cognitive and behavioral disturbances [1].

A triple transgenic mouse model of Alzheimer's disease (3xTg-AD) has been developed that produces both β -Amyloid plaques and neurofibrillary Tau tangles [6]. In a previous study we showed 3xTg-AD mice have severe impairments in long-term working memory using the 8-arm radial maze at 3 months old, an age generally considered to be presymptomatic [7]. In the current study, we explore the potential early behavioral changes that may occur in 3xTg-AD mice using behavioral (open field locomotor activity) assessments to investigate the onset and progression of disturbances in the general psychological state of the animal. Our findings show differences in locomotor activity, habituation to a novel environment, and center zone crossings between 3xTg-AD and NonTg mice beginning as early as 21 days old.

4.2 Methods

4.2.1 Animals and euthanasia

All animals used in this study were male mice and consisted of Alzheimer's disease model mice (3xTg-AD) homozygous for three mutant transgenes: APP(Swe), Psen1, and TauP301L, (B6/129-*Psen1*^{tm1Mpm} Tg(APP^{Swe}, tauP301L)1Lfa/Mmjax) obtained from the MMRRC (ID 034830-JAX) through Jackson Laboratories, and nontransgenic (NonTg) control mice (B6129SF2/J) from Jackson Laboratories (101045 JAX, Bar Harbor, ME). The generation of 3xTg-AD mice has been described elsewhere [6]. Briefly, two separate transgene constructs each encoding human *APP* cDNA (695 isoform) harboring the Swedish mutation (*KM670/671NL*), or human *Tau* cDNA (4R/0N) harboring the *P301L* mutation, each under control of mouse Thy1.2 regulatory elements, were comicroinjected into single-cell embryos from homozygous *PS1*_{M146V} knockin mice. Embryos were screened for cointegration of both cassettes to the same locus. Embryos were then reimplanted into foster mothers and the resulting offspring were genotyped to identify 3xTg-AD mice. Hemizygous F1 3xTg-AD mice were then crossed to produce 3xTg-AD mice homozygous for all three transgenes. Both 3xTg-AD and NonTg mice are on the same genetic and strain background (129/C57BL6 hybrid), except NonTg mice harbor the endogenous wild-type *PS1* gene. Breeding pairs for each group were obtained and animals were bred in house at the University of Georgia animal facilities. Mice were housed in an AAALAC accredited facility on a 12 hour light/dark timed schedule and had ad libitum access to food and water during this study. Behavioral testing occurred at three different time points: 21 days (20-22 days old), 2 months (60-67 days old), and 3 months (90-100 days old). Pre-weaned mice at 21 days

were tested instead of 1 month old mice to avoid any stress induced effects from the weaning process that could potentially influence behavioral measurements. Euthanasia of mice occurred under deep anesthesia with halothane followed by decapitation. The University of Georgia Institutional Animal Care and Use Committee approved all animal protocols and experiments.

4.2.2 Open field arena

Behavioral activity was measured in the open field arena, which consisted of a square chamber (43 x 43 cm) with clear plastic walls (30.5 cm high) and a removable smooth metal floor (Med Associates, St. Albans, VT, USA). The chambers are individually housed in sound attenuating cubicles with house lighting (20 lx) positioned in 2 of the 4 corners, and a ventilation fan which also provided ambient background noise. Two banks, each containing 16 infrared photobeams, are mounted at right angles to each other, with paired photodetectors mounted opposite each bank, creating a 16 x 16 photobeam grid 2 cm from the floor. Activity Monitor software counts photobeam breaks to determine both ambulatory (sequential) and stereotypic (repetitive; movement without displacement) movements based on patterning of beam breaks. For locomotor activity, mice were placed in the center of the open field arena and allowed to roam freely for 30 minutes. Both ambulatory and stereotypic counts were combined into total horizontal counts, and summed into 10 minute blocks. For center zone analysis, a defined square area of 26.3 x 26.3 cm (37.5% of total area) in the center of the chamber was designated as the center zone to count crossings into this area. All animals were subjected to a single 30 minute session in the midafternoon during the midpoint of their circadian light cycle.

4.2.3 Statistics

Tests of significance were performed using either ANOVA, or independent t-tests as appropriate.

4.3 Results

To determine if behavioral differences exist between 3xTg-AD and NonTg mice at 21 days, 2 months, and 3 months of age, open field behavior in a novel environment was measured to evaluate the general psychological state of the animal.

To evaluate general locomotor activity and anxiety, open field behavior in a novel environment was observed and total locomotor activity and center zone crossings were measured (Figure 4.1). Locomotor data for each genotype at each age were first subjected to individual ANOVA to assess the degree of habituation to a novel environment. All groups, except for the 21 day old NonTg group, showed a significant reduction in locomotor activity ($p < 0.01$) from 0-30 minutes, indicating habituation to the novel environment (Figure 4.1A, B, & C). The 21 day NonTg group did show a reduction in total locomotor activity over 30 minutes, but was not statistically significant ($p = 0.17$), suggesting NonTg mice at this age did not habituate to the novel environment as the 3xTg-AD mice did. Locomotor data for each age group were then subjected to a 2 genotype (NonTg versus 3xTg-AD) x 3 point elapsed time (0-30 minutes in 10 minute blocks) mixed ANOVA. At 21 days, 3xTg-AD mice ($n=11$) differed from NonTg mice ($n=12$) in total locomotor activity (Figure 4.1A). Within-subjects analysis showed there was a significant effect of time ($F(2,42)=18.469$, $p < 0.001$), and a significant interaction of time x genotype ($F(2,42)=3.486$, $p < 0.05$) on locomotor

activity, indicating NonTg mice habituate differently to the novel environment than 3xTg-AD mice, which was expected since NonTg mice did not show significant habituation. Between-subjects analysis showed there was a significant effect of genotype ($F(1,21)=5.493$, $p < 0.05$), and follow up between-subjects comparisons using independent t-tests showed NonTg mice remain more active than 3xTg-AD mice past 10 minutes. At 2 months, 3xTg-AD mice ($n=8$) also differed from NonTg mice ($n=8$) in total locomotor activity (Figure 4.1B). Within-subjects analysis showed there was a significant effect of time ($F(2,28)=102.372$, $p < 0.001$), but no significant interaction of time x genotype ($F(2,28)=0.408$, $p = 0.67$) on locomotor activity. Between-subjects analysis showed there was a significant effect of genotype ($F(1,14)=14.480$, $p < 0.01$), and follow up between-subjects comparisons using independent t-tests showed NonTg mice were again more active than 3xTg-AD mice at each increment tested, although unlike the 21 day group, NonTg mice did habituate to the novel environment similarly to 3xTg-AD mice. At 3 months, 3xTg-AD mice ($n=15$) did not differ from NonTg mice ($n=9$) in total locomotor activity (Figure 4.1C). Within-subjects analysis showed there was a significant effect of time ($F(2,44)=128.205$, $p < 0.001$), and a significant interaction of time x genotype ($F(2,44)=7.885$, $p < 0.01$) on locomotor activity, indicating NonTg mice habituate differently to the novel environment than 3xTg-AD mice, even though both genotypes do show a significant degree of habituation. This result is most likely a consequence of the last 10 minutes in which 3xTg-AD mice had less locomotor activity at 20 minutes, but higher locomotor activity by 30 minutes (although not significantly). This is in combination with NonTg mice continuing to show habituation from 20-30 minutes ($p < 0.001$), but 3xTg-AD mice do not ($p = 0.372$), despite both groups showing

an overall habituation from 0-30 minutes. Between-subjects analysis showed there was no significant effect of genotype ($F(1,22)=0.070$, $p = 0.794$), and follow up between-subjects comparisons using independent t-tests confirmed 3xTg-AD mice are not different from NonTg mice at any increment tested.

We also examined center zone crossings as a measure of anxiety. A defined square area in the center of the open field arena representing approximately 38% of the total area was designated as the center zone. This test assesses the tension between a rodent's natural exploratory behavior versus the instinct to remain in protected areas (such as close to a wall or in a corner) under stressful conditions. Our results showed crossings into the center zone were significantly less ($p < 0.01$) in 3xTg-AD mice ($n=11$) compared to NonTg mice ($n=12$) at 21 days old (Figure 4.1D). Center zone crossings at 2 months (3xTg-AD, $n=8$; NonTg, $n=4$) and 3 months (3xTg-AD, $n=13$; NonTg, $n=4$) were not significantly different between genotypes.

4.4 Discussion

In this study, we observed behavioral differences in 3xTg-AD mice compared to NonTg controls. Behavioral differences were found in 3xTg-AD mice using an open field assessment of locomotor activity. 3xTg-AD mice showed reduced locomotor activity at 21 days and 2 months of age, and reduced center zone crossings at 21 days old (Figure 4.1).

Locomotor activity following introduction to a novel environment is useful as an evaluation of the general psychological state of the animal. Exposure to psychopharmacological agents or certain pathological conditions can alter behavioral

circuitry that may express sensitivity through changes in locomotor activity [8-10]. In our current study, NonTg and 3xTg-AD mice both showed habituation to the novel open field environment at all ages tested except for the 21 day NonTg mice. 3xTg-AD mice displayed less exploratory behavior and greater habituation to the novel environment at 21 days than NonTg mice. At 2 months of age, 3xTg-AD mice continue to show less exploratory behavior, but habituate to the novel environment similarly to NonTg mice. At 3 months of age however, there is not a significant difference in overall locomotor activity between NonTg and 3xTg-AD mice, but 3xTg-AD mice show less habituation to the novel environment during the last 10 minutes of the open field assay. The results of the center zone analysis agree with the locomotor activity at these ages showing 3xTg-AD mice were less willing to explore away from the periphery by having less center zone crossings than NonTg mice, indicating a reduction in the natural exploratory behavior as compared to NonTg mice of similar age. Reservation to explore the central zone area can be used as an indicator of anxiogenic behavior, and our results suggest 3xTg-AD mice display an anxiogenic effect at 21 days. It should be noted however, that NonTg mice failed to adequately habituate to the novel environment, making it difficult to interpret center zone crossings in combination with locomotor data. It is the 3xTg-AD mice at 21 days that appear to respond normally to the open field environment rather than NonTg mice, thus we cannot exclude the possibility that the NonTg mice may have been hyperactive, rather than the 3xTg-AD mice being hypoactive due to an anxiogenic state. Comparison of our 21 day NonTg results to those of other studies was difficult due to a lack of similar studies in the current literature. By 3 months of age, the visual appearance of locomotor activity was not different between genotypes, but statistical

analysis revealed 3xTg-AD mice habituated to the open field environment differently than NonTg mice, most likely a result of the last 10 minutes of locomotor activity influencing the overall effect. Center zone entries were increased in 3xTg-AD mice over NonTg, something not observed at earlier ages, but this was not significant. Open field studies on young 3xTg-AD mice are limited, although one study has shown 3xTg-AD mice have less locomotor activity than NonTg mice at 20-22 days old [11], which somewhat agree with our own results, however this study only evaluated open field behavior for 5 minutes, making comparisons of habituation to a novel environment difficult. Most studies of locomotor behavior in 3xTg-AD mice however, are with substantially older animals (9-15 months on average) after AD pathology is present, and measure subtly different variables. Those studies indicate that older 3xTg-AD mice have less locomotor activity, and make less center zone entries [12], but spend more time in the central zone [13] compared to NonTg mice. These results in combination with our own observations suggest 3xTg-AD mice are behaviorally different from a very early age, long before the presence of characteristic AD pathology (plaques and tangles), and this difference seems to persist throughout the life of the animal.

In the current study, we show 3xTg-AD mice exhibit less locomotor activity than NonTg mice at 21 days and 2 months of age, but have similar activity at 3 months of age. In addition, at 21 days and 3 months of age, but not at 2 months of age, the genotype influences how locomotor activity changes with time. All groups habituate to the novel environment, with the exception of the NonTg mice at 21 days, which also show significantly higher center zone crossings. Further evaluation of behaviors such as those measured by the open field arena may provide a more thorough understanding

of the behavioral changes observed in AD patients, and may potentially influence strategies for behavioral treatment.

Acknowledgments

Funding for this work was provided by NIH R01 N5046451 (www.ninds.nih.gov) to R. Furukawa and M. Fechheimer. Disclosure statement: There are no conflicts of interest. All animal protocols and experiments were approved by the University of Georgia Institutional Animal Care and Use Committee.

References

1. Querfurth, H.W. and F.M. LaFerla, *Alzheimer's disease*. N Engl J Med, 2010. **362**(4): p. 329-44.
2. Sadowsky, C.H. and J.E. Galvin, *Guidelines for the management of cognitive and behavioral problems in dementia*. J Am Board Fam Med, 2012. **25**(3): p. 350-66.
3. Seignourel, P.J., et al., *Anxiety in dementia: a critical review*. Clin Psychol Rev, 2008. **28**(7): p. 1071-82.
4. Morris, M., et al., *The many faces of tau*. Neuron, 2011. **70**(3): p. 410-26.
5. LaFerla, F.M., K.N. Green, and S. Oddo, *Intracellular amyloid-beta in Alzheimer's disease*. Nat Rev Neurosci, 2007. **8**(7): p. 499-509.
6. Oddo, S., et al., *Triple-transgenic model of Alzheimer's disease with plaques and tangles: intracellular Abeta and synaptic dysfunction*. Neuron, 2003. **39**(3): p. 409-21.
7. Clark, J.K., et al., *Alterations in synaptic plasticity coincide with deficits in spatial working memory in presymptomatic 3xTg-AD mice*. Neurobiol Learn Mem, 2015. **125**: p. 152-162.
8. Pierce, R.C. and P.W. Kalivas, *A circuitry model of the expression of behavioral sensitization to amphetamine-like psychostimulants*. Brain Res Brain Res Rev, 1997. **25**(2): p. 192-216.
9. Prut, L. and C. Belzung, *The open field as a paradigm to measure the effects of drugs on anxiety-like behaviors: a review*. Eur J Pharmacol, 2003. **463**(1-3): p. 3-33.
10. Keralapurath, M.M., et al., *Cocaine- or stress-induced metaplasticity of LTP in the dorsal and ventral hippocampus*. Hippocampus, 2014. **24**(5): p. 577-90.
11. Blaney, C.E., et al., *Maternal genotype influences behavioral development of 3xTg-AD mouse pups*. Behav Brain Res, 2013. **252**: p. 40-8.
12. Pietropaolo, S., J. Feldon, and B.K. Yee, *Environmental enrichment eliminates the anxiety phenotypes in a triple transgenic mouse model of Alzheimer's disease*. Cogn Affect Behav Neurosci, 2014. **14**(3): p. 996-1008.
13. Filali, M., et al., *Cognitive and non-cognitive behaviors in the triple transgenic mouse model of Alzheimer's disease expressing mutated APP, PS1, and Mapt (3xTg-AD)*. Behav Brain Res, 2012. **234**(2): p. 334-42.

Figures

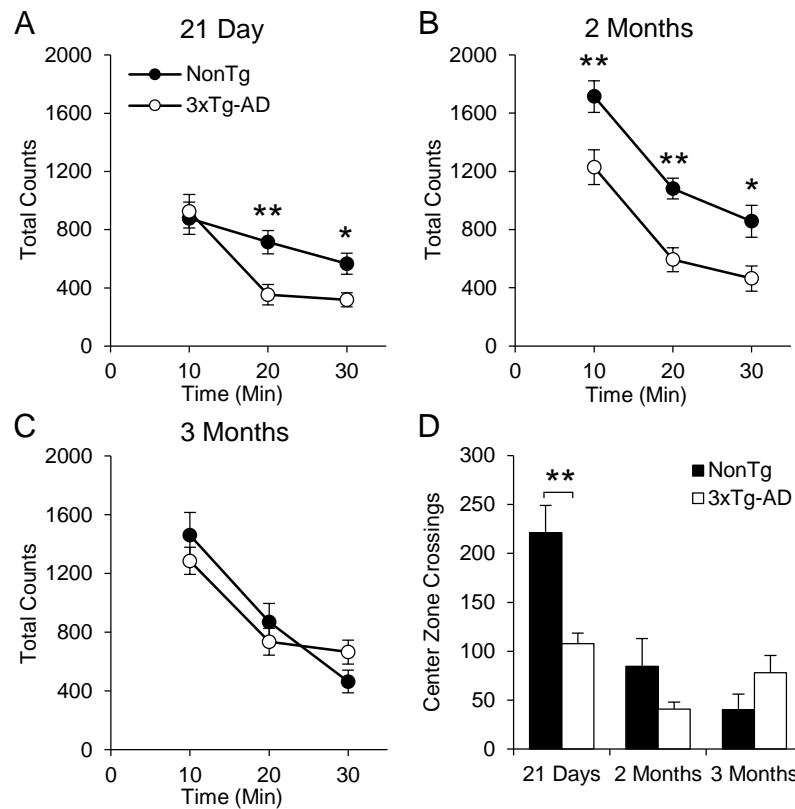


Figure 4.1. Open field behavior in 3xTg-AD and NonTg control mice. A) Locomotor activity in 21 day old 3xTg-AD (open circles, n=11) and NonTg (black circles, n=12) mice measured for 30 min, and summed into 10 minute blocks. B) Same as panel A except at 2 months of age for 3xTg-AD (n=8) and NonTg (n=8) mice. C) Same as panel A except at 3 months of age for 3xTg-AD (n=15) and NonTg (n=9) mice. D) Center zone entries during the 30 minutes of locomotor activity for 3xTg-AD (black bars, 21 days, n=11; 2 months, n=8; 3 months, n=13) and NonTg (open bars, 21 days, n=12; 2 months, n=4; 3 months, n=4) mice. Values represent the mean \pm SEM from n animals. Significance was determined using repeated measures ANOVA and independent t-tests (* $p < 0.05$, ** $p < 0.01$).

CHAPTER 5
IMPAIRMENTS IN SPATIAL WORKING MEMORY IN A NOVEL MOUSE MODEL OF
HIRANO BODY EXPRESSION¹

¹ Clark JK, Ferguson M, Crystal JD, Wagner JJ, Fechtmeier M, Furukawa R. *Hirano body expression impairs spatial working memory in a novel mouse model*. Acta Neuropathologica Communications. 2014 Sep 2;2(1):131.
Reprinted here with permission.

Abstract

Hirano bodies are actin-rich intracellular inclusions found in the brains of patients with neurodegenerative conditions such as Alzheimer's disease or frontotemporal lobar degeneration-tau. While Hirano body ultrastructure and protein composition have been well studied, little is known about the physiological impact of Hirano bodies due to the lack of an animal model system. Utilizing a Lox/Cre system, we have generated a new mouse model, which develops an age-dependent increase in the number of Hirano bodies present in both the CA1 region of the hippocampus and frontal cortex. These mice develop normally and experience no overt neuronal loss. Mice containing Hirano bodies have no abnormal anxiety or locomotor activity as measured in an open field arena. Mice with Hirano bodies do however, develop age-dependent spatial working memory impairments. Despite this cognitive impairment, basal synaptic responses, paired-pulse facilitation, and long-term potentiation measurements in the CA1 region of ventral hippocampus were not different compared to control mice. In addition, an inflammatory response can be detected at 8 months of age as measured by presence of reactive astrocytes. These findings suggests that Hirano bodies may contribute to disease progression. This new model mouse provides a tool to now investigate how Hirano bodies interact with other pathologies associated with Alzheimer's disease. Hirano bodies likely play a complex and region specific role in the brain during neurodegenerative disease progression.

5.1 Introduction

Neurodegenerative diseases are characterized by the progressive loss of neural structure or function, which can result in cognitive decline, motor impairments, and changes in behavior [1]. Two of the most prevalent neurodegenerative conditions affecting cognition are Alzheimer's disease (AD) and Frontotemporal lobar degeneration (FTLD) [2, 3]. Both of these diseases are characterized pathologically by the deposition of protein aggregates [1]. While the brains of AD patients develop extracellular β -Amyloid plaques and intracellular neurofibrillary Tau tangles (NFT), FTLD patients develop only NFTs without any overt Amyloid pathology [4, 5]. In addition, patients with AD, FTLD, and other neurodegenerative diseases, may also develop a secondary pathology known as Hirano bodies [6-10].

Hirano bodies are intracellular, eosinophilic rod-shaped inclusions that may be found in the soma and axons of CNS (brain and spinal cord) neurons and glia in a variety of conditions including Alzheimer's disease, FTLD, Amyotrophic Lateral Sclerosis, Creutzfeldt–Jakob disease, and occasionally in normal individuals of advanced age [6-12]. Hirano bodies are paracrystalline structures primarily composed of filamentous actin (F-actin) and actin-associated proteins [7, 13], and are differentiated from other types of actin inclusions based on their ultrastructure [14]. They have a distinct orientation and spacing of F-actin, the appearance of which changes based on the plane of section. These filaments are approximately 6-10 nm wide with 10-12 nm spacing between parallel filaments [7, 15, 16]. In addition to actin-associated proteins, Amyloid Precursor Protein Intracellular Domain (AICD) and Tau are also present in Hirano bodies, implicating these structures in AD and FTLD [17-19].

Despite decades of research, very little is known about the impact of Hirano bodies on cellular physiology. Due to the lack of a vertebrate model system, research has been limited to studying Hirano body frequency, components, and structure in post-mortem tissue. However, an *in vitro* model system for studying Hirano bodies does exist in the slime mold *Dictyostelium discoideum* through expression of a 34 kDa actin-binding protein truncation mutant that results in the production of the carboxy-terminal (CT) protein fragment [20, 21]. Expression of the CT peptide does not affect total actin levels, but does cause a redistribution in the ratio of globular-actin to F-actin, and the formation of rod shaped, actin-rich, intracellular inclusions [21]. These structures slow the growth and development of *Dictyostelium*, but only moderately, and are not detrimental to cell survival [21]. Ultrastructural analysis of these CT induced actin-rich deposits reveal highly ordered F-actin filaments identical to those found in Hirano bodies from human tissue [21]. Formation of model Hirano bodies through expression of CT has also been successful in mammalian cell lines, including primary neurons, and model Hirano bodies formed in mammalian cells contain many of the same protein components as authentic Hirano bodies found in humans, including the same hallmark ultrastructure and filament spacing [22-24].

The physiological impact of model Hirano bodies has been investigated, although studies are very limited. Hirano bodies found in both humans and model systems are often seen enclosed in membranes thought to be derived from autophagosomes [12, 22]. Consistent with this hypothesis, model Hirano bodies are degraded through both autophagy and proteasome pathways that have been assessed through the use of pharmacology, and an autophagy mutant of *Dictyostelium* [25]. The influence of model

Hirano bodies on AICD and Tau biology has been investigated in cell culture studies since these proteins colocalize with both human and model Hirano bodies [19, 22-24]. AICD has been shown to play a role in transcription [26, 27], but the presence of model Hirano bodies drastically reduces AICD nuclear localization [23]. This resulted in a decrease in AICD-induced transcription, and surprisingly, a reduction in AICD- and Tau-induced cell death [23, 24]. These results imply Hirano bodies may serve as a sink for aberrant production that may result in the inadvertent protection of cellular integrity.

While cell culture models may provide some useful insight into the physiological impact of Hirano bodies at a cellular level, an animal model is required to study the physiological impact at a systems level in complex disease states. Recently, we have created a mouse model with brain specific expression of CT by crossing a CT-GFP transgenic mouse (R26CT) with a Thy1.2-CRE mouse [28]. These mice develop rod-shaped eosinophilic inclusions in the CA3 region of the hippocampus that are identical in ultrastructure to authentic Hirano bodies [28]. The formation of Hirano bodies in CA3 did not induce neuron loss, but did result in electrophysiology measurements that were different from control mice for both short-term and long-term synaptic plasticity at CA3→CA1 synapses. Behavioral studies such as locomotor and cognitive tasks however, were not evaluated. Furthermore, Hirano bodies in human disease are found predominately in the hippocampal CA1 region, not CA3, as observed in our previous mouse model [12, 16, 28]. In order to generate Hirano bodies with increased expression in the hippocampal CA1 region, R26CT mice were crossed with a CaMKIIa-CRE mouse, which directs CRE expression predominately to hippocampal CA1 and forebrain [29, 30]. In our current study, this new mouse model is characterized using

histopathological (H&E, IHC, TEM), behavioral (spatial working memory using an 8-arm radial maze), and neurophysiological (extracellular recording from *ex vivo* slices in the CA1 region of ventral hippocampus) methods to evaluate the impact of Hirano bodies on cognitive and neurophysiological processes.

5.2 Methods

5.2.1 Animals and euthanasia

All mice used in this study were generated by crossing male transgenic mice homozygous for a mutation producing a truncated carboxy-terminal fragment of an actin binding protein tagged with a green fluorescent protein (CT-GFP) targeted to the *Rosa26* locus (*C57Bl/6-Gt(ROSA)26Sor^{tm1(CT-GFP)UGA}*) (R26CT) [28] with CaMKIIa-CRE female mice (*B6.Cg-Tg(Camk2a-cre)T29-1Stl/J*, Jax ID: 005359) [29] to produce offspring that express the CT-GFP peptide (R26CT-CRE), and others that do not (R26CT), and serve as control mice. All R26CT-CRE mice used in this study were homozygous for the CT-GFP transgene. All R26CT and R26CT-CRE mice used in behavioral and neurophysiological experiments were male. Mice were housed individually in an AAALAC accredited facility on a 12 hour light/dark timed schedule and had ad libitum access to food (except during behavioral studies) and water during this study. Mice began testing in the radial arm maze at approximately 2.5 and 7.5 months of age. After completion of maze testing, 5 days elapsed before testing in the open field arena. After completion of open field testing, 5 days elapsed before electrophysiological studies commenced to reduce any potential temporary enrichment from exposure to the maze or open field environment. Euthanasia of mice occurred under deep anesthesia

with halothane followed by decapitation. The University of Georgia Institutional Animal Care and Use Committee approved all animal protocols and experiments.

5.2.2 Chemicals and reagents

Except where noted, specialty chemicals and antibodies were obtained from Sigma Aldrich (St. Louis, MO).

5.2.3 Genotyping

PCR was utilized to genotype mice for the presence of the R26CT transgene with the primers: P1 5' -TTGGAGGCAGGAAGCACTTG -3' ; P2 5' –CATCAAGGAAACCC TGGACTACTG- 3' ; and P3 5' –CCGACAAAACCGAAAATCTGTG-3' using genomic DNA obtained from tail snip biopsies as a template. Amplification using P1 and P2 yields a 230 bp product from the R26CT allele and P1 and P3 yields a 369 bp product from the wild type Rosa26 allele. To detect the presence of the Cre transgene, the primers were: 5' -CCAGGCCTTTTCTGAGCATACC- 3' and 5' –CAACACCATTTTTT CTGACCCG-3', producing a product of 641 bp.

5.2.4 Brain sectioning and histology

For cryosections utilized in immunofluorescence, dissected whole brains were fixed with 4% paraformaldehyde in phosphate buffered saline (PBS, pH 7.4) overnight, followed by cryoprotection in 30% sucrose, embedding in OCT (Optical Cutting Temperature, Tissue-Tek 4583), and storage in liquid nitrogen. Sagittal sections 8 µm thick were cut from frozen tissue using a cryostat (Leica CM3050 S, Richmond, IL) and electrostatically attached to Superfrost Plus glass slides (Fisher Scientific, Pittsburgh, PA). For paraffin sections, dissected brains were fixed with 4% paraformaldehyde in PBS, pH 7.4, at 4° C overnight, dehydrated in a graded series of 50, 75, 90, 96 and

100% ethanol, equilibrated with xylene, embedded in paraffin, and sectioned on a sliding microtome (Leica RM2155, Richmond, IL) at a thickness of 5-10 μm and mounted on slides. Staining was performed as follows: after dewaxing with xylene, sections were stained with Gill's No. 2 hematoxylin and counterstained with eosin (H&E) solution (Sigma-Aldrich Chemical Co., St. Louis, MO).

5.2.5 Immunohistochemistry

Mounted paraffin sections were dewaxed in xylene and rehydrated in graded ethanol solutions prior to antigen retrieval in boiling 50 mM sodium citrate plus 0.01% Tween20 for 25 minutes. Endogenous peroxidase activity was inhibited by incubating sections in 3% hydrogen peroxide for 10 minutes prior to washing with PBS and blocking with 10 mg/ml bovine serum albumin (BSA) in PBS overnight. Slices were incubated in mouse anti-GFAP (1/1000) (Sigma-Aldrich Chemical Co., St. Louis, MO) or mouse anti-ED1 (1/400) (Abcam, Cambridge, MA) primary antibodies. Secondary biotinylated goat anti-mouse and goat anti-rabbit antibodies were used at 1/450 dilution. Slices were incubated with streptavidin-HRP polymer complex (1/1000) (Vector Laboratory, Burlingame, CA). Slices were washed 3 times for 5 minutes each between antibody and enzyme incubations with TBST (10 mM Tris-HCl, pH 7.4; 150 mM NaCl; 0.1% Tween20). Diaminobenzidine (DAB) enhanced substrate system was used according to the manufacturer's instructions (Vector Laboratory, Burlingame, CA). After washing off excess DAB substrate, slides were counterstained with Gill's No. 2 Hematoxylin (Sigma-Aldrich Chemical Co., St. Louis, MO) prior to mounting. Sections were viewed with a Leica DM6000 B microscope (Wetzlar, Germany) with Hamamatsu ORCA-ER digital camera (Hamamatsu, Bridgewater, NJ).

5.2.6 Immunofluorescence

Cryosections were blocked for 1 hour in 2% BSA in TBST and incubated in primary antibody at room temperature overnight. The sections were washed x3 times in 4% milk in TBST for 5 minutes each, followed by 1 hour incubation with rabbit anti-GFP (1/500) (Sigma-Aldrich Chemical Co., St. Louis, MO), FITC labeled goat anti-rabbit secondary (1/1000) (Sigma-Aldrich Chemical Co., St. Louis, MO) and TRITC-phalloidin conjugated (1/40) (Sigma-Aldrich Chemical Co., St. Louis, MO), and 264 μ M Hoechst 33258 with appropriate washes in between. Slides were visualized with a Zeiss Axioobserver Z1 equipped with an AxioCam MRm controlled by AxioVision4.6 software.

5.2.7 Transmission electron microscopy

TEM was performed as previously described with slight modification [31]. Whole mouse brains were dissected to isolate the hippocampus. Hippocampal tissue blocks were fixed by immersion with 4% paraformaldehyde and 2% glutaraldehyde in 0.1 M cacodylate buffer, pH 7.4 overnight, and post-fixed in 1% osmium tetroxide for 2 hours. After serial dehydration in ethanol solutions, tissues were embedded in Epon (Embed-812; Electron Microscope Science, Hatfield, PA). Semithin sections were stained with 1% toluidine blue in 1% sodium tetraborate. Ultrathin sections were collected on nickel grids, counterstained with uranyl acetate for 30 minutes, and followed by lead citrate for 5 minutes at room temperature. Samples were observed with a JEOL 100CX with an accelerating voltage of 80 kV.

5.2.8 Western blot

Brain samples were dissected from mice and flash frozen in liquid nitrogen and stored at -80°C until processed. Tissues were homogenized in a Potter-Elvehjem

homogenizer containing 4 brain volumes of Tris buffered saline (25 mM Tris-HCl pH 7.4, 140 mM NaCl, 3 mM KCl, 5 mM EDTA, and 2 mM 1,10-phenanthroline) with 10 μ L protease inhibitor cocktail (5 mM EGTA, 1 mM DTT, 100 mM leupeptin, 10 mM pepstatin, 0.1 M PMSF, 0.1 M benzamidine, and 0.5 M ϵ -aminocaproic acid). Cell debris was separated from total homogenate by centrifugation at 13,000g for 15 minutes at 4°C. Supernatant was stored at -80°C until used. Protein concentrations of the supernatants were determined by bicinchoninic acid assay using BSA as a standard [32]. For western blot analysis, tissue samples were loaded at equal total protein, separated by SDS-PAGE, and transferred to nitrocellulose membranes. Blots were blocked in 5% nonfat dry milk in TBST and probed using either mouse anti-GFAP (1/2000) (Sigma-Aldrich Chemical Co., St. Louis, MO), rabbit anti-GFP (1/5000) (Sigma-Aldrich Chemical Co., St. Louis, MO), mouse anti-ED1 (1/5000) (Abcam, Cambridge, MA), mouse anti-synaptophysin (1/2000) (AbD Serotec, Raleigh, NC), or mouse anti-alpha tubulin (1/8000) (Millipore, Billerica, MA). After 3 washes with TBST, blots were incubated with either goat anti-mouse or goat anti-rabbit HRP conjugated secondary antibodies (1/10000) (Pierce-lab, Rockford, IL) and detected by chemiluminescence using SuperSignal Western Dura Extended Duration Substrate (Thermo Scientific, Rockford IL). Images were captured utilizing ChemiDoc™ MP system and Image Lab™ software (Bio-Rad Laboratories, Hercules, CA).

5.2.9 Open field arena

Behavioral activity was measured in the open field arena, which consisted of a square chamber (43 x 43 cm) with clear plastic walls (30.5 cm high) and a removable smooth metal floor (Med Associates, St. Albans, VT, USA). The chambers are

individually housed in sound attenuating cubicles with house lighting (20 lx) positioned in 2 of the 4 corners, and a ventilation fan which also provided ambient background noise. Two banks, each containing 16 infrared photobeams, are mounted at right angles to each other, with paired photodetectors mounted opposite each bank, creating a 16 x 16 photobeam grid 2 cm from the floor. Activity Monitor software counts photobeam breaks to determine both ambulatory (sequential) and stereotypic (repetitive; movement without displacement) movements based on patterning of beam breaks. Five days after completion of radial arm maze testing, mice were placed in the center of the open field arena and allowed to roam freely for 60 minutes to assess general locomotor activity. Both ambulatory and stereotypic counts were combined into total horizontal counts, and summed into 10 minute blocks. For center zone analysis, a defined square area of 26.3 x 26.3 cm (37.5% of total area) in the center of the chamber was designated as the center zone to count crossings into this area during the first 30 minutes of activity. All animals were subjected to a single 60 minute session in the midafternoon during the midpoint of their circadian light cycle.

5.2.10 Radial arm maze apparatus and animal preparation

Learning and memory assessments were conducted using an 8-arm radial maze (Med Associates, St. Albans, VT) as described previously for rats [33]. This maze consists of a central chamber with 8 equally spaced arms extending outward. The central chamber is equipped with motorized guillotine doors positioned at the interface of the central chamber and arms. Each arm has two sets of photosensors to track movement of the animals into and out of the arms. At the distal end of each arm is a food trough with a 20 mm food dispenser activated by a photosensor to detect mouse

head entries. The sides and top of each arm are composed of clear plastic to allow mice to use external visual cues to spatially navigate the maze. A computer in an adjacent room controls the maze events and data collection. Photosensor, food, and door data were collected using MED-PC software 4.0 (Med Associates, St. Albans, VT) with a resolution of 10 ms. A video camera was mounted above the maze to visualize the mice during the procedure.

Behavioral assessments in the radial arm maze were measured at either 3 or 8 months of age. Thirteen days prior to the start of behavioral testing, mice were individually housed and a 3 day average of individual animal body weight was determined. Mice were diet restricted to reduce and maintain a body weight of approximately 87.0% of their free fed body weight for the duration of the behavioral testing. Mice were behaviorally shaped to associate a single head entry with obtaining a single sucrose-flavored food reward (Bio-Serve F0071, Frenchtown, NJ) by allowing each animal free access to 4 of the 8 arms until a single food reward from each arm was retrieved. Behavioral shaping was carried out once a day for 4 consecutive days prior to testing.

The maze was cleaned between subjects with 1/1250 diluted Coverage Plus NPD disinfectant (Steris Life Sciences, Mentor, OH) to prevent a previous mouse's scent from interfering with a subsequent mouse's performance. To further prevent a mouse from using scent cues, the entire maze was scent saturated using cotton bedding from the mouse's home cage after cleaning the maze.

5.2.11 Radial arm maze testing to assess spatial short-term working memory

Spatial short-term working memory was assessed using a standard 8-arm uninterrupted task. Each mouse was placed in the central chamber for a 2 minute acclimation period, after which all 8 doors simultaneously opened allowing free access to all arms for the duration of the testing session (8 arms open, 8 arms baited). Only a single food reward is delivered per baited arm, and a revisit to a previously visited food trough is considered an error in spatial short-term working memory. After collecting the last food reward, or after 15 minutes of elapsed time, the session ends and the doors close. For this task, the dependent variable is the total number of errors. Comparisons are results obtained from the first 3 days and last 3 days of testing. The experiments are performed once a day, at the same time of day for 10 consecutive days. All mice achieved the criterion of no more than 2 errors within the first 10 choices for 3 consecutive days by the 10th day of testing and were continued in the study. Following 10 consecutive days of spatial short-term memory testing, animals proceeded directly to the spatial long-term working memory task containing a retention interval delay.

5.2.12 Radial arm maze testing to assess spatial long-term working memory

On the following day after completion of spatial short-term working memory testing, spatial long-term working memory was tested using a modified delayed spatial win-shift assay. This is a 2-phase procedure similar to a standard 8-arm task with an interposed delay. This test consisted of a study phase and test phase, conducted in the same day for 10 consecutive days. For the initial study phase, the mouse was placed in the central chamber of the maze for a 2 minute acclimation period. After acclimation, only 4 of the 8 doors simultaneously opened, allowing free access to all open arms for

the duration of the testing session (4 arms open, 4 arms baited). The 4 arm sequence during this phase was randomly chosen for each mouse on each day. Only a single food reward is delivered per baited arm, and a revisit to a previously visited food trough is considered an error in spatial short-term working memory. After collecting the last food reward, or after 15 minutes of elapsed time, the session ends and the doors close. The mouse was then subjected to a retention interval by returning to the home cage for 2 minutes while the maze is cleaned of any urine or feces that could potentially serve as visitation cues. The mouse was then returned to the central chamber to begin the subsequent test phase. After a 1 minute acclimation period (4 minute total interval), all 8 doors simultaneously opened allowing free access to all open arms for the duration of the testing session. Only arms that were previously closed during the study phase were baited during the test phase (8 arms open, 4 arms baited). Each animal must collect the food reward available at the end of each of the 4 newly baited arms. Only a single food reward is delivered per baited arm, and a visit to a previously baited food trough from the study phase was considered an error in spatial long-term working memory (maximum of 4 errors), and a revisit to any food trough during the test phase (whether baited in the training or test phase), was considered an error in spatial short-term working memory. Both short-term and long-term working memory errors were combined into a total working memory error variable that we report herein as working memory errors. After collecting the last food reward, or after 15 minutes of elapsed time, the session ends and the doors close. In the test phase, the dependent variable is the total number of errors. Comparisons are results obtained from the first 3 days and last 3 days of testing.

5.2.13 Extracellular field recording

Hippocampal slices were prepared from behaviorally tested 3 and 8 month old R26CT and R26CT-CRE mice 10-17 days after completion of radial arm maze testing. Mice were deeply anesthetized with halothane prior to decapitation. The brain was removed and submerged in ice-cold, oxygenated (95% O₂ / 5% CO₂) dissection artificial cerebrospinal fluid (ACSF) containing: 120 mM NaCl, 3 mM KCl, 4 mM MgCl₂, 1 mM NaH₂PO₄, 26 mM NaHCO₃, and 10 mM glucose. The brain was sectioned using a vibratome through the horizontal plane into 400 μm thick slices. The hippocampus was then dissected free from slices obtained between the levels of Bregma -4.0 mm to Bregma -2.4 mm. We estimate such slices were from the ventral 35-40% of the hippocampus with respect to the longitudinal axis. We also excluded slices from the extreme 10% of the ventral pole, where it is difficult to clearly distinguish the CA1 pyramidal region from the CA2/3 and subicular regions. Slices were placed in a submersion recording chamber and perfused at approximately 1 ml/min with oxygenated (95% O₂ / 5% CO₂) standard ACSF containing: 120 mM NaCl, 3 mM KCl, 1.5 mM MgCl₂, 1 mM NaH₂PO₄, 2.5 mM CaCl₂, 26 mM NaHCO₃, and 10 mM glucose at room temperature. Slices recovered for 45 minutes at room temperature and an additional 45 minutes at 30°C. A bipolar stimulating electrode (Kopf Instruments, Tujunga, CA) was placed within the stratum radiatum of CA1 and an extracellular recording microelectrode (1.0 MΩ tungsten recording microelectrode, World Precision Instruments, Sarasota, FL) was positioned in the same layer of CA1. Field Excitatory Post-Synaptic Potentials (fEPSPs) were recorded at Schaffer collateral→CA1 synapses using a stimulus pulse consisting of a single square wave of 270 μs duration. Data

were digitized at 10 kHz, low-pass filtered at 1 kHz, and analyzed with pCLAMP 10.2 software (Axon Instruments, Sunnyvale, CA). The initial slope of the population fEPSP was measured by fitting a straight line to a 1 ms window immediately following the fiber volley.

Stimulus response curves were obtained at the beginning of each experiment with stimulus pulses delivered at 30, 40, 50, 60, 75, 90, 110, 130, 150, and 170 μ A once every 60 s (0.0167 Hz). For baseline recording, the stimulation intensity was adjusted to obtain a fEPSP of approximately 35-40% of the maximum response. Paired-pulse stimulations were performed at intervals of 50, 100, 200, and 500 ms. Five pairs of pulses were performed and averaged together for each interval. The initial slope of the averaged second pulse was divided by the initial slope of the averaged first pulse to obtain the paired-pulse ratio for each slice. Synaptic responses for Long-Term Potentiation (LTP) experiments were normalized by dividing all fEPSP slope values by the average of the five responses recorded during the 5 minutes immediately prior to high frequency stimulation (HFS). LTP values for the 1, 2, and 3 hour time points were determined by averaging 5 minutes of normalized slope values immediately prior to the 60 minute, 120 minute, and 180 minute time points post-HFS, respectively. The HFS protocol used to induce LTP in all experiments consisted of 3 episodes of 100 Hz/1 s stimulus trains (100 pulses x3) administered at 20 s inter-train intervals. Reported n-values (x(y)) indicate the number of slices (x) and the number of animals (y) assessed.

5.2.14 Statistics

Tests of significance were performed using either ANOVA, or paired and independent t-tests as appropriate.

5.3 Results

5.3.1 Histopathology

Mice expressing CT-GFP in the hippocampus and frontal cortex were generated by crossing R26CT mice with CaMKIIa-CRE mic. To verify that CT-GFP expression, immunofluorescence was performed on cryosections of 1 month old R26CT and R26CT-CRE mice using anti-GFP antibodies (Figure 5.1). The presence of CT-GFP was also verified by western blot analysis using tissue from hippocampus and frontal cortex of R26CT and R26CT-CRE mice (Figure 5.1).

To determine if expression of CT-GFP resulted in the production of Hirano bodies, H&E staining was performed on paraffin sections of brains from 3 and 8 month old R26CT and R26CT-CRE mice. No eosinophilic inclusions were seen in 3 month old R26CT mice in either the cortex or the hippocampus (Figure 5.2). At low frequency, 3 month R26CT-CRE mice exhibited eosinophilic inclusions in the hippocampus, but not in the cortex (Figure 5.2). In 8 month old R26CT-CRE mice, eosinophilic inclusions appear predominately in the CA1 of the hippocampus and are found rarely in the cortex (Figure 5.3). To verify that the eosinophilic inclusions found in the brains of R26CT-CRE animals have the same ultrastructure as Hirano bodies found in human brains, hippocampal samples from 8 month old mice were processed and viewed using transmission electron microscopy. R26CT-CRE mice show electron dense inclusions with 10-12 nm spacing similar to human Hirano bodies (Figure 5.4). Structures with the characteristic features of Hirano bodies were not observed in R26CT mice.

Since inflammation is a common observation in neurodegenerative diseases, we wanted to determine if the presence of model Hirano bodies induces an inflammatory

response in the brains of 3 and 8 month old R26CT and R26CT-CRE mice. Paraffin embedded brain sections were stained with antibodies against known markers of reactive astrocytes (GFAP) and activated microglia (ED1) using DAB to visualize the product (Figure 5.5 and Figure 5.6). During inflammation the levels of GFAP are significantly higher in reactive astrocytes [34]. Therefore, GFAP antibodies were titrated to label only reactive astrocytes using a well-established 5xFAD model of Alzheimer's disease known to have inflammation (data not shown) [35]. At 3 months of age, neither R26CT nor R26CT-CRE mice show GFAP or ED1 staining in either hippocampus or frontal cortex showing that neither reactive astrocytes nor activated microglia are present (Figure 5.5). ED1 staining of 8 month old R26CT and R26CT-CRE brain sections revealed no activated microglia in either hippocampus or cortex (Figure 5.6). Further, 8 month old R26CT mice show no GFAP staining in either hippocampus or cortex. At 8 months however, R26CT-CRE mice have GFAP staining in the hippocampus but not cortex, indicating that the presence of model Hirano bodies induces inflammation at a later age (Figure 5.6). To verify these results, western blot analysis was performed using brain homogenate from 3 and 8 month old R26CT and R26CT-CRE mice (Figure 5.7). At 3 months of age, neither ED1 nor GFAP levels were significantly different between R26CT and R26CT-CRE mice (Figure 5.7A & B). At 8 months of age, ED1 levels were not different between R26CT and R26CT-CRE mice, but contrastingly, GFAP levels were approximately 4 fold higher in R26CT-CRE mice compared to R26CT mice (Figure 5.7C & D). These results are consistent with the immunohistochemistry results indicating that older R26CT-CRE mice have inflammation in the hippocampus as indicated by positive GFAP staining in reactive astrocytes.

5.3.2 Behavioral assessment

Changes in anxiety and cognition can be two clinical signs in patients suffering from neurodegenerative conditions with Hirano bodies [36]. To examine the behavior of R26CT and R26CT-CRE mice, we used an open field arena and an 8-arm radial maze to evaluate anxiety and cognition respectively. The open field test showed no difference in locomotor activity between R26CT (3 month, n=11; 8 month, n=11) and R26CT-CRE (3 month, n=12; 8 month, n=12) mice at either age (Figure 5.8A & B). R26CT and R26CT-CRE mice also made a similar number of entrances to the center zone, suggesting no differences in the general psychological state or anxiety at either age (Figure 5.8C).

For cognitive assessments, spatial memory was tested in an 8-arm radial maze utilizing two different protocols. The first tested spatial short-term working memory utilizing an 8-arm uninterrupted task as shown in the top schematic diagram of Figure 5.9, and the second tested spatial long-term working memory utilizing a delayed spatial win-shift task as shown in the middle schematic diagram of Figure 5.9. In the 8-arm uninterrupted task (8 arms open, 8 arms baited), R26CT (3 month, n=11; 8 month, n=11) and R26CT-CRE mice (3 month, n=12; 8 month, n=12) performed similarly, as both groups showed significant improvement in performance across sessions from day 1 to day 10 at both 3 and 8 months of age (Figure 5.9A & B). These observations were confirmed by subjecting data from the 8-arm uninterrupted task (Figure 5.9A & B) to a 2 genotype (R26CT versus R26CT-CRE) x 2 training levels (first 3 versus last 3 days) x 2 ages (3 versus 8 months) mixed ANOVA. The number of errors declined with

experience ($F(1,42)=56.94$, $p < 0.001$), none of the other variables or interactions were significant.

Beginning on day 11, the same mice from the 8-arm uninterrupted task were evaluated using a delayed spatial win-shift assay as shown in the middle schematic diagram of Figure 5.9. In the study phase (4 arms open, 4 arms baited), both 3 and 8 month old mice showed no difference between groups or improvement across sessions (data not shown). This was expected, as they had already displayed high performance for this type of task by the end the 8-arm uninterrupted task, and the study phase is a simplified version of this (4-arm uninterrupted task). Upon completion of the study phase, a 3 minute retention interval occurred before the subsequent test phase. In the test phase (8 arms open, 4 arms baited), 3 month old R26CT and R26CT-CRE mice showed improvement across sessions, but due to the high variability within the R26CT group, the improvement was not statistically significant, despite R26CT mice making less errors by the end of the 10 day testing period compared to the beginning (Figure 5.9C). At 8 months, R26CT mice showed significant improvement in performance across sessions, but in contrast, R26CT-CRE mice did not (Figure 5.9D). In addition, there was a statistically significant difference between R26CT and R26CT-CRE mice ($* p < 0.05$) by the end of the 10 day testing period (days 18-20) (Figure 5.9D). Data from the test phase (Figure 5.9C & D) were subjected to a 2 genotype (R26CT versus R26CT-CRE) x 2 training levels (first 3 versus last 3 days) x 2 ages (3 versus 8 months) mixed ANOVA. There was a significant effect of training ($F(1,42)=28.03$, $p < 0.001$), and a significant interaction of training x genotype x age ($F(1,42)=8.61$, $p < 0.01$). None of the other variables or interactions were significantly different. Next, we conducted

training x genotype ANOVAs separately for ages 3 and 8 months. At both ages, there was a significant effect of training (3 months, $F(1,21)=17.05$, $p < 0.001$; 8 months, $(F(1,21)=11.25$, $p < 0.01)$). However, the interaction of training x genotype was significant at 8 months ($F(1,21)=14.37$, $p < 0.05$) but not at 3 months ($F(1,21)=2.16$, $p = 0.16$). None of the other variables were significant. These results indicate that R26CT-CRE mice develop an impairment in spatial working memory by 8 months of age. Moreover, the 8 month old R26CT-CRE mice showed an impairment at the end of training that was absent in the 3 month old mice. Importantly, the impairment was selective to the test phase of our cognitive tasks, which isolates the impairment as driven by the memory load imposed by the retention interval. The absence of an impairment in the 8-arm uninterrupted task rules out nonspecific impairments (such as motivational or locomotor factors) and highlights the impairment as memory driven.

5.3.3 Neurophysiological assessment

Several neurodegenerative conditions are characterized by synaptic loss or reduction in synaptic density that correlate with cognitive impairment [37-40]. Since 8 month old R26CT-CRE mice show cognitive impairments in spatial working memory, levels of synaptophysin were measured as a qualitative indicator of synaptic density [35]. Synaptophysin levels were approximately equal between R26CT and R26CT-CRE mice at both 3 and 8 months of age, suggesting spatial working memory impairments in R26CT-CRE mice are not due to decreases in synaptic density (Figure 5.7).

In order to determine whether the presence of Hirano bodies impact synaptic function, fEPSPs were recorded at CA3→CA1 synapses in the stratum radiatum layer of ventral hippocampus. Stimulus response curves to test the functional range of

synaptic activity were generated at both 3 and 8 months. There was no difference in synaptic response between R26CT (3 month, n=10(19); 8 month, n=10(20)) and R26CT-CRE (3 month, n=12(18); 8 month n=12(19)) mice at any stimulus intensity tested at either age (Figure 5.10). Next, short-term synaptic plasticity was evaluated using paired-pulse stimulus protocols to determine the paired-pulse ratio. Both R26CT (3 month, n=10(19); 8 month, n=10(20)) and R26CT-CRE (3 month, n=12(18); 8 month, n=12(21)) mice exhibited paired-pulse facilitation at 50, 100, and 200 ms intervals at both 3 and 8 months, but there was no difference in the amount of facilitation between genotypes at either age, or at any stimulus interval tested (Figure 5.11). These results indicate that impairments in spatial working memory in 8 month R26CT-CRE mice are likely not attributed to synaptic density or short-term plasticity in the ventral hippocampal CA1 region.

Lastly, Long-term synaptic plasticity was evaluated by inducing Long-Term Potentiation (LTP) using a high frequency stimulus induction protocol (100 pulses x3). Following the induction of LTP, fEPSPs were recorded for 3 hours post-induction to measure early (< 3 hr) and late (> 3 hr) phases of LTP. At both 3 and 8 months of age, fEPSP slope values were not significantly different between R26CT (3 month, n=10(17); 8 month, n=9(18)) and R26CT-CRE (3 month, n=11(16); 8 month, n=11(18)) mice at 60, 120, or 180 minutes post-induction (Figure 5.12). Taken together, these results suggest that the expression of CT-GFP, and subsequent formation of Hirano bodies, have no impact on synaptic density, baseline synaptic responses, or synaptic plasticity in the CA1 region of ventral hippocampus, as late as 8 months of age.

5.4 Discussion

A new transgenic mouse model was created to study the impact of Hirano bodies on cognition and neurophysiology *in vivo*. A mouse model forming Hirano bodies had been previously studied by crossing homozygous R26CT mice with a Thy1.2-CRE mouse (R26CT x Thy1.2-CRE) [28]. These animals produced Hirano bodies in the hippocampus as well, but were predominately reported in the CA3 region. This is not surprising since the Thy1.2-CRE mouse has been shown to have higher expression of the CRE transgene in the CA3 region rather than CA1 [28]. In this study, R26CT mice were crossed with a CaMKIIa-CRE mouse (R26CT x CaMKIIa-CRE) because the CaMKIIa-CRE mouse is known to express CRE predominantly in the forebrain and CA1 region of the hippocampus [29, 30, 41]. This CRE driver was chosen in an attempt to more closely recapitulate human disease conditions in which Hirano bodies are normally found in the pyramidal cell layer of the CA1 region [6, 15, 16, 42, 43]. In our current study, R26CT-CRE mice expressed eosinophilic inclusions predominately in the CA1 region, instead of CA3. In contrast with the previously study, in which Hirano bodies were not detected by light microscopy until 6 months of age [28], our current study shows eosinophilic inclusions in the hippocampus of R26CT-CRE mice as early as 3 months, but not before. It is unclear why eosinophilic inclusions are detected earlier in R26CT mice crossed with CaMKIIa-CRE than in R26CT mice crossed with Thy1.2-CRE. Perhaps CA1 pyramidal neurons have a greater propensity to facilitate CT-induced Hirano body formation, or CaMKIIa has activity dependent expression, while Thy1.2 shows a ubiquitous basal level of expression. The CT-GFP construct is under control of the *Rosa26* promoter, which shows a basal level of expression, and

very well may be the limiting factor. If this were true, differences in expression levels of Cre wouldn't matter. Differences in Cre expression levels between CaMKIIa-CRE mice used in our current study, and Thy1.2-CRE mice used in our previous study were not compared. In human disease, Hirano body appearance is not observed in young patients below 11 years of age, and once present, increase with age and disease severity [15, 44, 45]. Consistent with these findings, an age-dependent increase in the formation of Hirano bodies was also observed in our mouse model.

There are several characterized actin inclusions found in human disease other than Hirano bodies such as ADF/cofilin rods (AC rods) and hyaline bodies [46-48]. Hirano bodies are differentiated from these other actin aggregates by their eosinophilic nature, ability to interact with phalloidin, and distinct ultrastructure [8, 44, 47, 49]. To definitively prove an actin inclusion is a Hirano body, electron microscopy must be performed for Ultrastructural analysis. In humans, they often appear as fingerprint or spheroid/spindle shaped [8]. Hirano bodies in R26CT-CRE mice also display these alternative patterns (Figure 5.4A & B). In humans, smaller Hirano bodies not visible through light microscopy are more frequent than larger Hirano bodies as assessed by electron microscopy [16]. These smaller Hirano bodies are noted as appearing less compact and more irregular than those visible through light microscopy [16]. R26CT-CRE mice also show smaller structures not visible by light microscopy, which contain both ordered filaments and amorphous electron dense material (Figure 5.4D). In *Dictyostelium*, small nascent model Hirano body structures observed by TEM fuse together by an unknown process involving microtubules and myosin II to form larger Hirano bodies [21, 50, 51]. Expression of CT in cell culture systems often results in

alternative fibrillar structures or small aggregates [22, 25]. These smaller structures have also been noted in the brains of humans [52] and in the brains of R26CT-CRE mice (Figure 5.4C). It is likely that a similar formation process of Hirano bodies is occurring in R26CT-CRE mouse brains since several small aggregates can be seen in close proximity in TEM samples (Figure 5.4C).

Inflammation is a phenomenon occurring in neurodegenerative conditions such as AD, and is characterized by activated microglia and reactive astrocytes [34]. Many mouse models of neurodegenerative disease recapitulate reactive microglia or reactive astrocytes as a predominant phenotype [35, 53-55]. Markers of reactive astrocytes or activated microglia were measured in order to determine if Hirano bodies accompany an innate immune response in the brain. Our study showed 3 month old R26CT-CRE mice had no signs of inflammation (Figure 5.5 and Figure 5.7). However, by 8 months of age R26CT-CRE mice had significantly higher levels of GFAP compared to aged matched R26CT mice (Figure 5.6 and Figure 5.7). There are several factors that can initiate astrogliosis, including cell damage, ischemia, neuronal hyperactivity, and foreign pathogens including abnormal protein aggregates [56]. In AD, reactive astrocytes are often found in close proximity to deposits of β -Amyloid plaques, and neurons containing intracellular NFTs [35, 57-61]. Reactive astrocytes have been reported to surround ghost tangles (extracellular NFTs) where they are thought to be clearing these structures from the brain [62, 63]. Hirano bodies have also been reported to be extruded from neurons, and model Hirano bodies can be cleared from cells through exocytosis [15, 25]. It is possible that extruded Hirano bodies or intermediate aggregates may initiate an astrocytosis response in the brain. While 3 month old

R26CT-CRE mice have sparse Hirano bodies, they are more abundant in 8 month old mice, and release of Hirano bodies may explain why 8 month old R26CT-CRE mice exhibit reactive astrocytes.

The most important goal of this study was to assess the impact of Hirano bodies on neural physiology in the brain. To determine if CT-GFP expression and subsequent formation of Hirano bodies impacts certain areas of cognition, behavioral studies were performed using both the open field arena and the 8-arm radial maze. The open field arena can be used as a measure of general locomotor activity, which can be indicative of the general psychological state of the animal, and a measure of factors such as anxiety [64]. At 3 and 8 months of age, R26CT and R26CT-CRE mice show similar levels of locomotor activity (Figure 5.8A & B). General anxiety was also evaluated by recording the number of center zone entries between R26CT and R26CT-CRE mice (Figure 5.8C). No differences between groups at either age were found, implying that the presence of Hirano bodies do not contribute to anxiety or impair general locomotor function.

In our test of cognition, the 8-arm uninterrupted task demonstrated that both R26CT and R26CT-CRE mice have intact spatial learning and navigation since both groups learn the rules associated with completion of the radial maze task. In addition, both R26CT and R26CT-CRE mice appear to have equivalent perception of spatial cues, levels of motivation, and motor control. The 8-arm uninterrupted task is continuous, and thus the working memory load is low, making the procedure primarily dependent upon immediately accessible information from short-term working memory [65, 66]. The incorporation of a time delay however, forces retention of trial-unique

spatial information. To successfully complete phase 2, the mice must remember which arms were visited in phase 1, which increases working memory load. At 3 months of age, spatial working memory appears unimpaired since both R26CT and R26CT-CRE mice perform equally well and improve with training. At 8 months however, a discrimination in performance between R26CT and R26CT-CRE mice was apparent. The test phase results suggest that 8 month R26CT-CRE mice have impaired spatial working memory since the 8-arm uninterrupted task results indicated intact acquisition of maze rules, making this a working memory impairment, and not a learning impairment. Furthermore, the working memory deficiencies observed at 8 months coincide with the observed increase in frequency of Hirano bodies.

Spatial memory performance is known to depend upon intact hippocampal function [65, 67, 68]. In the current studies, electrophysiological recordings in ventral hippocampal slices were utilized to determine if synaptic function is altered in R26CT-CRE mice. Short-term synaptic plasticity measurements at 3 and 8 months of age showed that paired-pulse facilitation was unchanged in R26CT-CRE mice compared to R26CT mice (Figure 5.12). This data is in contrast with the previous characterization of the R26CT-CRE mouse with a Thy1.2 CRE driver, which showed a paired-pulse depression at a 50 ms stimulus interval [28]. This is likely due to differences in the expression pattern of CT-GFP. In our current study, CT-GFP expression and Hirano body formation were more predominant in the CA1 region of the hippocampus, versus the previous mouse model that showed expression and Hirano body formation predominately in the CA3 region [28-30]. In both our current and previous studies, our field potential experiments were performed by stimulating the Shaffer collaterals of CA3

axons, and measuring the synaptic response at CA3→CA1 synapses on dendrites of CA1 pyramidal neurons. In the previous study using the Thy1.2-CRE driver, Hirano bodies were formed in presynaptic CA3 neurons [28]. In our current study that uses the CaMKIIa-CRE mice, Hirano bodies were formed in postsynaptic CA1 pyramidal neurons. Paired-pulse stimulation is a measurement that reflects the active transport recovery of Ca²⁺ and trafficking of neurotransmitter vesicles to replenish the ready releasable pool of vesicles [69]. Since the trafficking of these neurotransmitter vesicles is also modulated by the actin cytoskeleton, the paired-pulse depression seen in the R26CT-CRE mice driven by the Thy1.2-CRE driver was explained as a change in vesicular trafficking due to the presence of the Hirano body sequestration of F-actin [70], but this would not be the case in our current study since CaMKIIa-CRE is predominately expressed in the postsynaptic neuron, and the formation of Hirano bodies is predominately observed in postsynaptic CA1 neurons. Thus, the difference in the effect of Hirano bodies on paired-pulse facilitation in the Thy1.2-CRE and CaMKIIa-CRE driver models is readily explained. Further, these results show clearly that the effect of model Hirano bodies in the brain depend significantly on the location in which they form.

In addition to evaluating short-term synaptic plasticity, a form of long-term synaptic plasticity, LTP, that has been shown to be involved in spatial learning and memory was also investigated [71, 72]. Long-term potentiation has an early and a late phase. The early phase relies on redistribution and rearrangement of available synaptic proteins while the latter involves gene expression and protein synthesis to maintain changes in synaptic strength [73]. Both the early and late phases of LTP are associated

with an increase in actin assembly [74-76], and in the late phase can result in structural changes such as increases in the number and size of dendritic spines, and expansion of the postsynaptic density [74, 75]. Model Hirano bodies are known to shift the globular-actin to F-actin ratio [21], increasing the proportion of cellular F-actin, and may consequently impact synaptic plasticity. Therefore, LTP was measured for 3 hours post-induction to determine if the presence of Hirano bodies impact early (< 3 hr) or late (> 3 hr) phase LTP. Interestingly, despite the important role of actin in LTP, we found no measurable difference between R26CT and R26CT-CRE mice in the induction, expression, and maintenance of LTP at either 3 or 8 months of age (Figure 5.12). These results are in contrast to those in the previous study, in which the R26CT-CRE mouse with the Thy1.2-CRE driver showed a deficit in the early, but not the late, phase of LTP [28]. Thus, presence of Hirano bodies in the CA1 region of ventral hippocampus for our current R26CT-CRE mouse with the CaMKIIa-CRE driver appears to be benign as assessed by our paired-pulse and LTP measurements.

Despite no apparent deficits in either short-term or long-term synaptic plasticity measurements, 8 month R26CT-CRE mice do show an impairment in spatial working memory in the 8-arm radial maze [77-79]. Both the hippocampus and prefrontal cortex work together in spatial working memory tasks, and this seeming discrepancy between hippocampal LTP and working memory performance could be due to prefrontal cortex impairments rather than hippocampal impairments [65, 80]. The CaMKIIa promoter that is used to drive Cre expression is activated in both the hippocampus and prefrontal cortex [29, 30], and we show that R26CT-CRE mice develop Hirano bodies in the prefrontal cortex in addition to the hippocampus at 8 months of age (Figure 5.3). Thus,

it is possible that our electrophysiological measurements in the CA1 of ventral hippocampus is either not sensitive enough to detect changes in synaptic physiology, or the hippocampus is resistant to the impact of Hirano bodies in R26CT-CRE mice under the CaMKIIa-CRE driver. In the future, it will be important to perform electrophysiological experiments in the prefrontal cortex as well as the hippocampus to evaluate the contribution of each brain region to working memory.

In conclusion, the physiological impact of Hirano bodies in the brain has remained elusive. The transgenic mouse generated in this study provides an animal model of Hirano body formation in the brain. Consistent with humans, this transgenic mouse develops Hirano bodies in the CA1 region of the hippocampus as well as in the frontal cortex. Behavioral analyses of Hirano body model mice indicate that Hirano bodies negatively impact spatial working memory. This study shows that Hirano body formation initiates an inflammatory response in the hippocampus and suggests that Hirano bodies may independently contribute to disease progression, or exacerbate the disease state. This model mouse serves a useful tool to investigate how Hirano bodies interact with other pathologies associated with neurodegenerative diseases such as AD.

Author contributions

All authors in this manuscript contributed to the design of the study, analysis, interpretation of data, and drafting of this manuscript. JKC and MFerguson carried out all experiments under the supervision of JJW, MFechheimer, or RF. JKC performed the electrophysiology, radial arm maze, and open field experiments. MFerguson performed the immunohistochemistry, western blot analysis, immunofluorescence,

electron microscopy, and radial arm maze experiments. JDC provided and designed the radial arm maze protocol and performed statistical analysis of the radial arm maze data.

Acknowledgements

Funding for this work was provided by NIH R01 N5046451 (www.ninds.nih.gov/) to R. Furukawa and M. Fechheimer. Disclosure statement: There are no conflicts of interest. We would like to thank Dr. Richard Meagher and Dr. Steve Hajduk for providing access to their microscopes. We would also like to thank the UGA College of Veterinary Medicine, Electron Microscopy Laboratory for their technical support and expertise with a special thanks to Mary Ard, lab coordinator. Finally, we would like to thank Dr. Jim Lauderdale and Dr. Nancy Manley for providing access to their cryostat and microtome. All animal protocols and experiments were approved by the University of Georgia Institutional Animal Care and Use Committee.

References

1. Ross, C.A. and M.A. Poirier, *Protein aggregation and neurodegenerative disease*. Nat Med, 2004. **10 Suppl**: p. S10-7.
2. Ratnavalli, E., et al., *The prevalence of frontotemporal dementia*. Neurology, 2002. **58**(11): p. 1615-21.
3. Alzheimer's, A., W. Thies, and L. Bleiler, *2011 Alzheimer's disease facts and figures*. Alzheimers Dement, 2011. **7**(2): p. 208-44.
4. Terry, R.D., *The Fine Structure of Neurofibrillary Tangles in Alzheimer's Disease*. J Neuropathol Exp Neurol, 1963. **22**: p. 629-42.
5. Lynch, T., et al., *Clinical characteristics of a family with chromosome 17-linked disinhibition-dementia-parkinsonism-amyotrophy complex*. Neurology, 1994. **44**(10): p. 1878-84.
6. Gibson, P.H. and B.E. Tomlinson, *Numbers of Hirano bodies in the hippocampus of normal and demented people with Alzheimer's disease*. J Neurol Sci, 1977. **33**(1-2): p. 199-206.
7. Hirano, A., et al., *The fine structure of some intraganglionic alterations. Neurofibrillary tangles, granulovacuolar bodies and "rod-like" structures as seen in Guam amyotrophic lateral sclerosis and parkinsonism-dementia complex*. J Neuropathol Exp Neurol, 1968. **27**(2): p. 167-82.
8. Schochet, S.S., Jr., P.W. Lampert, and R. Lindenberg, *Fine structure of the Pick and Hirano bodies in a case of Pick's disease*. Acta Neuropathol (Berl), 1968. **11**(4): p. 330-7.
9. Martinez-Saez, E., et al., *Hirano body - rich subtypes of Creutzfeldt-Jakob disease*. Neuropathol Appl Neurobiol, 2011.
10. Cartier, L., S. Galvez, and D.C. Gajdusek, *Familial clustering of the ataxic form of Creutzfeldt-Jakob disease with Hirano bodies*. J Neurol Neurosurg Psychiatry, 1985. **48**(3): p. 234-8.
11. Okamoto, K., S. Hirai, and A. Hirano, *Hirano bodies in myelinated fibers of hepatic encephalopathy*. Acta Neuropathol, 1982. **58**(4): p. 307-10.
12. Gibson, P.H., *Light and electron microscopic observations on the relationship between Hirano bodies, neuron and glial perikarya in the human hippocampus*. Acta Neuropathol (Berl), 1978. **42**(3): p. 165-71.
13. Galloway, P.G., G. Perry, and P. Gambetti, *Hirano body filaments contain actin and actin-associated proteins*. J Neuropathol Exp Neurol, 1987. **46**(2): p. 185-99.

14. Hirano, A., *Hirano bodies and related neuronal inclusions*. Neuropathol Appl Neurobiol, 1994. **20**(1): p. 3-11.
15. Ogata, J., G.N. Budzilovich, and H. Cravioto, *A study of rod-like structures (Hirano bodies) in 240 normal and pathological brains*. Acta Neuropathol, 1972. **21**(1): p. 61-7.
16. Schochet, S.S., Jr. and W.F. McCormick, *Ultrastructure of Hirano bodies*. Acta Neuropathol, 1972. **21**(1): p. 50-60.
17. Maciver, S.K. and C.R. Harrington, *Two actin binding proteins, actin depolymerizing factor and cofilin, are associated with Hirano bodies*. Neuroreport, 1995. **6**(15): p. 1985-8.
18. Galloway, P.G., et al., *Hirano bodies contain tau protein*. Brain Res, 1987. **403**(2): p. 337-40.
19. Munoz, D.G., D. Wang, and B.D. Greenberg, *Hirano bodies accumulate C-terminal sequences of beta-amyloid precursor protein (beta-APP) epitopes*. J Neuropathol Exp Neurol, 1993. **52**(1): p. 14-21.
20. Lim, R.W.L., et al., *Three distinct F-actin binding sites in the Dictyostelium discoideum 34,000 dalton actin bundling protein*. Biochemistry, 1999a. **38**: p. 800-812.
21. Maselli, A.G., et al., *Formation of Hirano bodies in Dictyostelium and mammalian cells induced by expression of a modified form of an actin cross-linking protein*. J Cell Sci., 2002. **115**: p. 1939-1952.
22. Davis, R.C., R. Furukawa, and M. Fechheimer, *A cell culture model for investigation of Hirano bodies*. Acta Neuropathol, 2008. **115**(2): p. 205-217.
23. Ha, S., R. Furukawa, and M. Fechheimer, *Association of AICD and Fe65 with Hirano bodies reduces transcriptional activation and initiation of apoptosis*. Neurobiol Aging, 2011. **32**(12): p. 2287-98.
24. Furgerson, M., M. Fechheimer, and R. Furukawa, *Model Hirano bodies protect against tau-independent and tau-dependent cell death initiated by the amyloid precursor protein intracellular domain*. PLoS One, 2012. **7**(9): p. e44996.
25. Kim, D.H., et al., *Autophagy contributes to degradation of Hirano bodies*. Autophagy, 2009. **5**: p. 44-51.
26. Cao, X. and T.C. Südhof, *A transcriptionally active complex of APP with Fe65 and histone acetyltransferase Tip60*. Science, 2001. **293**: p. 115-120.

27. Cao, X. and T.C. Südhof, *Dissection of amyloid-beta precursor protein-dependent transcriptional transactivation*. J. Biol. Chem., 2004. **279**: p. 24601-14611.
28. Ha, S., et al., *Transgenic mouse model for the formation of Hirano bodies*. BMC Neurosci, 2011. **12**(1): p. 97.
29. Tsien, J.Z., et al., *Subregion- and cell type-restricted gene knockout in mouse brain*. Cell, 1996. **87**(7): p. 1317-26.
30. Shimizu, E., et al., *NMDA receptor-dependent synaptic reinforcement as a crucial process for memory consolidation*. Science, 2000. **290**(5494): p. 1170-4.
31. Wegiel, J., et al., *The role of microglial cells and astrocytes in fibrillar plaque evolution in transgenic APP(SW) mice*. Neurobiol Aging, 2001. **22**: p. 49-61.
32. Smith, P.K., et al., *Measurement of protein using bicinchoninic acid*. Anal. Biochem., 1985. **150**: p. 76-85.
33. Babb, S.J. and J.D. Crystal, *Episodic-like memory in the rat*. Curr. Biol., 2006. **16**: p. 1317-1321.
34. Glass, C.K., et al., *Mechanisms underlying inflammation in neurodegeneration*. Cell, 2010. **140**(6): p. 918-34.
35. Oakley, H., et al., *Intraneuronal beta-amyloid aggregates, neurodegeneration, and neuron loss in transgenic mice with five familial Alzheimer's disease mutations: potential factors in amyloid plaque formation*. J Neurosci, 2006. **26**(40): p. 10129-40.
36. Rosen, H.J., et al., *Utility of clinical criteria in differentiating frontotemporal lobar degeneration (FTLD) from AD*. Neurology, 2002. **58**(11): p. 1608-15.
37. Koffie, R.M., B.T. Hyman, and T.L. Spires-Jones, *Alzheimer's disease: synapses gone cold*. Mol Neurodegener, 2011. **6**(1): p. 63.
38. Picconi, B., G. Piccoli, and P. Calabresi, *Synaptic dysfunction in Parkinson's disease*. Adv Exp Med Biol, 2012. **970**: p. 553-72.
39. Terry, R.D., et al., *Physical basis of cognitive alterations in Alzheimer's disease: synapse loss is the major correlate of cognitive impairment*. Ann Neurol, 1991. **30**(4): p. 572-80.
40. Scheff, S.W. and D.A. Price, *Alzheimer's disease-related alterations in synaptic density: neocortex and hippocampus*. J Alzheimers Dis, 2006. **9**(3 Suppl): p. 101-15.

41. Rondi-Reig, L., et al., *CA1-specific N-methyl-D-aspartate receptor knockout mice are deficient in solving a nonspatial transverse patterning task*. Proc Natl Acad Sci U S A, 2001. **98**(6): p. 3543-8.
42. Schmidt, M.L., V.M. Lee, and J.Q. Trojanowski, *Analysis of epitopes shared by Hirano bodies and neurofilament proteins in normal and Alzheimer's disease hippocampus*. Lab Invest, 1989. **60**(4): p. 513-22.
43. Lass, R. and C. Hagel, *Hirano bodies and chronic alcoholism*. Neuropath. and Appl. Neurobiol., 1994. **20**: p. 12-21.
44. Hirano, A., et al., *The fine structure of some intraganlionic alterations*. J. Neuropathol. Expt. Neurol., 1968. **27**(2): p. 167-182.
45. Laas, R. and C. Hagel, *Hirano bodies and chronic alcoholism*. Neuropathol Appl Neurobiol, 1994. **20**(1): p. 12-21.
46. Ono, S., et al., *Colocalization of ADF and cofilin in intranuclear rods of cultured muscle cells*. J. Mus. Res. and Cell Motil., 1993. **14**: p. 195-204.
47. Goebel, H.H. and N.G. Laing, *Actinopathies and myosinopathies*. Brain Pathol, 2009. **19**(3): p. 516-22.
48. Bamberg, J.R. and G.S. Bloom, *Cytoskeletal pathologies of Alzheimer's disease*. Cell Motility and the Cytoskeleton, 2009. **66**: p. 635-649.
49. Nishida, E., K. Iida, and N. Yonezawa, *Cofilin is a component of intranuclear and cytoplasmic actin rods induced in cultured cells*. Proc. Natl. Acad. U. S. A., 1987. **84**: p. 5262-5266.
50. Reyes, J.F., et al., *Formation of Hirano bodies after inducible expression of a modified form of an actin-cross-linking protein*. Eukaryot Cell, 2009. **8**(6): p. 852-7.
51. Griffin, P., et al., *Requirements for Hirano Body formation*. Eukaryot Cell, 2014.
52. Izumiyama, N., et al., *Elucidation of three-dimensional ultrastructure of Hirano bodies by the quick-freeze, deep-etch and replica method*. Acta Neuropathol, 1991. **81**(3): p. 248-54.
53. Zaheer, S., et al., *Enhanced expression of glia maturation factor correlates with glial activation in the brain of triple transgenic Alzheimer's disease mice*. Neurochem Res, 2013. **38**(1): p. 218-25.
54. Duyckaerts, C., M.C. Potier, and B. Delatour, *Alzheimer disease models and human neuropathology: similarities and differences*. Acta Neuropathol, 2008. **115**(1): p. 5-38.

55. Mineur, Y.S., et al., *Genetic mouse models of Alzheimer's disease*. Neural Plast, 2005. **12**(4): p. 299-310.
56. Sofroniew, M.V. and H.V. Vinters, *Astrocytes: biology and pathology*. Acta Neuropathol, 2010. **119**(1): p. 7-35.
57. Akiyama, H., et al., *Inflammation and Alzheimer's disease*. Neurobiol Aging, 2000. **21**(3): p. 383-421.
58. Wyss-Coray, T., et al., *Adult mouse astrocytes degrade amyloid-beta in vitro and in situ*. Nat Med, 2003. **9**(4): p. 453-7.
59. Sheffield, L.G., J.G. Marquis, and N.E. Berman, *Regional distribution of cortical microglia parallels that of neurofibrillary tangles in Alzheimer's disease*. Neurosci Lett, 2000. **285**(3): p. 165-8.
60. Sheng, J.G., R.E. Mrazek, and W.S. Griffin, *Glial-neuronal interactions in Alzheimer disease: progressive association of IL-1alpha+ microglia and S100beta+ astrocytes with neurofibrillary tangle stages*. J Neuropathol Exp Neurol, 1997. **56**(3): p. 285-90.
61. DiPatre, P.L. and B.B. Gelman, *Microglial cell activation in aging and Alzheimer disease: partial linkage with neurofibrillary tangle burden in the hippocampus*. J Neuropathol Exp Neurol, 1997. **56**(2): p. 143-9.
62. Cras, P., et al., *Microglia are associated with the extracellular neurofibrillary tangles of Alzheimer disease*. Brain Res, 1991. **558**(2): p. 312-4.
63. Probst, A., J. Ulrich, and P.U. Heitz, *Senile dementia of Alzheimer type: astroglial reaction to extracellular neurofibrillary tangles in the hippocampus. An immunocytochemical and electron-microscopic study*. Acta Neuropathol, 1982. **57**(1): p. 75-9.
64. Crawley, J.N., *Exploratory behavior models of anxiety in mice*. Neurosci Biobehav Rev, 1985. **9**(1): p. 37-44.
65. Floresco, S.B., J.K. Seamans, and A.G. Phillips, *Selective roles for hippocampal, prefrontal cortical, and ventral striatal circuits in radial-arm maze tasks with or without a delay*. J Neurosci, 1997. **17**(5): p. 1880-90.
66. Baddeley, A., *Working memory*. Curr Biol, 2010. **20**(4): p. R136-40.
67. Jarrard, L.E., *On the role of the hippocampus in learning and memory in the rat*. Behav Neural Biol, 1993. **60**(1): p. 9-26.
68. Olton, D.S. and B.C. Papas, *Spatial memory and hippocampal function*. Neuropsychologia, 1979. **17**(6): p. 669-82.

69. Rizzoli, S.O. and W.J. Betz, *Synaptic vesicle pools*. Nat Rev Neurosci, 2005. **6**(1): p. 57-69.
70. Dillon, C. and Y. Goda, *The actin cytoskeleton: integrating form and function at the synapse*. Annu Rev Neurosci, 2005. **28**: p. 25-55.
71. Davis, S., S.P. Butcher, and R.G. Morris, *The NMDA receptor antagonist D-2-amino-5-phosphonopentanoate (D-AP5) impairs spatial learning and LTP in vivo at intracerebral concentrations comparable to those that block LTP in vitro*. J Neurosci, 1992. **12**(1): p. 21-34.
72. Borroni, A.M., et al., *Role of voltage-dependent calcium channel long-term potentiation (LTP) and NMDA LTP in spatial memory*. J Neurosci, 2000. **20**(24): p. 9272-6.
73. Citri, A. and R.C. Malenka, *Synaptic plasticity: multiple forms, functions, and mechanisms*. Neuropsychopharmacology, 2008. **33**(1): p. 18-41.
74. Fukazawa, Y., et al., *Hippocampal LTP is accompanied by enhanced F-actin content within the dendritic spine that is essential for late LTP maintenance in vivo*. Neuron, 2003. **38**(3): p. 447-460.
75. Lin, B., et al., *Theta stimulation polymerizes actin in dendritic spines of hippocampus*. J. Neurosci., 2005. **25**(8): p. 2062-2069.
76. Ramachandran, B. and J.U. Frey, *Interfering with the actin network and its effect on long-term potentiation and synaptic tagging in hippocampal CA1 neurons in slices in vitro*. J. Neurosci., 2009. **29**(39): p. 12167-12173.
77. Baddeley, A., et al., *Dementia and working memory*. Q J Exp Psychol A, 1986. **38**(4): p. 603-18.
78. Moser, E., M.B. Moser, and P. Andersen, *Spatial learning impairment parallels the magnitude of dorsal hippocampal lesions, but is hardly present following ventral lesions*. J Neurosci, 1993. **13**(9): p. 3916-25.
79. Bubser, M. and W.J. Schmidt, *6-Hydroxydopamine lesion of the rat prefrontal cortex increases locomotor activity, impairs acquisition of delayed alternation tasks, but does not affect uninterrupted tasks in the radial maze*. Behav Brain Res, 1990. **37**(2): p. 157-68.
80. Yoon, T., et al., *Prefrontal cortex and hippocampus subserve different components of working memory in rats*. Learn Mem, 2008. **15**(3): p. 97-105.

Figures

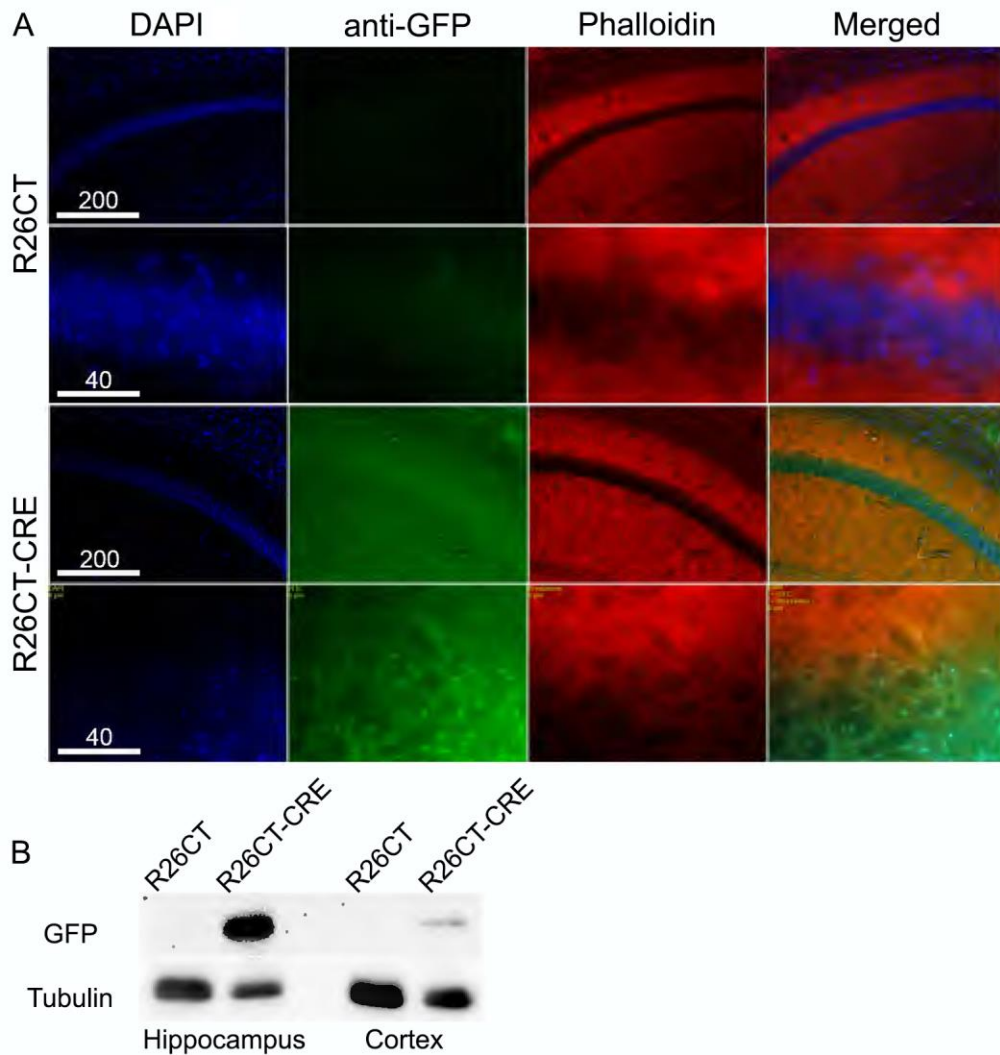


Figure 5.1. Immunofluorescence and western blot of CT-GFP expression in R26CT-CRE mice. A) Immunofluorescence on cryosections from 1 month old R26CT and R26CT-CRE mouse hippocampus. Sections were stained with anti-GFP antibodies to visualize expression of CT-GFP and counterstained with DAPI and TRITC-labeled phalloidin to visualize nuclei and F-actin, respectively. R26CT-CRE mice show expression of CT-GFP in the hippocampus while R26CT mice do not. B) A western blot was performed using brain homogenate from hippocampus and frontal cortex of 1

month old R26CT and R26CT-CRE mice using anti-GFP antibodies to detect CT-GFP expression. To ensure no expression of CT-GFP is detectable in R26CT mice, twice the amount of protein from R26CT samples was loaded compared to R26CT-CRE samples. R26CT-CRE mice show strong expression of CT-GFP in the hippocampus and weak expression in the cortex. R26CT mice have no detectable CT-GFP in either hippocampus or cortex. Scale bar represents 40 or 200 μm .

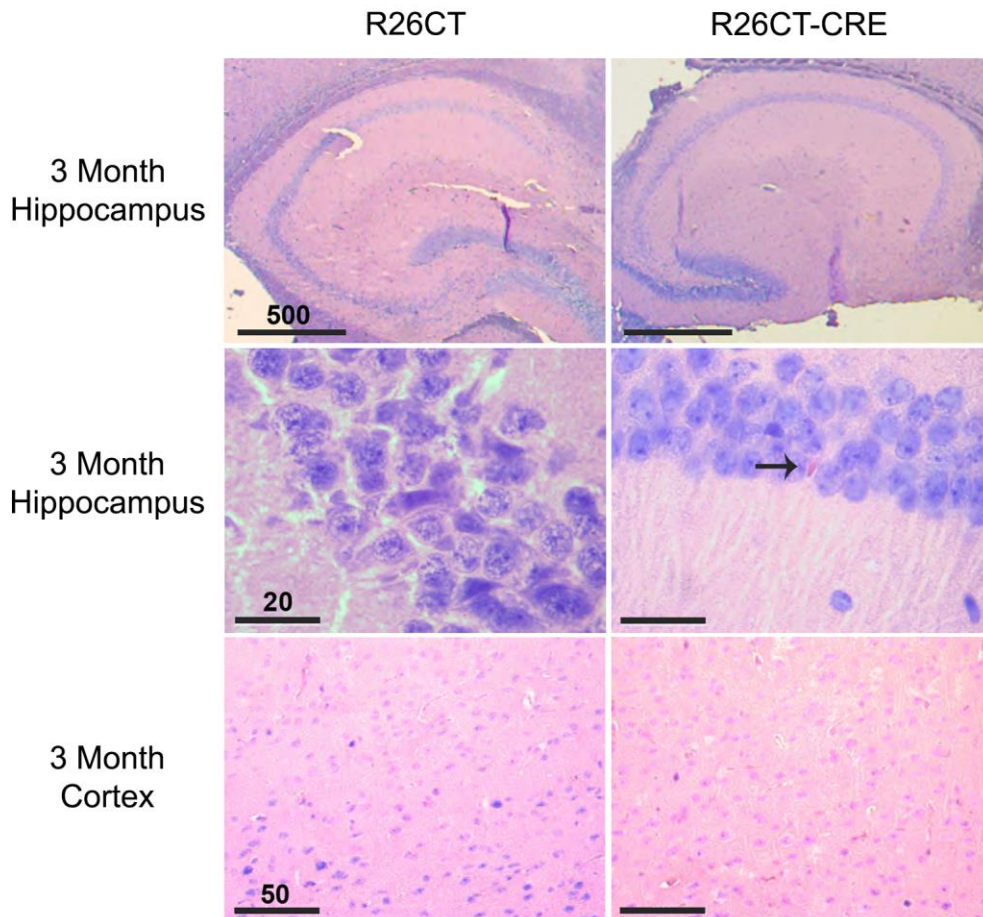


Figure 5.2. Model Hirano bodies detected as eosinophilic inclusions in 3 month old R26CT-CRE mice. Paraffin embedded brain sections from 3 month old R26CT and R26CT-CRE mice were dewaxed and stained with Gill's hematoxylin and counterstained with eosin. 3 month old R26CT mice show no rod-shaped eosinophilic inclusions in the pyramidal cells of the hippocampus or cerebral cortex. 3 month old R26CT-CRE mice show no inclusions in the cerebral cortex, but contain rare eosinophilic inclusions in CA1 pyramidal cells of the hippocampus indicated by the arrow. Scale bars represent 20, 50, or 500 μm .

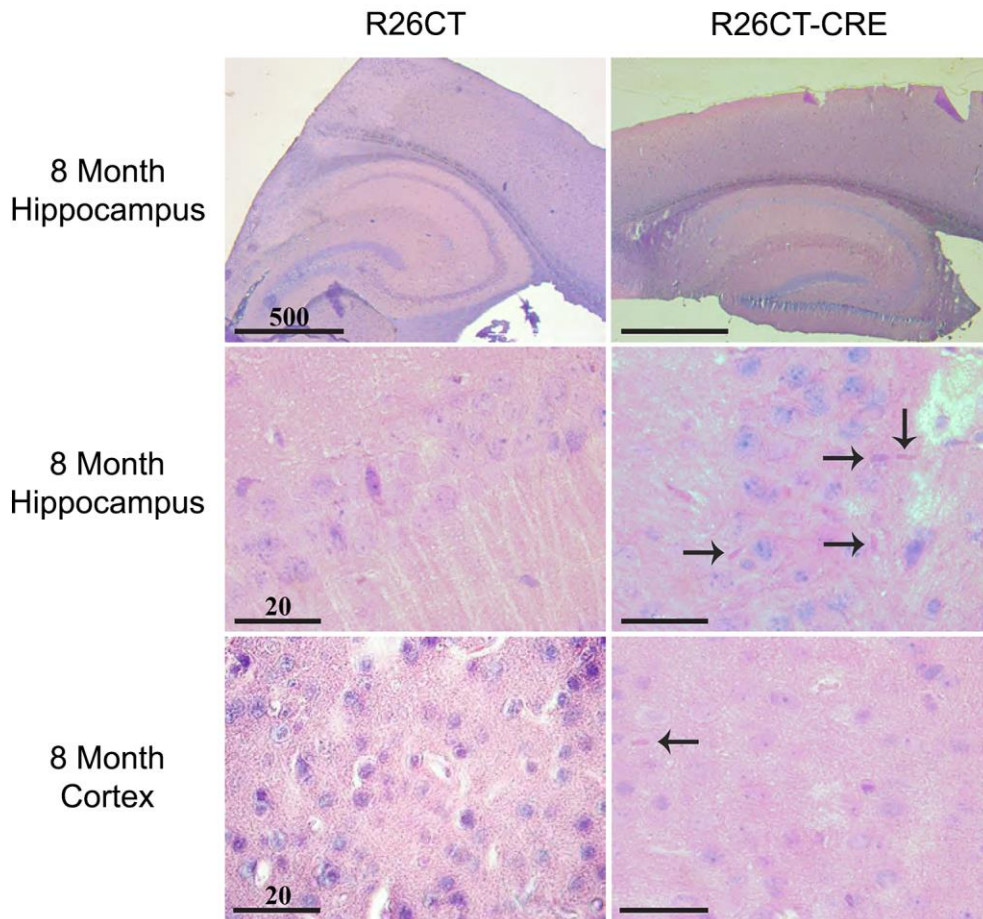


Figure 5.3. Model Hirano bodies detected as eosinophilic inclusions in 8 month old R26CT-CRE mice. Paraffin embedded brain sections from 8 month old R26CT and R26CT-CRE mice were dewaxed and stained with Gill's hematoxylin and counterstained with eosin. 8 month old R26CT mice show no rod-shaped eosinophilic inclusions in the pyramidal cells of the hippocampus or cerebral cortex. R26CT-CRE mice have eosinophilic inclusions predominately in the CA1 pyramidal cell layer of the hippocampus and rarely in the cerebral cortex. Arrows indicate inclusions. Scale bars represent 20 or 500 μm .

R26CT-CRE Hippocampus

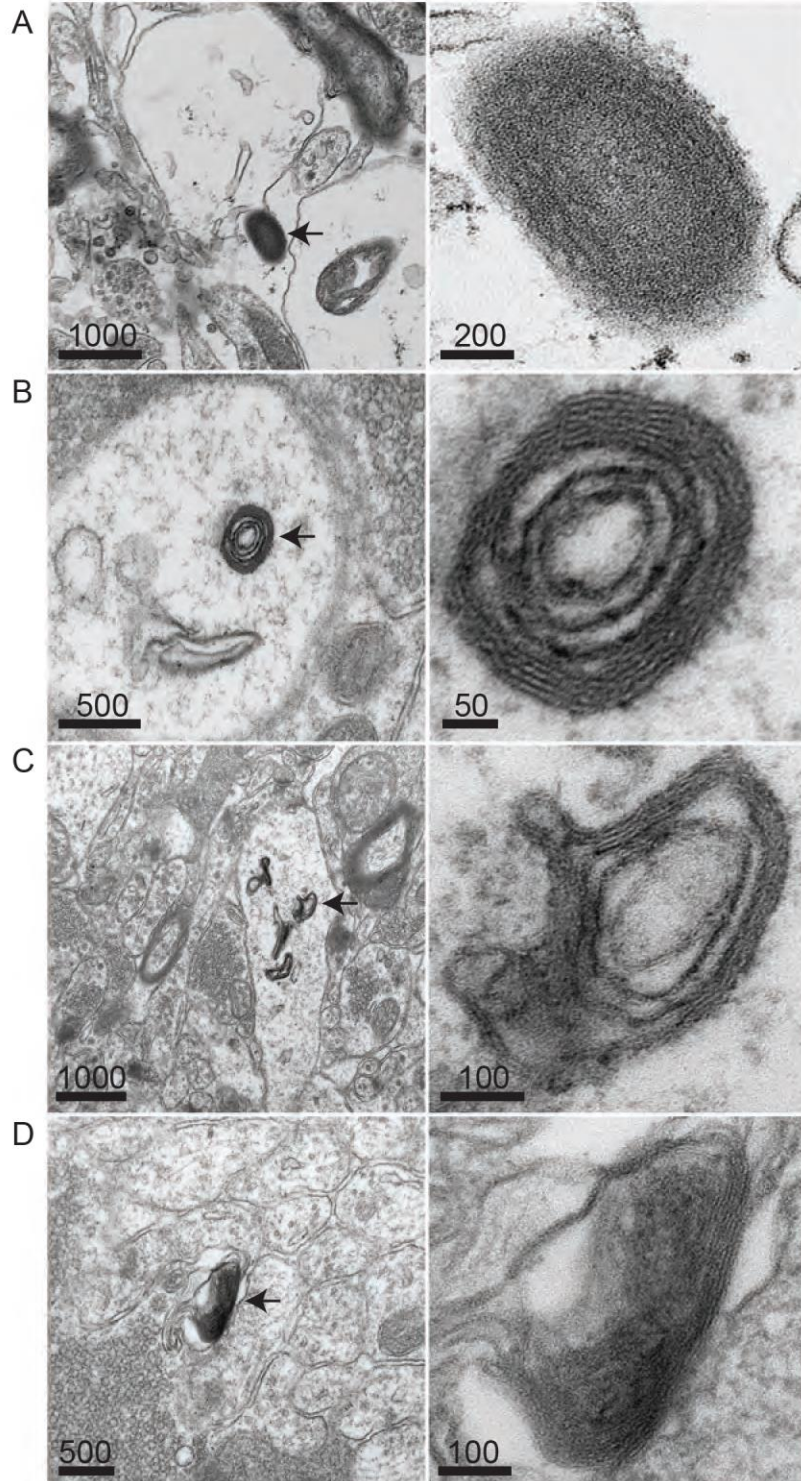


Figure 5.4. Electron micrographs of inclusions in 8 month R26CT-CRE mice.

Hippocampal tissue from 8 month old R26CT and R26CT-CRE mice was isolated and prepared for transmission electron microscopy. R26CT-CRE tissue contained electron dense inclusions which are identical to the ultrastructure of Hirano bodies. These structures were not observed in R26CT mice (data not shown). A, B) The ultrastructure of model Hirano bodies resembling a spheroid or fingerprint pattern similar to those seen in humans [8]. C) Intermediate structures were seen in the brains of R26CT-CRE mice similar to those seen in humans and cell culture models [22, 25, 52]. D) R26CT-CRE mice exhibit model Hirano bodies which contain both ordered filaments and amorphous electron dense material. Arrows indicate Hirano bodies or intermediates magnified in the panels to the right. Scale bars are in nm.

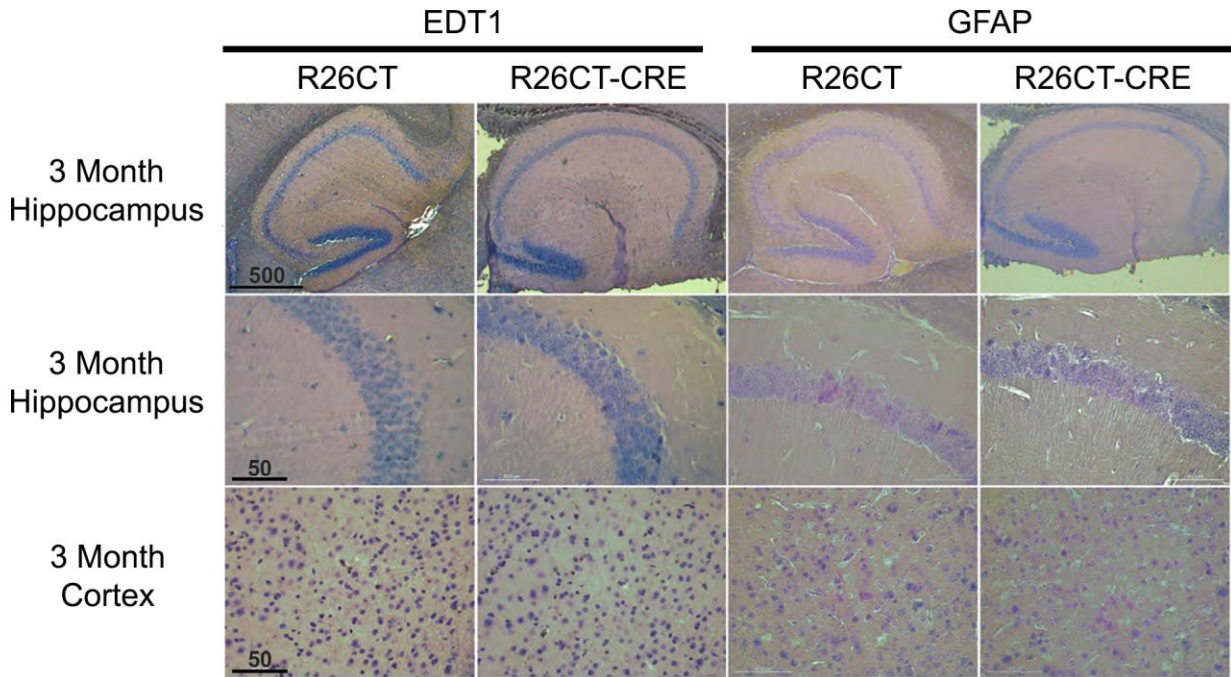


Figure 5.5. Lack of inflammation in microglia and astrocytes of 3 month old R26CT and R26CT-CRE mice. Paraffin embedded brain sections from 3 month old R26CT and R26CT-CRE mice were dewaxed and stained with DAB using antibodies against ED1 or GFAP to label activated microglia and reactive astrocytes, respectively. At 3 months, R26CT and R26CT-CRE mice show no GFAP or ED1 staining in either the hippocampus or cortex. Scale bars represent 50 or 500 μm .

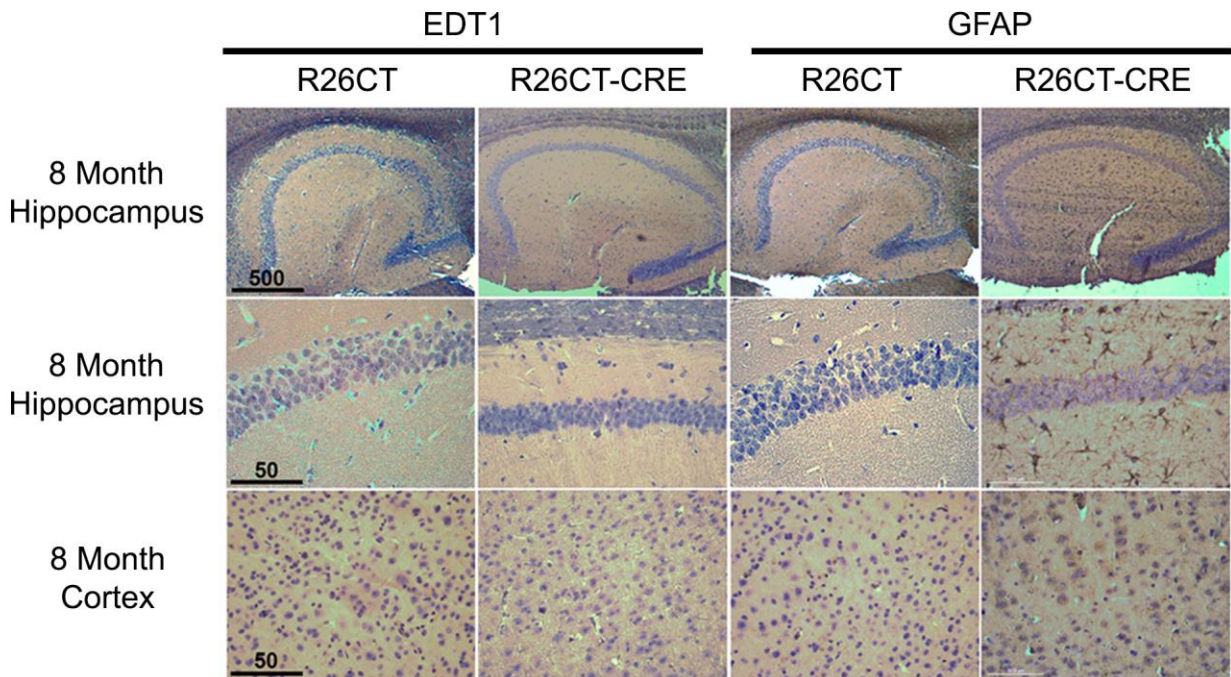


Figure 5.6. Inflammatory response in astrocytes, but not microglia of 8 month old R26CT-CRE mice. Paraffin embedded brain sections from 8 month old R26CT and R26CT-CRE mice were dewaxed and stained with DAB using antibodies against ED1 or GFAP to label activated microglia and reactive astrocytes, respectively. At 8 months, R26CT and R26CT-CRE show no ED1 staining in the hippocampus or cerebral cortex. R26CT mice also show no GFAP staining in either hippocampus or cerebral cortex. R26CT-CRE mice have GFAP staining in the hippocampus but not cerebral cortex. Scale bars represent 50 or 500 μm .

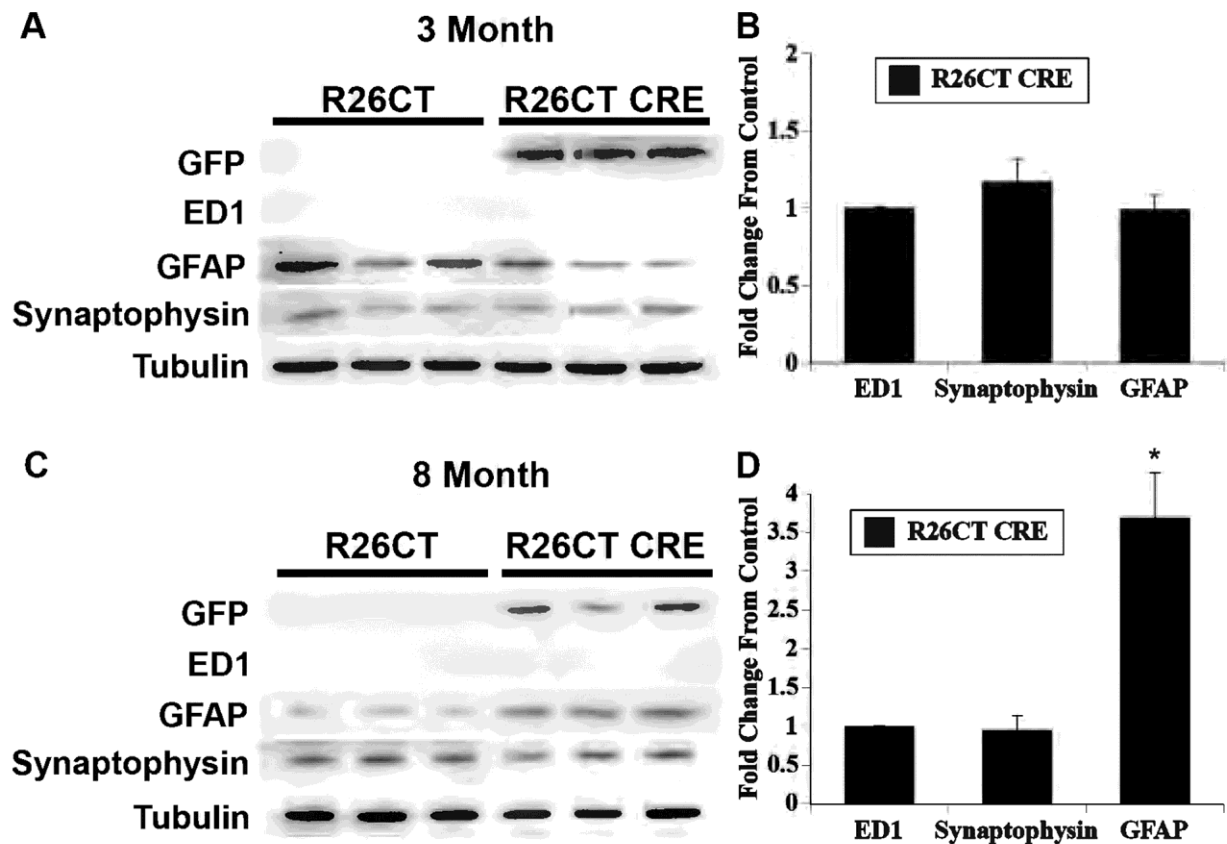


Figure 5.7. Western blot analysis of inflammatory response in 3 and 8 month old mice. Brain homogenate from 3 and 8 month old R26CT and R26CT-CRE mice was separated by SDS-PAGE and transferred to nitrocellulose. Blots were probed using anti-ED1 and GFAP antibodies. A) At 3 months, there is no difference in levels of synaptophysin, GFAP, or ED1 between R26CT and R26CT-CRE mice. B) Quantification of data in A. C) At 8 months, there is no difference in levels of ED1 or synaptophysin between R26CT and R26CT-CRE mice. However, R26CT-CRE mice show an increase in GFAP. D) Quantification of data in C.

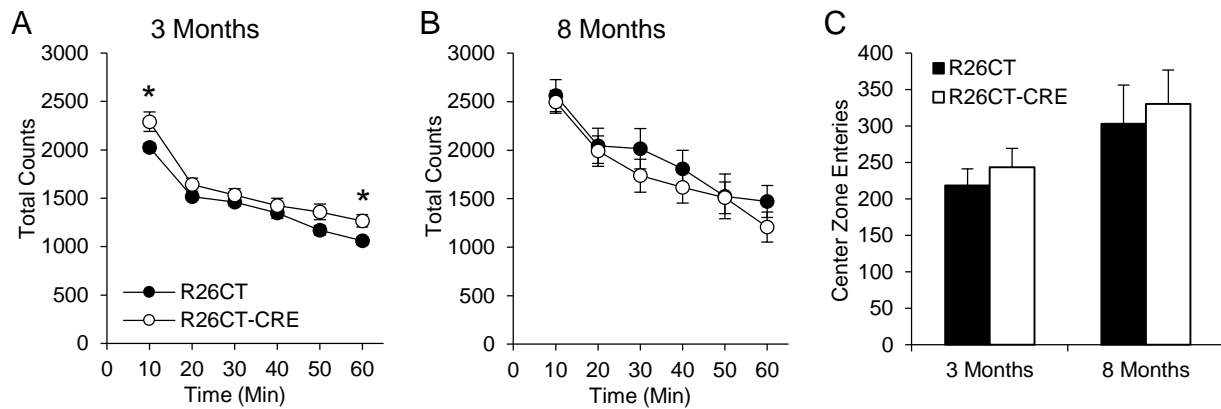
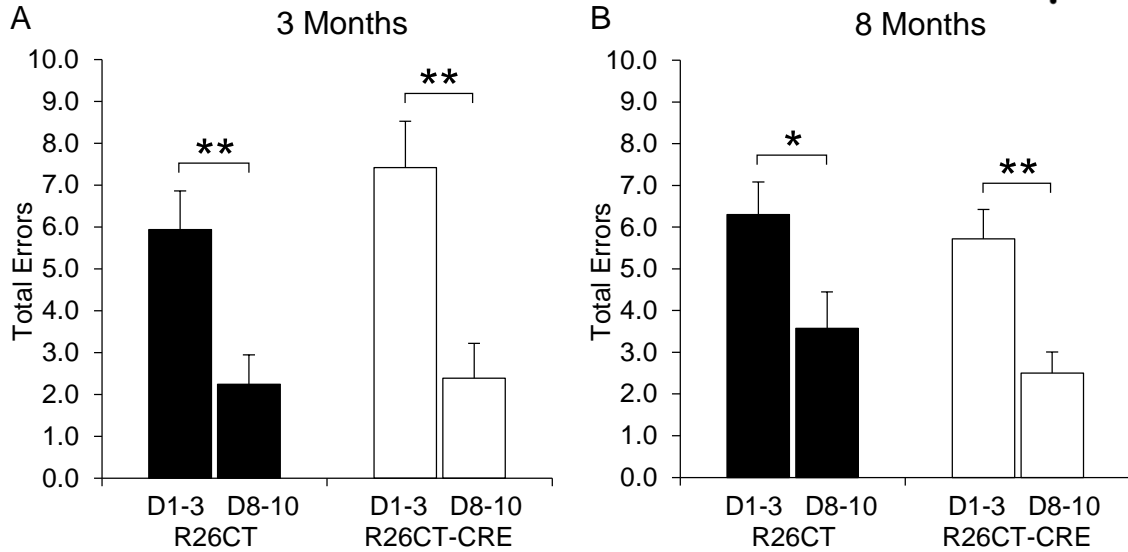
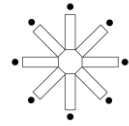
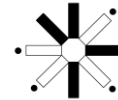


Figure 5.8. Open field behavior in R26CT control mice and R26CT-CRE mice. A) Locomotor activity in 3 month old R26CT (black circles, n=11) and R26CT-CRE (open circles, n=12) mice measured for 60 min, and summed into 10 minute blocks. B) Same as panel A except at 8 months for R26CT (n=11) and R26CT-CRE (n=12) mice. C) Center zone entries during the 30 minutes of locomotor activity for R26CT and R26CT-CRE mice. Values represent the mean \pm SEM from n animals. Significance was determined using independent t-tests (* $p < 0.05$, ** $p < 0.01$).

8-Arm uninterrupted task: 8 Arms Open; 8 Arms Baited



Study Phase: 4 Arms Open; 4 Arms Baited



Retention Interval (3 min)

Test Phase: 8 Arms Open; 4 Arms Baited

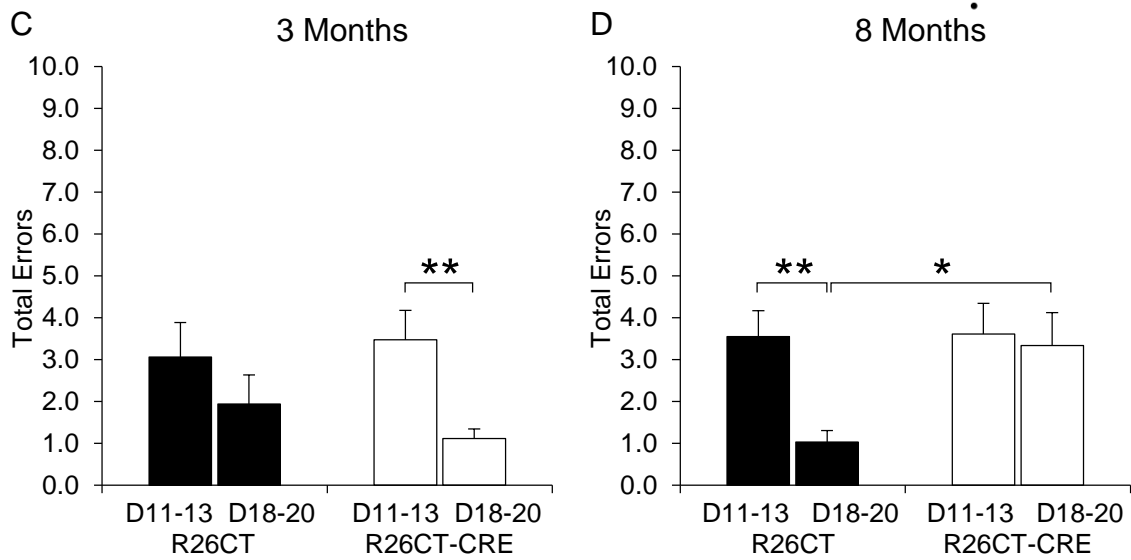
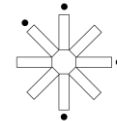


Figure 5.9. Short-term and working memory in the 8-arm radial maze. The Schematic above each data set illustrates the protocol used for testing. (•) represents baited arms. Blacked out arms represent inaccessible arms. A & B) 8-arm uninterrupted task for R26CT control mice and R26CT-CRE mice at 3 and 8 months. A) R26CT (black bars, n=11) and R26CT-CRE (open bars, n=12) mice at 3 months of age. B) R26CT (black bars, n=11) and R26CT-CRE (open bars, n=11) at 8 months of age. C & D) Test phase of the delayed spatial win-shift assay for R26CT control mice and R26CT-CRE mice at 3 and 8 months. C) R26CT (black bars, n=11) and R26CT-CRE (open bars, n=12) mice at 3 months of age. D) R26CT (black bars, n=11) and R26CT-CRE (open bars, n=11) mice at 8 months of age. Values represent the mean \pm SEM of the first 3 days or the last 3 days of testing for each phase from n animals. Significance was determined using mixed ANOVA, 2-way ANOVA, and paired and independent t-tests (* $p < 0.05$, ** $p < 0.01$).

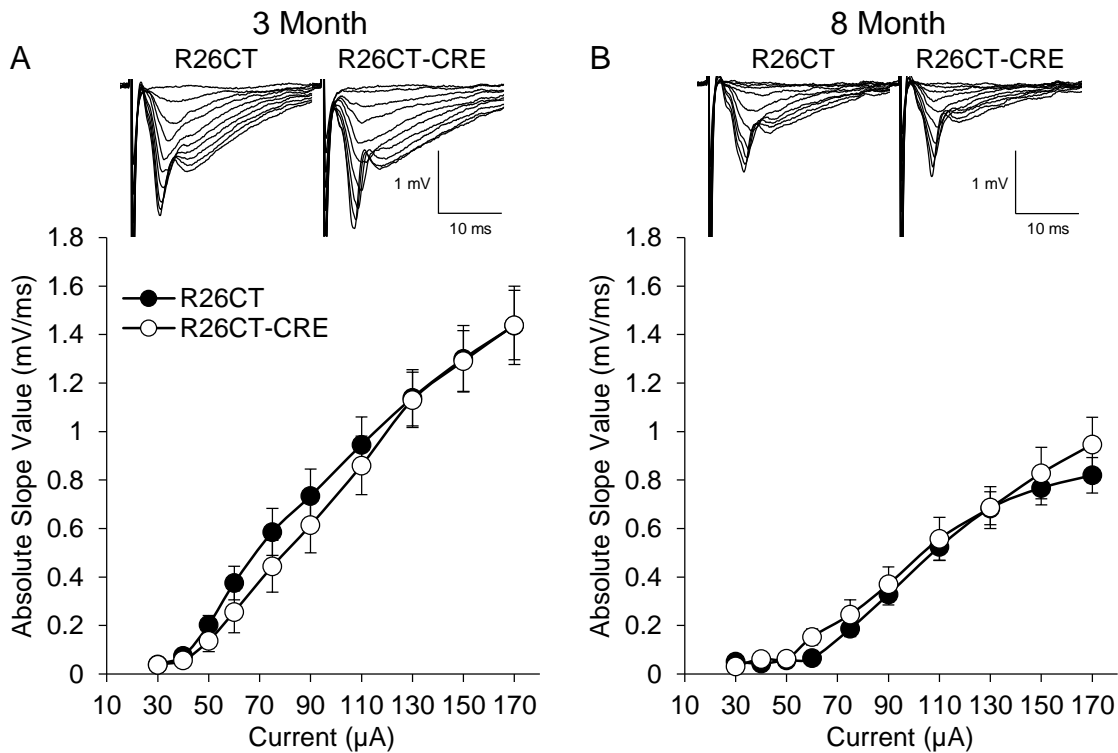


Figure 5.10. Field Excitatory Post-Synaptic Potentials (fEPSP) recorded from the CA1 region of ventral hippocampus in R26CT control mice and R26CT-CRE mice. A) Stimulus response curves for R26CT (black circles, n=19(10)) and R26CT-CRE (open circles, n=18(12)) mice at 3 months of age. Input intensities are 30, 40, 50, 60, 75, 90, 110, 130, 150 and 170 μ A. The averaged fEPSP sweeps are shown above the stimulus response curves. B) Same as panel A except at 8 months of age for R26CT (n=20(10)) and R26CT-CRE (n=19(12)) mice. Values represent the mean \pm SEM from n slices(animals). Significance was determined using independent t-tests (* p < 0.05, ** p < 0.01).

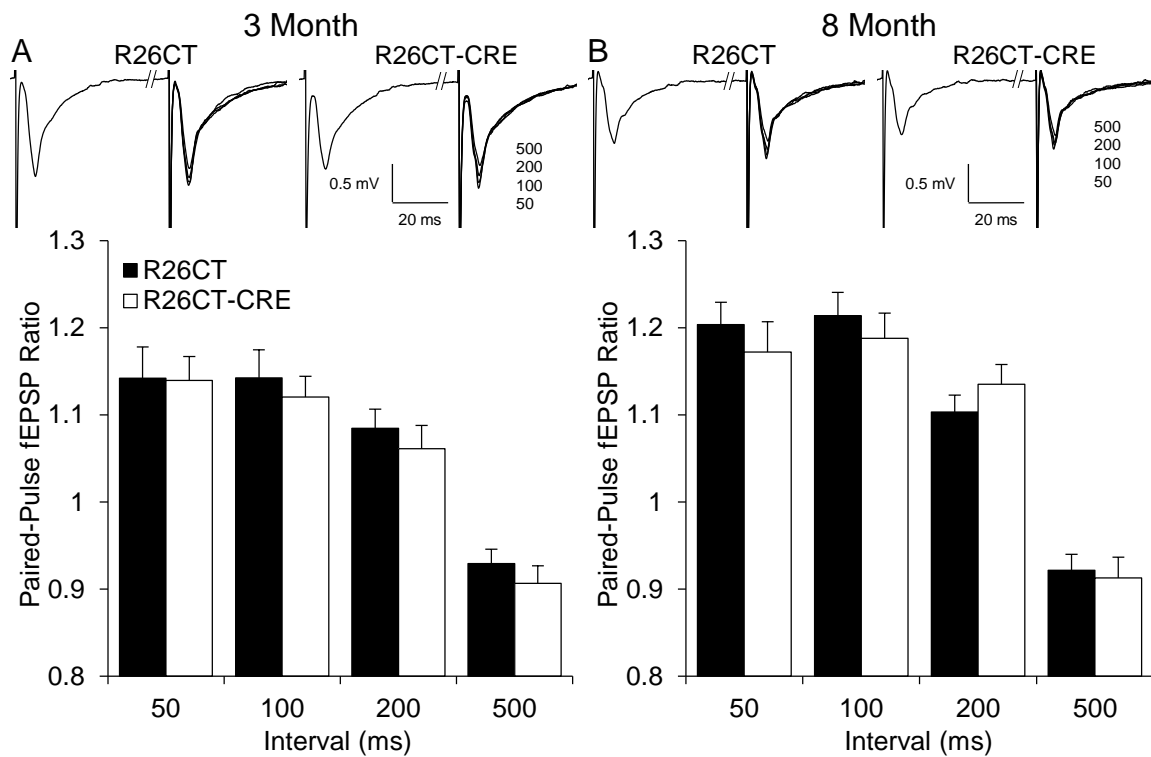


Figure 5.11. Paired-pulse field Excitatory Post-Synaptic Potentials (fEPSP) recorded from the CA1 region of ventral hippocampus in R26CT control mice and R26CT-CRE mice. A) Paired-pulse ratios at 50, 100, 200, and 500 ms intervals in R26CT (black bars, n=19(10)) and R26CT-CRE (open bars, n=18(12)) mice at 3 months of age. The averaged fEPSP sweeps are shown above the paired-pulse ratios. B) Same as panel A except at 8 months of age for R26CT (n=20(10)) and R26CT-CRE (n=21(12)) mice. Values represent the mean \pm SEM from n slices(animals). Significance was determined using independent t-tests (* p < 0.05, ** p < 0.01).

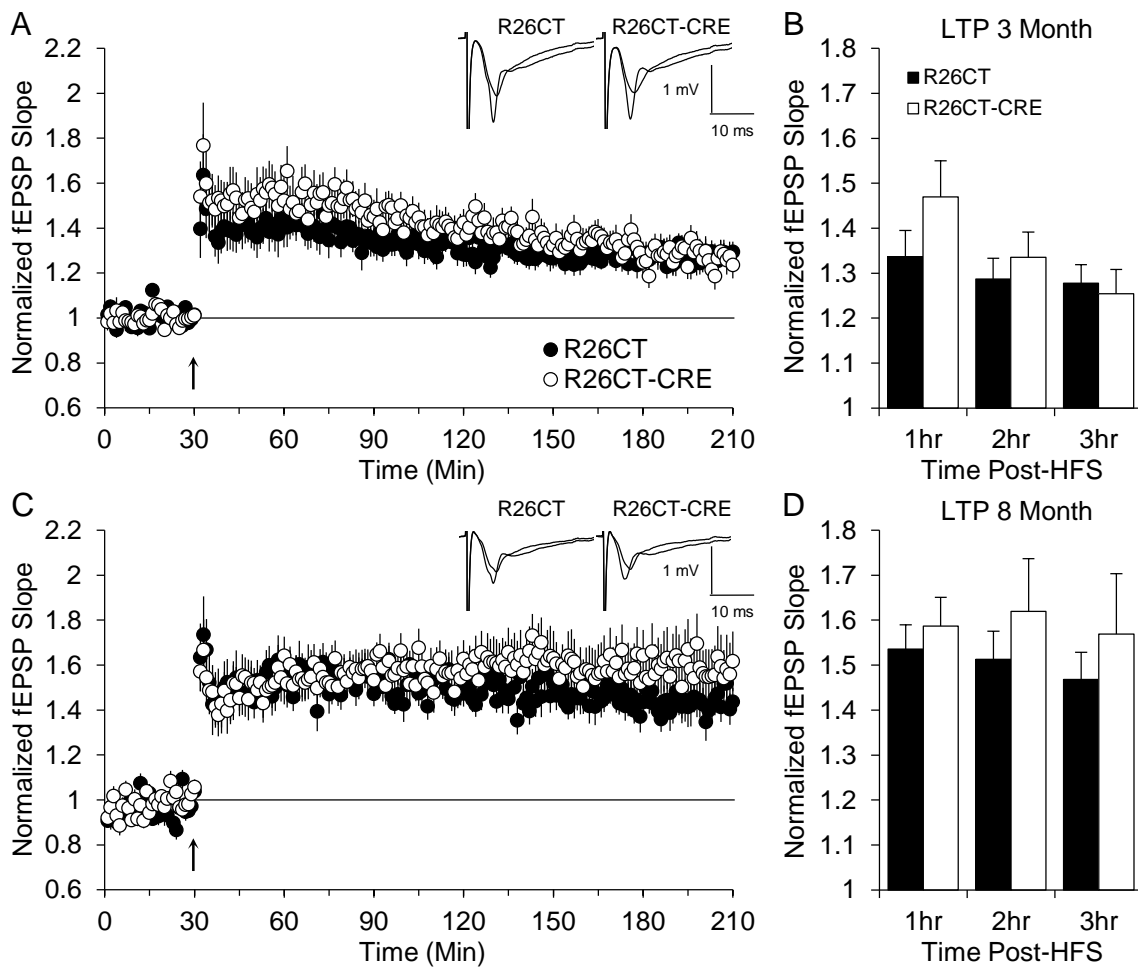


Figure 5.12. Long-Term Potentiation (LTP) of field Excitatory Post-Synaptic Potentials (fEPSP) recorded from the CA1 region of ventral hippocampus in R26CT control mice and R26CT-CRE mice. A) Summary plot of normalized fEPSP slope values in 3 month old R26CT control mice (black circles, $n=17(11)$) and R26CT-CRE mice (open circle, $n=16(11)$) before and after high frequency stimulation (HFS) ($3 \times 100\text{Hz}/1 \text{ s}$ at 20 s intervals) indicated by the arrow at 30 minutes. Insets show the averaged fEPSP sweeps before and after HFS. B) Summary quantification of LTP for R26CT and R26CT-CRE mice at 1, 2, and 3 hours post-HFS. C & D) Same as A & B above except

at 8 months of age for R26CT (black square, (n=18(9)) and R26CT-CRE (open circle, (n=18(11)). Values represent the mean \pm SEM from n slices(animals). Significance was determined using independent t-tests (* p < 0.05, ** p < 0.01).

CHAPTER 6

CONCLUSIONS AND FINAL THOUGHTS

6.1 Summary of Experimental Findings

Alzheimer's disease is a neurodegenerative condition of aging believed to be initiated by the production of Amyloid- β peptide, which leads to synaptic dysfunction and progressive memory loss, and the eventual formation of β -Amyloid plaques and neurofibrillary Tau tangles. Using a triple transgenic mouse model of Alzheimer's disease (3xTg-AD) carrying mutations for APP, PS1, and Tau, an 8-arm radial maze was employed to assess spatial working memory. Unexpectedly, the younger (3 month old) 3xTg-AD mice were just as impaired in the spatial working memory task as were the older (8 month old) 3xTg-AD mice when compared with age-matched NonTg control mice. Field potential recordings from the CA1 region of ventral hippocampal slices were obtained to assess synaptic transmission and capability for synaptic plasticity. At 3 months, basal synaptic transmission was largely similar between 3xTg-AD and NonTg mice except at high stimulus inputs ($\geq 130 \mu\text{A}$). An evaluation of short-term synaptic plasticity showed 3xTg-AD mice have significantly reduced paired-pulse facilitation compared to NonTg mice, indicating an impairment in short-term synaptic plasticity. Evaluation of long-term synaptic plasticity showed 3xTg-AD mice have a significant reduction in the NMDAR-dependent component of LTP, despite having a total LTP that is not different from NonTg mice. This was a result of the non-NMDAR-dependent

component of LTP being concomitantly increased. The reduction in paired-pulse facilitation and NMDAR LTP coincided with impairments in spatial working memory, which also coincided with the presence of intracellular A β 42 in hippocampal CA1 pyramidal neurons, and an increase in hippocampal A β 42 levels that significantly correlated with spatial working memory impairments. Results at 8 months were similar to those at 3 months, with the exception that total LTP in 3xTg-AD mice was now also significantly reduced compared to NonTg mice, and histological preparations showed the presence of β -Amyloid plaques and neurofibrillary Tau tangles. The early presence of this cognitive impairment, and the associated alterations in synaptic plasticity, demonstrate that the onset of some behavioral and neurophysiological consequences can occur before the detectable presence of plaques and tangles in the 3xTg-AD mice, lending further support to the Amyloid hypothesis, and that the emergence of extracellular β -Amyloid plaques are secondary to soluble or intraneuronal A β 42 in regards to disease pathogenesis.

These findings prompted us to explore the progression of synaptic changes in young presynaptic 3xTg-AD mice, and determine the nature of the non-NMDAR component of LTP. The 21 day old animals showed no difference between genotypes in any electrophysiological measurements or response to antagonism of NMDARs or VDCCs. At 2 months however, 3xTg-AD mice had reduced paired-pulse facilitation and were resistant to NMDAR antagonism with AP5. By 3 months, 3xTg-AD mice showed a reduction in synaptic response at higher stimulus inputs, reduced paired-pulse facilitation, and LTP that was independent of NMDAR or VDCC activation. Antagonism of NMDARs and VDCCs failed to prevent LTP expression, producing LTP that was not

different from total LTP. A weaker HFS induction protocol revealed a substantial difference between 3xTg-AD and NonTg mice for post-tetanic potentiation (PTP) and short-term potentiation (STP) expression, indicating differences in neurotransmitter facilitation similar to our paired-pulse results, and differences in the decay of STP. These leveled out to similar LTP levels that were not different between genotypes after 1 hour. Measurements of NMDAR-mediated fEPSPs indicate there is no difference between genotypes in NMDAR-mediated neurotransmission, and the differences in the induction of LTP between 3xTg-AD and NonTg mice originate from mechanisms other than the normal mechanisms of extracellular Ca^{2+} entry.

6.2 The Big Picture

Alzheimer's disease is a complex and formidable disease. There are many groups around the world working on many aspects of AD in an effort to understand exactly how this particular disease inflicts so much damage, and better yet, how to treat it. But the more questions that are answered, the more questions that are generated. Conquering AD begins with understanding AD, which begins with useful model systems that accurately recapitulate specific aspects of the disease process. There are many AD model mice available, but the 3xTg-AD model is one of the only, if not the only, models that produces both plaques and tangles. These mice are an ideal choice for study due to their natural progression of AD pathology that mimics the human condition. Since there is no such thing as an ideal model however, there are some points of interest that we have observed in our own studies that may be of importance to AD field in moving forward with studies involving this model. The first is that these mice may not

be truly presymptomatic, maybe not at any age. While we did not find any neurophysiological deficits at 21 days, we did observe a reduction in locomotor activity at 21 days. It is unclear if this behavioral phenotype constitutes a functional impairment or not, but behavioral testing of cognition at this age, or sooner, is likely to be unreliable. Our radial arm maze results for assessment of spatial working memory at 3 months represent the earliest reported cognitive impairment to date in 3xTg-AD mice, at least 1 month before subtle impairments in reference memory, and 3 months before full long-term reference memory impairments. This observation is the second point of interest. In human AD patients, impairments in working memory of this type are generally the first observed, and these findings confirm that working memory is affected before reference memory in the 3xTg-AD model, adding another criterion by which 3xTg-AD mice mimic the human AD condition.

We have also learned something new about learning and memory in general, and its relation to cellular models of information storage such as LTP. Measurements such as paired-pulse facilitation, PTP, or STP may be more predictive of working memory performance rather than LTP, which is traditionally associated with long-term reference memory. A reevaluation of data from chapter 2 that compares working memory errors from the test phase of the radial arm maze with paired-pulse facilitation or total LTP across both age groups (3 and 8 months) supports this hypothesis (Figure 6.1). A comparison of working memory errors with total LTP does not show a functional correlation between these two factors (Figure 6.1B). However, when working memory errors are compared against paired-pulse facilitation ratios, a significant correlation exists for NonTg animals (Figure 6.1A). This correlation does not hold up in 3xTg-AD

mice. The important observation is that NonTg mice show a strong relationship between short-term synaptic plasticity and working memory performance, but 3xTg-AD mice do not, which have both impaired short-term synaptic plasticity and impaired working memory. The ideal scenario would show a relationship in both genotypes, with the 3xTg-AD performance data shifted below that of NonTg mice, but since we did not observe this however, we would simply argue that a relationship exists under nonimpaired conditions, but completely falls apart under the disease state due to the breakdown of associated regulatory mechanisms. Thus, measurements such as paired-pulse facilitation may be useful as early indicators of neurophysiological impairments associated with AD or other cognitive disorders. In light of these observations, we have potentially uncovered a possible cellular mechanism to explain early working memory deficits that are observed in AD patients, although additional work is needed to confirm this hypothesis.

6.3 Where do we go from here?

Studying AD has the potential to not only solve the problems that occur as a result of AD, but to also answer important basic science questions about general learning and memory processes. With regards to our own work, we have formulated a working model of how we believe synaptic plasticity becomes dysregulated in the early AD patient. This model is based on our own studies, as well as those of others exploring related questions, but still requires further investigation for conformation.

We show 3xTg-AD mice are resistant to NMDAR and VDCC antagonists during the induction of LTP, but it is still unclear if there is a change in NMDAR or VDCC

density, current, or activation kinetics in animals in our 3 month age range, the first indication when the changes to LTP induction and expression seem to be fully developed. Our studies only looked at NMDAR-mediated synaptic response, which is informative, but not a complete picture. Studies suggest there is no change in NMDAR or VDCC current until at least 12 months of age in 3xTg-AD mice [1], indicating there should not be a change at 3 months either, but this has not been confirmed. It is also unclear at 12 months if these changes occur as a result of increased NMDAR or VDCC expression, or a change in activation kinetics, although whole cell current data indicate there may be an increase in VDCC density, but channel kinetics were not evaluated. Interestingly, the current is shown to increase, not decrease. This increase occurs at a time when there should be decreased synaptic response and impairments in LTP, potentially as a compensatory effort to boost synaptic efficacy just before complete synaptic collapse, but none of the studies that compared NMDAR and VDCC current examined any form of synaptic response or synaptic plasticity. Thus, the first goal is to determine if NMDARs and VDCCs are expressed at control levels, produce control level currents, and follow control activation kinetics. If and when these factors change (and studies show they will), when and why? Our current model does not explain differences in LTP in the early AD patient by changes in NMDAR or VDCC expression or activity.

The induction of LTP requires a transient rise in intracellular Ca^{2+} concentration. Our current model suggests there is a transient rise in intracellular Ca^{2+} despite blocking the normal routes for external Ca^{2+} entry into neurons. The second goal is to determine if 3xTg-AD mice do in fact show an increase in intracellular Ca^{2+} concentration in the presence of NMDAR and VDCC antagonists. Studies indicate 3xTg-AD mice have

enhanced Ca^{2+} release from the ER via increases in Ryanodine receptor (RyR) expression, although these studies are in mice 6-8 weeks of age [2]. If mice in our age range do show a transient increase in intracellular Ca^{2+} concentration, we should confirm (or refute), the source is in fact, ER Ca^{2+} released via RyRs. A combination of fluorescent Ca^{2+} imaging and a variety of high frequency stimulation induction protocols sufficient to elicit LTP can be performed in the presence of NMDAR, VDCC, and RyR antagonists to sufficiently answer this question.

Since RyRs are Ca^{2+} activated channels, there would still need to be an initial Ca^{2+} trigger. The most likely candidate is the ER-associated IP_3R . Activation of the IP_3R by IP_3 may occur after activation of PLC, which metabolizes PIP_2 to form DAG and IP_3 . PLC is a target of G-protein activation coupled to Group I mGluRs located on postsynaptic neurons. Exogenous application of $\text{A}\beta$ to hippocampal slices indicates $\text{A}\beta$ interferes with glutamate reuptake, prolonging glutamate clearance and excessively activating mGluRs [3]. Performing LTP experiments as before (blocking activation of NMDARs and VDCCs) but with an antagonist for IP_3Rs instead of RyRs would be a logical next step, followed by antagonism of Group I mGluRs instead of ER-associated Ca^{2+} channels. If these experiments produce positive results, determining the nature of mGluR activation would follow by determining if glutamate uptake was in fact delayed by impaired glutamate transporter function by performing glutamate reuptake assays for comparison between genotypes. Attempts to normalize this process with the use of glutamate scavenger systems would confirm this mechanism. While this represents an ideal scenario, there are some potential pitfalls to consider. If blocking IP_3Rs still yields a Ca^{2+} response from RyRs, there is the small possibility that T-type Ca^{2+} channels may

be in play. T-type Ca^{2+} channels are low voltage activated regulatory channels that modulate membrane potential, and could potentially be a source of external Ca^{2+} if activation properties are altered in AD. T-type channels are beginning to be looked at in both aging and AD as a potential source of Ca^{2+} dysregulation [4, 5]. If blocking mGluRs still produces a response, the next likely candidate would be extrasynaptic NR2B containing NMDARs. Studies have suggested that extrasynaptic NR2B containing receptors can be activated by glutamate spill over [6]. In addition, $\text{A}\beta$ has also been shown to stimulate glutamate release from astrocytes via $\alpha 7$ nicotinic receptors to activate extrasynaptic NMDARs [7]. NMDARs are unique in that they have recently become the only described receptor to show both ionotropic and metabotropic capabilities [8-10]. In other words, it may function as both an ion channel, and a G-protein coupled receptor.

$\text{A}\beta$ has been shown to elicit synaptic depression through activation of the metabotropic function of extrasynaptic NR2B containing receptors [9], and metabotropic NMDAR activity is required for LTD [8]. On a related note, this finding may also explain decades of subtle, inconsistent results between different NMDAR antagonists such as AP5 (a competitive antagonist) and MK-801 (a noncompetitive channel blocker).

In summary, others have demonstrated a dysregulation in intracellular Ca^{2+} homeostasis in very young animals, but not in adult or older animals. Others have shown there are no changes in NMDA or VDCC current or density, or changes in synaptic density, but none have demonstrated functional consequences of these findings. We have shown there are changes in paired-pulse facilitation and LTP induction that lead to altered expression of LTP, but we have not demonstrated this

results as a dysregulation of intracellular Ca^{2+} homeostasis. Our data, as well as others, have also characterized the onset of different types of learning and memory impairments in 3xTg-AD mice. Together, these data allow for the construction of our current model of synaptic plasticity impairments in the early AD state. Moving forward, the mechanisms driving dysregulation of intracellular Ca^{2+} homeostasis need to be verified as having a functional effect on synaptic plasticity, which leads to behavioral impairments.

Taken together, we have summarized the following model for synaptic impairment in the early-stage AD patient: Mutated APP and PS1/2 result in a shift in amyloidogenic processing that leads to an increase in $\text{A}\beta$ production, predominately $\text{A}\beta_{42}$ for most mutations. Release of glutamate as a result of synaptic activity results in prolonged glutamate clearance due to $\text{A}\beta$ interaction with glutamate transporters. This results in excessive activation of AMPARs, NMDARs, and mGluRs. This may also result in glutamate spillover which could potentially activate extrasynaptic NR2B containing NMDARs. In addition, $\text{A}\beta$ induces glutamate release from astrocytes, which augments activation of extrasynaptic NR2B containing receptors. These events result in an enhanced rise in intracellular Ca^{2+} concentration, that is further enhanced by Ca^{2+} activated Ca^{2+} release from increased expression of RyRs, and a potentiated Ca^{2+} current from RyRs mediated by mutated PS1 that functions independently from Presenilins involved in $\text{A}\beta$ production. There is also Ca^{2+} release from IP_3Rs activated by mGluR signaling. This results in a dysregulation of Ca^{2+} homeostasis that allows for excitotoxic mechanisms, and altered regulation of synaptic plasticity processes. Eventually, excessive activation over time of mGluRs and extrasynaptic NR2B NMDARs

results in LTD mechanisms that remove AMPARs from the synaptic membrane and impair AMPAR trafficking. Excessive Ca^{2+} dysregulation eventually results in excitotoxic mechanisms that cause oxidative stress and mitochondrial collapse, eventually ending in apoptosis and wide spread neurodegeneration in the late-stage AD patient.

6.4 A Final Thought on the Future of Alzheimer's Disease Research

The ultimate success of AD research is to learn enough to prevent it from ever occurring in the first place. Until that happens however, we are faced with the daunting task of characterizing what seems to be an overwhelming number of divergent effects all stemming from the overproduction of a single peptide. The scientific literature is filled with novel approaches that claim to offer some improvement for cognitive abilities, but these findings rarely progress on to human studies. Current FDA approved therapeutics fall into two classes: Cholinergic esterase inhibitors, and the NMDAR low-affinity channel blocker Memantine [11]. The RyR antagonist Dantrolene has gained in popularity, producing positive results in animal models of AD, restoring cognition [12, 13] and neurophysiology [14]. Dantrolene and other RyR antagonists have been involved in clinical trials, but for cardiovascular and musculoskeletal related diseases, not for AD. In addition, antibody therapies against $\text{A}\beta$ have also shown great promise in AD models [15-20], but have ultimately failed in clinical trials [21, 22]. Despite setbacks, Amyloid immunotherapy remains one of the most optimistic approaches by the research community. Current therapies directed at regulating cellular processes down stream of $\text{A}\beta$ production are likely to be unsuccessful. Once $\text{A}\beta$ is produced, there is simply too many avenues for destruction of cellular processes. It seems the most beneficial

strategy at this point would be to focus efforts on limiting the production of A β at the source. With this in mind, BACE-1 (β -secretase) inhibition is an attractive therapeutic strategy, however many BACE-1 inhibitors show undesirable side effects due to the role of BACE-1 in other systems, particularly muscle physiology [23]. Despite this, Merck and AstraZeneca currently have BACE-1 inhibitors in Phase III clinical trials. Thus, in all likely hood, the successful treatment of AD will ultimately be a multifaceted approach through enzymatic inhibition, antibody targeting, and nutritional, physical, and lifestyle modification. Until then, understanding the intricate details of cellular and synaptic impairment as a result of AD pathology is both a necessary and valuable endeavor for both the future of AD research, and the field of learning and memory as a whole.

References

1. Wang, Y. and M.P. Mattson, *L-type Ca²⁺ currents at CA1 synapses, but not CA3 or dentate granule neuron synapses, are increased in 3xTgAD mice in an age-dependent manner*. *Neurobiol Aging*, 2014. **35**(1): p. 88-95.
2. Chakroborty, S., et al., *Deviant ryanodine receptor-mediated calcium release resets synaptic homeostasis in presymptomatic 3xTg-AD mice*. *J Neurosci*, 2009. **29**(30): p. 9458-70.
3. Li, S., et al., *Soluble oligomers of amyloid Beta protein facilitate hippocampal long-term depression by disrupting neuronal glutamate uptake*. *Neuron*, 2009. **62**(6): p. 788-801.
4. Rice, R.A., et al., *Age-related downregulation of the CaV3.1 T-type calcium channel as a mediator of amyloid beta production*. *Neurobiol Aging*, 2014. **35**(5): p. 1002-11.
5. Proft, J. and N. Weiss, *T-type Ca(2+) channels: New players in the aging brain*. *Commun Integr Biol*, 2014. **7**(1): p. e28424.
6. Li, S., et al., *Soluble Aβ oligomers inhibit long-term potentiation through a mechanism involving excessive activation of extrasynaptic NR2B-containing NMDA receptors*. *J Neurosci*, 2011. **31**(18): p. 6627-38.
7. Talantova, M., et al., *Aβ induces astrocytic glutamate release, extrasynaptic NMDA receptor activation, and synaptic loss*. *Proc Natl Acad Sci U S A*, 2013. **110**(27): p. E2518-27.
8. Nabavi, S., et al., *Metabotropic NMDA receptor function is required for NMDA receptor-dependent long-term depression*. *Proc Natl Acad Sci U S A*, 2013. **110**(10): p. 4027-32.
9. Kessels, H.W., S. Nabavi, and R. Malinow, *Metabotropic NMDA receptor function is required for beta-amyloid-induced synaptic depression*. *Proc Natl Acad Sci U S A*, 2013. **110**(10): p. 4033-8.
10. Chung, C., *NMDA receptor as a newly identified member of the metabotropic glutamate receptor family: clinical implications for neurodegenerative diseases*. *Mol Cells*, 2013. **36**(2): p. 99-104.
11. *Alzheimer's disease medications fact sheet*. NIH Publication No. 15-3431 2015; Available from: <https://www.nia.nih.gov/alzheimers/publication/alzheimers-disease-medications-fact-sheet>.
12. Oules, B., et al., *Ryanodine receptor blockade reduces amyloid-beta load and memory impairments in Tg2576 mouse model of Alzheimer disease*. *J Neurosci*, 2012. **32**(34): p. 11820-34.

13. Peng, J., et al., *Dantrolene ameliorates cognitive decline and neuropathology in Alzheimer triple transgenic mice*. *Neurosci Lett*, 2012. **516**(2): p. 274-9.
14. Chakroborty, S., et al., *Stabilizing ER Ca²⁺ channel function as an early preventative strategy for Alzheimer's disease*. *PLoS One*, 2012. **7**(12): p. e52056.
15. Billings, L.M., et al., *Intraneuronal Ab causes the onset of early Alzheimer's disease-related cognitive deficits in transgenic mice*. *Neuron*, 2005. **45**: p. 675-688.
16. Oddo, S., et al., *Abeta immunotherapy leads to clearance of early, but not late, hyperphosphorylated tau aggregates via the proteasome*. *Neuron*, 2004. **43**(3): p. 321-32.
17. Bacskai, B.J., et al., *Imaging of amyloid-beta deposits in brains of living mice permits direct observation of clearance of plaques with immunotherapy*. *Nat Med*, 2001. **7**(3): p. 369-72.
18. Wang, A., et al., *Robust amyloid clearance in a mouse model of Alzheimer's disease provides novel insights into the mechanism of amyloid-beta immunotherapy*. *J Neurosci*, 2011. **31**(11): p. 4124-36.
19. Buttini, M., et al., *Beta-amyloid immunotherapy prevents synaptic degeneration in a mouse model of Alzheimer's disease*. *J Neurosci*, 2005. **25**(40): p. 9096-101.
20. Dorostkar, M.M., et al., *Immunotherapy alleviates amyloid-associated synaptic pathology in an Alzheimer's disease mouse model*. *Brain*, 2014. **137**(Pt 12): p. 3319-26.
21. Wisniewski, T. and F. Goni, *Immunotherapeutic approaches for Alzheimer's disease*. *Neuron*, 2015. **85**(6): p. 1162-76.
22. Panza, F., et al., *Is there still any hope for amyloid-based immunotherapy for Alzheimer's disease?* *Curr Opin Psychiatry*, 2014. **27**(2): p. 128-37.
23. Ghosh, A.K. and H.L. Osswald, *BACE1 (beta-secretase) inhibitors for the treatment of Alzheimer's disease*. *Chem Soc Rev*, 2014. **43**(19): p. 6765-813.

Figures

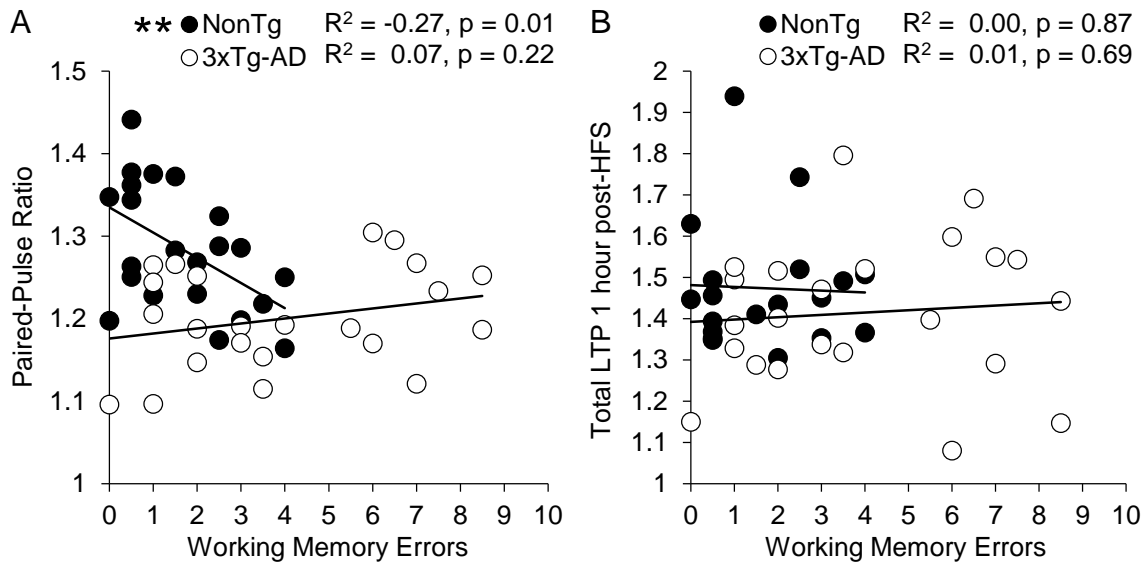


Figure 6.1. Neurophysiology relation to maze performance in 3xTg-AD and NonTg control mice. A) Scatter plot showing the relationship between paired-pulse facilitation ratio (100 ms interval) and total working memory errors in the test phase of our working memory task in 3xTg-AD (open circles, $n=23$) and NonTg (black circles, $n=22$) mice. B) Scatter plot showing the relationship between total LTP and total working memory errors in the test phase of our working memory task in 3xTg-AD (open circles, $n=23$) and NonTg (black circles, $n=19$) mice. Values represent individual subject electrophysiological measurements and individual subject maze performance. Significance was determined using Pearson correlation with Bonferroni probability statistic (* $p < 0.05$, ** $p < 0.01$).